Design considerations and implementation of a RF front-end for a CDMA adaptive array system

By
Kelesh D. Roopram (BSc. Eng)
University of Natal
December 2000

Submitted in fulfilment of the academic requirements for the Degree of Master of Science in the Programme of Electronic Engineering, University of Natal.

ABSTRACT

Recent studies have shown that considerable system capacity gains in mobile communication systems can be obtained by exploiting the use of antenna arrays at the base station. Unfortunately, these studies make little mention of practical issues concerning implementation. It is thus one of the objectives of the Centre of Excellence (CoE) in Radio Access Technologies at the University of Natal to investigate the development of a wideband CDMA adaptive array transceiver using Alcatel software radios as the transceiver platforms. Such a transceiver system can be subdivided into three major sections: RF front-end, signal digitization and baseband processing stages. Due to the enormity of such an undertaking, the research outlined in this thesis is focused on (but not isolated to) some aspects of the RF front-end implementation for the proposed system.

The work in this thesis can be catergorized into two sections. The first section focuses on the theoretical and practical (or implementation) aspects of antenna arrays and beamforming. In particular, it is evident that digital (rather than analogue) beamforming in a multiuser environment, is a more viable option from both a cost and implementation standpoint. The second section evaluates the impact of RF component noise and local oscillator generated phase noise in a DS-CDMA system. The implementation of a RF front-end for a BPSK transceiver also forms part of the work in this section. LO phase noise and Error Vector Magnitude (EVM) measurements are performed on this system to support relevant theory. By use of the HP89410A phase noise measurement utility and the phase noise theory developed in this thesis, a quantitative phase noise comparison between two frequency sources used in the system were made. EVM measurement results conclusively verified the importance of an LNA in the system. It has also been shown that the DS-CDMA simulated system exhibits superior performance to the implemented BPSK system. Furthermore, an EVM troubleshooting methodology is introduced to identify possible impairments within the BPSK receiver RF front-end. However, this thesis was written with the intention of bridging the gap between the

theoretical and practical/implementation aspects of RF wireless communication systems. It is the author's opinion that this has been achieved to a certain extent.

PREFACE

The research work discussed in this thesis was performed by Mr Kelesh Roopram, under the supervision of Mr Stephen McDonald, in the Programme of Electronic Engineering, University of Natal. The work forms part of the Centre of Excellence (CoE) programme. Part of the work documented in this thesis has been presented by the student author at the SATNAC '99 conference in Durban and the COMSIG 2000 conference in Cape Town. The publications in respect of these conference presentations are:

- K.D. Roopram and S.A. McDonald, "Design considerations towards the implementation of a CDMA adaptive array receiver," in Proc. South African Telecommunications Networks Applications Conference (SATNAC), Durban, South Africa, September 1999, P432 – 437.
- K.D. Roopram and S.A. McDonald, "The impact of oscillator generated phase noise on DS-CDMA performance," IEEE South African conference on Communications and Signal processing (COMSIG), incorporated in SATCAM 2000 conference, Somerset West, South Africa, September 2000.
- K.D. Roopram and S.A. McDonald, "The effect of internally generated RF component noise in a DS-CDMA system," IEEE South African conference on Communications and Signal processing (COMSIG), incorporated in SATCAM 2000 conference, Somerset West, South Africa, September 2000.

The whole thesis, unless specifically indicated to the contrary in the text, is the student author's work, and has not been submitted in part, or in whole to any other university.

ACKNOWLEDGEMENT

It is impossible to acknowledge all those people who have had an influence on the conception and fruition of both this project and thesis. To the best of my ability I shall attempt to do so: A project of this magnitude and stature requires considerable funding. To this end, I would first and foremost like to thank the sponsors of the Centre of Excellence (CoE). They are Telkom S.A., Alcatel Altech Telecoms (AAT) and THRIP. Hardware, both primary and secondary to this project were obtained through their financial assistance. In particular, the development of an antenna test facility (anechoic chamber) was made possible through their generosity. Furthermore, I would like to express my sincere appreciation to AAT for the donation of the software radio. Both the anechoic chamber and software radio (shown on page vi) are set to form the testbed and the core of the CoE adaptive array research project.

Knowledge is cumulative. It is not based on each person's reinventing everything that is known, but rather on accumulating what has been learned in the past, synthesizing new ideas from old formulas and principles, and creating completely new insights. I want to acknowledge the contributions of all those whose work has added to my understanding of the various topics in this thesis. I am grateful to my former associates at Reutech Defence Industries (RDI) where I gained that real understanding comes from experience rather than from a textbook.

I would like to acknowledge Agilent Technologies for the donation of the Advanced Design System (ADS) software which has allowed us to simulate the complete project before implementation. Their technical support and interest in this project has been overwhelming.

I would like to express my most profound gratitude to my project supervisor/mentor, Mr S. McDonald for his encouragement and help in establishing an elective stream in high-frequency circuit design, which has resulted in the proposal of this project. He has tirelessly answered many of my questions regarding the implementation details of this

project. His patience and invaluable suggestions are much appreciated. I am really grateful for the happy and profitable years I spent working under his supervision.

In closing, I would like to express my sincere appreciation to the special group of research engineers within the COE who challenged me everyday on the engineering and operational details of a complex CDMA system. In particular, special thanks to my team members, G. Parry and T. Ellis for their immense contribution to the baseband and signal processing stages of this project.

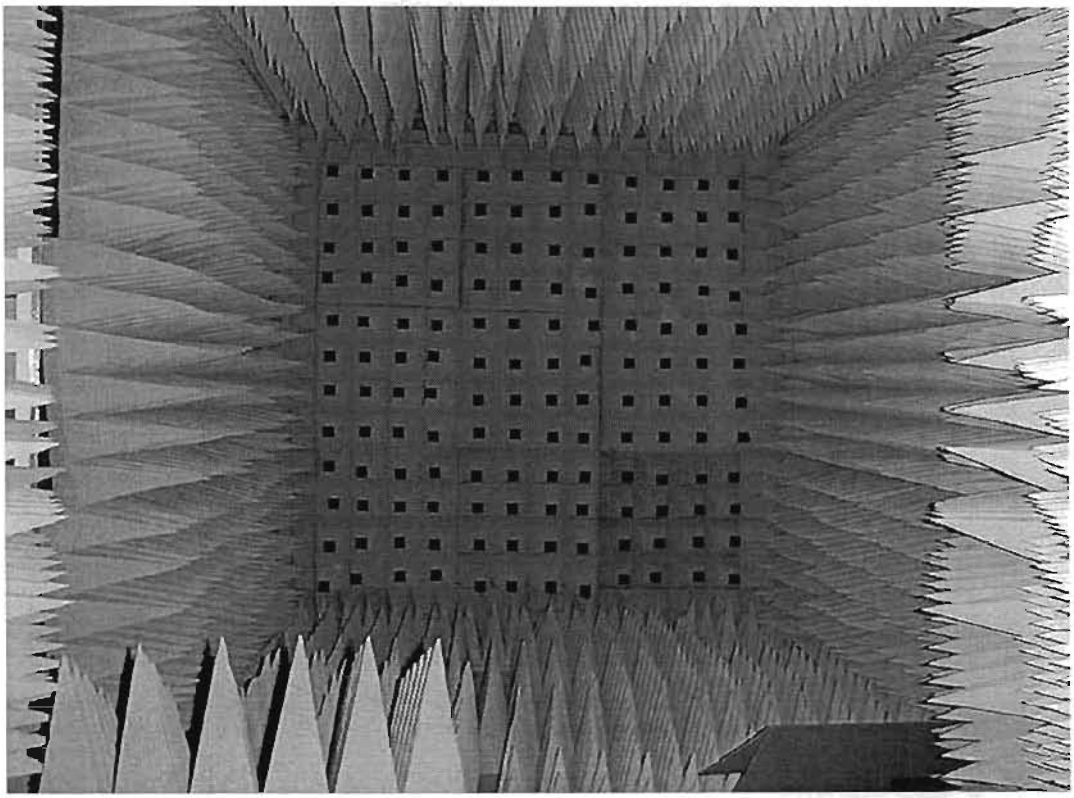

Anechoic chamber developed for antenna array testing and characterization

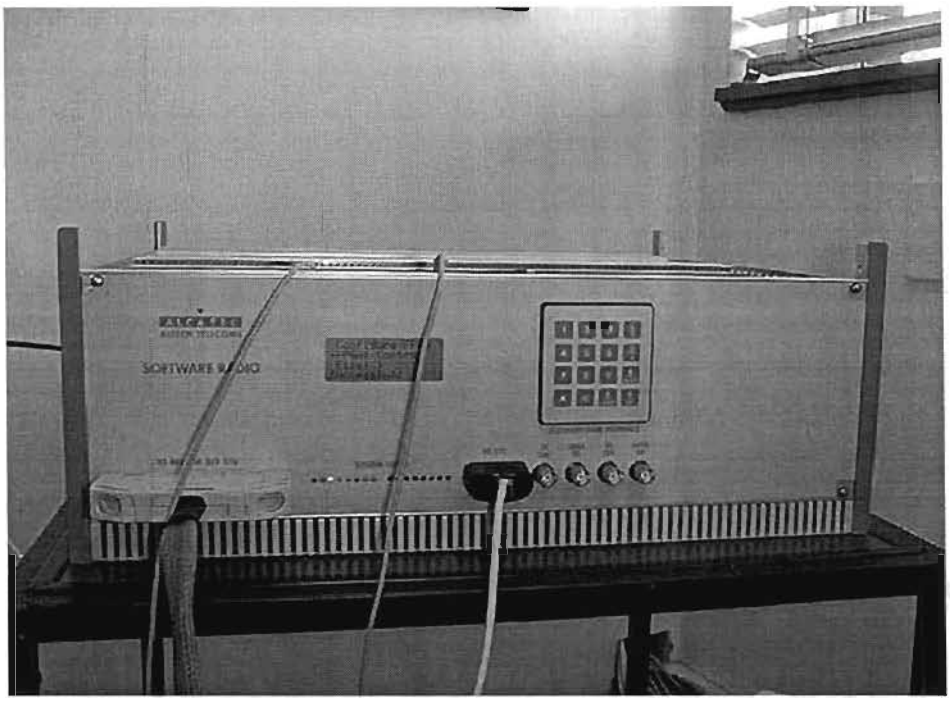

Alcatel software radio intended as the test platform for the CDMA adaptive array transceiver

TABLE OF CONTENTS

LIST OF FIGURES / TABLES

CHAPTER 2

CHAPTER 3

CHAPTER 4

CHAPTER 5

APPENDIX

CHAPTER 1

INTRODUCTION

1.1 Motivation and focus of thesis

Code Division Multiple Access (CDMA) technology is proving to be a promising and definite approach for spectrally efficient and high quality, digital wireless communication systems. CDMA is currently deployed in certain areas across the world under the IS-95 standard and has been selected as the main multiple access technology for third generation wireless systems [1]. However, emerging requirements for higher rate data services and greater spectrum efficiency, has led to the proposal of wideband CDMA (WCDMA) for third generation systems [1]. In general, the most complex and expensive part of the radio path for these systems is the base station. As a result, systems have been designed to have high efficiency in terms of bandwidth occupied and the number of users per base station. Recent studies ([2], [3], [4], [5], [6]) have shown that considerable system capacity gains are available from exploiting the use of antenna arrays at the base station. Unfortunately, there is very little literature concerning the practical and development aspects of such a system. The CoE at the University of Natal, which has adopted both a research and development stance, has thus taken an initiative to investigate the development of a wideband CDMA adaptive array system. Due to both the anticipated research intensiveness and implementation complexity of such a system, some aspects of the RF front-end was the focus of the author's research.

The increasing development of wireless communication products in recent years has led to an interest in improved circuit design in the radio frequency (RF) and microwave frequency ranges. Even though the majority of interest and activity for these systems is occurring at frequencies below 2GHz, there is increasing interest above 2GHz. One technical reason for the use of frequencies below 2GHz is that signal attenuation in the propagation medium (atmosphere) rises with frequency. Secondly, the active circuits that are used during transmission and modulation of the signals in the past have had little gain at higher frequencies. However, with advances

in IC technology, this latter limitation is changing. Also, more importantly, due to an ever-increasing demand for services below 2GHz, researchers are forced to consider the spectrum above 2GHz to support more users and services.

The development of commercial markets for digital wireless communications in recent years has also been a blessing to many RF and microwave engineers affected by the downsizing of the defense industry of the late 1980s and 1990s. However, the technology required to address these new markets are different from the traditional high-power consuming RF/microwave electronics which has provided discrete analog solutions with emphasis on performance rather than cost. Due to the aggressive cost targets associated with the competitive consumer market, the communication industry is continually seeking monolithic, low-power operation solutions to microwave/RF circuit design.

The implementation of a CDMA adaptive array requires a thorough understanding of RF issues in addition to a background in digital communication techniques and familiarity with various wireless communication protocol standards. In the wireless communication industry it is well known that the RF front-end transceiver is one of the key elements of the communication system. Chapter 2 presents an overview of antenna array theory. The chapter begins with a summary on the basic concepts of antenna arrays. This is followed by a discussion on the application of arrays in mobile communication systems and the performance improvement thereof. The theory behind linear arrays are explicitly described. This is used to discuss the principles of beamscanning and pattern multiplication. Also described are antenna element spacing criteria for the avoidance of grating lobes. All these concepts are demonstrated by a simple simulation that plots the array beam pattern as a function of the number of elements, element spacing and scan angle. A half-wavelength dipole is used in this simulation. This chapter closes with a subsection on the effects of mutual coupling on the antenna radiation pattern.

The implementation implications of adaptive antennas at RF, IF or baseband are discussed in chapter 3. This chapter begins with a description of both analogue and digital beamforming. In the analogue case, a discussion on the different types of array feeds and phase shifters are provided. The bandwidth effects due to both phase shifter

and feed effects are also described. The next subsection focuses on digital beamforming. Here, the ideal concept of digital beamforming is introduced. This ideal digital topology describes a straightforward approach that digitizes the RF input signal directly and processes the digitized data to extract the needed information. However, this approach is currently impractical given the usually high operating frequencies that are part of real communication systems and also the relatively low sampling rates of present-day analog-to-digital converters. Three (practical) receivers for digital beamforming are proposed where the microwave/RF input signals are downconverted to IF before digitization. The merits and demerits of each receiver are also discussed. The penultimate section describes an adaptive beamforming configuration for CDMA and the implementation issues thereof. The final section includes a case study of various adaptive antenna systems and their implementation trends.

Chapter 4 provides a comprehensive overview on CDMA theory and concepts. A brief background on CDMA and spread spectrum is provided. Also included are descriptions of other multiple access schemes such as FDMA and TDMA and the advantages of CDMA over them. A descriptive subsection on the all-important process of filtering, to reduce channel bandwidth, is included. The three most common types of filters are discussed: raised cosine, square root raised cosine and Gaussian filters. This subsection also extends briefly into the efficiency of different modulation techniques. Finally, the practicalities of Gaussian filtering (in conjunction with MSK modulation) as used in the GSM standard, are discussed. The CDMA theory and concepts in this chapter are reinforced by simulation work using Advanced Design System (ADS) software [7]. The work here forms the basis for the simulation models utilized in the following chapters.

Chapter 5 looks at the effect of internally generated RF component noise on the bit error rate of the DS-CDMA system. This investigation is warranted since it is intended to utilize off-the-shelf/commercial RF components in the implementation of the adaptive CDMA system. The chapter begins with a discussion on receiver noise and characterization. Here, the well-known concepts of noise figure and Friis' formula are defined. Following this is a description of the DS-CDMA transceiver system architecture and the simulation. Simulation results are presented and

analyzed. Part of the analysis and results include some theory on mixer noise figures and the effect of mixer noise on system performance. This is justified since in addition to being the "noisiest" component in RF front-end, it also dominates the receiver chain performance ahead of the LNA. Finally, some concluding remarks are mentioned.

Chapter 6 examines the impact of local oscillator generated phase noise on the bit error rate of the DS-CDMA system. These circuits often form the "heart" of any communication system in the sense that they provide precise reference frequencies for modulation/demodulation and frequency conversion. As a result, their performance is crucial for an overall acceptable system performance. The local oscillator generates spurious signals, amplitude (AM) noise and phase noise. Spurious signals and AM noise are initially discussed. Thereafter, a thorough discussion and analysis of phase noise from an RF engineer's perspective is provided. The effect of local oscillator generated phase noise on DS-CDMA system performance is investigated via simulation. Some concluding remarks are made with regard to the simulation results and the phase noise performance of commercially-available local oscillators.

An overview on mixer theory is presented in chapter 7. The usually high operating frequencies that are associated with wireless communication systems coupled with the non-availability of signal processing and digitization at these frequencies, has inevitably led to the use of a mixer for frequency downconversion in the receiver. As mentioned previously, this fundamental device is usually the dominant source of distortion/noise in the receiver. In addition to the brief discussion on mixer noise figure in chapter 5, other important issues and properties concerning mixers are covered in this chapter. Amongst them are the process of mixing or frequency changing and the parasitic signals generated by this process. Also discussed are the principal characteristics such as conversion gain/loss, VSWR, isolation, dynamic range, 1dB compression point, etc. Intermodulation products (as a result of the mixing process) and conversion gain are demonstrated by a simple ADS simulation. This chapter is concluded by a discussion on intermodulation distortion and design techniques/suggestions to avert these unwanted responses.

In wireless communication systems, a fundamental function of the RF front-end is signal amplification. Chapter 8 is therefore devoted to the design, simulation, construction and characterization of a low noise microwave amplifier for possible use in the proposed CDMA adaptive array system. A firm theoretical and practical basis on microwave low noise amplifier design is laid down in this chapter. Each stage of the design process from defining the specifications right up to verifying that the constructed amplifier meets these specifications, are explicitly described. The initial stage of this process involves determining the stability of the active device. "Traditional" techniques utilizing a Smith chart to determine this, are demonstrated. Other stages involve the simulation, optimization and microstrip implementation of the circuit. S parameter measurement results (using the HP8510A network analyzer) are obtained. Noise figure measurements on this amplifier are also performed using the HP346B noise source and HP8970B noise figure meter. The theory behind the workings of these noise figure instruments are described. A comparison between simulated and measured results are also made. Finally, some concluding remarks about this low noise amplifier design process, are mentioned.

The measurements chapter (chapter 9) is intended to support the theory and simulation results of the preceding chapters (specifically chapters 5 and 6). A receiver RF front-end for a BPSK system was implemented using commercially available (off-the-shelf) components. This chapter begins with a description of this BPSK system. Waveforms at most of the stages of the system are shown. Component parameters such as gain, conversion loss or insertion loss are computed and compared with the ones specified in manufacturer's datasheets. This is followed by a description of two phase noise measurement techniques that support the phase noise theory in chapter 6. Phase noise measurements are performed on two signal generators used in the system and the phase noise variance, computed and compared. The effect of RF component noise on DS-CDMA system performance was evaluated in chapter 5. Simulation results here established that RF component noise (as a result of the noise figure) cause degradation of the signal-to-noise ratio (SNR) and hence an increase in the bit error rate (BER). Thus it is intended to replicate the SNRs within the measurement setup and compare the performance degradation between simulated and measured results. Instead of the BER being used as a figure of merit to quantify system performance, this chapter introduces another type of measurement, the Error

Vector Magnitude (EVM), which has been gaining rapid acceptance in the wireless communication industry. It has already been included in standards such as GSM, NADC and PHS (Personal Handyphone System). In addition to providing a figure of merit for system performance, it allows a methodology for troubleshooting to identify the possible impairments within a transceiver system that cause the signal degradation. This methodology is described to identify/trace impairments such as residual PM noise, phase noise, IQ imbalance, quadrature error, amplitude nonlinearities, adjacent channel interference, filter distortion, etc. Finally, this troubleshooting methodology is demonstrated on the BPSK transceiver system.

Chapter 10, the final chapter, presents a summary and conclusions of this thesis. Some possible extensions and/or further topics of study to this research are also included.

CHAPTER 2

ANTENNA ARRAY THEORY

2.1 Introduction

Antennas are the front-end building block of most communication systems. By increasing the performance characteristics, it often places reduced requirements on the remaining stages of the communication system, for example, increased antenna gain has direct mobile communication system benefits in terms of received signal strength and the reduced requirements on front-end amplifiers.

Usually the radiation pattern of a single element antenna is relatively wide, and each element provides low values of directivity (gain). In many applications it is necessary to design antennas with very directive characteristics (very high gains) to meet the demands of long distance communications. This can be accomplished by increasing the electrical size of the antenna. Enlarging the dimensions of single elements often leads to more directive characteristics. Another way to enlarge the dimensions of the antenna, without necessarily increasing the size of the individual elements, is to form an assembly of radiating elements in an electrical or geometrical configuration. This new antenna, formed by multi-elements, is referred to as an array. In most cases the elements of an array are identical. This is not necessary, but is often convenient, simpler, and more practical.

A single element antenna is such that any modification of the radiation pattern is only obtained by mechanical movements that generally involve rotation of the entire antenna about one or more axes, movement of all or part of the reflector or movement of the primary source. In this instance the single element antenna only provides a rotatable fixed radiation pattern. This has three main consequences:

(a) Any modification of the radiation is slow.

(b) It is not possible to modify the radiation pattern significantly.

(c) It is not possible in practice to control the pattern in the secondary radiation directions (characterized by the antenna sidelobes). The direct result of this is that it is not possible to change the principal radiation direction rapidly. Therefore in

changing from one direction of interest to another that is quite different, it is necessary to pass systematically through a large number of other directions of no interest in which the energy transmitted by the antenna is lost. A second result is that if a system with a number of very different patterns is required in order to provide different functions, it is essential to use as many antennas as there are functions. On the otherhand, a multi-element antenna (array) eliminates or alleviates the above-mentioned problems thereby allowing more precise control of the radiation pattern, thus resulting in lower sidelobes or careful pattern shaping.

However, the primary reason for using arrays is to produce a directive beam that can be repositioned (scanned) electronically thus eliminating the need for servo-mechanism rotation of the entire antenna. Although arrays can be used to produce fixed (stationary) beams and multiple stationary beams, the primary emphasis today is on arrays that are scanned electronically.

The total field of the array is determined by the vector addition of the fields radiated by the individual elements ([8], [9], [10], [11]). This assumes that the current in each element is the same as that of the isolated element. This is usually not the case and depends on the separation between the elements. To provide very directive patterns, it is necessary for the fields from the elements of the array to interfere constructively (add) in the desired directions and to interfere destructively (cancel each other) in the remaining space. Ideally this can be accomplished, but practically it is only approached. In an array of identical elements, there are five controls that can be used to shape the overall pattern of the antenna [11]. These are:

(a) The geometrical configuration of the overall array.

(b) The relative displacement between the elements.

(c) The excitation amplitude of the individual elements.

(d) The excitation phase of the individual elements.

(e) The relative pattern of the individual elements.

2.2 Basic concepts of antenna arrays

An array antenna consists of a number of individual radiating elements suitably spaced with respect to one another. The relative amplitudes and phases of the signals applied to each of the elements are controlled to obtain the desired radiation pattern from the combined action of all the elements. Two common geometrical forms of array antennas of interest are the linear array and the planar array. A linear array consists of elements arranged in a straight line in one dimension. A planar array is a two-dimensional configuration of elements arranged to lie in a plane. The planar array may be thought of as a linear array of linear arrays. A broadside array is one in which the direction of maximum radiation is perpendicular, or almost perpendicular to the line (or plane) of the array. Figure (2.1) shows a broadside array pattern for a linear array with elements situated on the z-axis. An endfire array has its maximum radiation parallel to the array. Figure (2.2) shows endfire array patterns for a linear array with elements situated on the z-axis. As can be seen, the maximum radiation can be directed at either ends of the linear array. An array whose elements are distributed on a nonplanar surface is called a conformal array.

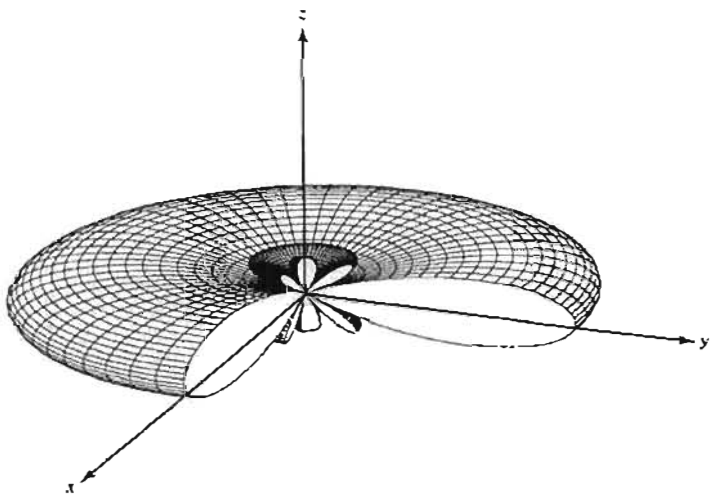

Fig. 2.1: Broadside array pattern for a linear array placed on the z-axis (from [11])

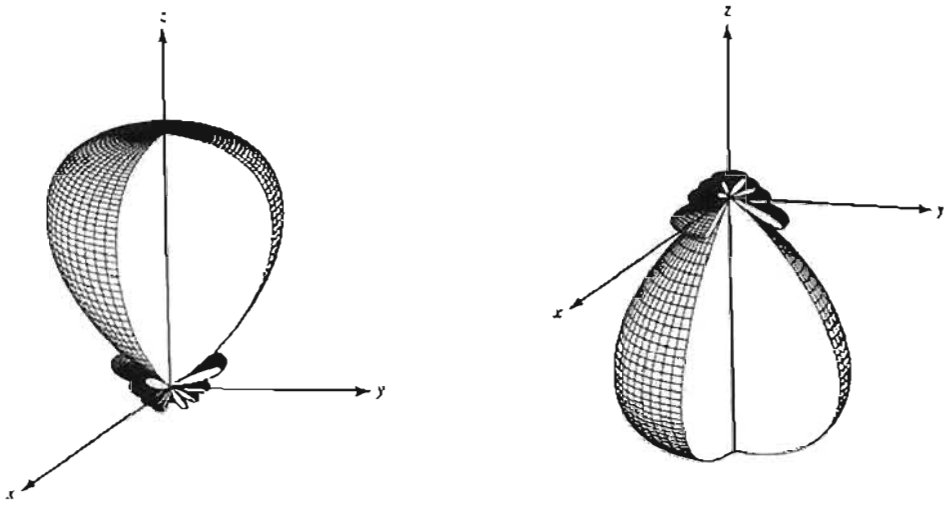

Fig. 2.2: Endfire array patterns for a linear array placed on the z-axis (from [11])

Antennas in general may be classified as omnidirectional, directional, phased array, adaptive and optimal [12]. An omnidirectional antenna has equal gain in all directions and is also known as an isotropic antenna. Directional antennas, on the other hand, have more gain in certain directions and less in others. The direction in which the gain of these antennas is maximum is referred to as the boresight direction of the antenna. The gain of directional antennas in the boresight is more than that of the omnidirectional antenna and is measured with respect to the gain of the omnidirectional antenna [12]. For example, a gain of 10dBi means the power radiated by this antenna is 10dB more than that radiated by an isotropic one. It should be noted that the same antenna may be used as a transmitting antenna or a receiving antenna. The gain of the antenna remains the same in both cases. The gain of a receiving antenna indicates the amount of power it delivers to the receiver compared to an omnidirectional antenna.

A phased array antenna uses an array of simple antennas, such as omnidirectional antennas, and combines the signal induced on these antennas to form the array output. Each antenna forming the array is known as the element of the array. The direction where the maximum gain would appear is controlled by adjusting the phase between different antennas. The phases of signals induced on various elements are adjusted such that the signals due to a source in the direction where maximum gain is required

are added in phase. This results in the gain of the array (or equivalently, the gain of the combined antenna) being equal to the sum of the gains of all individual antennas.

The term adaptive antenna is used for the phased array when the gain and phase of the signals induced on various elements are changed before combining to adjust the gain of the array in a dynamic fashion, as required by the system. In a way, the array adapts to the situation, and the adaption process is normally under the control of the system [13]. A block diagram of a typical adaptive antenna array system is shown in figure (2.3).

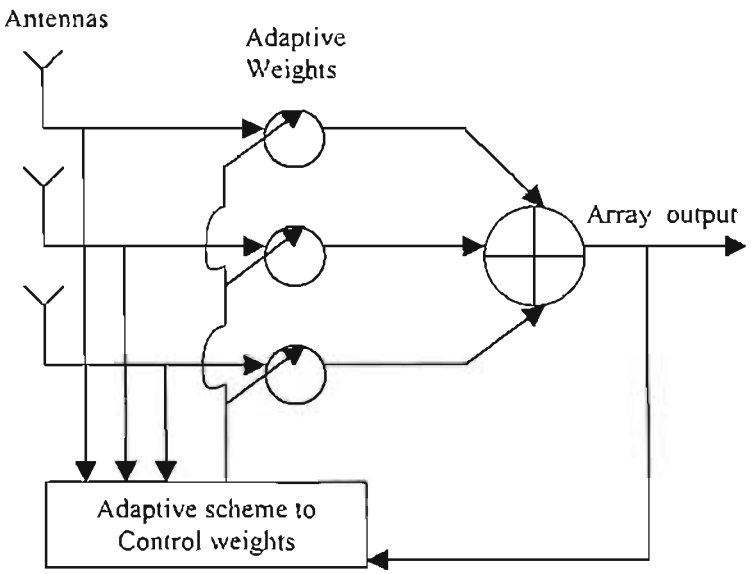

Fig. 2.3: Block diagram of a narrow-band adaptive antenna system (from [13])

An optimal antenna is one in which the gain and phase of each antenna element is adjusted to achieve the optimal performance of the array in some sense. For example, to obtain maximum output SNR by cancelling unwanted interferences and receiving the desired signal without distortion may be one way of adjusting the gain and phases of each element. This arrangement where the gain and phase of each antenna element is adjusted to obtain maximum output SNR (sometimes also referred to as signal-to-interference-and-noise ratio, SINR) is also referred to as optimal combining in the mobile communications literature ([14], [15], [16]).

(a) Beam steering and switching

The signals induced on different elements of an array are combined to form a single output of the array. A plot of the array response as a function of the angle is normally

referred to as the array pattern or the beam pattern. It is also called a power pattern when the power response is plotted. It shows the power received by the array at its output from a particular direction due to a unit power source in that direction. This process of combining the signals from different elements is known as beamforming. The direction in which the array has maximum response is said to be the beam pointing direction. Thus, this is the direction where the array has the maximum gain. For a linear array, when signals are combined without any gain and phase change, this is broadside to the array, that is, perpendicular to the line joining all elements of the array.

The array pattern drops to a low value on either side of the beam pointing direction. The place of the low value is normally referred to as a null. Strictly speaking, a null is a position where the array response is zero. However, the term is generally misused to indicate the low value of a pattern. The pattern between the two nulls on either side of the beam pointing direction is known as the main lobe. The width of the beam (main lobe) between the two half-power points as called the half-power beamwidth. These concepts are illustrated in figure (2.4).

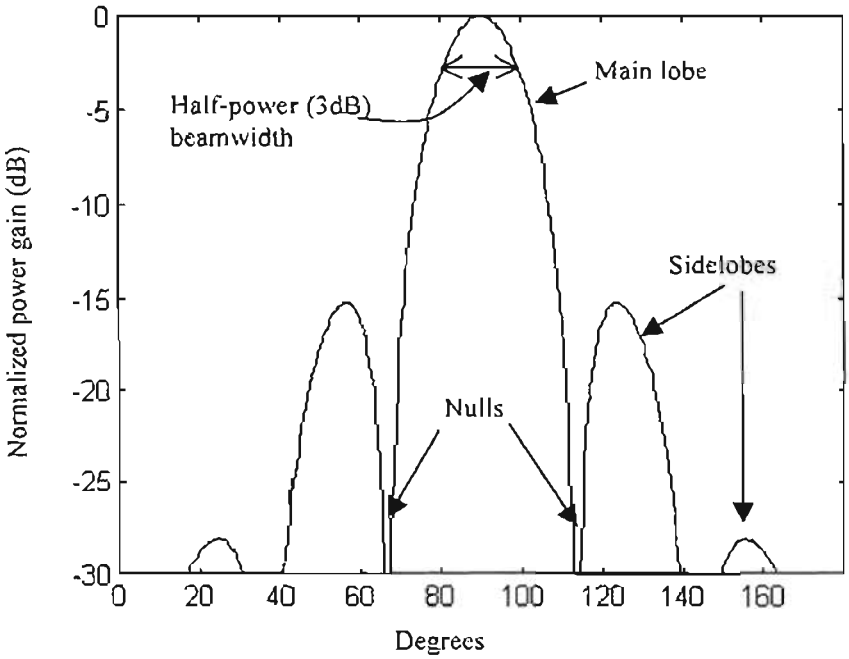

Fig. 2.4: A typical array pattern illustrating some array concepts

A smaller beamwidth results from an array with a larger extent. The extent of the array is known as the aperture of the array. Thus, the aperture of the array is the

distance between the two farthest elements in the array. For a linear array, it is equal to the distance between the elements on either side of the array.

(b) Conventional beam forming

Adjusting only the phase of signals from different elements to point a beam in a desired direction is the conventional method of beam pointing or beam forming. When the main beam is pointed in different directions by adjusting various phases, the relative positions of the sidelobes with respect to the main lobe change. By adjusting both the gain and phase of each signal, the pattern can be shaped as required. The amount of change depends upon the number of elements in the array. When only the gain of each of the elements are changed, the shape of the array pattern is fixed, that is, the positions of the sidelobes with respect to the main beam and their levels are unchanged.

The gain and phase applied to the signals derived from each element may be thought of as a single complex quantity referred to as the weighting applied to the signals. If there is only one element, no amount of weighting can change the pattern of that antenna. With two elements, however, changing the weighting of one element relative to the other may adjust the pattern to the desired value at one place, that is, one is able to place one minima or maxima anywhere in the pattern. Similarly with three elements, two positions may be specified, and so on. Thus, with an N-element array, one is able to specify N-1 positions. These may be one maxima in the direction of the desired signal and N-2 minimas (nulls) in the directions of unwanted interferences. This flexibility of an N-element array to be able to fix the pattern at N-1 places is known as the degree of freedom of the array.

(c) Null beam forming

The flexibility of array weighting to being adjusted to specify the array pattern is an important property. This may be exploited to cancel directional sources operating at the same frequency as that of the desired source, provided these are not in the direction of the desired source. In situations where the directions of these interferences are known, cancellation is possible by placing the nulls in the pattern corresponding to these directions and simultaneously steering the main beam in the direction of the desired signal. Beam forming in this way, where nulls are placed in

the directions of interferences, is normally known as null beam forming or null steering. The cancellation of one interference by placing a null in the pattern uses one degree of the freedom of the array.

Null beam forming uses the direction of sources towards which nulls are placed for estimating the required weighting on each element. There are other schemes that do not require directions of all the sources.

2.3 Application of arrays in mobile communication systems [12]

Arrays may be used in various mobile communication systems, for example, base-mobile, indoor-mobile, satellite-mobile, and satellite-to-satellite communication systems. Only the base-mobile system will be considered here. The use of arrays in the remaining systems are discussed in [12].

The base-mobile system consists of a base station situated in a cell and serves a set of mobiles within the cell. It transmits signals to each mobile and receives signals from them. It monitors their signal strength and organizes the handoff when the mobiles cross the cell boundary. It provides the link between the mobiles within the cell and the rest of the network.

In this section various scenarios are presented to show how an array could be used in such a system. The discussion will concentrate on the use of an array at the base station. A base station having multiple antennas is sometimes referred to as having antenna diversity or space diversity.

2.3.1 Use of an array at a base station

(a) **Formation of multiple beams:** Multiple antennas at the base station may be used to form multiple beams to cover the whole cell site. For example, three beams with a beamwidth of 120° each or six beams with a beamwidth of 60° each may be formed for the purpose. Each beam may then be treated as a separate cell, and the frequency assignment may be performed in the usual manner. Mobiles are handed to the next beam as they leave the area covered by the current beam, as is done in a normal handoff process when the mobiles cross the cell boundary.

(b) Formation of adaptive beams: An array of antennas with the capability to form independent beams may be used at the base station. The array is used to find the location of each mobile, and then beams are formed to cover different mobiles or groups of mobiles. Each beam may be considered as a cochannel cell, and may be able to use the same frequency or code, as the case may be. Figure (2.5) shows a typical setup involving different beams covering various mobiles along with the directions of moving mobiles. It illustrates the situation at two time instants.

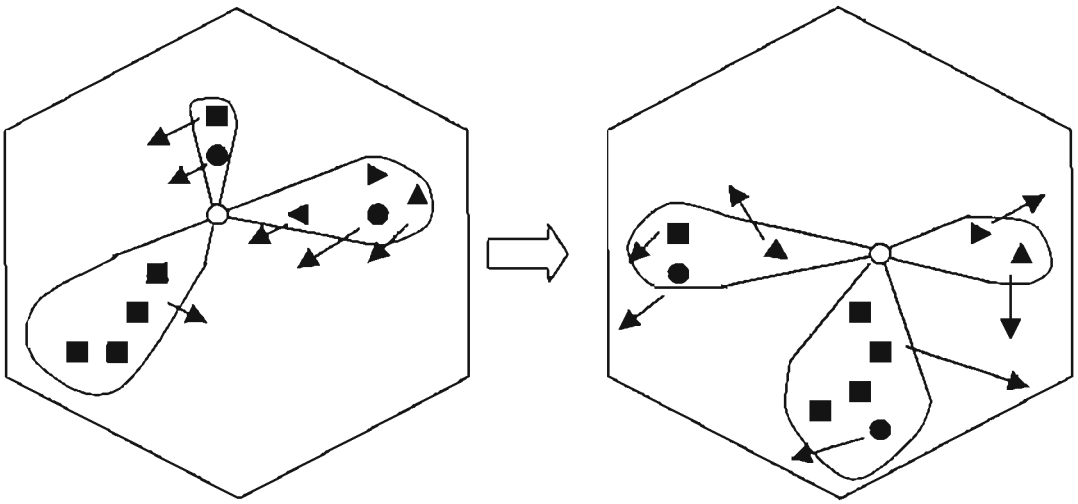

Fig. 2.5: A typical setup showing different beams covering various mobiles

This setup is different from the one discussed previously where a number of beams of fixed shape cover the whole cell. Here, the beams are shaped to cover traffic. As the mobiles move, the different beams cover different clusters of mobiles, offering the benefit of transmitting the energy toward the mobiles. The arrangement is particularly useful in situations where the mobiles move in clusters or along confined paths, such as highways. Each mobile can also be covered by a separate beam. Each beam would then follow the mobile, reducing the handoff problem to the bare minimum.

(c) Null formation: In contrast with steering beams toward mobiles, one may adjust the antenna pattern such that it has nulls towards other mobiles. Formation of nulls in the antenna pattern toward cochannel mobiles helps to reduce the cochannel interference in two ways. In the transmit mode, less energy is transmitted from the base towards these mobiles, reducing the interference from

the base to them. In the receiving mode, this helps to reduce the contribution from these mobiles at the base.

(d) Optimal combining: Canceling unwanted cochannel interferences while an array is operating in receiving mode is a very effective use of an antenna array. The process combines signals received on various antennas in such a way that the contribution due to unwanted interferences is reduced while that due to a desired signal is enhanced. Knowledge of the directions of the interferences is not essential to the process's functioning, while some characteristic of the desired signal are required to protect it from being cancelled.

By using constrained beamforming techniques, one may be able to combine the formation of nulls in the directions of unwanted mobiles while keeping the specified response in the direction of a desired mobile. For proper operation, the direction of the desired signal is required. It is used for maintaining a specified response in that direction. Though constrained beam-forming is very effective when the desired signal is a point source, its use in mobile communications is limited, particularly in situations of multipaths. Optimal combining using a reference signal is more appropriate for this case. It requires a signal that is correlated with the desired signal. The scheme that protects all signals that are correlated with this reference signal and adds them in phase to maximize their combined effect. It simultaneously cancels all waveforms that are not correlated with this signal, resulting in a removal of cochannel interferences. Thus, optimal combining using a reference signal is able to make use of multipath arrivals of the desired signal, whereas constrained beamforming treats them as interferences and cancels them. Further discussion on these techniques are provided in [13] and [17].

(e) Dynamic cell formation: The concept of adaptive beam-forming may be extended to dynamically changing cell shapes [12]. Instead of having cells of fixed size, the use of array antennas allows the formation of a cell based upon traffic needs, as shown in figure (2.6). An architecture to realize such a base station requires the capability of locating and tracking the mobiles to adapt the system parameters to meet the traffic requirements.

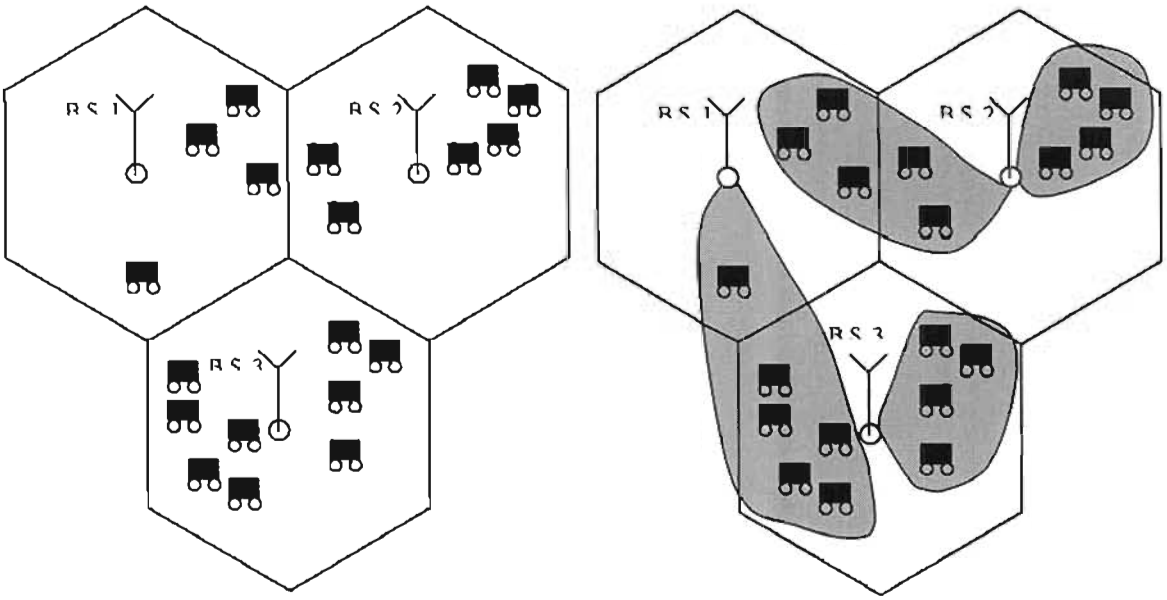

(a) (b)

Fig. 2.6: Cell shape based upon traffic needs. (a) Cells of fixed shape. (b) Cells of dynamic shape

(f) Blind estimation of cochannel signals: A base station employing arrays may be able to exploit the fact that signals arriving from different mobiles follow different paths and arrive at various elements at different times. This allows independent measurements of signals superimposed from different mobiles. This, along with the properties of the modulation techniques used, allows separation of signals arriving from different mobiles. Thus, by using the measured signals at various elements of the array at the base, one is able simultaneously to separate all signals. The process is referred to as the blind estimation of cochannel signals ([12], [13], [17]). It does not require knowledge of the directions or other parameters associated with mobiles, such as a reference signal, but exploits the temporal structure that might exist in signals inherited from the source of their generation, for example, the modulation techniques used.

2.3.2 Performance improvement using an array

An antenna array is able to improve the performance of a mobile communication system in a number of ways. It provides the capability to reduce cochannel interferences and multipath fading, resulting in better quality of services, such as reduced bit error rate (BER) and outage probability. Its capability to form multiple beams could be exploited to serve many users in parallel resulting in an increased

spectral efficiency. Its ability to adapt beam shapes to suit traffic conditions is useful in reducing the handoff rate.

This section discusses the advantages of an array of antennas in a mobile communications system and improvements that are possible by using multiple antennas in a system rather than a single one.

(a) Reduction in delay spread and multipath fading [12]: Delay spread is caused by multipath propagation where a desired signal arriving from different directions gets delayed due to the different travel distances involved. An array with the capability to form beams in certain directions and nulls in the others is able to cancel some of these delayed arrivals in two ways. In the transmit mode, it focuses energy in the required direction, which helps to reduce multipath reflections causing a reduction in the delay spread. In the receive mode, an antenna array provides compensation in multipath fading by diversity combining, by adding the signals belonging to different clusters after compensating for delays, and by canceling delayed signals arriving from directions other than that of the main signal.

(i) ***Use of diversity combining:*** Diversity combining achieves a reduction in fading by increasing the signal level based upon the level of signal strength at different antennas, whereas in multipath cancellation methods, it is achieved by adjusting the beam pattern to accommodate nulls in the direction of late arrivals, assuming them to be interferences. For the latter case, a beam is pointed in the direction of the direct path or a path along which a major component of the signal arrive, causing a reduction in the energy received from other directions and thus reducing the components of multipath signal contributing to the receiver.

(ii) ***Combining delayed arrivals:*** A radiowave originating from a source arrives at a distant point in clusters after getting scattered and reflected along the way. This is particularly true in scenarios with large buildings and hills were delayed arrivals are well separated. These clustered signals could be used constructively by grouping them as per their delays compared to a signal available from the shortest path. Individual paths of

these delayed signals may be resolved by exploiting their temporal or spatial structure.

The resolution of paths using temporal structures depends upon the bandwidth of the signal compared to the coherence bandwidth of the channel and increases as this bandwidth increases. When the paths are well separated spatially, an antenna array may be used. This could be done, for example, by determining their directions. In some situations, it is possible to separate the signals from each cluster by forming multiple beams in the directions of each component of these clusters, with nulls pointing toward the other ones. Combining signals belonging to different users after compensating for delays leads to a reduction in delay spread and cochannel interference.

(iii) ***Nulling delayed arrivals:*** An antenna array can reduce delay spread by nulling the delayed signals arriving from different directions.

(b) Reduction in cochannel interference: An antenna array has the property of spatial filtering, which may be exploited in transmitting and receiving modes to reduce cochannel interferences. In the transmitting mode, it can be used to focus radiated energy by forming a directive beam in a small area where a receiver is likely to be. This in turn means that there is less interference in other directions where the beam is not pointing. Cochannel interference in transmit mode could be further reduced by forming specialized beams with nulls in the direction of other receivers. This scheme deliberately reduces transmitted energy in the direction of cochannel receivers and requires knowledge of their positions.

The reduction of cochannel interference in the receive mode is a major strength of antenna arrays. It does not require knowledge of the cochannel interferences. If these were available, however, an array pattern might be synthesized with nulls in these directions. In general, an adaptive array requires some information about the desired signal, such as the direction of its source, a reference signal, or a signal that is correlated with the desired signal.

(c) **Spectral efficiency and capacity improvement:** Spectrum efficiency refers to the amount of traffic a given system with certain spectrum allocation could handle. An increase in the number of users of the mobile communications system without a loss of performance causes the spectrum efficiency to increase. Channel capacity refers to the maximum data rate a channel of given bandwidth could sustain. An improved channel capacity leads to more users of a specified data rate, implying a better spectral efficiency.

TDMA and CDMA result in an increase in channel capacity over the standard FDMA, allowing different time slots and different codes to be assigned to different users [18]. This may be further improved by using multiple antennas and combining the signals received from them. Firstly, the increased quality of service resulting from the reduced cochannel interferences and reduced multipath fading, as discussed, may be traded to increase the number of users. Thus, the use of an array results in an increase in channel capacity while the quality of service provided by the system remains the same, that is, it is as good as that provided by a system using a single antenna. Secondly, an array may be used to create additional channels by forming multiple beams without any extra spectrum allocation, which results in potentially extra users and thus increases the spectrum efficiency.

(i) ***Multiple-beam antenna array at the base station:*** By first using a base-station array in receive mode to locate the positions of mobiles in a cell and then transmitting in a multiplexed manner toward different clusters of mobiles one at a time, using the same channel, the spectral efficiency increases many times over and depends upon the number of elements in the array and the amount of scattering in the vicinity of the array. By pointing beams with directed nulls towards other mobiles in a cell, the array is used more efficiently than by reducing the cell size and the reuse distance. The use of a multiple-beam antenna array at the base-station to improve spectral efficiency by resolving the angular distribution of mobiles is discussed in [3], where it is shown that spectral efficiency increases as the number of beams increases. Formulas, which are helpful in predicting interference reduction and capacity increase provided by a switched-beam antenna system employed by a base station, also predict

that the number of subscribers in a cell increases as the number of beam increases [19].

(ii) ***Antenna array at a CDMA base station:*** By using an array of antennas for a CDMA system, the number of mobiles a cell may be able to sustain increases many fold (on the order of the number of elements) for a given outage probability and bit error rate (BER) ([15], [20], [21]). For example, at an outage probability of 0.01, the system capacity increases from 31 for a single antenna system to 115 for a five-element array. Using an array of seven elements increases the capacity to 155 [21]. The study reported in [15] is for both mobile-to-base and base-to-mobile links and derives expressions for the outage probability considering the effects of cochannel interferences

(d) BER improvement: A consequence of a reduction in cochannel interference and multipath fading by using an array in a mobile communications system to improve the communications quality is a reduction in BER and symbol error rate (SER) for a given signal-to-noise ratio (SNR), or a reduction in required SNR for a given BER.

(e) Reduction in outage probability: Outage probability is the probability of a channel being inoperative due to increased error rate in the received data. It may be caused by cochannel interference in a mobile communications system. Using an array helps to reduce outage probability by decreasing cochannel interference. It decreases as the number of beams used by a base station increases.

(f) Increase in transmission efficiency: Electronically steerable antennas are directive compared to fixed omnidirectional antennas, that is, they have high gains in the directions where the beam is pointing. This fact may be useful in extending the range of a base station resulting in a bigger cell size, or it may be used to reduce the transmitted power of the mobiles. By using a highly directive antenna, the base station may be able to pick a weaker signal within the cell than by using an omnidirectional antenna. This in turn means that the mobile has to transmit less power and its battery will last longer, or it would use a smaller battery, resulting in a smaller size and weight. This is important for hand-held mobiles.

It is also advantageous to use an antenna array at the base station in transmit mode. In a single antenna system, all the power of the base station is transmitted by one antenna. However, when the base station uses an array of antennas and transmits the same amount of power as that of the single antenna system, the power transmitted by each antenna of the array is much lower compared to the case where the total power is transmitted by one antenna. Furthermore, for a given SNR at the mobile site, the base station using an array has to transmit less power compared to the single omnidirectional antenna due to the directive nature of the array. This further reduces the power transmitted by each antenna. These reductions in transmitted power level using an array allow the use of electronic components of lower power rating in the transmitting circuitry. This results in lower system cost, leading to a more efficient transmission system.

(g) **Dynamic channel assignment:** In mobile communications, channels are generally assigned in a fixed manner depending upon the position of a mobile and the available channels in the cell where the mobile is positioned. As the mobile crosses the cell boundary, a new channel is assigned. In this arrangement, the number of channels in a cell are normally fixed. The use of an array provides an opportunity to change the cell boundary and thus to allocate the number of channels in each cell as the demand changes due to changed traffic situations. This provides the means whereby a mobile or group of mobiles may be tracked as it moves and the cell boundary may be adjusted to suit this group.

Dynamic channel assignment is also possible in a fixed cell boundary system and may be able to reduce the frequency reuse factor up to a point where frequency reuse in each cell might be possible. There may be situations when it is not possible to reduce cochannel interferences in certain channels, and the call may be dropped due to high BER caused by strong interferences. Such a situation may arise when a desired mobile is close to the cell boundary and the cochannel mobiles are near the desired mobile's base-station. This could be avoided by dynamic channel assignment, where the channel of a user is changed when the interference is above a certain level.

(h) **Reduction in handoff rate:** When the number of mobiles in a cell exceeds its capacity, cell capacity is used to create new cells, each with its own base-station and new frequency assignment. A consequence of this is an increased handoff due to reduced cell size. This may be reduced using an array of antennas. Instead of cell splitting, the capacity is increased by creating independent beams using more antennas. Each beam is adapted or adjusted as the mobile locations change. The beam follows a cluster of mobiles or a single mobile, as the case may be, and no handoff is necessary as long as the mobiles served by different beams using the same frequency do not cross each other.

(i) **Reduction in cross talk:** Cross talk may be caused by unknown propagation conditions when an array is transmitting multiple cochannel signals to various receivers. Adaptive transmitters based upon the feedback obtained from probing the mobiles could help eliminate this problem. The mechanism works by transmitting a probing signal periodically. The received feedback from mobiles is used to identify the propagation conditions, and this information is then incorporated into the beamforming mechanism.

2.4 Demonstration of beamscanning using linear arrays

2.4.1 The linear array

Appendix A.1 shows and describes the three dimensional coordinate system used in this section to analyze the array response as a result of beamscanning. The mathematical models developed here may be found in one form or another in many texts on array theory, see for example [12], [13] and [54].

Consider a N element linear array of isotropic point sources placed along the z-axis as shown in figure (2.7). The elements are spaced a distance d apart from one another. Assume that all elements have identical amplitudes but each succeeding element has a β progressive phase lead current excitation relative to the preceding one (β represents the phase by which the current in each element leads the current of the preceding element). An array of identical elements all of identical magnitude and each with a progressive phase is referred to as a uniform array. Although isotropic elements are not realizable in practice, they are a useful concept in array theory, especially for the

computation of radiation patterns. The effect of practical elements with nonisotropic elements will be considered in section (2.4.1.1).

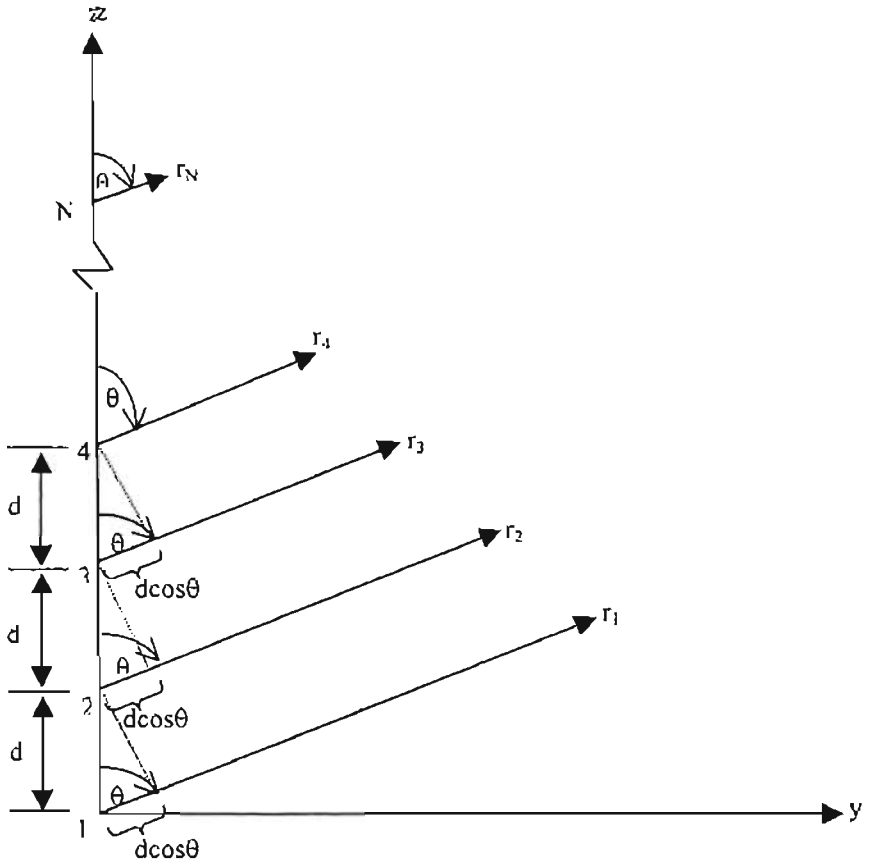

Fig. 2.7: Far-field geometry of N element array of isotropic point sources positioned along the z-axis

The time delay of a signal between two successive elements is given by:

$$\tau = \frac{d\cos\theta}{c} \tag{2.1}$$

where c is the free-space signal propagation velocity.

This time delay corresponds to a phase shift of

$$\begin{aligned} \psi &= \omega\tau + \beta \\ &= 2\pi f \frac{d\cos\theta}{c} + \beta \\ &= \frac{2\pi}{\lambda} d\cos\theta + \beta \\ &= kd\cos\theta + \beta \end{aligned} \tag{2.2}$$

where f is the frequency and $k = \frac{2\pi}{\lambda}$ is the wave number.

The array factor (AF) is now introduced. It is basically a mathematical concept that is a function of the time delay (or phase shift) between the array elements. For a uniform array, the array factor is given by

$$AF = 1 + e^{+j(kd\cos\theta+\beta)} + e^{+j2(kd\cos\theta+\beta)} + ... + e^{+j(N-1)(kd\cos\theta+\beta)}$$
$$= \sum_{n=1}^{N} e^{+j(n-1)(kd\cos\theta+\beta)} \qquad (2.3)$$

which can be written as

$$\boxed{AF = \sum_{n=1}^{N} e^{+j(n-1)\psi} \quad where\ \psi = kd\cos\theta + \beta} \qquad (2.4)$$

Since the total array factor for the uniform array is a summation of exponentials, it can be represented by the vector sum of N phasors each of unit amplitude and progressive phase ψ relative to the previous one. Graphically this is illustrated by the phasor diagram in figure (2.8).

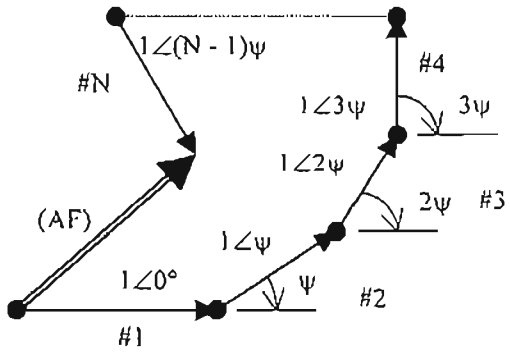

Fig. 2.8: Phasor diagram of N element linear array

It is apparent from the phasor diagram that the amplitude and phase of the AF can be controlled in uniform arrays by properly selecting the relative phase ψ between the elements.

The array factor of equation (2.4) can also be expressed in an alternate, compact and closed form whose functions and their distribution are more recognizable. This is accomplished as follows:

Multiplying both sides of equation (2.4) by $e^{j\psi}$ it can be written as

$$(AF)e^{j\psi} = e^{j\psi} + e^{j2\psi} + e^{j3\psi} + ... + e^{j(N-1)\psi} + e^{jN\psi} \qquad (2.5)$$

Subtracting equation (2.4) from equation (2.5) reduces to

$$AF(e^{j\psi} - 1) = (-1 + e^{jN\psi}) \qquad (2.6)$$

which can also be written as

$$AF = \left[\frac{e^{jN\psi} - 1}{e^{j\psi} - 1}\right] = e^{j[(N-1)/2]\psi}\left[\frac{e^{j(N/2)\psi} - e^{-j(N/2)\psi}}{e^{j(1/2)\psi} - e^{-j(1/2)\psi}}\right] = e^{j[(N-1)/2]\psi}\left[\frac{\sin(\frac{N}{2}\psi)}{\sin(\frac{1}{2}\psi)}\right] \quad (2.7)$$

If the reference point is the physical centre of the array, the array factor of equation (2.7) reduces to

$$AF = \left[\frac{\sin(\frac{N}{2}\psi)}{\sin(\frac{1}{2}\psi)}\right] \quad (2.8)$$

The maximum of equation (2.8) occurs when $\psi=0$ but the array factor (AF) is indeterminate since both the numerator and denominator are zero. However, by applying L'Hopital's rule (differentiating numerator and denominator separately) and setting $\psi=0$ results in equation (2.8) having a maximum value of N. To normalize the array factors so that the maximum value of each is unity, equation (2.8) is written in the normalized form as

$$(AF)_n = \frac{1}{N}\left[\frac{\sin(\frac{N}{2}\psi)}{\sin(\frac{1}{2}\psi)}\right] \quad (2.9)$$

$$where\ \psi = kd\cos\theta + \beta$$

2.4.1.1 Principle of pattern multiplication

The reasons for using isotropic elements for computation of the array factor becomes apparent in the ensuing discussion. The array factor is a function of the geometry of the array and the excitation phase. By varying the separation d and and/or the phase β between the elements, the characteristics of the array factor and of the total field of the array can be controlled. The far-zone field of a uniform array of identical elements is equal to the *product of the field of a single element, at a selected reference point (usually the origin), and the array factor of that array* [11]. That is

$$E(total) = [E(single\ element\ at\ reference\ point)] \times [array\ factor] \quad (2.10)$$
$$E_T = E_e E_a$$

This is referred to as *pattern multiplication* for arrays of identical elements. Each array has its own array factor. The array factor, in general, is a function of the number

of elements, their geometrical arrangement, their relative magnitudes, their relative phases, and their spacing. Since the array factor does not depend on the directional characteristics of the radiating elements themselves, it can be formulated by replacing the actual elements with isotropic (point sources). Once the array factor has been derived using the point source array, the total field of the actual array is obtained by use of equation (2.10). Each point source is assumed to have the amplitude, phase and location of the corresponding element it is replacing. Squaring both sides of equation (2.10) converts it into a relationship of power density-patterns (radiation patterns) in which the squares of the electric-intensity factors may be replaced by corresponding power-density pattern factors i.e. $P_T = P_e P_a$.

In using the principle of pattern multiplication, certain rules must be observed [25]:

(a) The pattern to be used for the array elements is the pattern that a single element would have if it were isolated, that is, not in the "array environment".

(b) The array pattern to be used is the one calculated for isotropic point-source elements spaced and phased the same as the actual elements. The phasing cannot be calculated on the basis of a transmission-line feed system designed for the input impedances of the elements operating as isolated elements. Their actual input impedances will be affected by mutual coupling with other elements.

(c) All the array elements must be alike; they must have similar patterns, similarly orientated. For example, if the elements are dipoles, they must have their axes parallel to one another. If the elements are horns, they must be of the same form and size, and all "aimed" in the same direction.

Equation (2.10) is only an approximation for many problems of array design. It ignores mutual coupling (section (2.5)) and it does not take account of the scattering or diffraction of radiation by the adjacent array elements. These effects cause the element pattern to be different when located within the array in the presence of the other elements than when isolated in free space. In order to obtain an exact computation of the array radiation pattern, the presence of each element must be measured in the presence of all the others. The array pattern may be found by summing the contributions of each element, taking into account the proper amplitude and phase.

2.4.1.2 Phased (scanning) array

In many applications it is desired to orientate/steer the maximum radiation in a particular direction to form a scanning array. Assume that the maximum radiation of the array is required to be oriented at an angle θ_o ($0^o \leq \theta_o \leq 180^o$). Referring to equation (2.9), the maximum of the array factor occurs when $\Psi=0$,

$$\begin{aligned} &\psi = kd\cos\theta + \beta\big|_{\theta=\theta_o} = 0 \\ &\Rightarrow \beta = -kd\cos\theta_o \end{aligned} \tag{2.11}$$

The array factor of equation (2.9) now becomes

$$(AF)_n = \frac{\sin\left[\frac{N\pi d}{\lambda}(\cos\theta - \cos\theta_o)\right]}{N\sin\left[\frac{\pi d}{\lambda}(\cos\theta - \cos\theta_o)\right]} \tag{2.12}$$

Two arrays that are of interest are the broadside and the endfire arrays. In the broadside array, the maximum radiation is directed normal to the axis of the array ($\theta = 90^o$ in figure (2.7)). Substituting $\theta_o = 90^o$ into equation (2.11) yields $\beta = 0$. Thus for a broadside array, the elements have zero progressive phase lead current excitation. However, it is necessary that all the elements have the same phase excitation (in addition to the same amplitude excitation). For an endfire array, the maximum radiation can be directed at either $\theta_o = 0^o$ or 180^o i.e. along the axis of the array. To direct the maximum toward $\theta_o = 0^o$, the progressive lead current excitation (β) should be $-kd$ while if the maximum is desired towards $\theta_o = 180^o$, then $\beta = kd$.

2.4.1.3 Antenna element spacing to avoid grating lobes

One of the objectives in many designs is to avoid multiple maxima, in addition to the main maximum, which are referred to as grating lobes. A grating lobe is defined as a lobe, other than the main lobe, produced by an array antenna when the interelement spacing is sufficiently large to permit the in-phase addition of radiated fields in more than one direction. They are undesirable since, in addition to directing the main lobe in the desired direction, the array also directs grating lobes to undesired directions. Thus there is no maximization of power in the desired direction. Often it may be required to select the largest spacing between the elements but with no grating lobes.

Consider a broadside array ($\beta = 0$ and $\psi = kd\cos\theta = \frac{2\pi}{\lambda} d\cos\theta$). This value of ψ when substituted in equation (2.9) makes the array factor attain its maximum value when $\cos\theta = \frac{n\lambda}{d}$ for n = 1,2,3,... The maximum at $\cos\theta = 0$ defines the main beam. If the spacing between elements is a half-wavelength (d = 0.5λ), the first grating lobe (n = $\pm$1) does not appear in real space since $\cos\theta = 2$ which is undefined. Grating lobes appear at 0° and 180° when d = λ. For a nonscanning array this condition (d = λ) is usually satisfactory for the prevention of grating lobes. Practical antenna elements that are designed to maximize the radiation at θ = 90°, generally have negligible radiation in the directions θ = 0° and θ = 180° directions. To avoid any grating lobe in a nonscanning array, the largest spacing between the elements should be less than one wavelength ($d_{max} < \lambda$).

Using an argument similar to the nonscanning array described above, for a scanning array, grating lobes appear at an angle θ_g when the array factor of equation (2.12) attains its maximum value, or

$$\frac{\pi d}{\lambda}\left(\cos\theta_g - \cos\theta_o\right) = \pm n\pi$$
$$or \quad \frac{d}{\lambda} = \frac{\pm n}{\left|\cos\theta_g - \cos\theta_o\right|} \tag{2.13}$$

If a grating lobe is permitted to appear at θ_g = 0° when the main beam is steered to θ_o = 180°, it is found from equation (2.13) that d = λ/2. Thus the element spacing must not be larger than a half-wavelength if the beam is to be steered over a wide angle without having undesirable grating lobes. Therefore a criterion for determining the maximum element spacing for an array scanned to a given angle θ_o is to set the spacing so that the nearest greatest lobe is at the boundary of the visible region. Using equation (2.13) this leads to the condition

$$\frac{d}{\lambda} \le \frac{1}{\left|1 - \cos\theta_o\right|} \tag{2.14}$$

Therefore the common rule that half-wave spacing precludes grating lobes is not quite accurate, as part of the grating lobe may be visible for extreme scan angles.

Grating lobes can also be avoided by unequal spacing of the elements i.e. by making the array aperiodic [8]. In an aperiodic array, the element weights are made equal but all the design freedom is employed in the element locations. There is no restriction imposed on the element spacing. However, the elements are usually overspaced to avoid the effect of mutual coupling. This process of overspacing the array is known as thinning [8]. In addition to the hazard of grating lobes, which is avoided by unequal spacing of the elements, a thinned array introduces another problem. For an array of fixed length, the number of elements is reduced. While this lowers cost and mutual coupling, both highly desirable changes, the reduction in element numbers reduces the designer's control of the radiation pattern in the sidelobe region. This reduction in design control influences the level of the peak sidelobe, which is of major concern to the array designer. Since the number of degrees of freedom is reduced in direct proportion to the number of elements, deviations from the desired radiation pattern must be anticipated. The beamwidth and approximate shape of the main lobe are not severely altered by thinning (beamwidth is not affected since the length of the array is fixed). The dominant effect of thinning is observed in the sidelobes. [8] provides a detailed discussion on aperiodic arrays and thinning.

2.4.1.4 Simulation work

Appendix A.2 contains a MATLAB program for the analysis of linear arrays using the theory developed thus far. The program plots the array factor pattern (for elements placed along the z-axis) as a function of the number of elements, element spacing and scan angle. An extension is also made to illustrate the pattern multiplication rule (section 2.4.1.1) using the half-wavelength dipole antenna as the element. The concept of grating lobes is also illustrated.

2.5 Mutual coupling

Up until now, no discussion or definition of mutual coupling was given. The principal effects of mutual coupling are changing the effective/predicted element pattern and producing gain variations in scanning. Due to this detrimental effect on array performance, it needs to be considered during array design. A brief description of this phenomenon is thus warranted.

When two antennas are near each other, whether one and/or both are transmitting or receiving, some of the energy that is primarily intended for one ends up at the other. The amount depends primarily on the

(a) radiation characteristic of each element

(b) relative separation between them

(c) relative position/orientation of each element in the array

(d) feed of the array elements

(e) scan volume of the array

There are many different mechanisms that cause this interchange of energy. For example, even if both antennas are transmitting, some of the energy radiated from each will be received by the other because of the nonideal directional characteristics of practical antennas. Part of the incident energy on one or both antennas may be rescattered in different directions allowing them to behave as secondary transmitters. This interchange of energy is known as mutual coupling, and in many cases it complicates the analysis and design of an antenna.

In the theory developed thus far, it was implicitly assumed that each element in the array acts independently of all the others. This assumption is invalid in practice. Currents couple from one element to another by the parts illustrated in figure (2.9).

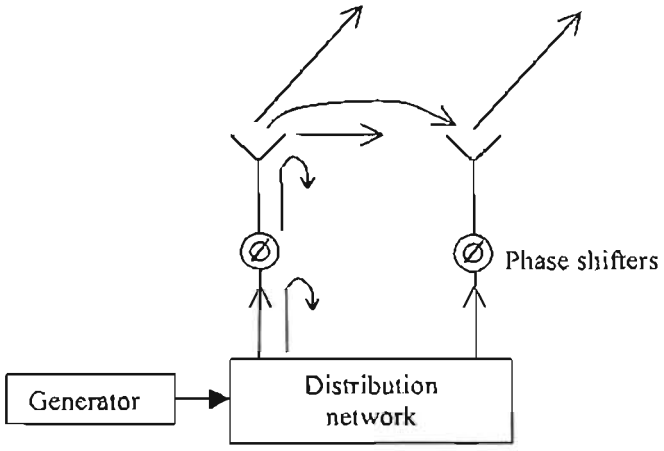

Fig. 2.9: Sources of coupled currents (from [8])

Two elements in a transmitting array are shown. Radiation from one element couples to its neighbours, as do currents that propagate along the surface of the array. In addition, current from the power-distribution network to the array element is partially reflected by mismatches, as shown in the figure. The reflected currents reach neighbouring elements through the distribution network. At each array element is the sum of the design value of the exciting current plus all the contributions from the various coupling sources from each of its neighbours.

The induced currents cause the input impedance and radiation resistance of an antenna to be different from the values that would be observed if the antenna were isolated. Therefore, the feed system of an array cannot be designed on the basis of isolated-antenna input impedance values, nor can the radiated power be calculated on the basis of isolated-antenna radiation resistance.

In using the principle of pattern multiplication (section (2.4.1.1)), it was assumed that the pattern used for array elements is the pattern that a single element would have if it were isolated, that is, not in the "array environment". This principle neglects the effect of mutual coupling. Another approach, discussed in [26], employs the effect of mutual coupling. In this case, the array pattern is obtained by superposing the fields of elements based on this pattern and by assuming a phasing that would occur if there were no mutual coupling. This pattern is found experimentally by connecting a receiver to only one element of the array, with all the other elements connected to terminating impedances of the value that would be effective if the array were operated

normally. This element pattern is measured physically. The currents induced in the single receiving element (as well as in the terminating elements) will be the same as in actual array operation, including mutual coupling effects. The pattern measured under these conditions is called "the element pattern in the array environment," and it is in general different from the pattern of an isolated element. In the practical design of arrays, the effects of mutual coupling are often evaluated experimentally, since theoretical calculation is quite difficult, although the theory is helpful in understanding the general nature of the effect.

Mutual coupling effects are greatest for closely spaced elements. It is also greater in an endfire array than in a broadside array. It can be reduced by overspacing the elements in the array (thinning). For an array of fixed length, thinning results in fewer elements, and hence, lower costs. These salutary effects, however are accompanied by grating lobes unless the array is made aperiodic (as discussed in section (2.4.1.3)) [8]. Thinning also reduces the designer's control of the radiation pattern in the sidelobe region.

CHAPTER 3

ANALOGUE AND DIGITAL BEAMFORMING

3.1 Introduction

The term beamforming relates to the function performed by a device or apparatus in which energy radiated by an antenna is focused along a specific direction in space. The objective is to preferentially receive or to transmit a signal from that direction. Energy from a source, which is assumed to be aligned with the antenna's preferred direction, arrives at the feed temporary aligned and is thereby summed coherently. In general, sources in other directions, arrive at the feed unaligned and add incoherently. For this reason, beamforming is often referred to as spatial filtering.

When an array is illuminated by a source, samples of the source's wavefront are recorded at the location of the antenna elements. The outputs from the antenna elements can be subjected to various forms of signal processing, wherein phase or amplitude adjustments are made to produce outputs that can provide concurrent angular information for signals arriving in several different directions in space. When the outputs of the elements are combined via some passive phasing network, the phasing will usually arrange for the outputs of all the elements to add coherently (in phase) for a given direction. The network that controls the phases and amplitudes of the excitation currents is usually called the beamforming network.

The weight and summing circuits of an adaptive antenna (figure (2.3) chapter 2) can operate at the antenna RF operating frequency, at a lower (downconverted) IF frequency or at baseband. At RF or IF, beamforming may be performed using analogue phase shifters and attenuators [27]. Alternatively, digital technology may be used at baseband. Digital technology may also be used at IF depending on the IF frequency. This chapter explores the implications, with respect to implementation, of adapting the antenna weights at RF, IF and baseband.

3.2 Analogue or digital beamforming?

Adaptive arrays may have either analogue or digital processing for the determination of the array element weight matrix. In the analogue case, all the received signals in the array are analogue, the usual operations performed by the analogue processor being frequency conversion, multiplication, correlation, integration, filtering, and so on. In an adaptive array with digital processing, all signals (analogue) received by the antenna are converted to digital form using analogue to digital converters (ADC) with the signal being processed subsequently only in this form. Sometimes, a digital to analogue converter (DAC) is used to provide an analogue output signal. It may be noted that chronologically, the first built were analogue systems [28], [29]. However, taking account of the impact of VLSI circuit development on this field, the situation is swiftly changing in favour of digital processors. The interest in digital implementation is further enhanced by its potential use in satellite communication systems where size, weight and power consumption become important design factors. Also technological advances in digital signal processing provide the possibility of developing a digital receiver. If such a receiver can be achieved, its performance may be superior in comparison to a conventional analog approach because of three major differences [30]:

(a) More information is maintained in the digital approach.

(b) The digitized data can be stored for long periods of time.

(c) More flexible signal processing methods are available to obtain the desired information directly from digitized signals.

3.3 Analogue beamforming

If beamforming is carried out at RF or IF, the analog beamforming network usually consists of devices that change the phase and power of the signals. Figure (3.1) gives an example of a RF beamformer that is designed only to form one beam.

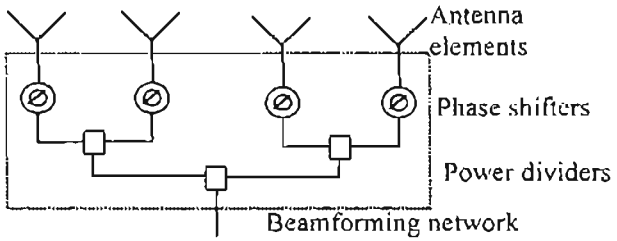

Fig. 3.1: An analog beamforming network (from [17])

It should be noted that an analog beamforming network consists of devices such as phase shifters and power dividers which are used to adjust the amplitude and phases of the antenna signals in such a way as to form a desired beam. It is sometimes desirable to form multiple beams that are offset by finite angles from each other. The design of a multiple-beam beamforming network is much more complicated than that of a single-beam beamforming network. A multiple-beam beamforming network is known as a beamforming matrix. The best example is given by the Butler matrix [31]. In a beamforming matrix, an array of hybrid junctions and fixed phase-shifters are used to achieve multiple beams.

3.3.1 Array feeds

If a single transmitter and receiver are utilized in an array, there must be some form of network to connect the single port of the transmitter and/or receiver to each of the antenna elements. The power divider used to connect the array elements to the single port is called an array feed. There are at least three basic concepts for feeding an array: the constrained feed, the optical space feed and the parallel plate feed ([32], [33], [34]). The constrained feed utilizes waveguide or other microwave transmission lines along with couplers, junctions or other power distribution devices. The optical space feed distributes the energy to a lens array in a manner analogous to a point-feed illuminating a lens or reflector antenna. The advantage of an optical beam-forming feed over the constrained feed is simplicity. Disadvantages are a lack of amplitude-tapering control and the excessive volume of physical space required to accommodate the feed system. The parallel plate feed uses the principles of microwave structures to

provide efficient power division. It is in some respects, a cross between the constrained feed and the optical space feed. The constrained feed is the commonest type of feed system and therefore warrants a further discussion. [33] and [34] provide a detailed description on the other two feed systems.

3.3.1.1 The constrained feed

The various types of constrained feeds can be classified into two groups: the series feed and the parallel feed. A description of the various types of feeds in each group follows.

(a) Series feed

In the series-fed arrangement, the energy may be transmitted from one end of the line (figure 3.2(a)), or it maybe fed from the centre out to each end (figure 3.2(b)).

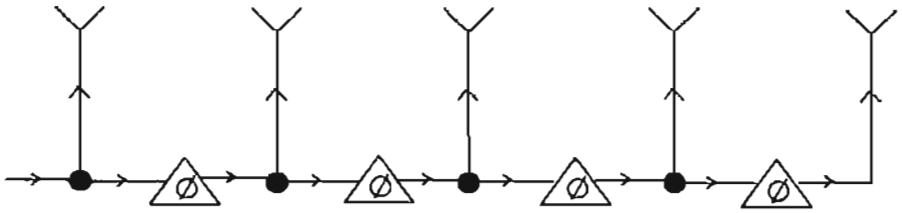

Fig. 3.2(a): End-fed series feed with series phase shifters

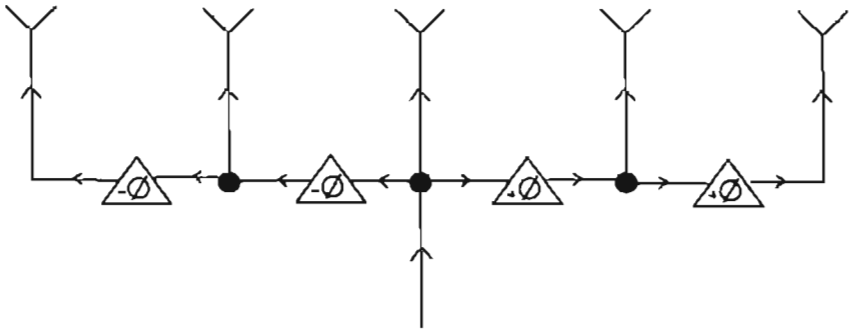

Fig. 3.2(b): Centre-fed series feed with series phase shifters

The elements are arranged serially along the main line. They consist of a main transmission line from which energy is tapped (in the case of transmission) through loosely coupled junctions to feed the radiating elements. The path length to each radiating element must be computed as a function of frequency and taken into account when setting the phase shifter. The adjacent elements are connected by a phase shifter with phase shift ϕ. All the phase shifters are identical and introduce the same amount of phase shift, which is less than 2π radians. To steer the beam, phase shifters

are added either in the main line, as shown in figure (3.2), or in the branch lines as shown in figure (3.3).

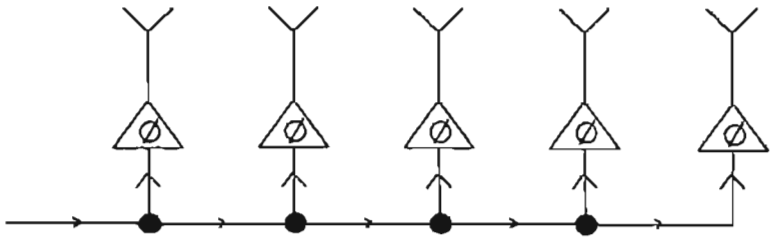

Fig. 3.3(a): End-fed series feed with parallel phase shifters

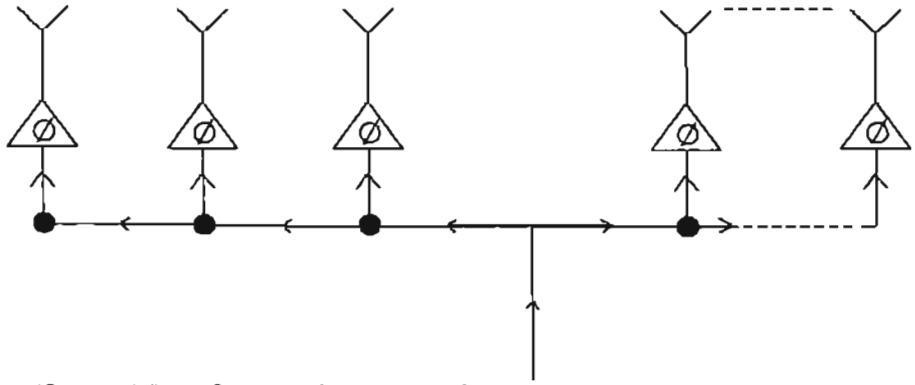

Fig. 3.3(b): Centre-fed series feed with parallel phase shifters

The end-fed series feed utilizing series phase shifters (figure 3.2(a)) and parallel phase shifters (figure 3.3(a)) provide mechanical simplicity – a great advantage over other feed configurations. They are easy to assemble and to construct. The configurations are easily adapted to construction in waveguides, using cross-guide directional couplers as junctions. They are potentially capable of handling full-waveguide power at the input (within the limitation of the phase shifters). However, they suffer losses associated with the corresponding length of waveguide plus that of the phase shifters. The most severe limitation of the end-fed series feed is its dependence of pointing angle on frequency. Thus it will be more limited in bandwidth than most array feed. The centre-fed series feed of figures (3.2(b)) and (3.3(b)) do not have this problem. Alternatively a parallel feed could be used.

The end-fed series feed with parallel phase shifter configuration places lower power handling demands on the phase shifters and also results in a lower system loss for a given phase shifter loss. On the otherhand, the end-fed series feed utilizing series phase shifters has an advantage in that all phase shifters will have identical phase shifts for a given pointing angle – a property which results in simplified array control.

However, the total system loss of the end-fed series feed with series phase shifters is higher than that utilizing parallel phase shifters. The bandwidth of a series feed can be increased by making the path lengths from the input to each output of the branch lines all equal as shown in figure (3.4).

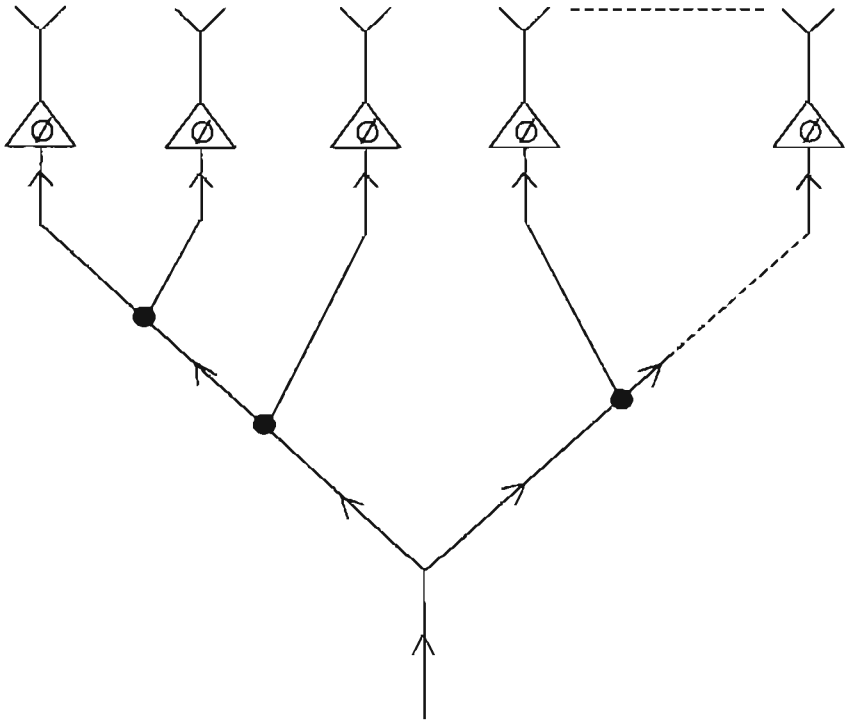

Fig. 3.4: Equal-path-length series feed

However, if the bandwidth is already limited by the phase shifters and the couplers, very little benefit can be derived from this approach at the cost of a considerable increase in size and weight. The network of figure (3.4) simplifies the beam-steering computation since the correction for path-length differences is no longer necessary.

(a) Parallel feeds

The frequency dependence (change in beam-pointing angle with frequency) associated with series feeds can be reduced by the use of parallel feeds at a cost of a slightly more complex mechanical structure. The frequency dependence of the parallel-feed configuration depends mainly on the frequency characteristics of the phase shifters and the couplers at the junctions of the feed, if the line lengths from the transmitter (or receiver) to the radiators are all made equal. Thus, if variable time-delay phase shifters were used in place of the constant-phase type phase shifters at each radiating element, the beam pointing angle would be essentially independent of

frequency. The frequency dependence of a parallel feed using constant-phase-type phase shifters is discussed in section (3.3.3).

The most common technique for realizing parallel feeds is the corporate feed structure of figure (3.5).

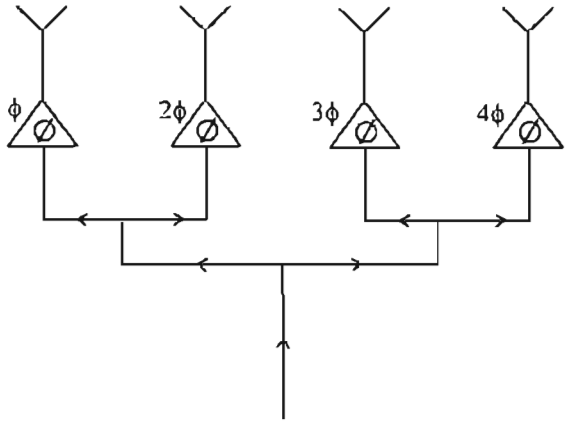

Fig. 3.5: Corporate feed

The energy to be radiated is divided between the elements by power splitters. Equal lengths of line transmits the energy to each element so that no unwanted phase differences are introduced by the lines themselves. If the lines are not of equal length, a compensation in the phase shift must be made. The proper phase change for beam steering is introduced by the phase shifters in each of the lines feeding the elements. When the phase of the first element is taken as the reference, the phase shifts required in the succeeding elements are ϕ, 2ϕ, 3ϕ,...., $(N-1)\phi$.

The maximum phase change required of each phase shifter in the parallel-fed array is many times 2π radians. Since phase shift is periodic with period 2π, it is possible in many applications to use a phase shifter with a maximum of 2π radians. However, if the pulse width is short compared with the antenna response time (if the signal bandwidth is large compared with the antenna bandwidth), the system response may be degraded. For example, if the energy were to arrive in a direction other than broadside, the entire array would not be excited simultaneously. The combined outputs from the parallel-fed elements will fail to coincide or overlap, and the received pulse will be smeared. This situation may be relieved by replacing the 2π modulo phase shifters with delay lines.

A similar phenomenon occurs in the series-fed array when the energy is radiated at or near the broadside direction. If a short pulse is applied at one end of a series-fed transmitting array, radiation of energy by the first element might be completed before the remainder of the energy reaches the last element. On reception, the effect is to smear or distort the pulse. It is possible to compensate for the delay in the series-fed array and avoid distortion of the main beam when the signal spectrum is wide by the insertion of individual delay lines of the proper length in series with the radiating elements.

In a series-fed array containing N phase shifters, the signal suffers the insertion loss of a single phase shifter N times. In a parallel-fed array, the insertion loss of the phase shifter is introduced effectively but once. Hence the phase shifter in a series-fed array must be of lower loss compared with that in a parallel-fed array. If the series phase shifters are too lossy, amplifiers can be inserted in each element to compensate for the signal attenuation.

Since each phase shifter in the end-fed series feed (with series phase shifters) has the same value of phase shift, only a single control signal is needed to steer the beam. The N-element parallel-fed linear array similar to that of figure (3.5) requires a separate control for each phase shifter or N-1 total (one phase shifter is always zero). A two-dimensional parallel-fed array of MN elements requires M+N-2 separate control signals. The two-dimensional series-fed array requires but two control signals.

3.3.2 Phase shifters for arrays

Phase shifters are crucial to analog beamforming to adjust the phases of the antenna signals in such a way as to form a desired beam. The difference in phase ϕ experienced by an electromagnetic wave of frequency f propagating with a velocity v through a transmission line of length l is

$$\phi = \frac{2\pi f l}{v} \tag{3.1}$$

The velocity v of an electromagnetic wave is a function of the permeability μ and the dielectric constant ε of the medium in which it propagates. Therefore a change in

phase can be obtained by a change in frequency, length of line, velocity of propagation, permeability or dielectric constant.

Phase shifting devices can either be reciprocal or nonreciprocal. In the reciprocal device, the phase change does not depend on the direction of propagation. On the otherhand, a nonreciprocal phase shifter must have different control settings for reception and transmission.

3.3.2.1 Selection criteria

There are currently two types of electronic phase shifters suitable for practical arrays: the ferrite phase shifter and the semiconductor-diode phase shifter (discussed in sections (3.3.2.2) and (3.3.2.3)). Selection of the type of phase shifter depends strongly on the operating frequency and the RF power per phase shifter. Above S band (2 to 4GHz), waveguide ferrite phase shifters have less loss than diode phase shifters. In situations in which RF powers are low and size and weight constraints dictate a miniaturized design, diode phase shifters are preferred. Other factors that have a bearing on the selection are listed below:

(a) *Insertion loss*: Insertion loss should be as low as possible. It results in a reduction of generated power on transmit and of low signal-to-noise ratio on receive. It also produces phase-shifter-heating problems.

(b) *Switching times*: The time to switch should be as short as possible. Times on the order of microseconds are adequate for most applications.

(c) *Drive power*: Drive power should be as small as possible. A large amount of drive power generates heat and also may require power supplies that are too large for a mobile system. Large drive power may also require expensive driver-circuit components. Diode phase shifters require holding power as well as switching power. Ferrite phase shifters can be latched i.e. they do not consume drive power except when switching.

(d) *Phase error*: Phase error should be as small as possible. It should not reduce antenna gain substantially or raise sidelobes in the radiation pattern. One cause of phase error is the size (in degrees) of the least significant bit of a digital phase shifter. Other phase errors are due to manufacturing tolerances in the phase shifter and driver.

(e) *Transmitted power*: The required power per phase shifter depends upon the maximum range and the data rate of the system design.

(f) *Physical size*: The phase shifter should fit within a $\lambda/2$ by $\lambda/2$ cross section so that it can be packaged behind each element, otherwise an expensive fan-out feed is required.

(g) *Weight*: Phase shifter weight should be minimized in mobile and especially in airborne or spacecraft, installations.

(h) *Cost and manufacturing ease*: For arrays with thousands of elements, the unit cost must be low. Manufacturing tolerances must be as large as possible, consistent with allowable system phase and amplitude errors.

3.3.2.2 Ferrite phase shifters

Construction of ferrite phase shifters fall into two categories: those phase shifters enclosed by a waveguide structure and those built by using a microstrip configuration. While the construction of the microstrip ferrite phase shifter is extremely simple, the performance of the waveguide ferrite phase shifter is far superior, and is generally used for most applications.

Ferrite phase shifters use ferromagnetic materials that include families of both ferrites and garnets which are basically ceramic materials with magnetic properties. The change in the applied dc magnetic field of the ferrite produces a change in the propagation properties because of a change in the permeability, which results in a phase shift.

They may be analog or digital with either reciprocal or nonreciprocal characteristics. Several types of ferrite phase shifters have been developed, but those that have been of interest in applications are the toroidal, Reggia-Spencer and the faraday rotator phase shifters. Since these phase shifters are enclosed by waveguide structures, their manufacturing ease decreases, thus resulting in an increase in cost. Reference [33] and [34] provides extensive information on these ferrite phase shifters.

3.3.2.3 Diode phase shifters

The property of a semiconductor diode that is of interest in phase shifter design is that its impedance can be varied with a change in bias control voltage. This allows the diode to act as a switch. Phase shifters based on diode devices can be of relatively high power and low loss, and can be switched rapidly from one phase state to another. They are relatively insensitive to changes in temperature, they can operate with low control power, and are compact in size. They are well suited to microwave integrated circuit construction, and are capable of being used over the entire range of frequencies of interest. However, their losses are generally less and their power handling is generally higher at lower frequencies.

There are three basic methods for employing semiconductor diodes in digital phase shifters, depending on the circuit used to obtain the individual phase bit. These are: (a) the switched-line, (b) the hybrid-coupled and (c) the loaded line phase shifter.

(a) Switched-line phase shifter [33]

A change in phase can be obtained by utilizing one of a number of lengths of transmission lines to approximate the desired value of phase. The various lengths of line are inserted and removed by high-speed electronic switching.

There are at least two methods for switching lengths of transmission lines. These are the parallel-line configuration and the series-line or cascaded configuration. Due to the discrete nature of the digitally switched phase shifter, the exact value of required phase shift cannot be achieved without a quantization error. However, this error can be made as small as possible.

(i) Parallel-line configuration

Figure (3.6) illustrates the parallel-line configuration of the digitally switched phase shifter in which the desired length is obtained by means of a pair of one-by-N switches. Each of the boxes labelled S represents a single-pole single throw (SPST) switch.

The N ports of each one-by-N switch are connected to N lines of different lengths l_1, l_2, ..., l_N. The number of lines depends on the degree of phase quantization that can be tolerated. This number is limited by the quality of the switches, as measured by

the difference between their impedance in the "off" and "on" positions. With many switches in parallel, the "off" impedance of each must be high if the combined impedance is to be large compared to the "on" impedance of a single switch. A parallel line configuration with 16 lengths of line provides a phase quantization of 22.5° (±11.25°), assuming the nth line is of length nλ/16.

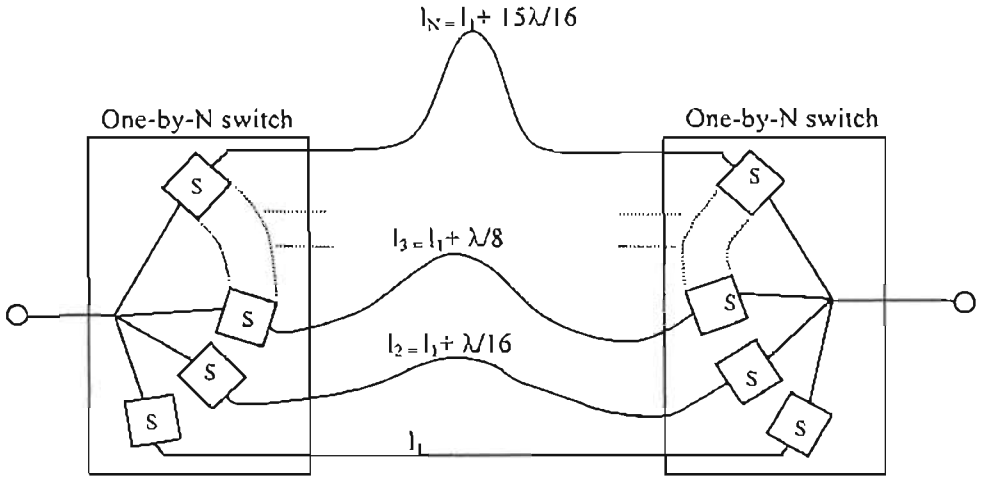

Fig. 3.6: Digitally switched parallel-line phase shifter with N switchable lines (from [33])

A suitable form of switch is the semiconductor diode. The diodes attached to the ends of the particular line selected are operated with forward bias to present a low impedance. The remaining diodes attached to the unwanted lines are operated with reverse-bias to present a high impedance. The switched lines can be any standard RF transmission line. An advantage of the parallel-line configuration is that the signal passes through only two switches and in principle, should therefore have lower insertion loss than the cascaded or series line digitally switched phase shifter described below. A disadvantage is the relatively large number of lines and switches required when it is necessary to minimize the quantization error. The parallel-line configuration has also been used when phase shifts greater than 2π radians are needed, as in broadband devices that require true time delays rather than phase shift which is limited to 2π radians.

(ii) Series-line (cascaded) configuration

The series-line (cascaded) digitally switched phase shifter (figure (3.7)) is more commonly used than the parallel line configuration. A cascaded digitally switched phase shifter with four phase bits capable of switching in or out lengths of line equal

to λ/16, λ/8, λ/4 and λ/2 yields a phase shift with a quantization of λ/16, similar to the parallel-line shifter with 16 lengths of line described above.

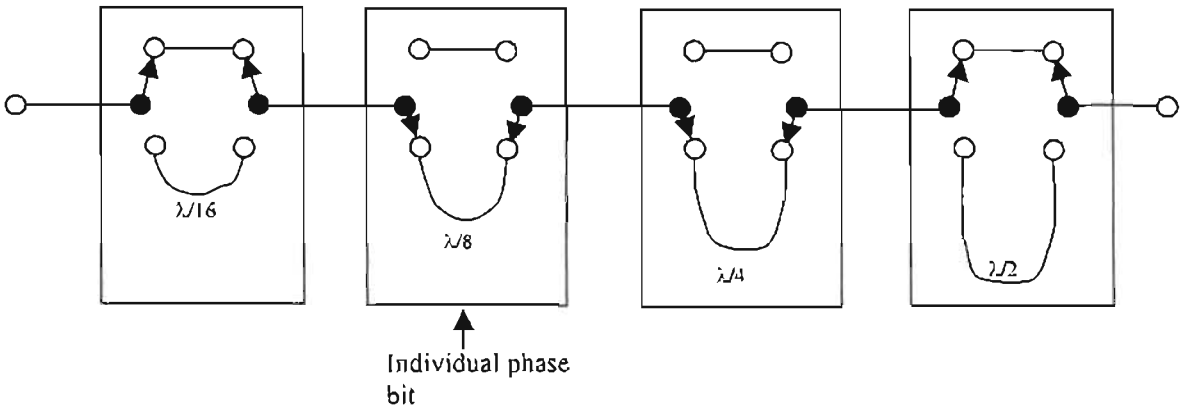

Fig. 3.7: Cascaded four-bit digitally switched phase shifter with λ/16 quantization. Arrangement shown gives 135^0 (3/8 wavelengths) phase shift

The binary quantization of line lengths make it convenient to apply digital techniques for actuating the phase shifter (figure (3.8)).

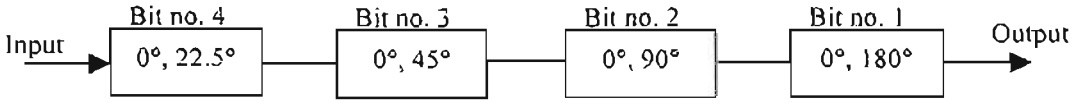

Fig. 3.8: Schematic of a 4-bit phase shifter with λ/16 quantization

Figure (3.7) shows a four-bit digital phase shifter consisting of four cascaded modules. Each module consists of two single-pole double throw (SPDT) switches and two line lengths for each bit. The minimum number of diodes per bit is four (16 diodes in total for a 4 bit phase shifter). It gives 16 steps in increments of 22.5°. The SPDT switch in each module inserts either "zero" phase change or a phase change of $360/2^n$ degrees, where n=1,2,3,4. When the upper two switches are open, the lower two are closed, and vice-versa. Note that in the "zero" phase state, the phase shift is generally not zero, but is some residual amount ϕ_o. Thus the two states provide a phase shift of ϕ_o and $\phi_o+\Delta\phi$. The difference $\Delta\phi$ between the two states is the desired phase shift required of the module.

(b) The hybrid coupled phase shifter (reflection phase shifter) [33], [35]

Each module used in the series-line (cascaded) phase shifter can be replaced by a 3dB hybrid junction. The hybrid-coupled phase bit, as shown in figure (3.9) uses a 3dB

hybrid junction with balanced reflecting terminations connected to the coupled arms. Alternatively, a circulator could be used if a nonreciprocal phase shifter is desired. Two switches (diodes) control the phase change.

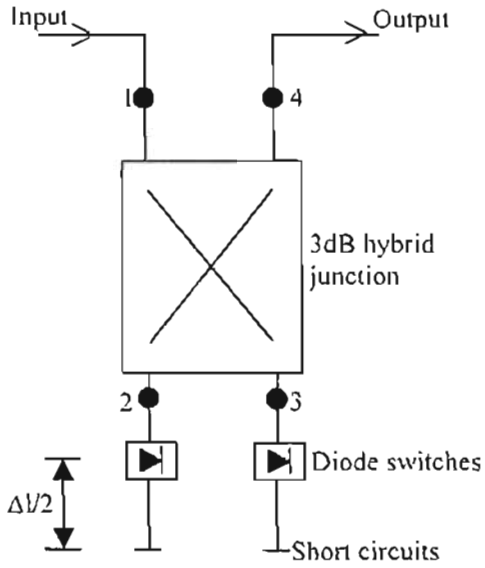

Fig. 3.9: Hybrid coupled phase bit (from [33])

The 3dB hybrid has the property that a signal input at port 1 is divided equally in power between ports 2 and 3. No energy appears at port 4. The diodes act to either pass or reflect the signals. When the impedance of the diode is such as to pass the signals, the signals will be reflected by the short circuits located farther down the transmission line. The signals at ports 2 and 3, after reflection from either the diode switches or the short circuits, combine at port 4. None of the reflected energy appears at port 1.

The difference in path length with the diode switches open and closed is Δl. The two-way path Δl is chosen to correspond to the desired increment of digitized phase shift. A N bit phase shifter can be obtained by cascading N such hybrids. Moderately wide bandwidths can be achieved with the hybrid coupled phase shifter.

(c) The loaded-line phase shifter [33], [35]

This phase shifter (figure (3.10)) consists of a transmission line periodically loaded with spaced, switched impedances or susceptances. Diodes are used to switch between the two states of susceptances. The spacing between diodes is approximately one-quarter wavelength at the operating frequency. Adjacent quarter-wavelength-spaced loading susceptances are equal and take either of two values.

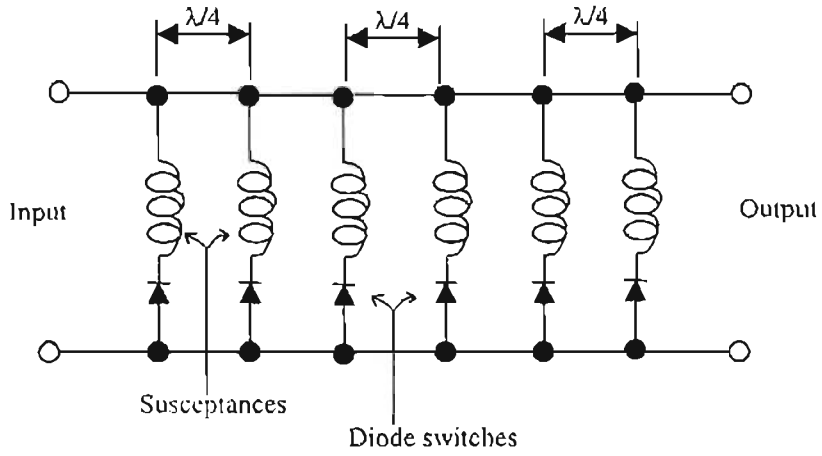

Fig. 3.10: Periodically loaded-line phase shifter (from [33])

If the magnitude of the normalized susceptance is small, the reflection from any pair of symmetrical susceptances can be made to cancel so that matched transmission will result for either of the two susceptance conditions. Each pair of diodes spaced a quarter-wavelength apart produces an increment of the desired phase. The number of pairs that are cascaded determines the value of the transmission phase shift. To achieve high-power capacity, many such sections with small phase increments can be used so that there are many diodes to share the power. The ability to operate with high power is the advantage of the loaded-line diode phase shifter. If the largest and practical phase shift per diode pair is $\lambda/16$ or 22.5°, 32 diodes are required to shift the phase 360°.

The hybrid coupled phase shifter generally has lower loss than the other two (loaded-line and switched-line phase shifters) and uses the least number of diodes. It can be made to operate over a wide band. The switched-line phase shifter uses more diodes than the other types and has an undesirable phase-frequency response which can be corrected at the expense of a higher insertion loss. This configuration is generally restricted to true time-delay circuits and to low-power, miniaturized phase shifters where loss is not a major consideration. For a four-bit phase shifter covering 360°, the minimum number of diodes needed in the periodically loaded-line is 32, the switched-line requires 16, and the hybrid-coupled circuit needs only 8. The theoretical peak power capability of the switched-line is twice that of the hybrid-coupled circuit since voltage doubling is produced by the reflection in the hybrid circuit. The switched-line phase shifter has the greatest insertion loss, but its loss

does not vary with the amount of phase shift as it does in the other two types of circuits.

3.3.3 Bandwidth of arrays

The bandwidth of an array antenna depends upon the types of components, such as radiators, phase shifters, and feed networks, comprising the array. The bandwidth is also affected by many factors, including change of element input impedance with frequency, change in array spacing in wavelengths that may allow grating lobes, change in element beamwidth, etc.

In practice, most radiators for phased arrays are matched over a broadband of frequencies. Therefore, the radiator design is not a primary factor in the determination of bandwidth. The more severe limitation in bandwidth are determined by the frequency characteristics of the phase shifters and feed networks. In general, the effects due to the phase shifters and feed networks are additive, so that if the phase shifter causes the beam to scan by an amount equal to $\Delta\theta_p$ and the feed causes it to scan by $\Delta\theta_f$, then the total beam scan is given by $\Delta\theta_p + \Delta\theta_f$.

3.3.3.1 Phase-shifter effects

To evaluate effects caused by the phase shifter alone, a corporate feed (equal-line-length parallel feed) is used to illuminate all the radiator elements (see figure (3.11)). The corporate parallel feed exhibits no feed effects since a signal at the input illuminates all the radiating elements with the same phase regardless of frequency. The bandwidth in this case is completely determined by the type of phase shifter used in the array. In this discussion, two basic types of phase shifters will be considered: (a) time delay phase shifters (b) constant phase-type phase shifters.

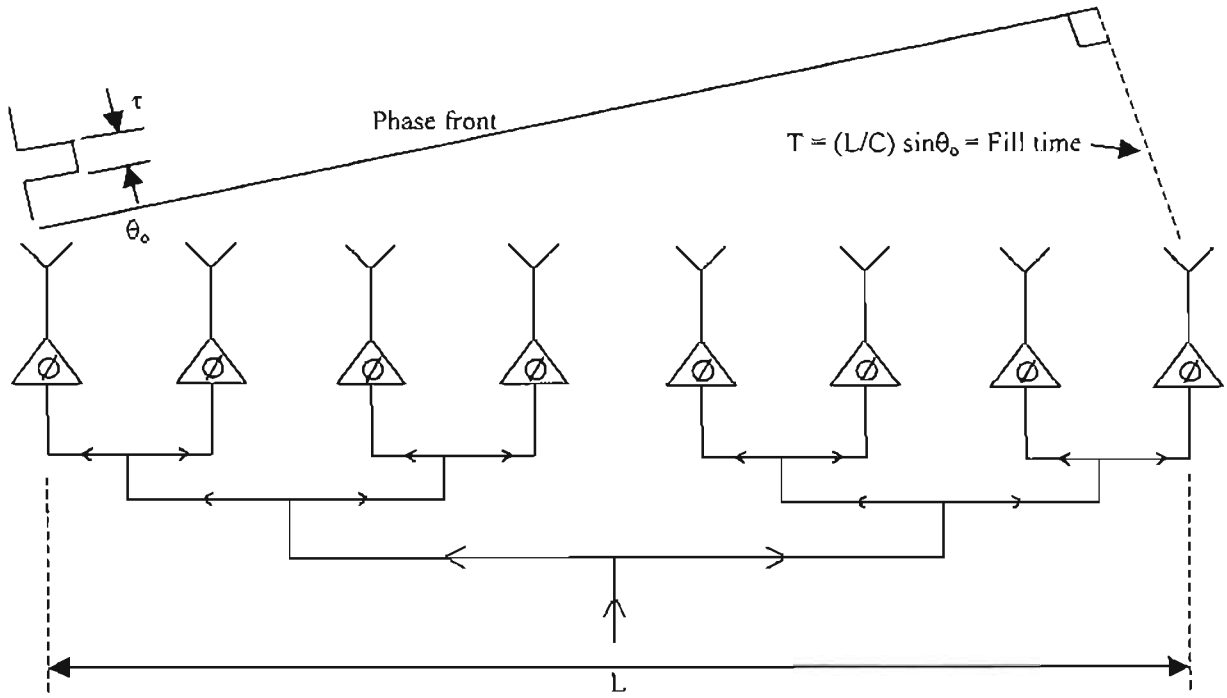

Fig. 3.11: Equal-line-length corporate (parallel) feed

(a) Time delay phase shifters

When time-delay phase shifters are used at each radiating element, the signals received by the elements from an incident wavefront at an angle θ_o are appropriately time delayed so that they all arrive at the output terminal. For example, the amount of time delay at the first element of the array shown in figure (3.11) is equal to the additional time required for the wavefront to travel to the last element after arriving at the first element. This time delay τ, known as the aperture fill time, is given by

$$T = \frac{L}{c}\sin\theta_o \tag{3.2}$$

where L = total length of the array aperture

c = velocity of propagation of the signal (in freespace this is equivalent to the speed of light)

θ_o = angle of incidence of wavefront from array normal

The phase distribution across the array aperture produced by the time-delayed feed matches that of the incident wavefront independently of frequency. Consequently, the beam position remains stationary with frequency change, and the array has infinite bandwidth. When the angle of incidence of the incoming wavefront changes, the amount of time delays at each element must be changed accordingly to maintain the bandwidth. This time-delayed feed network is commonly known as a time-delayed

beam-steering feed. The above discussion is valid for either a continuous wave (CW) or a pulsed incidence signal. For the pulsed incidence signal, the time-delayed feed preserves the shape of the pulse without any distortion.

(b) Constant phase-type phase shifter

When constant phase-type phase shifters (phase shifters whose phase shift is independent of carrier/centre frequency) are used at each element, the output phase distribution of the feed matches that of the incident phase front only at one frequency f_0 and for a particular incidence angle θ_0. At a different frequency f_1, the output phase distribution of the feed network remains fixed, hence the array is phased to receive at a difference incidence angle θ_1. The amount of beam squint with frequency is given by the following relationship:

$$f_1 \sin\theta_1 = f_0 \sin\theta_0$$
$$or \quad \sin\theta_1 = \frac{f_0}{f_1}\sin\theta_0 \tag{3.3}$$

Figure (3.12) shows this behavior.

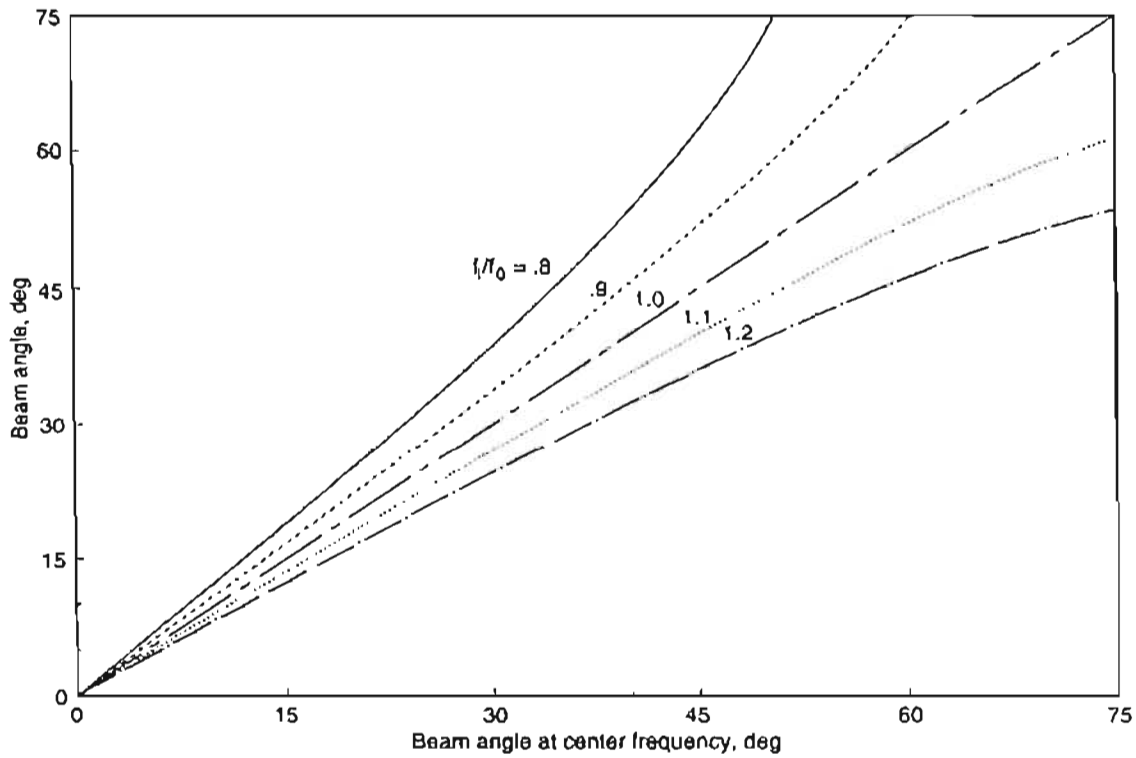

Fig. 3.12: Beam angle shift with frequency (from [32])

The beam peak angle is reduced for frequencies above the design frequency (f_o) and increased for frequencies below the design frequency. For a small change in frequency, equation (3.3) shows that the change in scan angle is given by

$$\Delta\theta_o = -\left(\frac{\Delta f}{f}\right)\tan\theta_o \tag{3.4}$$

The above expression shows the amount of beam squint depends upon the original scan angle as well as on percent frequency change. At broadside ($\theta_o = 0°$), there is no scanning regardless of the amount of change in frequency, and the array has infinite bandwidth. When the beam scans away from broadside, the amount of beam squint with frequency increases with scan angle. Therefore, the bandwidth of an array must be specified in terms of the desired maximum scan angle. For most practical applications, the desired maximum scan angle is ±60° from array broadside.

There is a direct relationship (equation (3.5)) between actual bandwidth and array size [22],

$$L\sin\theta_o = 0.886B_b(300)/\Delta f_M \tag{3.5}$$

where Δf_M is the bandwidth in megahertz

L is the array length in meters

B_b is the beam broadening factor – chosen as unity for the uniformly illuminated array

Equation (3.5) shows that the bandwidth becomes smaller as the array is made larger or as the scan angle is increased.

3.3.3.2 Feed effects

When a feed other than an equal-length parallel feed (corporate feed) is used, phase errors due to the feed alone are produced across the array aperture. An example is the end-fed series feed shown in figure (3.13).

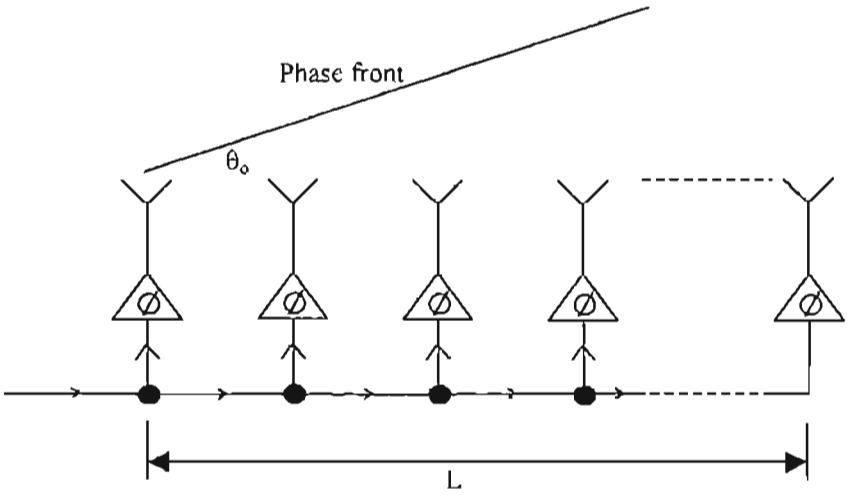

Fig. 3.13: End-fed series feed

The total phase shift across the length of the feed is $\Phi = \frac{2\pi}{\lambda} L$ radians with free-space propagation assumed. When the frequency is changed, the change in phase across the array aperture will be

$$\Delta\Phi = \frac{2\pi L}{c}\Delta f \tag{3.6}$$

This linear change in phase across the aperture scans the beam just as phase shifters would. To observe just how far the beam is scanned, it is essential to examine the way in which the aperture is scanned with phase. For a given scan angle θ_o, the required phase across the array is

$$\psi = \frac{2\pi L}{\lambda}\sin\theta_o \tag{3.7}$$

The required change in ψ for a change in scan angle is

$$\begin{aligned} \frac{\partial\psi}{\partial\theta_o} &= \frac{2\pi L}{\lambda}\cos\theta_o \\ or \quad \Delta\psi &= \frac{2\pi L}{\lambda}\cos\theta_o\Delta\theta_0 = \frac{2\pi Lf}{c}\cos\theta_o\Delta\theta_0 \end{aligned} \tag{3.8}$$

When the change in phase across the array is induced by the feed, $\Delta\psi = \Delta\Phi$ or

$$\frac{2\pi L}{c}\Delta f = \frac{2\pi Lf}{c}\cos\theta_o\Delta\theta_0 \tag{3.9}$$

Hence the amount of beam scan for a change in frequency is given by

$$\Delta\theta_o = \left(\frac{\Delta f}{f}\right)\frac{1}{\cos\theta_o} \tag{3.10}$$

For a 60° scan angle, the scanning caused by the feed alone is slightly greater than that caused by the aperture. Therefore, the bandwidth of the series feed is essentially half of that of the equal-line-length parallel feed (corporate feed).

3.4 Digital beamforming

Digital beamforming (DBF) for signal reception is conceptually simple. Each antenna element in the array is connected to a pre-amplifier (LNA) and then to an A/D converter, as shown in figure (3.14).

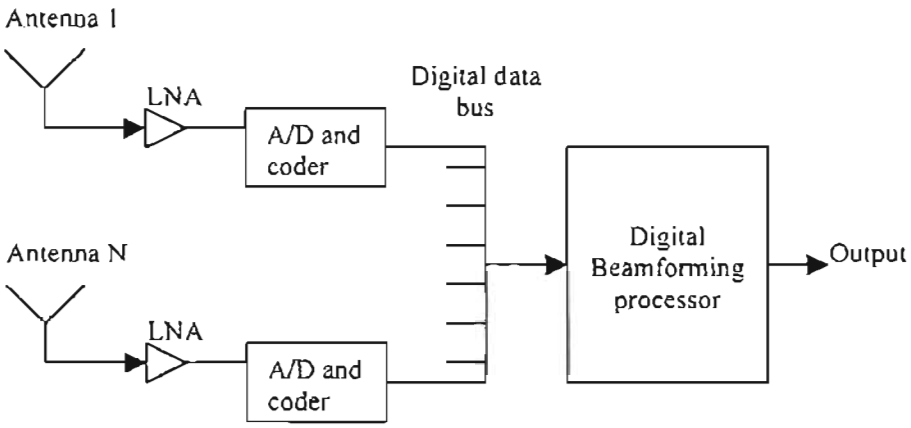

Fig. 3.14: Digital topology

The outputs of the A/Ds are connected to a digital data bus. A DBF processor can then manipulate this data to form any number of multiple beams, perform rapid beam scan, produce low-sidelobe beams and perform adaptive nulling.

Because the element combining algorithms can be formulated in true time delay form, there are no bandwidth limitations in the digital beamformer. The serious limitation is the bit-bandwidth product of the A/D. The sampling rates and resolutions (number of bits) provided by present-day (June 2000) A/D converters cover a wide rage of values. Invariably, a balance between these two parameters must be sought because it is difficult to achieve both a high sampling rate and a high resolution. In CDMA systems, 4 to 6 bit A/Ds have been noted to provide adequate performance [36]. At the present time, A/D hardware appears suitable only for low microwave frequencies and below. Table (3.1) lists the resolution and sampling rates of the state-of-the-art ADC technology ([37]-[43]).

DESIGNER	RESOLUTION (Bits)	SAMPLING RATE
F.G. Weiss [37]	8	1GHz
T. Ducourant et al. [38]	4	3GHz
Crystal Semiconductor [39]	20	256kHz
Phillips research lab [40]	8	650MHz
H. Kimura [41]	10	300MHz
A.N. Karanicolas [42]	15	1MHz
HP Co. [43]	8	4GHz
Signal Processing Tech.	12	30MHz

Table 3.1: Performance of state-of-the-art ADCs reported in [37]-[43]

These ADCs were cited as state-of-the-art in [17] as at 1996. It should be pointed out that very few of the converters are commercially available. As pointed out in [44], commercially available ADCs are the result of market demand rather than technology enhancement. Currently, commercially available products range from 8bit, 80MHz to 10 bit, 200MHz, by Texas Instruments and Analog Devices, respectively. Advances in superconducting ADCs are promising, but commercial realization of this hardware is years away.

The processor used in an all-digital beamforming array has two speed regimes: the handling of digitized RF requires coherent beam formation at the A/D converter upper frequency, while the calculation and change of amplitude and phase tapers for sidelobe control, etc., can proceed at a much slower rate. That is, the RF data handling requires a very fast processor while for the array control functions a much slower processor will suffice. Beam-formation and tracking of mobiles depends on the speed of the mobiles. The mobiles need to tracked by beams when moving from one cell to another. It is intuitive from the contrast in speed of the mobile and digitized RF data, that a much slower processor be required for array control functions than that for RF data handling. Some array functions such as adaptive nulling, may require a specialized and/or separate processor for such tasks as matrix inversion, singular value decomposition, etc. All of the digital hardware and software is available, only the A/D capability is awaited.

The above digital topology describes a straight-forward approach that digitizes the input signal directly and processes the digitized data to extract the needed information. Clearly, an all-digital adaptive array is currently impractical given the usually high operating frequencies that are part of real communication systems.

One compromise is to down-convert the microwave/RF input signals to IF. The digitizing is then performed on the IF signals. The main component of the down-conversion process is the multiplication device or mixer which would probably remain analog for a long time to come. It should also be noted, even if the incoming signal is down-converted in frequency, its allocated bandwidth could be too wide to be handled digitally.

The performance of a digital beamforming (DBF) receiving array is, to a large extent, determined by the capabilities of the receivers that are used at the antenna elements. The receivers perform the functions of frequency conversion, filtering, and amplification of the signal to a power level that is commensurate with the input requirements of the A/D converters or with the output power requirements. Since the elemental receivers are a significant factor in determining the cost of a DBF antenna, it is important when designing receivers to adopt an architecture that leads to receivers that are low in cost and yet meet performance requirements.

3.4.1 Receivers for digital beamforming

3.4.1.1 Single-channel receiver

A basic down-conversion receiver scheme is shown in figure (3.15).

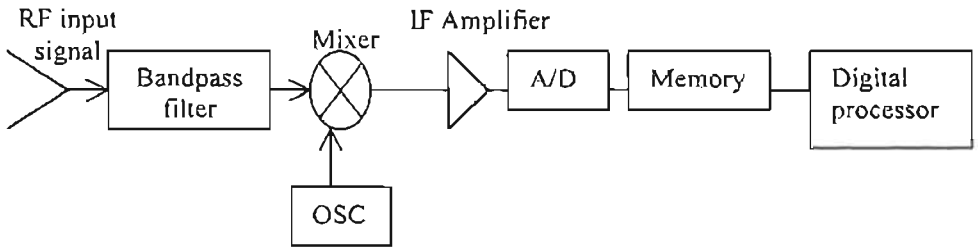

Fig. 3.15: A basic single-channel receiver

A filter is used at the input for image suppression. Following the filter is a mixer that converts the input signals into an IF. An IF amplifier is used to amplify the input signals to a proper level to be digitized by the A/D converter. After the A/D converter a digital memory unit is used to store the information for further processing. The memory unit and digital processor may be combined in a single unit.

To fulfil the Nyquist criterion, the A/D converter must operate at more than twice the frequency of the upper IF range (the IF amplifier has a bandwidth from DC to its

upper frequency limit. If the low-pass cut-off frequency of the IF amplifier is infinitely sharp, the sampling rate can be at the Nyquist criterion. However, this cut-off frequency response has some finite slope, thus, the sampling rate must be higher than the Nyquist rate (approximately 2.5 to 3 times the input bandwidth). Two undesirable aspects should be considered for this down-conversion approach [30]: spurious output and image problems. A frequency mixer used to down-convert an input signal to a proper IF range is usually considered as a linear device, but strictly speaking, it is a non-linear device. The spurious output or harmonics are filtered out by the low-pass filtering effect of the IF amplifier at the output of the mixer. The image frequencies entering the IF passband can be filtered out with a RF bandpass filter at the input to limit the input bandwidth.

3.4.1.2 Two-channel receiver

Another approach to building a digital receiver extends the basic down-conversion idea to a two-channel approach: an in-phased channel-I; and 90° out-of-phased channel-Q [30]. The basic structure of this receiver is shown in figure (3.16).

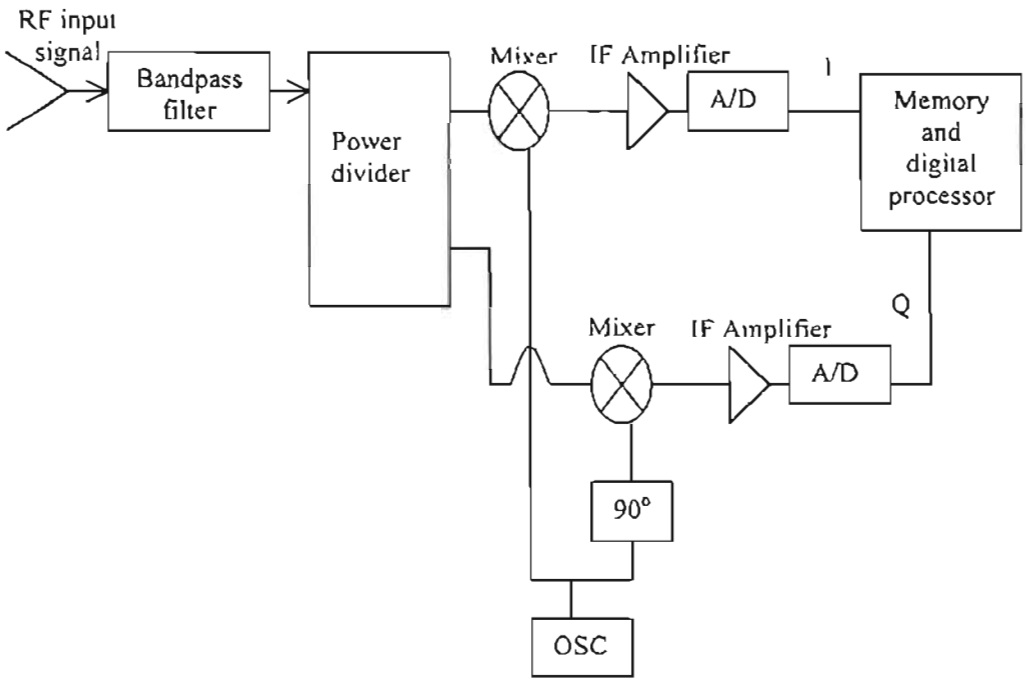

Fig. 3.16: A two channel digital receiver: in-phase input and out-of-phase local oscillator (from [30])

The input signals pass through a bandpass filter and an in-phase power divider that divides the input into two parallel channels. Two mixers are used to down-convert the input signals into two IF channels. The two mixers are fed by one local oscillator.

The local oscillator is fed directly to the I channel mixer but through a 90° hybrid to the Q channel. Therefore, the two local oscillator frequencies are the same but 90° out of phase with each other. Following each mixer is an IF amplifier, an A/D converter and the processing unit. One digital processor can process the data from both the I and Q channels for all antenna inputs.

Theoretically, a two-channel digital receiver can be accomplished through a slightly different arrangement: replacing the in-phase power divider in front of the receiver by a 90° hybrid and keeping the local oscillators in phase, as shown in figure (3.17).

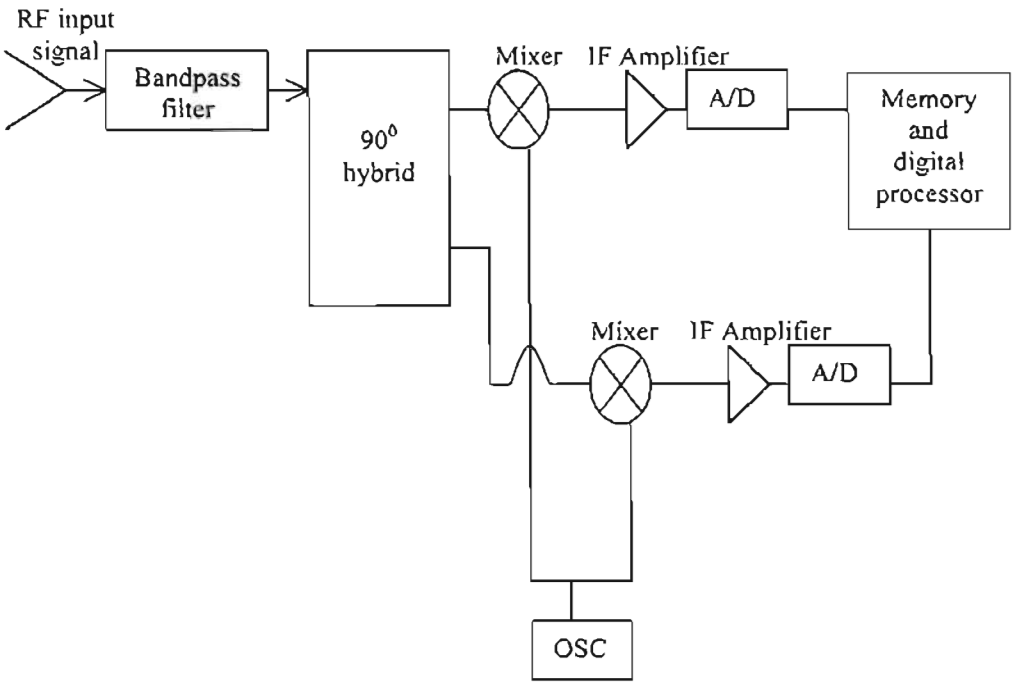

Fig. 3.17: A two-channel digital receiver: out-of-phase input and in-phase local oscillator

The advantages of the two-channel approach are twofold. First the input bandwidth can be doubled without increasing the digitizing speed of the A/D converters. One cycle is equivalently sampled four times; therefore the bandwidth can be doubled. Second, it is possible to solve the image problem [30]. Although one input signal will appear in both IF channels, if the data are properly processed, the true frequency of the input signal can be identified.

However, the two-channel receiver has a number of deficiencies. The overall bandwidth in the receiver is defined by the IF amplifiers in the I/Q baseband signals.

Because of the way in which the I and Q signals are derived, they may suffer from the following performance limitations [17]:

(i) There may be a poor match between the characteristics of the I and Q signals over the receiver bandwidth.

(ii) The I and Q channels may not maintain phase quadrature over the receiver bandwidth.

(iii) The I and Q channels may have separate dc offsets. In baseband sampling, dc offsets occur at the output of the I and Q mixers when the RF frequency is equal to the local oscillator frequency but with a phase difference. The I and Q dc offsets are different, since no two mixers are perfectly identical.

(iv) Nonlinearities of the components used in the I and Q channels may produce spurious noise.

A major drawback of the two-channel approach is its cost of implementation due to the fact that each antenna input requires two sets of mixers, IF amplifiers and A/Ds (for both the I and Q channel).

3.4.1.3 Direct sampling receiver

The amplitude matching and the phase orthogonality of the I and Q channels are extremely critical. This has created interest in an alternative conversion technique (figure (3.18)), in which the signal is sampled and digitized at IF and the I/Q signal is generated digitally.

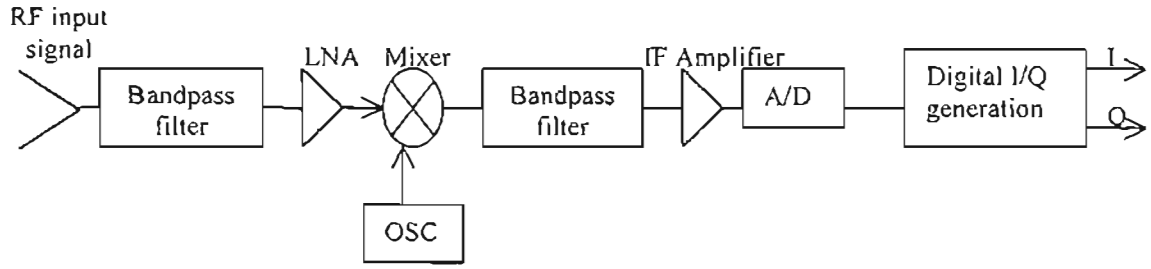

Fig. 3.18: Direct sampling receiver (from [17])

In this receiver, the I and Q outputs are formed using a digital filter, thereby eliminating I and Q matching problems from the channel. This approach eliminates the need for two sets of mixers, IF amplifiers and A/Ds at the expense of one faster A/D and some additional digital circuitry. The bandpass filter at the input is used to eliminate out-of-band interference. This bandpass filter can be placed before or after

the low-noise amplifier (LNA) with different consequences. By placing the filter before the LNA, the highest dynamic range (at the expense of a higher system noise figure) can be achieved, whereas by placing the filter after the LNA, the maximum receiver sensitivity can be obtained. A low-noise amplifier is essential since it establishes the system noise figure.

There are two methods for carrying out the direct sampling: Nyquist sampling and down-sampling (also called direct down-conversion). The Nyquist sampling theorem for sampling a bandpass analog signal (a signal having no frequency components above a certain frequency f_{max}) requires that the sampling rate be at least two times the highest frequency component of the analog signal (i.e. $2f_{max}$). For an RF signal with a bandwidth B centred at f_{RF}, the sampling rate must then be $2(f_{RF} + B/2)$ where the highest frequency component in the signal f_{max} is given by $f_{max} = f_{RF} + B/2$. It is possible to use sampling rates lower than $2f_{max}$ and still get an exact reconstruction of the information contained in the analog signal. This approach is referred to as direct down-conversion. It allows A/Ds with slower sampling rates to be used in applications where performance, power consumption, and cost are critical. For a bandpass signal with bandwidth B, the minimum sampling rate for information extraction is two times the bandwidth B. References [45] and [46] derive the constraints for a bandpass signal using down-sampling. To ensure that spectral overlap does not occur, the sampling frequency f_s must satisfy [46]

$$f_s \leq 2B\left(\frac{k-1}{N-1}\right) \tag{3.11}$$

and

$$f_s \geq 2B\left(\frac{k}{N}\right) \tag{3.12}$$

in which $k = f_{max}/B$ and $k \geq N$ since $f_s \geq 2B$. For example, in order to digitize a RF signal (directly) with bandwidth of 4MHz centred at 2GHz, application of equations (3.11) and (3.12) with k = 500.5, yields sampling frequencies in the range from 8MHz (twice the bandwidth) to 4.004GHz (Nyquist sampling rate) for integer values $N \leq 500.5$. At first glance, it seems possible to use down-sampling at the 2GHz RF frequency at a rate of twice the signal bandwidth, thus eliminating the need for frequency downconversion. However, there is a practical limitation: the ADC must still be able to operate on the highest frequency component in the signal ($f_{RF} + B/2$).

This is usually specified as the analog input bandwidth for the ADC. Also, conventional ADCs are designed such that their sampling rates are twice that of the maximum input frequency i.e. designed for Nyquist sampling. Performance of ADCs typically degrades with increasing input frequencies. Down-sampling also introduces another problem: a reduction in sampling rate results in a decrease in the width of the guard band, thus causing a filtering problem. Stringent requirements for analog bandpass filters (e.g. steep rolloffs) are needed to prevent distortion of the desired signal from unwanted adjacent frequency components. Furthermore, an IF down-conversion stage may be required for effective down-sampling. The sampling jitter requirements of the sampler must also be high to ensure that the carrier frequency is accurately sampled to recover the signal phase information that is required for PSK demodulation.

In order to carry out the coherent phase detection necessary for generating the digital I and Q signals, a digital down-converter (DDC) is used. A DDC contains a synthesizer, a quadrature pair of digital multipliers (which act as mixers in the digital domain) and some filters that implement both low-pass filtering and decimation [17]. It extracts a narrowband signal from a wideband digital input and decimates it to a reduced data rate. Since the new data rate is proportional to the bandwidth, all of the information in the digital signal has been captured without excess bandwidth being carried by the digital signal. A benefit derived from the reduced data rate is that the digital signal processor (DSP) (following the DDC) is better able to cope with it. Digital downconversion not only eliminates the need for another IF stage but it also overcomes many of the problems related to analog downconversion and lowpass digitization. Digital downconversion can also be performed by this same DSP. Alternatively, stand-alone DDCs can be used. However, by relieving the DSP from the processing burden associated with the digital downconversion functions, more computational power becomes available for the tasks required for array processing (updating of adaptive beamforming weights, etc).

The direct sampling receiver architecture is very attractive from a cost point of view. Also because of its potentially superior technical performance, it suitable for high-performance DBF system applications.

3.5 Adaptive beamforming in CDMA

The use of an adaptive array in a communication system requires some degree of compatibility between the signalling waveforms and the adaptive array. There are several reasons for this [47]:

(a) The adaptive weights are random processes, and they modulate the desired signal. The desired signal must be chosen so this modulation does not destroy the effectiveness of the communication system.

(b) There must be some difference between the desired signal and the interference waveforms, so these signals can be distinguished in the array.

(c) There must be some method for reference-signal generation and for acquiring system timing or frequency when the array is in the system.

Adaptive beamforming for CDMA wireless communications has been drawing more and more attention from both the communications and antenna communities [47]. Adaptive beamforming is highly suitable for a CDMA system, because the spreading codes can be used as a reference for beamforming.

3.5.1 Reference signal acquisition

An important function performed by the digital processor in the previously mentioned receiver configurations is that of adaptive beamforming. There are a number of criteria and algorithms for adaptive beamforming [17]. They all require some sort of reference signal in their adaptive optimization process. Reference signal refers to *a priori* and explicit information about the signals of interest. Explicit reference can be divided into two categories: spatial reference and temporal reference. Spatial reference is mainly referred to as the angle-of–arrival (AOA) information of a desired signal. A temporal reference signal may be a pilot signal that is correlated with the desired signal, a pseudo-noise (PN) code in the case of a CDMA system. The form of available reference depends on the particular system where adaptive beamforming is to be implemented. If an explicit reference signal is available in a system, it should be used as much as possible for less complexity, high accuracy and fast convergence. Adaptive beamforming is highly suitable for a CDMA system, because the spreading codes can be used as a reference for beamforming. The common implementation of adaptive beamforming in a CDMA wireless communication system is the use of

Compton's reference generation loop [47]. A generic implementation configuration for adaptive beamforming in a CDMA wireless communication system is shown in figure (3.19).

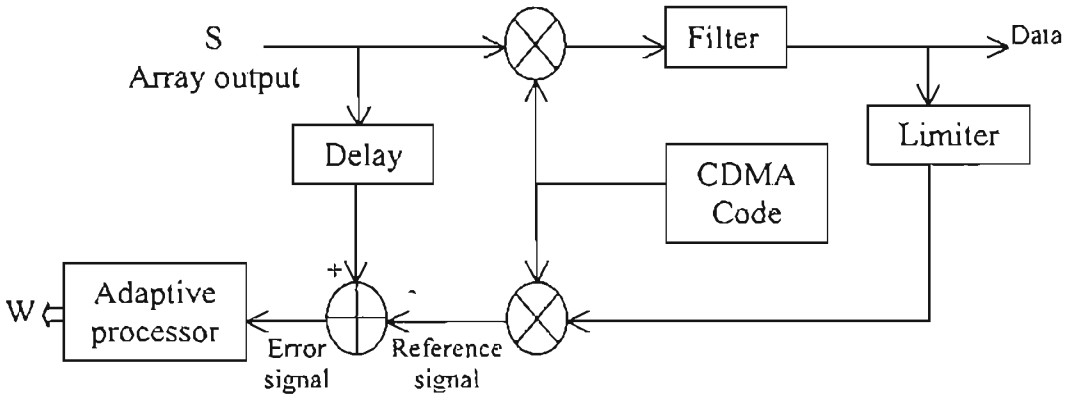

Fig. 3.19: Configuration for adaptive beamforming in CDMA (from [47])

In this configuration, the demodulation is carried out after beamforming. The array output S is first mixed with a CDMA-coded local oscillator signal, which is filtered and limited. The limited signal is re-modulated by mixing with the corresponding CDMA coded local oscillator signal. The re-modulated signal is used as the reference signal, which is compared with the delayed array output to produce an error signal. The error signal drives the adaptive processor to update the beamforming weights. This feedback loop is nonlinear due to the limiter operation.

The output of the 1st mixer contains both desired and interference components. These interference components are mainly multiuser interference i.e. the signals of undesired users. Some channel and receiver noise are also present. Because the CDMA code modulation matches that on the desired signal, the desired signal component at the 1st mixer output is compressed to data bandwidth, while the interference is not. The filter bandwidth is chosen wide enough to pass the desired signal, which now has only data modulation, but not wide enough to pass the interference, which has full-code bandwidth. As a result, the filter removes all but the centre portion of the interference spectrum. The signal is passed through a limiter, which controls the amplitude of the reference signal. The desired signal passes through this loop unchanged, except for the amplitude adjustment at the limiter and the envelope time delay associated with the filter.

An interference signal without the proper PN-code modulation, however has its waveform drastically altered by this loop. For example, a CW interfering signal which has a single line spectrum at the array output produces a reference signal with the full-bandwidth of the PN-code modulation (and with lower power than at the array array output). The correlation between the interference signal at the array output and the reference signal has been essentially destroyed by the loop.

There are several reasons why the reference signal amplitude must be controlled [47]:

(a) The amplitude of the reference signal determines the amplitude of the signals present at the array output, which should fall within a certain range for proper operation of the multipliers, etc., in the feedback loops.

(b) The reference-signal amplitude should be fixed so that the array will yield a maximum ratio of signal power to interference and noise power at the output.

(c) The reference-signal amplitude cannot be linearly dependent on the array output amplitude, because then there is a problem with the operation of the array weights. For example, if the reference loop were linear and its gain (to the desired signal) were greater than unity, the loop will return a reference signal larger than the array output signal, causing the array weights to increase without limit. Conversely, a loop gain less than unity returns a reference signal smaller than the array output, causing the array weights to drop to zero. Thus stable operation requires a fixed reference-signal amplitude.

(d) When the reference-signal amplitude is fixed, the desired signal voltage at the array output will also be fixed, regardless of the incident power of the desired signal. This behavior is important for the delay-lock loop [47] used for track code timing; it makes the threshold setting for code acquisition independent of incoming signal strength.

The processing loop in figure (3.19) not only generates the reference signal, but also delivers the desired signal with the PN-code removed at the output of the data-bandwidth filter. The desired signal is available at this point once the interference has been nulled. Thus, the reference-signal loop incorporates spectrum despreading. This configuration is also compatible to an asyncronous uplink CDMA system where despreading is done after beamforming [17]. It should be noted that this reference loop only operates properly as long as the local PN code is timed properly with

respect to the code on the desired incoming signal. This timing or synchronization is accomplished by a delay-lock loop. References [47] and [48] describe a novel delay-lock tracking loop that is designed to lock and track in the presence of data modulation on the desired signal, a feature that is only possible with an adaptive array in front of the loop. This adaptive array system is thus able to automatically lock on and track a desired signal with the correct code, while a signal with the incorrect code or no code at all is rejected.

3.5.2 Implementation issues for CDMA adaptive beamforming

Due to the fact that each CDMA user would require a separate loop, it would be cost-effective in a multiuser system to implement this loop in software in baseband.

The loop can also be implemented at IF using hardware followed by digital processing. This setup not only places increased requirements on the digital processor (which now has to process a much higher frequency signal), but is also costly in a multiuser system where hardware would be required for each user. The loop cannot be processed at RF (digital technology at RF is awaited). Although analogue beamforming and loop implementation (using hardware) can be performed at RF, the RF error signal would not be able to be processed by a present-day adaptive processor. Hence RF adaptive beamforming of the above loop is presently impossible. However, the weights themselves can be implemented in hardware using analog phase shifters and attenuators at either RF (following the antenna elements) or IF (following the IF amplifiers). The processing of the weights in this case can be performed at baseband/IF. In a large array, this setup is costly and increases the complexity of the front-end. The best alternative is to perform adaptive beamforming at baseband with the weights being implemented digitally in software.

3.6 Synopsis of some implemented adaptive array systems

This section provides a brief description/study of some adaptive antenna systems and the advantages and disadvantages of their implementation trends.

Reference [49] focuses on the stability problem that exists in adaptive antenna arrays when the weighting functions operate at a nonzero frequency. This paper shows how stability can be achieved by a simple time-compensation procedure. As a result, the weight processor can be implemented digitally. Nonzero frequency weighting in adaptive antenna arrays was introduced as a means to overcome some drawbacks encountered during implementation of conventional arrays whose weights operate around dc. Some of these drawbacks are dc offsets, feedthrough component imbalance, etc, and are usually associated with analog devices. The paper also cites an implementation of a four-element adaptive array with weights at an IF of 410MHz. Performance improvement in interference rejection over the conventional baseband array is also demonstrated. Also cited, is an array whose weight processor is implemented entirely with analog components. As a result, precise adjustments are difficult to achieve due to drifts and nonlinearity effects. Furthermore, analog integrators in adaptive processors suffer from imprecision, have a voltage limitation, and face an uncertain storage of information. This study was initially prompted by the desire to design the nonzero frequency weight processor by digital means in order to make this storage digital, and hence improve upon the analog integration.

Reference [50] discusses a phase-locked HF (30MHz) receiving array using separate RF amplifiers for each element (6 elements in total). The signals from each element are combined at an intermediate frequency of 3.7MHz. The type of array considered corrects essentially all phase errors between the distant transmitter and the point where the received signals are combined. This includes errors due to the propagation path, array element motion, near-field obstructions, and instabilities in electronic equipment and RF cables. The array also corrects phase shifts due to changes in angle of arrival, thus giving it the highly desirable property of automatically tracking a desired signal.

An adaptive antenna for a TDMA mobile telephony system is described in [51]. The adaptive array operates at a centre frequency of 1721MHz and consists of 10 elements arranged in a circular configuration. The weighting and summing of the received signals are performed on the received RF signal allowing the use of an ordinary base station as a receiver. The weighting is performed on the received RF signal using a phase shifter and an attenuator. The phase shifter accuracy is 1 degree and the attenuator is adjustable in 1dB steps down to –50dB. The RF signal is split and down-converted to the baseband and separated into I and Q channels where sampling at bit rate is done (270kHz). The ADC used has an 8 bit resolution with a dynamic range from –32dBm (0.631μW) to –80dBm (10pW). Digital signal processing is thereafter employed.

Reference [52] discusses an adaptive antenna for CDMA cellular systems. The performance of the adaptive antenna in various scenarios has been studied. There are four antenna elements in the array and the modulation scheme is QPSK. A processing gain of 128 was used. The spread spectrum signal received by the antenna elements is first processed by a weighting summing circuit. The output is then fed into two branches, one for symbol detection using a rake receiver and the other for comparing with the reference signal. The advantage of this scheme is that only one Rake receiver is needed and the path searcher operates in an environment of high signal to interference ratio (SIR) once an appropriate beam is formed. In a real system, the pilot signal can be used as part of the reference signal, but in the work reported in this paper, the antenna array is operated in a decision directed mode which means that the reference signal is obtained by respreading the detected symbols with phase and amplitude adjustment.

In [53], a new type of adaptive antenna is presented, which is intended for use in mobile receivers. A nonlinear, adaptive, analog feedback controller has been developed to control the phase relationship between two receiving elements. Both the controller and RF prototype are described in this paper. The prototype system described in this paper would be noteworthy for several reasons: First, the antenna diversity does not come at the price of additional expensive RF parts. This is in contrast to the multiple antenna systems that do the combining in baseband

processing, which requires that each antenna have its own LNA and mixer. It is common in modern spatial diversity systems to perform a down-conversion on each antenna signal before processing. The signals are digitized, then the computational power of a DSP is brought to bear on the problem of intelligent combining. This approach to building spatial diversity systems can be expensive; each new diversity branch requires its own LNA, mixer and ADC. However, the prototype system in [53] is much more cost effective. Second, the adaptive antenna would be completely modular, essentially a stand-alone "smart" antenna. The command level voltage could either be derived from the IF/baseband block or be simple, fixed reference. Third, the command level essentially sets the level of the automatic gain control at the receiving antenna, which relaxes the linearity requirement of the LNA. Finally, the nonlinear, analog controller proposed is a novel design and for this application, more cost efficient than traditional microprocessor-driven approaches.

From the above discussion, it is evident that antenna diversity comes at the expense of additional expensive RF parts (LNA, mixer and ADC). These systems are also very complex and expensive due to the large number of receivers required. They also require accurate calibration procedures for the phase and amplitude mismatches between channels. In [54] a multichannel measurement system using a single receiver is described. The system is based on a complex wideband radio channel sounder and a fast RF switch. The carrier frequency of the sounder is 2.154GHz and the bandwidth is 100MHz. The system provides real-time recording of signals from multiple input channels and this enables real dynamic array measurements of the radio channel of a moving mobile. The continuously recorded path lengths can be over one hundred metres. This method simulates a real adaptive array and therefore gives a realistic picture of the operation of practical adaptive array radio systems. In order to measure multiple antenna elements with a single receiver, a fast RF switching unit is required behind the antenna. The switching unit is based on a TTL-controlled GaAs switch with a switching time of 3ns. The system used in this paper has 8 channels.

The worldwide cellular and PCS infrastructure build-out has provided market incentives to develop better radio receivers. Better means smaller, lower power dissipation, high sensitivity, less factory tweaking, high manufacturing yields, field programmability, and operational flexible. Reference [55] discusses a new chipset

that has been developed that can be used to design high sensitivity, lower power digital receivers for a variety of cellular and PCS standards, including AMPS, IS-136, PDC, GSM and CDMA. One of them, the AD6600 is a dual channel, gain ranging receiver ADC that can sample IF signals from 70MHz to 250MHz at 20 mega samples per second (MSPS). It has on chip peak detectors, and received signal strength indicator (RSSI). It also has two analog input pins that can be used to sample separate diversity antennas. At the rated IF frequencies, 90dB of dynamic range is achieved: 30dB from the gain ranging and 60dB from the 11 bit ADC. The other chip, the AD6620 is a dual channel digital decimation programmable filter designed to interface directly with the AD6600 and subsequent DSPs. This chip can accept 16 bit input words at up to 65MSPS; the decimated data can be accessed by serial or parallel words. The combination of high IF over-sampling with programmable digital filtering allows designers to replace many analog/RF functions with digital functions.

Due to the difference in application (centre frequency, bandwidth, technology, etc.), a performance comparison of the above systems cannot be made.

CHAPTER 4

CDMA CONCEPTS

4.1 Introduction

In chapter 3, an adaptive beamforming scheme for CDMA using Compton's loop was described. It was assumed that the reader was familiar with CDMA theory. This chapter provides a comprehensive overview on CDMA. This theory is reinforced by simulation work using Advanced Design System (ADS) software [7]. This chapter forms the basis for the simulation models utilized in the following chapters. The list of references for CDMA is exhaustive. However, the reader is referred to [1], [56], [57] and [58] for further reading.

CDMA (Code Division Multiple Access) is a form of spread spectrum. Instead of using frequencies or time slots as in FDMA and TDMA technologies, it uses codes to transmit and distinguish between multiple users. Because the users are distinguished by codes, many users can share the same bandwidth simultaneously. This universal frequency reuse is crucial to CDMA's distinguishing high spectral efficiency. As a result CDMA has gained international acceptance by cellular radio system operators as an upgrade from current technologies. CDMA systems provide operators and subscribers with significant advantages over analog and conventional TDMA-based systems. Some of the advantages of CDMA are as follows:

- Increased capacity
- Improved voice quality, eliminating the audible effects of multipath fading
- Enhanced privacy and security
- Improved coverage characteristic which reduce the number of cell sites
- Simplified system planning reducing deployment and operating costs
- Reduced average transmitted power, thus increasing talk time for portable devices
- Reduction in the number of calls dropped due to handoff failures
- Development of a reliable transport mechanism for wireless data communications

- Coexistence with previous technologies due to CDMA and analog multiple access protocols operating in two spectras with no interference.

4.2 Background

To understand why there is a demand for CDMA, it is necessary to know the background behind previous spread spectrum systems. Spread spectrum communications have been used for encrypting military communications for many years. Its strength in the military arena lie in its ability to resist enemy jamming and to provide secure communications. It is difficult to interfere with or intercept a CDMA signal because of its use of a spread signal. The great attraction of CDMA technology from the beginning was its inherent ability to boost communications capacity and reuse frequencies to a degree unheard of in narrowband multiple access wireless technology. Its civilian mobile radio application was proposed theoretically in the late 1940's, but its practical application in the market did not take place until 40 years later due to the many technical obstacles that still needed to be overcome. However, the rapid development of high density digital integrated circuits (ICs), combined with the realization that regulating all transmitter powers to the lowest level required for a link would achieve optimal multiple access communication, allowed CDMA to materialize as a working technology. In 1991, promising results of the first field trials demonstrated that CDMA could work as well in practice as it did in theory. Commercial CDMA was introduced, tested, standardized, and initially deployed in less than seven years. This is a relatively rapid maturation cycle compared to other technologies such as TDMA. The first commercial CDMA service was launched in Hong Kong in 1995, followed by a launch in Korea and Pennsylvania. It has rapidly become the primary choice of carriers in the United States.

4.3 Comparison between FDMA, TDMA and CDMA

FDMA (Frequency Division Multiple Access), TDMA (Time Division Multiple Access) and CDMA are the three basic multiple access schemes.

FDMA divides radio channels into a range of radio frequencies and is used in traditional analog cellular systems. With FDMA utilizing a single carrier per channel (SCPC), only one subscriber is assigned to a channel at a time. Other users can access

this channel only after the subscriber's call has terminated or after the original call is handed off to a different channel by the system. FDMA cellular standards include AMPS (Advanced Mobile Phone Service) and TACS (Total Access Communications System).

TDMA is a common multiple access technique employed in digital cellular systems. It divides radio channel into time slots to obtain higher capacity. Its standards include North American Digital cellular (NADC), Global System for Mobile communication (GSM) and Personal Digital Cellular (PDC). As with FDMA, no other user can access an occupied TDMA channel until the channel is vacated.

CDMA uses a radically different approach. As mentioned earlier, it assigns a unique code to each subscriber to put multiple users on the same wideband channel at the same time. The codes, called "pseudo-noise (PN) code sequences", are used by both the mobile and the base station to distinguish between users. The IS-95 CDMA standard was adopted by the TIA (Telecommunications Industry Association) and became a digital cellular standard in 1992. The J-STD-008 standard for personal communication systems (PCS) was also accepted by ANSI (American National Standards Institute). CDMA is the first digital technology which meets the exact standards of the CTIA (Cellular Telecommunications Industry Association) [1]. Depending on the mobility of the system, CDMA provides 10 to 20 times the capacity of AMPS, and 4 to 7 times the capacity of TDMA. CDMA is the only one of the three technologies that can efficiently utilize spectrum allocation and offer service to many subscribers without requiring extensive frequency planning. All CDMA users can share the same frequency channel because their conversations are distinguished only by a digital code, while TDMA operators have to coordinate the allocation of channels in each cell in order to avoid interfering with adjacent channels. The average transmitted power required by CDMA is much lower than that required by analog, FDMA and TDMA technologies.

4.4 Spreading the spectrum

Spread spectrum multiple access transmits the entire signal over a bandwidth that is much greater than that required for standard narrowband transmissions in order to

gain signal-to-noise (S/N) performance. In channels with narrowband noise, increasing the transmitted signal bandwidth results in an increased probability that the received information will be correct. Because each signal is a compilation of many smaller signals at the fundamental frequency and its harmonics, increasing the bandwidth results in a more accurate reconstruction of the original signal. The effective drawback of narrowband data communications is the limitation of bandwidth. Thus signals must be transmitted with enough power so the corruption by gaussian noise is not as effective and the probability that the data received is correct will remain low. This means that the effective S/N must be high enough so that the receiver can recover the transmitted code without error.

From a system viewpoint, the performance increase for very wideband systems is referred to as "processing gain". This term is used to describe the received signal fidelity gained at the cost of bandwidth. Errors introduced by a noisy channel can be reduced to any desired level without sacrificing the rate of information using Claude Shannon's equation describing channel capacity ([18], [46]):

$$C = W \log_2 (1 + S/N) \tag{4.1}$$

where C = channel capacity in bits per second

W = bandwidth

S/N = Signal power / Noise power =Energy per bit x bit rate / Noise power

The S/N ratio may be decreased without decreasing the bit error rate. This means that the signal may be spread over a large bandwidth with smaller spectral power levels and still achieve the required data rate. If the total signal power is interpreted as the area under the spectral density curve, then signal with equivalent total power may have either a large signal power concentrated in a small bandwidth or a small signal power spread over a large bandwidth (figure (4.1)).

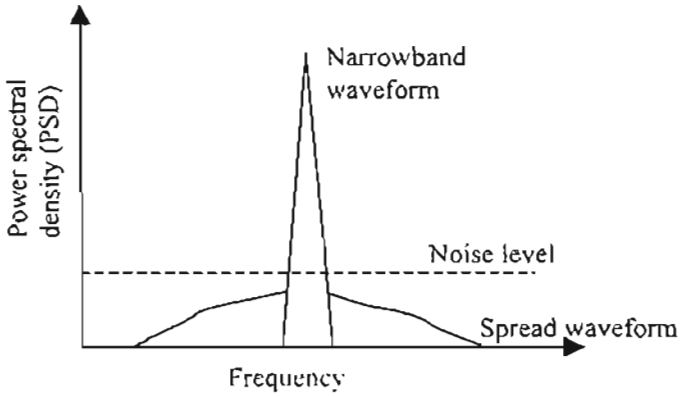

Fig. 4.1: Spread spectrum illustration

A CDMA spread spectrum signal is created by modulating the radio frequency (RF) signal with a spreading sequence (a code consisting of a series of binary pulses) known as a pseudo-noise (PN) digital signal because they make the signal appear wideband and noise-like. The spread spectrum receiver uses a locally generated replica PN code and a receiver correlator to separate the coded information from all possible signals. The correlator can be thought of as a specially matched filter that responds only to signals that are encoded with a PN code that matches its own code. Thus a spread spectrum correlator (signal demodulator) can be tuned to different codes simply by changing its local code. This correlator does not respond to man-made, natural or artificial noise or interference. It only responds to spread spectrum signals with identical matched signal characteristics and encoded with the identical PN code. Because of this, spread spectrum radios can tolerate a high level of interference unlike conventional radios, providing much greater capacity increase in frequency reuse [58]. The spread of energy over a wideband, or lower power spectral density makes spread spectrum signals less likely to interfere with narrowband communications, because the spreaded signal power is near that of gaussian noise levels. Narrowband communications, conversely, cause little or no interference to spread spectrum systems because the correlation receiver effectively integrates over a very wide bandwidth to recover the signal. The correlator then "spreads" out a narrowband interferer over the receiver's total detection bandwidth.

For this thesis, CDMA technology focuses primarily on the "direct sequence" method of spread spectrum. Direct sequence is a spread spectrum technique in which the bandwidth of a signal is increased by artificially increasing the bit data rate. This is

done by breaking each bit into a number of sub-bits called "chips". Assuming this number is 42, each bit of the original signal would be divided up into 42 separate bits, or "chips". This results in an increase in the data rate by 42. The increased data rate is often called the chip rate. By increasing the data rate by 42, the bandwidth is also increased by 42. The ratio of chip rate to data rate is termed the "processing gain" and represents the gain in bandwidth. The data signal is divided into chips by multiplying it by the PN code. The PN code is a sequence of chips ranging form –1 to 1 (polar or NRZ) or 0 to 1 (non-polar). The chipped or spread sequence in ADS [7] can be obtained by two methods depending on the format of the data signal and PN code. In the case of both the data and PN code signals being in polar or NRZ format, the spread sequence is obtained by simple multiplication. However, when both the data and PN code signals are in non-polar or binary format, the spread sequence is obtained by an Exclusive-NOR (XNOR) operation of both signals.

The basic operation of the transmitter and receiver for direct sequence spread spectrum will now be described briefly (figure (4.2)).

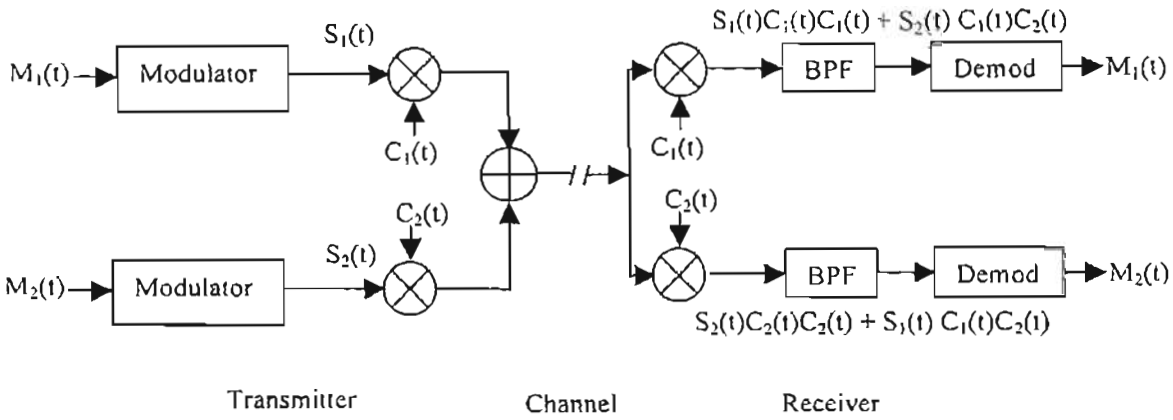

Fig. 4.2: Direct sequence transmitter and receiver

Assume there are two transmitters (refer to figure (4.2)) with two different messages to be transmitted. Each transmitter can be thought of as being two separate mobiles/subscribers. The messages $M_1(t)$ and $M_2(t)$ first go through a modulator to modulate the message at a higher frequency. For spread spectrum all messages are modulated on the same carrier frequency. The output of each of the modulators is $S_1(t)$ and $S_2(t)$. After the modulator, each signal is multiplied by its own unique PN code, $C_1(t)$ and $C_2(t)$. For this example assume that the PN codes are in NRZ or

bipolar format (-1 to 1). After spreading the bandwidth, each signal is transmitted. Because many signals can be transmitted from different transmitters at the same time, these transmissions are represented by simply summing their spectrums. At the receiver end, the incoming signal is the spread spectrum signal. In order for the receiver to extract a single message, it must multiply the incoming signal by the correct PN code. Because the PN code was chosen to range from –1 to1, this technique of multiplying by the PN code works perfectly. Since the original signal at the transmitter end was multiplied by the PN code, and again multiplied by the same PN code at the receiver end, the PN code for that particular message is effectively cancelled out. By eliminating the PN code, the spread spectrum effects for that particular message is eliminated. The receiver circuit that does this is called a correlator, and it collapses the spread signal back down to just the original narrow bandwidth centred at the modulated carrier frequency. The resulting signal is then passed through a bandpass filter (BPF) centred at the carrier frequency. This operation selects only the desired signal while rejecting all surrounding frequencies due to other messages in the spread spectrum. Lastly, the desired signal is demodulated to eliminate the carrier frequency.

4.5 Filtering

One of the primary requirements of any communication system is the channel bandwidth. The design objective is to use this resource as efficiently as possible. Channel bandwidth can be reduced by utilizing an efficient modulation technique and/or premodulation (baseband) filtering.

The modulation technique used has an effect on the channel bandwidth. Due to restricted spectrum allocation, only bandwidth-efficient modulation techniques can be chosen. Also, with ever increasing demand for service, the problem of restricted bandwidth allocation can cause significant degradation of the system. There is thus a need to provide subscribers with a quality of service which is demand independent.

The property of the baseband data has a significant effect on the channel bandwidth. To constrain the bandwidth of a modulated carrier, one must examine the baseband signal. The baseband waveform is usually a NRZ (non-return-to-zero) binary

waveform (here logic 1 is represented by an arbitrary voltage V_b held for the bit duration and logic 0 by the voltage $-V_b$ held for an equal time). The power spectral density (PSD) of a baseband waveform is determined by the waveform associated with an individual bit (or symbol). The waveform for an individual bit (or symbol) is a waveform of finite extension of time; its duration being the bit or symbol time. Any such waveform of limited time duration has a spectrum which extends throughout the frequency range ($f = -\infty$ to $f = +\infty$). The PSD of the NRZ data is shown in figure (4.3).

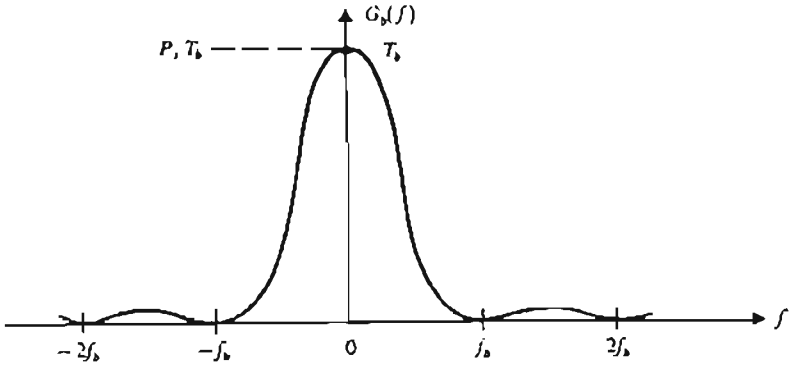

Fig. 4.3: Power spectral density of NRZ data (from [46])

Since the spectrum of the data extends over all frequencies, there is a corresponding increase in the spectrum of the modulated carrier, hence the importance of filtering. This is shown in figure (4.4) for BPSK modulation.

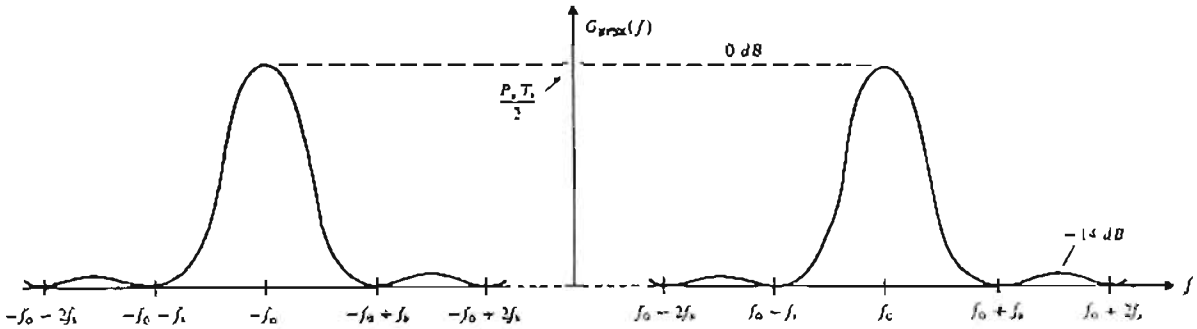

Fig. 4.4: Power spectral density of BPSK (from [46])

In cellular communications where different carrier frequencies or many channels are employed, there would inevitably be overlap in the spectra of the various signals and correspondingly a receiver tuned to one carrier would also receive, albeit at a lower level, a signal in a different channel. This overlapping of spectra causes interchannel

interference. For example, in the case of BPSK (also QPSK and OQPSK), the 1st sidelobe is relatively large when compared to the main lobe (sidelobe is only 14dB down the mainlobe). Since efficient spectrum utilization is extremely important in order to maximize the number of simultaneous users in a multi-user communication system, standardization agencies such as the FCC (Federal Communications Commission) require that the sidelobes produced in different modulation schemes be reduced below certain specified limits. This interchannel interference problem is so serious that standardization agencies will not permit these systems to be used except with bandpass filtering at the carrier frequency (i.e. at the transmitter output) to suppress the sidelobes.

In addition to bandpass filtering at the carrier frequency, filtering is also performed on the data waveform. Any fast transition in a signal, whether it be amplitude, phase or frequency will require a wide occupied bandwidth. Filtering helps to slow down and smoothen these transitions (in I and Q) thereby narrowing the occupied bandwidth. Filtering reduces interference because it reduces the tendency of one signal or one transmitter to interfere with another (especially in a FDMA system). At the receiver, reduced bandwidth improves sensitivity because more noise and interference are rejected. The spectrum can be minimized by passing the baseband waveform through a lowpass filter to remove the offending spectral range and sidelobes. However, it should be noted that this premodulation filtering distorts the signal and as a result, there is a partial overlap of a bit (symbol) and its adjacent bits in a single channel. This overlap is called intersymbol interference (ISI). ISI can be somewhat alleviated by the use of equalizers (filter-type structures) at the receiver. Equalizers are implemented in baseband. Basically, they undo the adverse effects introduced by the premodulation filter. So any unfiltered baseband waveform must cause interchannel interference and if it is filtered, interchannel interference can be reduced but only at the expense of causing intersymbol interference. Thus a tradeoff has to be made. Other tradeoffs are that filtering makes the radio more complex and can make them larger, especially if implemented in an analog fashion.

In order to determine the bandwidth efficiency of the different modulation techniques used in cellular communications, it is necessary to consider the different definitions of bandwidth. The two most commonly used bandwidth definitions are:

(a) Null-to-null bandwidth – is the width of the main spectral lobe where most of the signal power is contained.

(b) 99% of power – adopted by the FCC and states that the occupied bandwidth is the band which leaves exactly 0.5% of the signal power above the upper band limit, and exactly 0.5% of the signal power below the lower band limit. Thus, 99% of the signal power is contained inside the occupied band.

Using the 99% of power bandwidth criterion for a channel data rate (f_b) of 4.096MHz (data rate after spreading) for the proposed third generation WCDMA [1], BPSK modulation would require nearly $8f_b$ or 32.768MHz, which makes it unsuitable. This poor bandwidth efficiency can be improved using QPSK (or OQPSK) where twice the information can be carried in the same amount of channel bandwidth (compared to BPSK). Using the 99% of power bandwidth criterion, the total channel bandwidth equals $4f_b$ or 16.384MHz for a data rate (after spreading) of 4.096MHz. Thus, QPSK modulation provides a substantial savings (factor of 2) in channel bandwidth over BPSK.

The null-to-null bandwidth criterion is also often used. In BPSK, QPSK and OQPSK this translates to the mainlobe power. In these cases 90% of the power is contained in the mainlobe. To accommodate this mainlobe power, the premodulation filters and bandpass filters would have to have passbands of $2f_b$ in the case of BPSK and f_b in the case of QPSK and OQPSK. Again, using the proposed WCDMA with a data rate 4.096MHz (after spreading), BPSK would require an RF bandwidth of 8.192MHz while QPSK and OQPSK would require 4.096MHz. In the IS-95 CDMA system employing QPSK (at mobile) and OQPSK (at base) modulation the rate of the final spread signal is 1.2288MHz resulting in an RF bandwidth of approximately 1.25MHz. The 3dB bandwidth is 1.23MHz. The baseband signal after spreading is bandlimited by a digital filter that provides a sharp frequency roll-off and results in a nearly square spectral shape that is 1.23MHz wide at the 3dB point. In the case of third generation proposals, a nominal bandwidth of 5MHz has been proposed. This bandwidth is commensurate with the minimum chip rate of 4.096MHz specified by WCDMA [1]. Other proposed chipping rates are 8.192MHz and 16.384MHz resulting in an RF bandwidth of 10MHz and 20MHZ respectively [1]. It should be noted that all these bandwidths were proposed using QPSK/OQPSK modulation.

The most common varieties of baseband filtering are

- Raised cosine (Nyquist)
- Square-root raised cosine (transmitter receiver matched filter)
- Gaussian filtering

4.5.1 Nyquist or raised cosine filter

The raised cosine filter is a class of Nyquist filters. Nyquist filters have the property that their impulse response rings at the symbol rate. The filter is chosen to ring or have the impulse response cross through zero at the symbol clock frequency. The time response of the filter goes through zero with a period that exactly corresponds to the symbol spacing. Adjacent symbols do not interfere with each other at the symbol times because the response equals zero at all symbol times except the centre (desired) one. Nyquist filters filter the signal without blurring the symbols together at the symbols times. This is important for transmitting information without errors caused by intersymbol interference. Note that intersymbol interference does exist at all times except at the symbol (decision) times.

4.5.2 Square root raised cosine filter (transmitter-receiver matched filters)

In the square root raised cosine filter, the raised cosine filter described above is split, half being in the transmit path and half in the receiver path. In this case root Nyquist filters (commonly called root raised cosine) are used in each path, so that the combined response is that of a Nyquist filter.

Filtering is desired at both the transmitter and receiver. Filtering in the transmitter reduces the adjacent power radiation of the transmitter, and thus its potential for interfering with other transmitters. Filtering at the receiver reduces the effect of broadband noise and also interference from other transmitters in nearby channels. To get zero intersymbol interference, both filters are designed until the combined result of the filters and the rest of the system is a full Nyquist filter. Potential differences can cause problems in manufacturing because the transmitter and receiver are often manufactured by different companies. The receiver may be a small hand-held portable and the transmitter may be a large base station. If the design is performed correctly the results are the best data rate, the most efficient radio, and reduced effects

of interference and noise. This is the reason for root Nyquist filters being used in transmitters and receivers as $\sqrt{Nyquist} \times \sqrt{Nyquist} = Nyquist$.

4.5.2.1 Filter bandwidth parameter (α)

The sharpness of a raised cosine filter is described by the filter bandwidth parameter (α). α gives a direct measure of the occupied bandwidth of the system and is calculated as

$$\text{occupied bandwidth} = \text{symbol rate} \times (1 + \alpha) \tag{4.2}$$

Figure (4.5) shows raised cosine filter responses for different α.

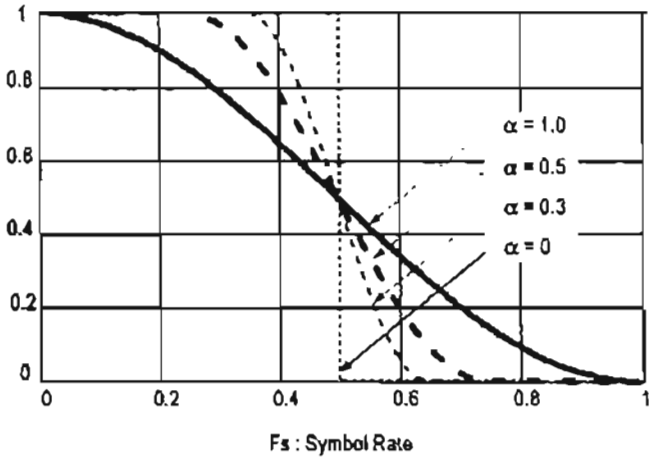

Fig. 4.5: Raised cosine filter responses as a function of (α)

If the filter had a perfect (brick wall) characteristic with sharp transitions, α is zero and the occupied bandwidth (using equation (4.2)) would be the symbol rate. However, this as an ideal case but this is not practical. α = 0 is impossible to implement. α is also known as the excess bandwidth factor since it indicates the amount of occupied bandwidth that will be required in excess of the ideal occupied bandwidth (which would be the same as the symbol rate). At the other extreme, a broader filter with α = 1 is easier to implement and has an occupied bandwidth of twice the symbol rate. Thus an α = 1 uses twice as much bandwidth than that of α = 0. In practice, it is possible to implement α < 0.2 and make good, compact, practical radios. The lower the α, the smaller the occupied bandwidth and the smoother the transitions between I and Q states. Typical values range from 0.35 to 0.5 though some video systems use an α as low as 0.11.

4.5.3 Gaussian filter

Gaussian filters are used in GSM. GSM uses GMSK (Gaussian Minimum Shift Keying) modulation. There is a small blurring of symbols on each of the four states in a GSM signal because the Gaussian filter does not have zero intersymbol interference. The phase states vary somewhat thereby causing blurring of the symbols. Thus the wireless system designer must decide on the amount of intersymbol interference that can be tolerated and combine that with noise and interference. However, Gaussian filters are used in GSM because of their advantages in carrier power, occupied bandwidth and symbol clock recovery. It is Gaussian in shape in both the time and frequency domains and it does not ring as in the case of raised cosine filters. Its effect in the time domain are relatively short and each symbol interacts significantly with only the preceding and succeeding symbols thereby causing intersymbol interference. This reduces the tendency for particular sequences of symbols to interact which makes amplifiers efficient and easier to build.

The corresponding term for the filter bandwidth parameter in a Gaussian filter is the bandwidth time product (B_bT). Occupied bandwidth cannot be stated in terms of B_bT because a Gaussian filter's frequency response does not go identically to zero, as does a raised cosine. Common values of B_bT are 0.3 to 0.5. More details of the Gaussian filter and B_bT are provided in the next section.

4.5.3.1 Gaussian filtering as used in MSK modulation

Filtering, in certain situations using QPSK or OQPSK does not resolve the problem of interchannel interference. These modulation techniques produce signals of constant amplitude, the information content being borne by phase changes. These phase changes are abrupt (90° in the case of OQPSK and 180° in the case of QPSK). Now it turns out that when such waveforms with abrupt phase changes, are filtered to suppress sidebands, the effect of the filter, at the times of the abrupt phase changes, is to cause substantial changes in the amplitude of the waveform. Such amplitude variations can cause problems in QPSK communication systems which employ repeaters (i.e. stations which receive and rebroadcast signals). These stations employ nonlinear power amplifier stages in their transmitters. Because of their nonlinearity, they generate spectral components outside the range of the mainlobe thereby undoing the effect of bandlimiting filtering and causing interchannel interference. In this

matter QPSK is a substantially worse offender than OQPSK because of its larger phase change.

The above-mentioned problem can be resolved using another modulation technique, called minimum shift keying (MSK) which is a form of OQPSK in which the symbol pulse shape is a half-cycle sinusoid, rather than the usual rectangular form. MSK has the following distinctive properties:

(a) The baseband waveform that multiplies the quadrature carrier is much "smoother" than the abrupt rectangular waveform of QPSK. The spectrum of MSK has a main centre lobe which is 1.5 times as wide as that of QPSK. However, the sidelobes with respect to the mainlobe is smaller than that of QPSK (the first sidelobe of BPSK, QPSK and OQPSK is only 14dB down the mainlobe!). Thus filtering is much easier in MSK.

(b) The MSK waveform exhibits phase continuity i.e. there are no abrupt phase changes as in QPSK. As a result interchannel interference caused by nonlinear amplifiers is avoided.

The spectral efficiency of MSK is considerably greater than that of QPSK/OQPSK. Using the 99% of signal power bandwidth criterion, MSK would require a bandwidth of $1.2f_b$ compared to $4f_b$ for QPSK/OQPSK. For a 4.096MHz data rate, this translates to an RF bandwidth of 4.9152MHz for MSK and 16.384MHz for QPSK/OQPSK. The null-to-null bandwidth criterion yields 6.144MHz (1.5 x 4.096MHz) for MSK and 4.096MHz for QPSK/OQPSK (main lobe for MSK is 1.5 times as large as that for QPSK and OQPSK).

As mentioned previously, GSM makes use of MSK modulation. A baseband Gaussian filter is used as the premodulation filter to obtain a linear phase characteristic. This filtered version of MSK is known as GMSK. Both the sidelobe power level and the width of the mainlobe is reduced by this Gaussian filter. In spite of its increased spectral efficiency over QPSK/OQPSK, MSK modulation has not been proposed for third generation CDMA systems. Instead linear modulation techniques (BPSK, QPSK and OQPSK) have been proposed for wideband third generation CDMA because of their good modulation efficiency [1]. Another reason can be speculated to be that the VLSI implementation of a GMSK modulator is

difficult to realize. The use of constant-envelope modulation schemes such as MSK are limited to a spectral efficiency of approximately 1bit/sec/Hz, regardless of the number of modulation levels used. However, linear modulation schemes such as shaped PSK, which uses linear power amplifiers, can achieve efficiencies greater than 1bit/sec/Hz. Greater efficiencies can be attained with a higher number of modulation levels used at the expense of a higher bit error rate (BER) due to the reduced distance between constellation points. Because of the use of linear amplifiers, linear modulation techniques can provide better out-of-band radiation performance, increasing the spectral efficiency of the system further. Advances in technology and devices have made the use of linear amplifiers feasible and cost-effective.

Bandlimited linear modulation methods utilizing nonlinear power amplifiers result in spectrum leakage to adjacent carriers [59]. Therefore, especially in the uplink (mobile to base), the modulated signal should be able to tolerate nonlinear power amplifier effects. Once the modulation method has been fixed, pulse shaping at baseband determines the final spectrum properties. The roll-off factor depends on the power amplifier (PA) linearity and adjacent channel attenuation. Spectrum leakage to adjacent channels can be controlled by backing off the PA or by using some linearization method to equalize the nonlinearities of the power amplifier. However, both methods decrease the achievable PA efficiency when compared to modulation schemes that have constant envelope and can be amplified with power efficient nonlinear power amplifiers [59].

The CTIA standardization agency has recommended that the adjacent-channel interference should be below –60dB for cellular radio [60]. One of the parameters of interest in the design of the Gaussian baseband filter is the bandwidth time product (normalized 3dB bandwidth), B_bT where T is the data pulse width. The power spectrum density plot as a function of normalized frequency difference from the carrier centre frequency $(f - f_c)T$, with the normalized 3dB bandwidth of the baseband Gaussian filter (B_bT) as a parameter is shown in figure (4.6).

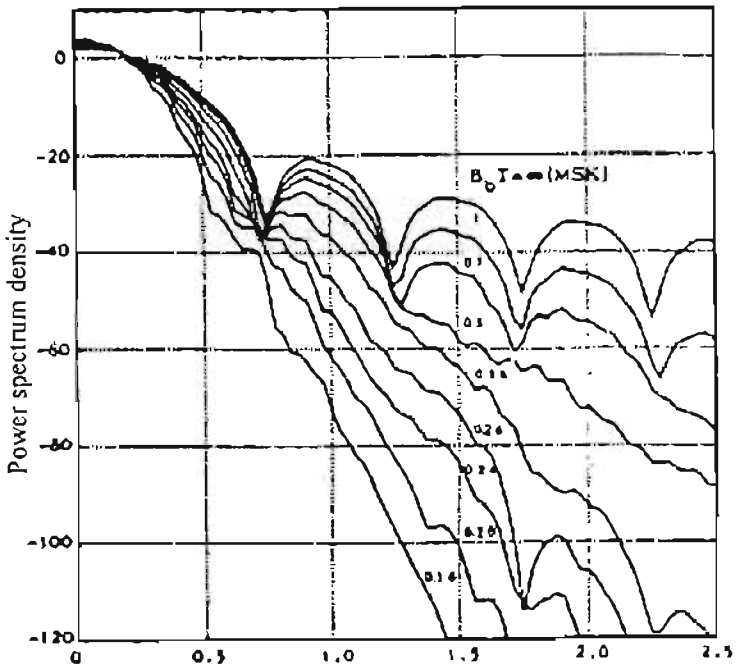

Fig. 4.6: PSD versus normalized frequency difference for GMSK (source [60] P328)

A B_bT value of ∞ represents a normal MSK power spectrum density. The normalized frequency difference for GSM can be computed from the specified channel spacing (200kHz) and the data rate (270.8kbps). For a normalized frequency difference of 1.5 for GSM (representing $(f - f_c)$ = 200kHz, R_d = 270.8kHz, $(f - f_c)T = 2 \times 200/270.8 = 1.5$) and with $B_bT = 0.36$, the power spectrum density has a value below –60dBc.

Figure (4.7) shows a plot of the spurious radiated power in the adjacent-channel relative to the desired channel power, with normalized frequency difference as abscissa and B_bT as a parameter. For a normalized frequency difference of 1.5 (calculated from GSM's data rate of 270.8kHz and 200kHz), the power in the adjacent channel is below 60dB for $B_bT = 0.24$.

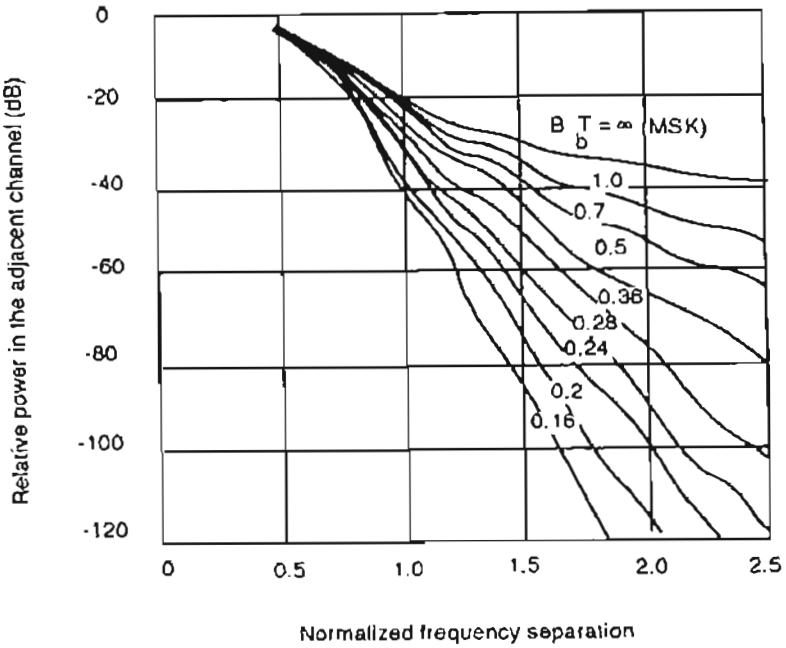

Fig. 4.7: Relative power radiated in adjacent channel (source [60] P329)

Thus, the baseband Gaussian filter of GMSK can have a maximum normalized 3dB bandwidth or bandwidth time product (B_bT) of 0.24 in order to satisfy the adjacent–channel requirement of –60dB.

In addition to the European GSM system, GMSK has also been adopted by DECT (Digital European Cordless Telephone). For GSM, the normalized bandwidth of B_bT is 0.3 with a total channel data rate of 270.8kbps has been adopted. Thus the bandwidth of the lowpass filter is 81kHz (0.3 x 270.8kbps).

From figure (4.7), it can be seen that the CTIA recommended value of –60dB adjacent-channel interference cannot be met in the GSM system employing $B_bT = 0.3$. The choice of B_bT of 0.3 for GSM is influenced by BER performance at the expense of not meeting the CTIA's recommended value of –60dB for adjacent-channel interference. A B_bT value of less than 0.3 increases the BER exponentially due to a drastic reduction in signal power. DECT has adopted $B_bT = 0.5$ with a data rate of 1.152Mbps. This corresponds to a filter bandwidth of 576kHz (0.5 x 1.152Mbps). DECT also does not meet the CTIA's –60dB recommended adjacent-channel interference. An adjacent-channel interference of nearly –40dB can only be met. Since the DECT system reassigns channels as the interference goes up, -40dB adjacent-channel interference may be tolerable. Figure (4.8) shows a plot of BER

versus signal-to-noise ratio (SNR) with the normalized 3dB bandwidth (B_bT) as the parameter.

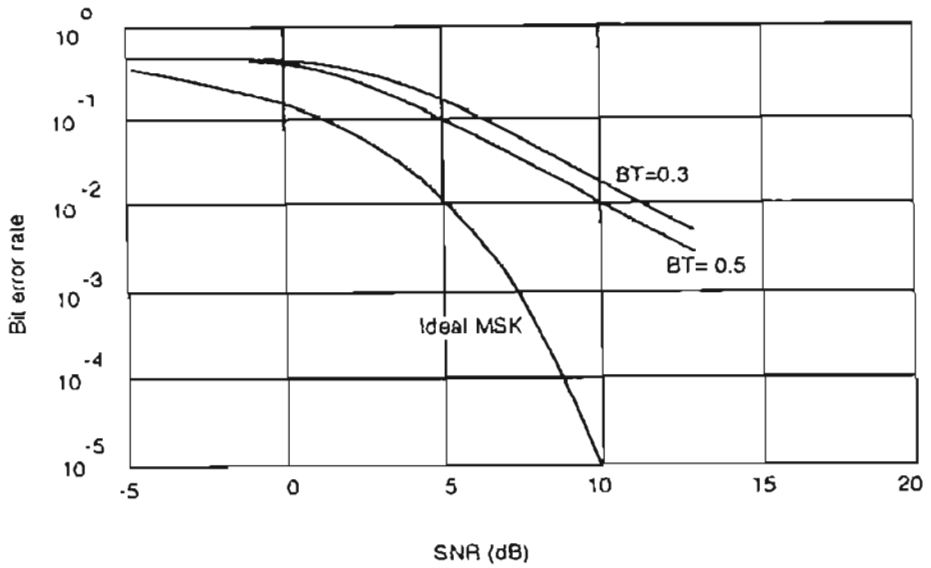

Fig. 4.8: BER versus SNR for GMSK (source [60] P333)

From this figure it can be seen that the BER with B_bT=0.3 (as in GSM) requires additional signal power by nearly 2dB compared to B_bT=0.5 (as in DECT). Also for a fixed SNR, an increase in the normalized 3dB bandwidth (B_bT) brings about a decrease in the bit error rate. This once again establishes the fact that the choice of B_bT=0.3 for GSM is influenced by better BER performance than that for B_bT=0.24. However, this is achieved at the expense of an increase in adjacent-channel interference.

4.6 Simulation of a simple CDMA system

This section reinforces the relevant CDMA theory covered in the preceding sections. A simple CDMA transceiver system is simulated using ADS software [7]. Waveforms for each stage of the transceiver are shown. The transmitter and receiver schematics, as implemented in ADS are shown in figures (4.9) and (4.10), respectively. A brief discussion on the component blocks used in the simulation will be provided initially. The reader is referred to the ADS documentation for further information.

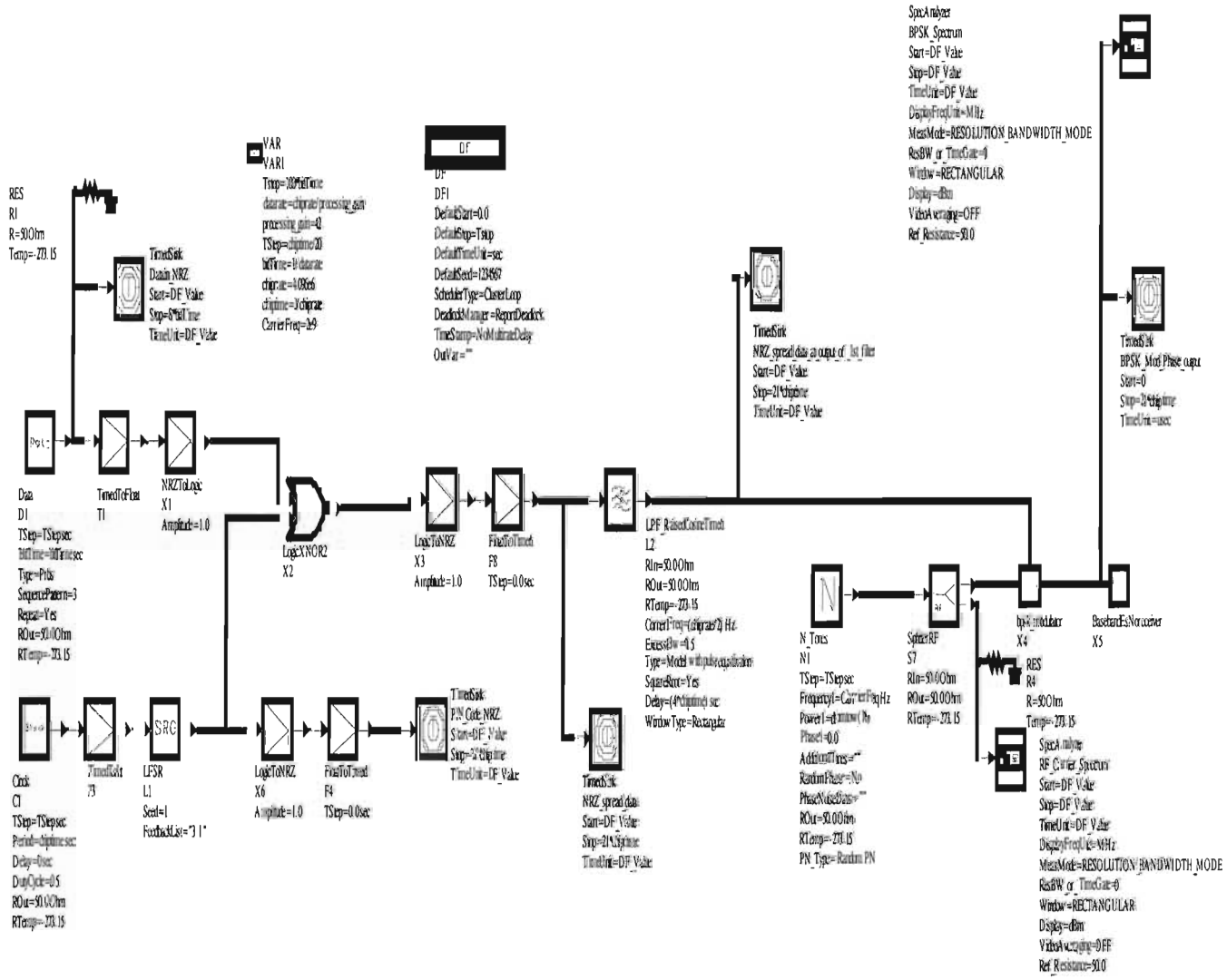

Fig. 4.9: ADS transmitter schematic

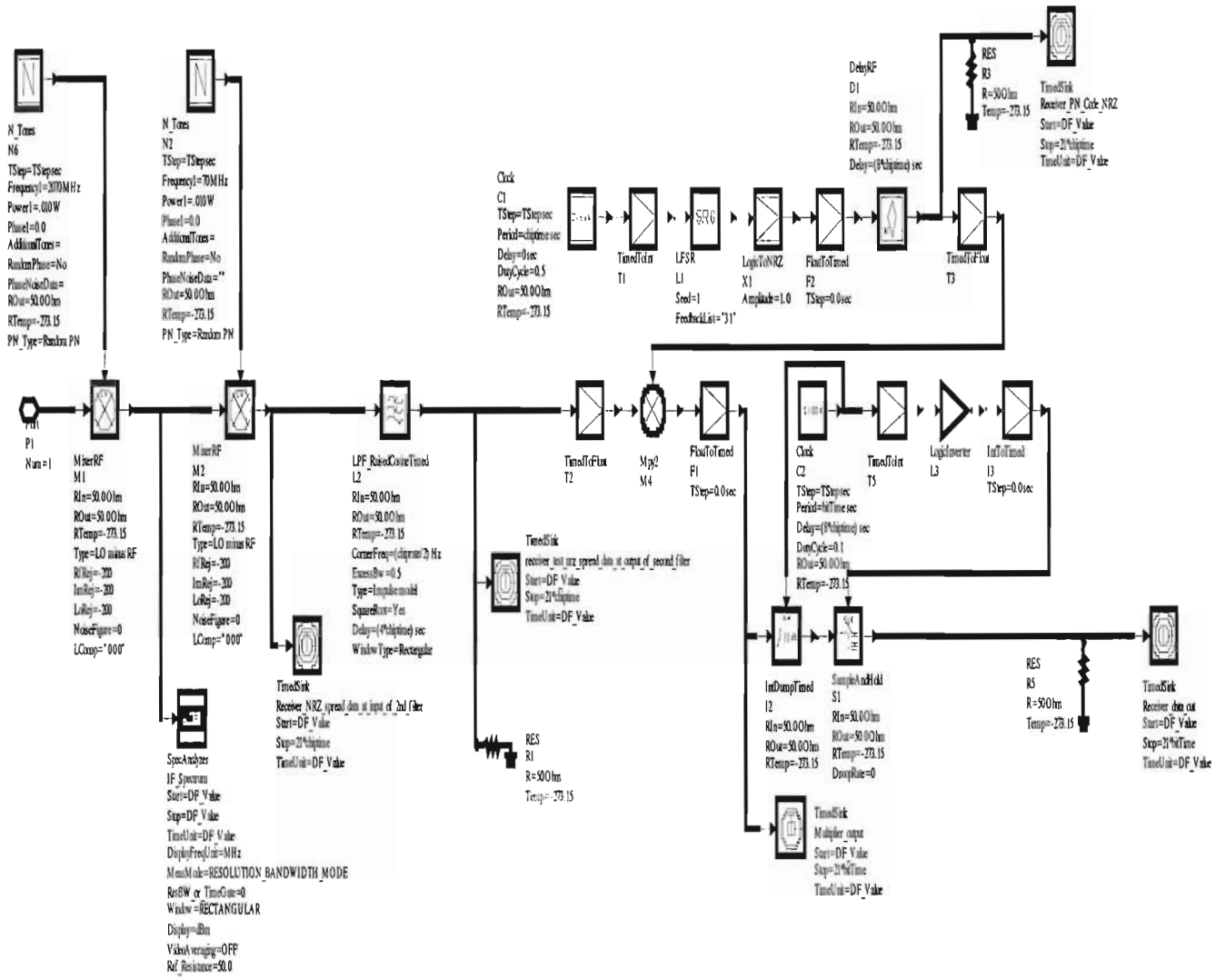

Fig. 4.10: ADS receiver schematic

ADS block label glossary

VAR: This block allows variables to be declared. Values are also assigned to these variables. Variables such as the simulation stop time (Tstop), data rate, processing gain, simulation sampling time (TStep) are declared in this block. The simulation sampling time (TStep) is of importance. Its value is chosen such that TStep<1/Maximum baseband data rate. In this case, the maximum baseband data rate corresponds to the chip rate (4.096MHz). A value of one-twentieth of the chip time interval was used for Tstep. It should also be noted that a decrease in the sampling time results in an increase in the simulation run time.

DF controller: The Data Flow (DF) controller is used to control the simulation start and stop times. The DefaultStop field in this instance is specified to be the variable Tstop (declared in the VAR block). The DefaultStart time is usually zero. The time unit can be specified in the DefaultTimeUnit field.

TimedSink: This enables display of waveforms as a function of time. The Start and Stop fields allow the waveform to be displayed over a specified time frame.

Data: This block generates data in NRZ format. A BitTime field exists for the input of the data/bit time. The length of the data can be specified in the SequencePattern field. The data is displayed in the time sink called Datain_NRZ.

NRZToLogic: Converts NRZ timed data to a binary datastream format.

LogicToNRZ: Converts a binary datastream to a NRZ timed data format.

TimedToInt, FloatToTimed, TimeToFloat, IntToTimed: These blocks enable conversion from one data format to another.

LogicXNOR2, LogicInverter: These are logic gates that perform the XNOR and inverter operations, respectively. The spreading process is performed using the 2 input XNOR gate (LogicXNOR2).

LFSR: This is a linear feedback shift register that was used to generate the PN code. In this case, the fields for the initial value (Seed) and the Feedback were set to 1 and "3 1", respectively. The Feedback field of "3 1" implies the use of a 3 stage shift register. Thus the PN code has a length of 7 (2^3-1).

Clock: This block (C1) was used to drive the shift registers (LFSR). Its period was set to the chip time. Thus the PN code generated by the LFSR is at the chip rate.

LPF_RaisedCosineTimed: This is a raised cosine low pass filter. Two of these filters (matched) were used in the transceiver. Some of the fields for this block were discussed in section (4.5.2).

N_tones: These blocks were used to generate the various carrier frequencies in the system. Fields exist for both frequency and power level.

SpecAnalyzer: This is a spectrum analyzer sink used to display the spectrum of signals. For example, the spectrum analyzer named BPSK_Spectrum is used to display the 2GHz BPSK spectrum at the transmitter. Fields are similar to those of a spectrum analyzer.

SplitterRF: This is a simulation device that splits or provides an alternate path for the signal. However, it is not a power splitter. The signal at the output legs of the device are a replica of that at the input.

bpsk_modulator, BasebandEsNoreceiver: These are subnetworks. For example, the subnetwork named BasebanEsNoreceiver was created by forming a network of all the receiver components. By clicking on this network, the receiver components (in figure (4.10)) can be viewed. Subnetworks simplify the schematic.

MixerRF: As the name suggests this is simply a mixer. In the receiver schematic (figure (4.10)), mixers M1 and M2 are used as a downconverter and demodulator, respectively.

Mpy2: This is a 2 input multiplier. In this context, it is used to perform the despreading operation (recall an XNOR gate could also be used).

DelayRF: This component is used to introduce a time delay. In the receiver it is used to synchronize the PN code with the demodulated (spread) data. The receiver PN code was delayed by 8 chips corresponding to the total delay of the two root raised cosine filters.

IntDumpTimed, SampleAndHold: These are just integrate and dump and sample and hold circuits. In the receiver (figure (4.10)), they are used (in conjunction with the despreading process) to retrieve the transmitted data.

The CDMA system will now be discussed: The input message signal is assumed to consist of an arbitrary chosen 97.5kbps data stream that is spread by a wideband CDMA signal with a chip rate of 4.096MHz. Thus this corresponds to a system processing gain of 42. The 4.096MHz chip rate is the minimum rate specified by WCDMA [1] in Europe and Japan. In the simulation, the message bit stream of bit time 10.254μs (1/97.5kHz) was set to consist of an eight bit (11010010) repetitive stream. For the purpose of simplicity in demonstrating CDMA concepts, a PN code

for a single user was generated using a 3 stage shift register with seed=1 and codelength=7. The repetitive code sequence consists of the code "0011101" of duration 1.709μs (7 times the chip time). Figures (4.11) to (4.13) show the data, PN code and spread data sequences with the time axis adjusted accordingly (the reader should constantly refer to the various sinks of figures (4.9) and (4.10) on pages 4-19 and 4-20, respectively for the source of the various waveforms shown). It should be noted that the 4.096MHz spread data in figure (4.13) was obtained by an exclusive-NOR operation of the input data stream (figure (4.11)) and the PN code sequence (figure (4.12)). The rate of the spread signal is equal to the PN code rate.

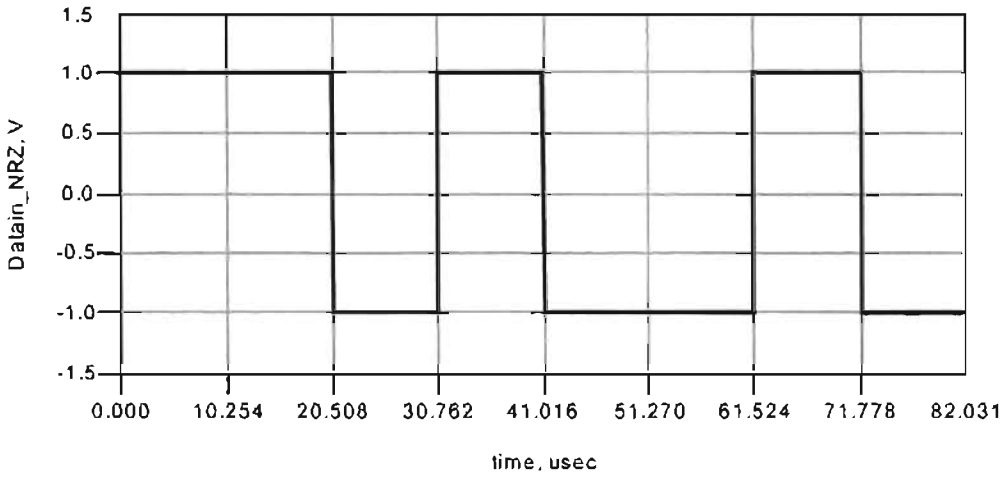

Fig. 4.11: Repetitive 8 bit 97.5kbps NRZ data stream (11-11-1-11-1)

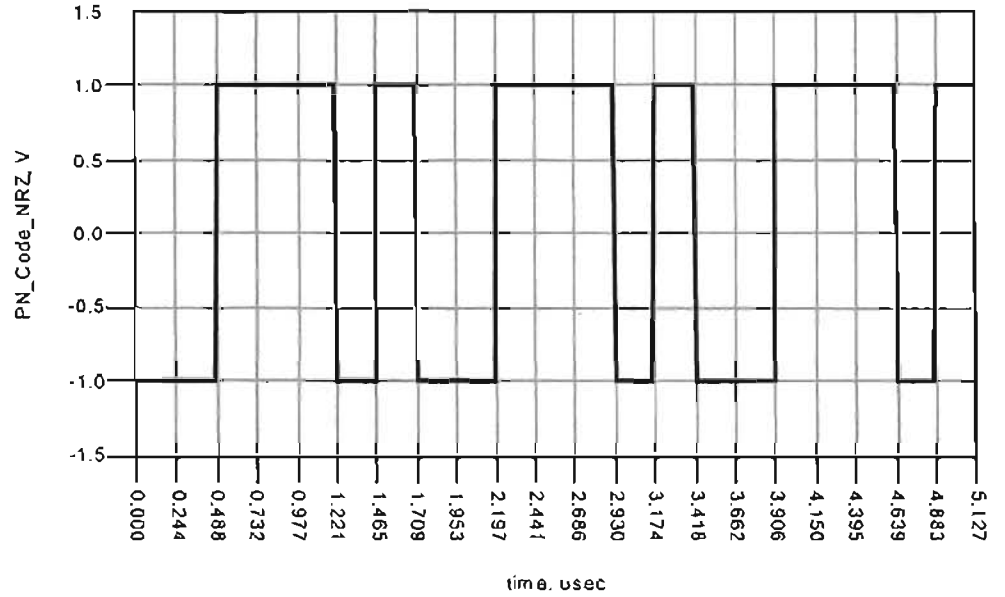

Fig. 4.12: Repetitive 4.096MHz NRZ PN code sequence (-1-1111-11) shown for three codelengths

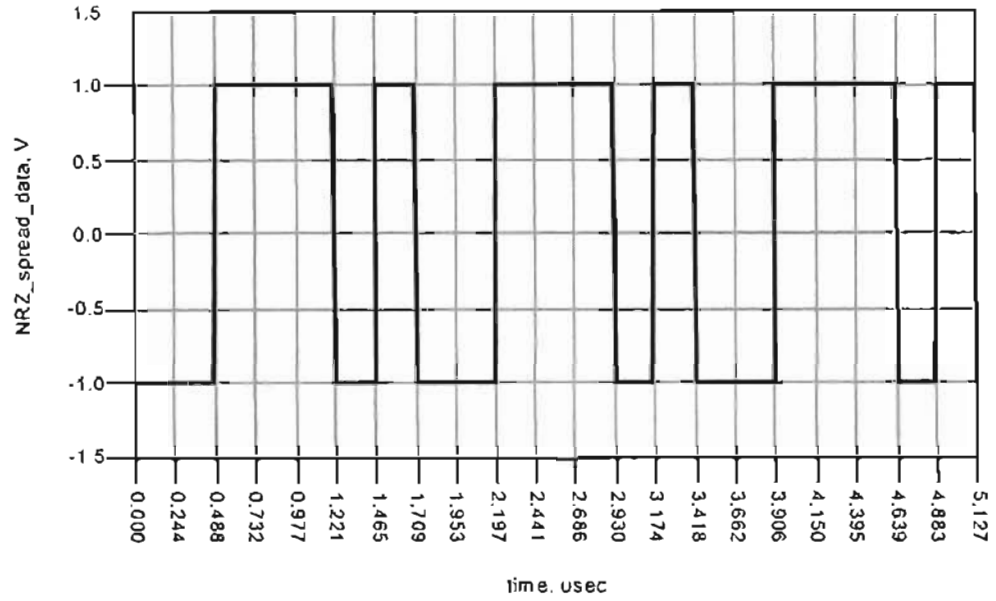

Fig. 4.13: NRZ 4.096MHz spread data shown for 3 codelengths

This NRZ spread data, after square root raised cosine premodulation filtering (figure (4.14)), is used to BPSK modulate an arbitrary chosen 2GHz, 10dBm (10mW) RF carrier. The root raised cosine filter (in both the transmitter and receiver) each have a delay of 4 chips or 976.6nS. Figure (4.15) shows the ADS implementation of the BPSK modulator. The BPSK spectrum is shown in figure (4.16).

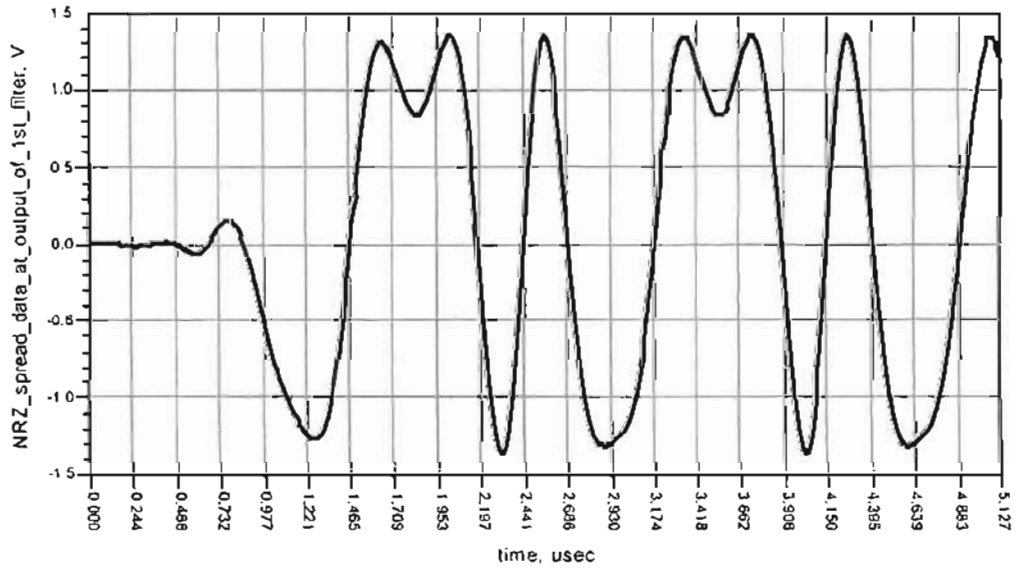

Fig. 4.14: NRZ 4.096MHz spread data after root raised cosine filtering at transmitter

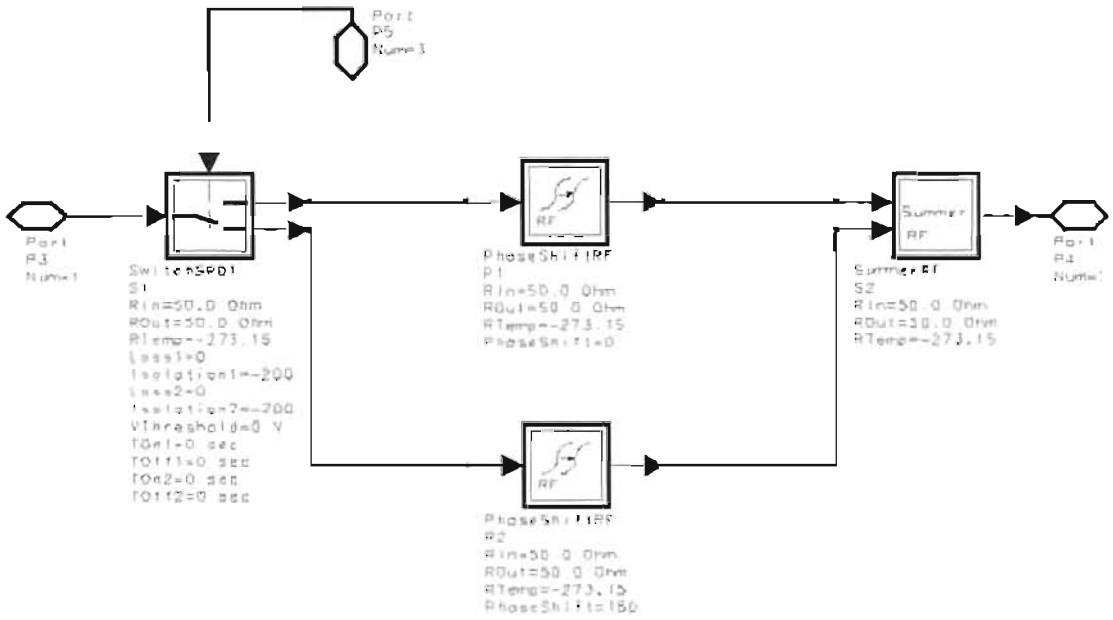

Fig. 4.15: BPSK modulator

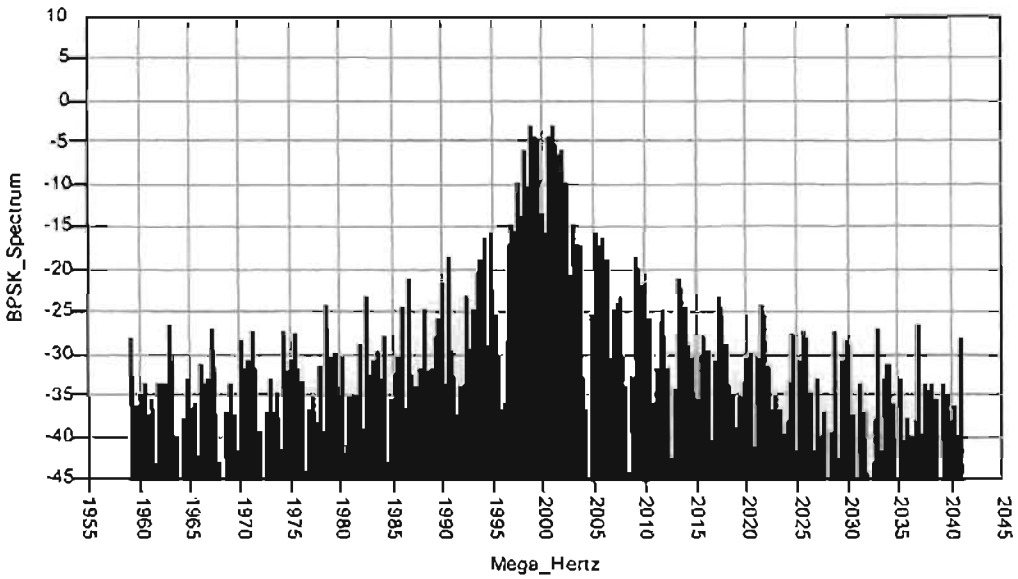

Fig. 4.16: 2GHz RF BPSK spectrum (ADS)

This simulated transmitted signal is then injected into the RF front-end receiver where downconversion and demodulation are performed. Downconversion to an IF of 70MHZ is performed using a mixer. The IF spectrum is shown in figure (4.17).

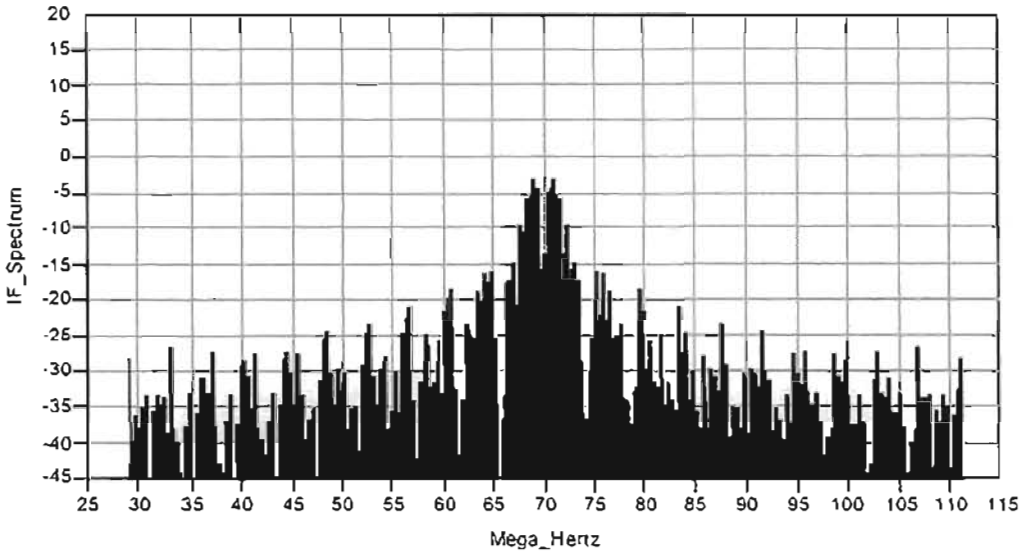

Fig. 4.17: 70MHz IF BPSK spectrum (ADS)

Figure (4.18) shows the 4.096MHz NRZ spread data after carrier demodulation.

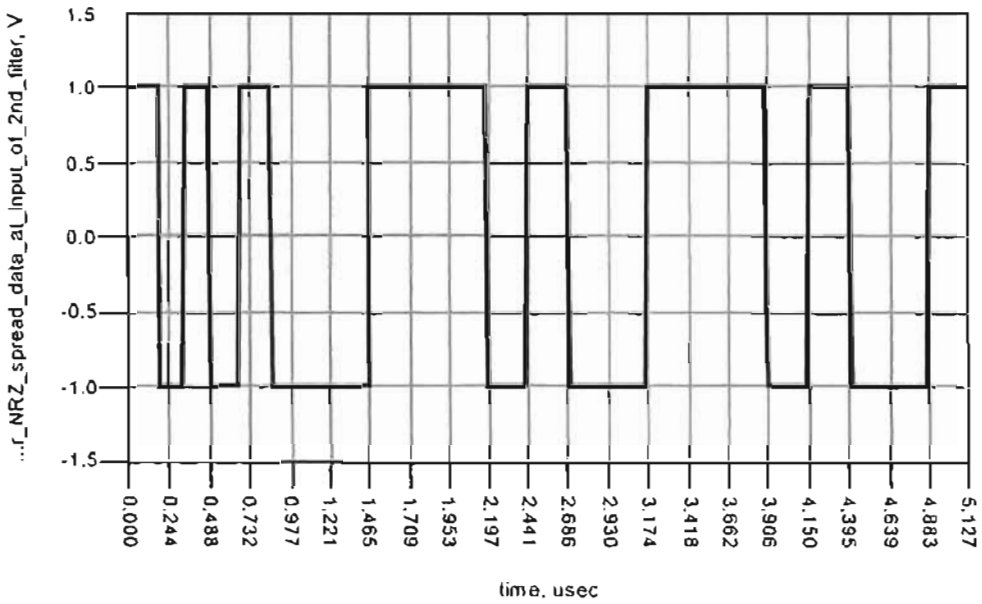

Fig. 4.18: NRZ spread data after demodulation (at input of receiver root raised cosine filter)

A comparison of NRZ spread data before premodulation filtering (input of transmitter raised cosine filter) and after post-modulation filtering (output of receiver raised cosine filter) is shown in figure (4.19). The receiver PN code (figure (4.20)) has been delayed by eight chips to enable synchronization of the despreading operation. Recall that the NRZ spread data has been delayed by 4 chips in each of the root raised cosine filters. The despreading operation in the receiver was performed by a simple

multiplier circuit. The waveform at the output of the multiplier circuit (displayed by TimedSink named "Multiplier_output" of figure (4.10) on page 4-20) is shown in figure (4.21). Finally, the received NRZ data stream (figure (4.22)) is recovered after the integration and dump and sample and hold circuitry. Integration and dump and sample and hold were performed for the duration of one bit interval (10.254μs). Once again the received data is delayed by 8 chips (1.953μS) (corresponding to the combined delay of both matched filters).

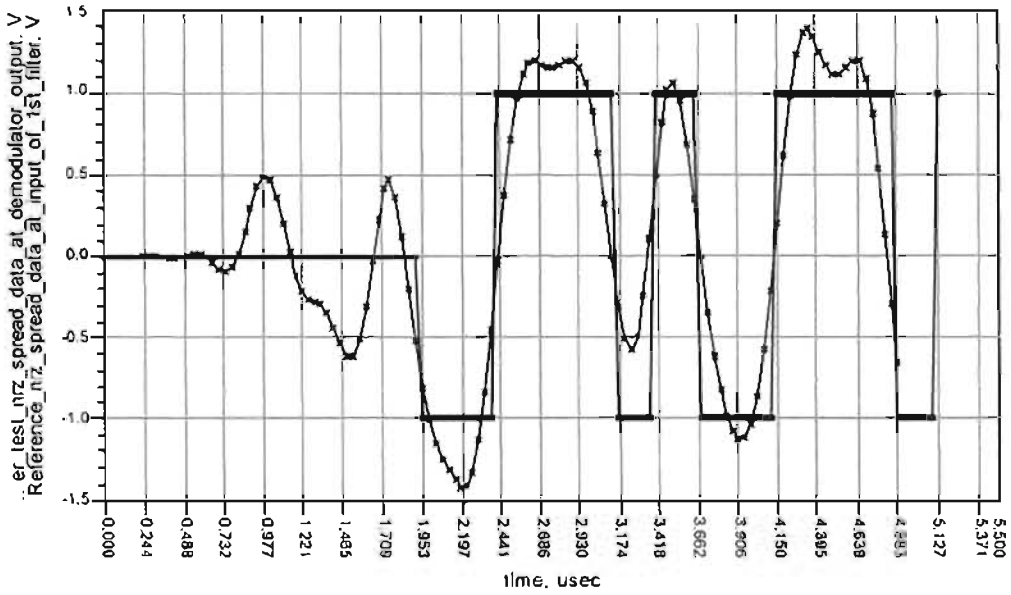

Fig. 4.19: Comparison of NRZ spread data before premodulation filtering and after post-modulation filtering

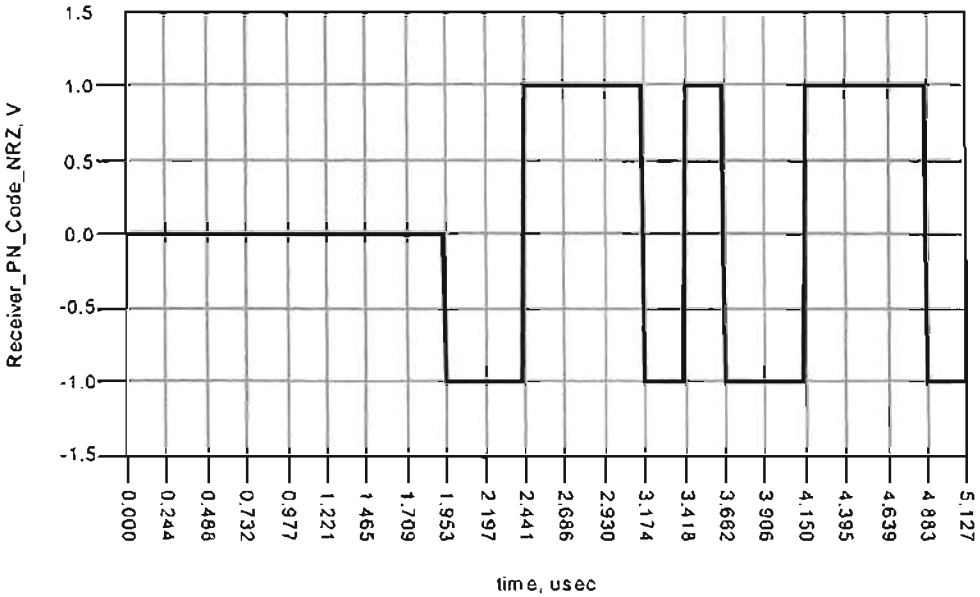

Fig. 4.20: Receiver PN code sequence (delayed by 8 chips)

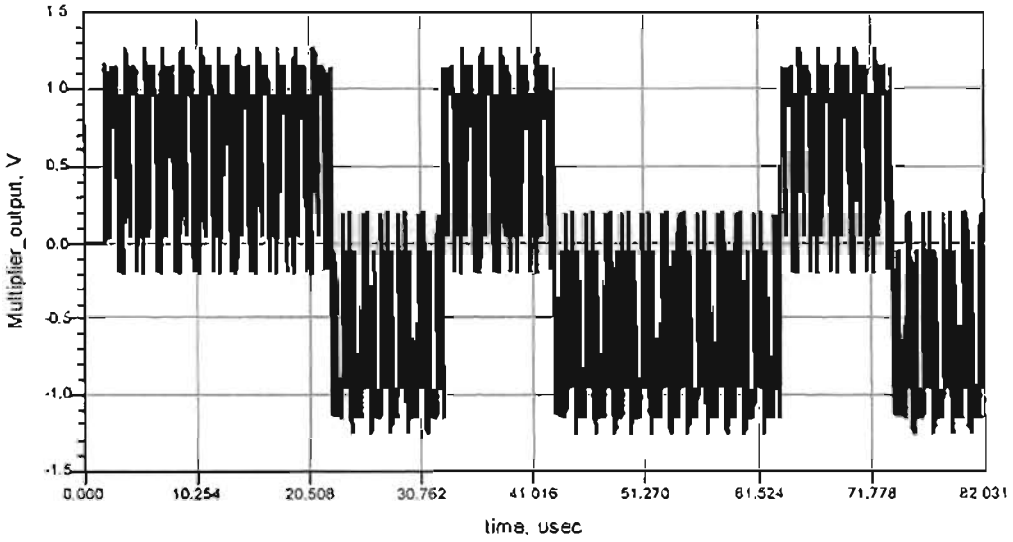

Fig. 4.21: Waveform at output of multiplier circuit

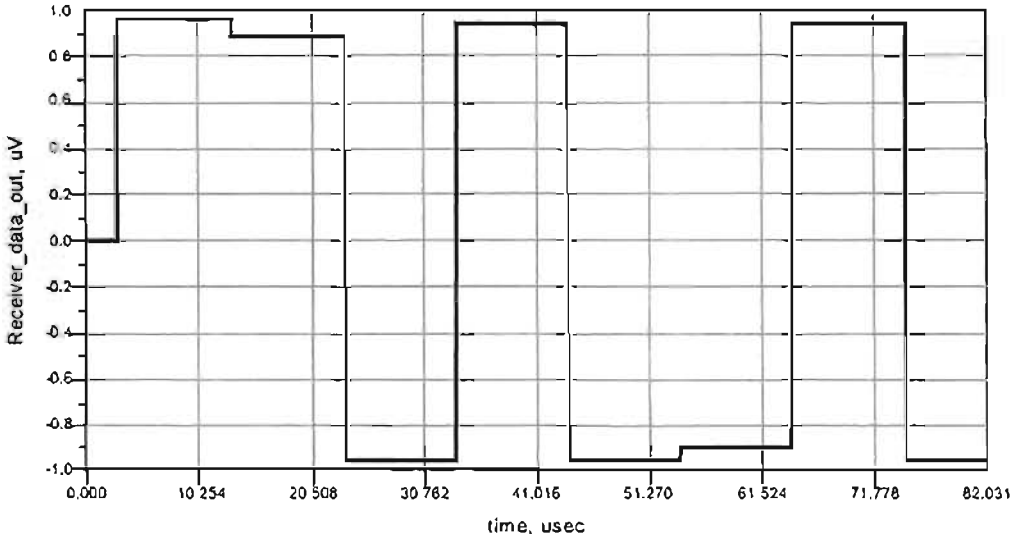

Fig. 4.22: Received NRZ data stream (11-11-1-11-1) after integration and dump and sample and hold (delayed by 8 chips)

4.7 Conclusion

This chapter has provided an understanding of CDMA. Its advantages over other multiple access schemes (such as FDMA and TDMA) were also highlighted. An overview on the fundamental process of filtering was also discussed. Finally, these concepts were reinforced by simulating a simple CDMA transceiver using ADS software. Here, signal waveforms for each stage of the transceiver chain were shown. The work presented here is a prerequisite for an understanding of the simulation models utilized in subsequent chapters.

CHAPTER 5

THE EFFECT OF INTERNALLY GENERATED RF COMPONENT NOISE ON DS-CDMA SYSTEM PERFORMANCE

5.1 Introduction

Now that the CDMA system and simulation model has been detailed, it is beneficial to examine certain aspects of the system in more detail. In the wireless communication industry, it is well known that the RF front-end transceiver is one of the key elements that determines the overall performance of the communication system. The noise generated within these systems contributes significantly to the total noise. The usually high operating frequencies that are part of mobile communication systems coupled with the fact that signal digitization and processing hardware are not commercially available for use at these frequencies, has inevitably led to the use of the mixer for frequency downconversion in the receiver. However, the mixer is the "noisiest" component in the RF front-end. It is thus common to find receivers with low noise amplifiers (LNAs) in the RF front-end stages. These optimize the most critical performance parameter, the noise figure. This quest for minimizing receiver noise (and hence the bit error rate) is usually achieved at the expense of a number of LNA stages. This chapter evaluates the impact of internally generated RF component noise in a simple DS-CDMA system with a view to identifying a method of quantifying the RF front-end component specifications for a given DS-CDMA system performance requirement.

5.2 Receiver noise and its characterization

Noise is a phenomenon inherent to all communication systems. It can be devastating in any communication system since it places a lower limit on the signals that can be detected and an upper limit on the amount of gain that can be used before distortion

occurs. The noise generated by electronic systems can be categorized as thermal noise, shot, flicker (1/f) noise and burst noise ([18],[61]). Most of the noise present at the input of a typical receiver consists of thermal and shot noise. Shot noise is proportional to the bias current in devices such as diodes, transistors, etc. For the sake of the noise characterization of devices and systems, only the combined effect of all internally generated noise will be considered. This combined noise effect is often referred to as the thermal noise (N_{th})of the system. It is proportional to temperature and bandwidth only as can be seen from Nyquist's equation [62]:

$$N_{th} = kTB \tag{5.1}$$

where N_{th} = thermal noise power in watts

T = absolute temperature in degrees Kelvin

=X °C + 273.15°

k = 1.38 X 10^{-23} watt/°K.Hz, Boltzmann's constant

B = bandwidth in Hz in which the measurement is made

For a noise source at room temperature (290K or 17°C), the noise power is −174dBm per Hertz of the system bandwidth. This thermal noise is characterized by a waveform that never repeats itself exactly i.e. it is purely random and, as predicted by the kinetic theory of heat, the power spectrum is flat with frequency. Since all frequencies are present in this thermal random noise, it is referred to as 'Johnson noise' or white noise due to an analogy with white light which has a uniform power distribution over the band of optical frequencies.

In many communication systems, the received signals are of low power and accompanied by noise. In these systems, the noise is generated within and outside the system. However, the noise generated within the system itself contributes a significant portion of the total noise, and in most cases, the internally generated noise is virtually the total noise [61]. Futher amplification is therefore necessary and this increases both signal and noise power levels. As the noise cannot be eliminated, it has been usual to use a criterion of performance, the ratio of signal power to noise power at various points in the system. This measure of system performance is not adequate in the case of certain active networks such as amplifiers or receivers. Consequently, it has been found necessary to use other criteria for measuring system performance.

The well-known concept of noise figure or noise factor F has thus been created to provide a standardized means of characterizing the internally generated noise of a system. In general, it measures the "noisiness" of a network which may be an amplifier or receiver by considering two signal-to-noise ratios, one at the input end and the other at the output of the network. This is illustrated in figure (5.1).

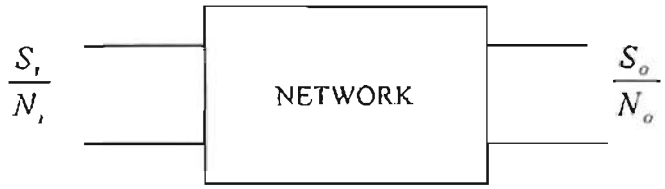

Fig. 5.1: Two port network

In terms of these quantities the noise factor F is widely defined as

$$F = \frac{S_i / N_i}{S_o / N_o}\Big|_{T_o=290K} \tag{5.2}$$

where S_i = input signal power

N_i = input noise power

S_o = output signal power

N_o = output noise power

From equation (5.2), it can be seen that the noise figure of the system or network is the degradation in the signal-to-noise ratio as a signal passes through the system. In defining the noise figure, a standard temperature of T_o=290K was adopted, originally by the IRE (forerunner of the IEEE), and this standard is widely accepted. Since the definition of F in equation (5.2) uses the signal-to-noise ratio at two different points in the system, it is sometimes more convenient to use an alternative expression obtained as follows:

$$F = \frac{S_i / N_i}{S_o / N_o} = \frac{N_o}{S_o / S_i \times N_i} \tag{5.3}$$

If G is the power gain of the network, then $G = S_o/S_i$ and also $N_i = N_{th} = kT_oB$. Hence

$$F = \frac{N_o}{GkT_oB} \tag{5.4}$$

In the above expression, N_o is the noise power output of the network, while GkT_oB is the noise power output of an ideal network i.e. a network which adds no further noise.

Thus the noise figure indicates the amount of noise generated in the device above the kT_oB thermal noise (referenced to a temperature of T_o = 290K).

The noise figure is also frequently expressed in terms of the internally generated noise N_e (equivalent noise power). N_e is the output noise power of the network when there is no noise power present at the input i.e. noise added by the system itself. Rearranging equation (5.2),

$$\begin{aligned} F &= \frac{S_i / N_i}{S_o / N_o} \\ &= \frac{S_i / N_i}{GS_i / N_o} \\ &= \frac{S_i / N_i}{GS_i /(N_e + GN_i)} \\ &= \frac{N_e + GN_i}{GN_i} \\ &= \frac{N_e + GkT_oB}{GkT_oB} \end{aligned} \tag{5.5}$$

It should be noted that the system noise figure is independent of the signal level as long as the system is levelled (constant gain).

The two-port network shown in figure (5.1) usually consists of a string of amplifiers and/or mixers as in the RF front-end of a typical communication system. In this instance, it would appear that every amplifier/mixer would degrade the signal-to-noise ratio by its noise figure. However, this is not the case. Each amplifier in a string of amplifiers produce a certain amount of noise over and above the thermal noise. As the input signal (and noise) is amplified, the signal becomes strong enough that the small amount of noise generated by succeeding stages adds relatively very little to the overall amount of noise. This concept leads to the familiar Friis' formula ([18], [61], [63]) for calculating the overall noise figure of a n-stage system:

$$F_{total} = F_1 + \frac{F_2 - 1}{G_1} + \ldots + \frac{F_n - 1}{G_1 G_2 \ldots G_{n-1}} \tag{5.6}$$

From equation (5.6) it can be seen that for a system processing very weak signals, F_{total} must be small in order to allow a high enough signal-to-noise ratio at the system output for the output signal to be detected. It is also observed that the noise figure of the first stage of the system F_1, contributes significantly to the overall noise figure, F_{total},

provided the gain G_1 in this stage is high. Hence it is necessary to have a low-noise and high-gain device as the first stage of a system processing weak signals.

5.3 System architecture and simulation work

In order to assess the effect that these RF components will have on system performance, it is necessary to simulate a complete CDMA transmit-receive system.

5.3.1 Transmitter architecture

Figure (5.2) shows the transmitter architecture for the proposed adaptive CDMA system.

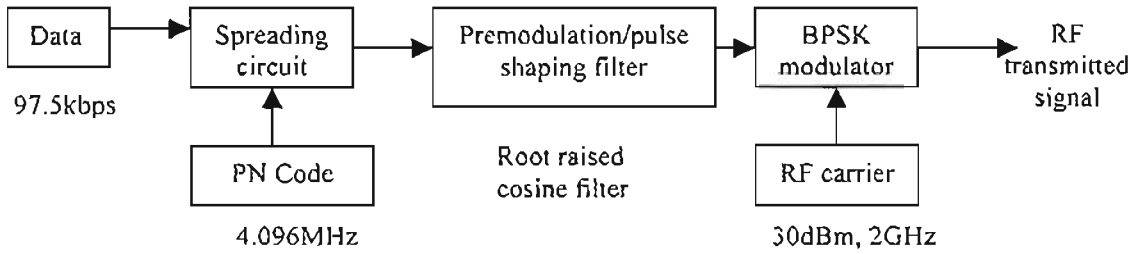

Fig. 5.2: Transmitter architecture

The transmitter system was configured as discussed in chapter 4. However, the power level of the 2GHz RF carrier was chosen to be 30dBm (1W) (not 10dBm as used previously). The transmitter utilizes a root raised cosine premodulation filter since the raised-cosine pulse is seen to have a faster spectral rolloff than rectangular pulses. Thus for a channel with a bandwidth wide enough to include the first lobe, transmitting raised cosine pulses will result in the reception of more power with less pulse distortion than for rectangular pulses. The receiver baseband filter would also consists of a similar (matched) root raised cosine filter as utilized in the transmitter.

5.3.2 Receiver architecture

This simulated transmitted signal is then injected into the RF front-end receiver where downconversion and demodulation are performed. Downconversion to an IF of 68MHz is performed using a mixer. The choice of this particular IF is based on an adaptive antenna system developed by Virginia Polytechnic Institute and State University [64]. It is envisaged that a system similar to that used in [64] will be used for signal digitization and baseband processing. Demodulation is performed on this IF

signal. Figure (5.3) shows the receiver architecture for the proposed adaptive CDMA system.

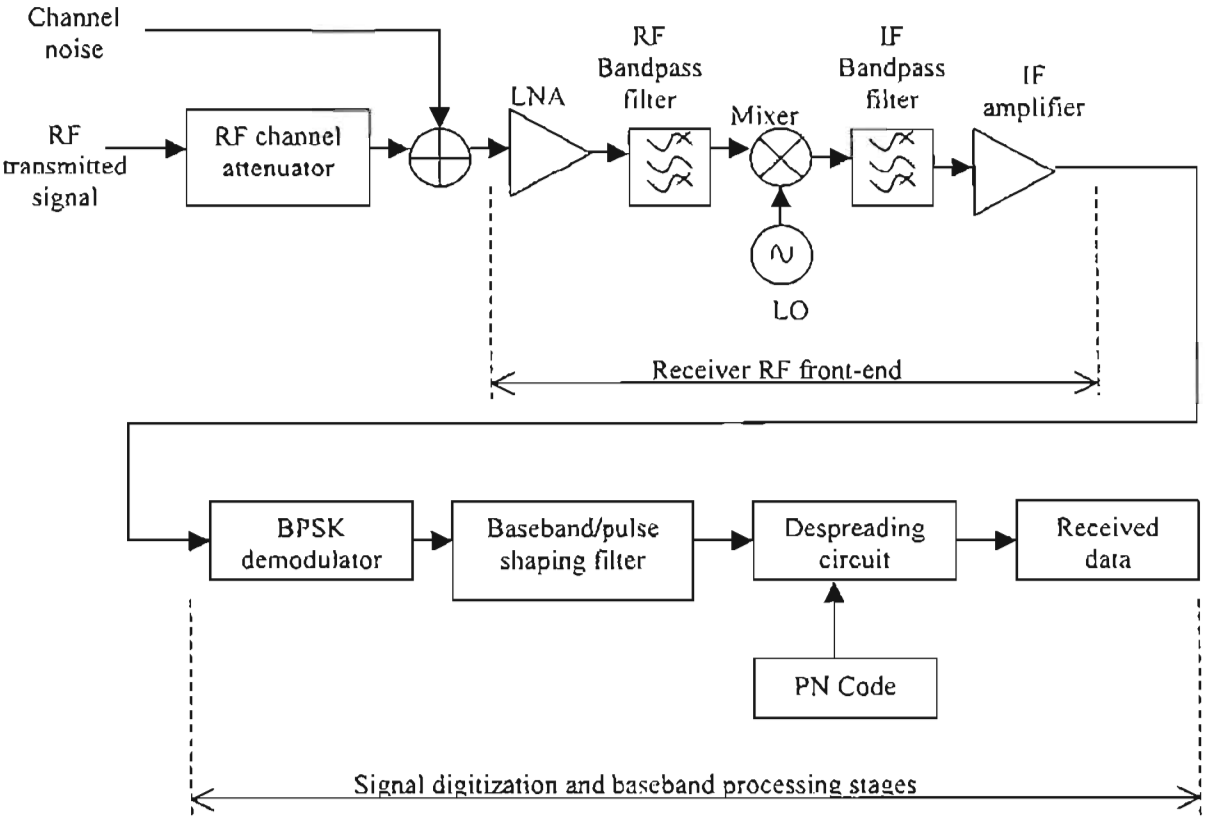

Fig. 5.3: Receiver architecture

5.3.2.1 Systematic analysis of receiver design

In receiver design, it is often advantageous to have *a priori* idea of the performance of each receiver component technology (specifications) before it is integrated. In order to assess the effect of internally generated RF component noise on the system, it is essential that the RF component specifications are known. The specifications of interest (noise figure and gain) can be traded-off to assess how a required system specification (such as the bit error rate) can be met. Table (5.1) lists the baseline specifications for each receiver RF front-end block in the proposed system. The specifications in table (5.1) are derived from a range of Avantek's RF and microwaves product catalogues. The RF LNA data is based on the AFT4231 wideband amplifier. It has a typical gain and noise figure of 12dB and 3.6dB, respectively over the 2 to 4GHz range. The RF and IF bandpass filters used are based on Avantek's AFP21851 and AFP41851 broadband YIG bandpass filters with maximum insertion loss of between 6 and 9dB with a 3dB minimum bandwidth of 20 MHz in the 1 to 18GHz

frequency range. The mixer noise figure is based on Avantek's UMX series mixers (TFX-72M) with conversion losses varying from 5 to 7dB. The IF amplifier used is based on the PPA-1043 that has a minimum gain and maximum noise figure of 10dB and 4dB, respectively over the 10MHz to 1GHz frequency range.

Receiver Block	NF (dB)	Gain (dB)
LNA	3	13
RF Bandpass filter	3	-3
Mixer	5	-5
IF Bandpass filter	3	-3
IF amplifier	4	10

Table 5.1: Baseline noise figure and gain for proposed receiver RF front-end

The overall noise figure of the baseline system using Friis' equation ([18], [61], [63]) is 5.478dB. It should be noted that 0.5 to 2dB tends to be the state of the art range of noise figures for solid state microwave receivers [18]. Currently, the noise figures of commercially available receiver front-ends for PCS, CDMA and FM systems produced by RF Microdevices (e.g. RF9906, RF9936 and RF9986), range from 2.5dB to 5.1dB. From figure (5.3), it can be seen that the 30dBm RF transmitted signal is directly coupled to the receiver front-end via an attenuator. The attenuator was included in the simulation since direct injection of the 30dBm RF signal into the front-end would not only drive the LNA, mixer and IF amplifier into compression but more importantly, would exceed the operating power rating of these devices thereby damaging them. Hence an attenuator with −120dB attenuation was used. Thus the signal power into the front-end is −90dBm (1pW or 7.071μV into 50Ω). The typical minimum and maximum RF sensitivity of an IS-55 receiver is −110dBm and −25dBm, respectively [65]. Thus the -90dBm signal power level is within the dynamic range or sensitivity range of typical wireless receivers. Channel noise power of approximately −100dBm was introduced into the receiver RF front-end to establish a SNR in the order of 10dB at the input of the LNA. A link budget analysis performed on an an IS-55 system uses a SNR of 13dB at the input of the receiver [65]. Thus the SNR of 10dB is a reasonable estimate for which the bit error rate would be determined after the simulation. It should be noted that this noise power is valid over a bandwidth of 24.576MHz which is the RF bandwidth or RF frequency span used by the ADS software. This bandwidth

is the reciprocal of the time step or sampling time (T_{step}) used by the software. The sampling time should be chosen such that $T_{step} < 1/f_m(\max)$ where $f_m(\max)$ is the highest baseband frequency component. In this instance, $f_m(\max)$ is the frequency of the chipped data (4.096MHz). Each chip was sampled 6 times (T_{step} = 40.69ns). The sampling time can be reduced but at the expense of a longer simulation run time. The baseband bandwidth or frequency span (after carrier demodulation) is 12.288MHz i.e. one half of the RF bandwidth.

5.4 BER Measurement methodology

A useful parameter that can be used to gauge the quality of a digital communication system is the probability of bit error (denoted either as P_e or BER). Most wireless voice systems can tolerate one bit error in every 1000 bits received (P_e=10^{-3}), before their performance is deemed unacceptable. Other applications, such as data transfer, demand a much lower P_e. Typical values of P_e in this instance are 10^{-8} to 10^{-10} for systems such as Ethernet and token ring networks [65].

ADS has two techniques for the computation of P_e. These are the Monte Carlo and the Improved Importance Sampling (IIS) ([66], [67], [68]) techniques. The Monte Carlo measurement technique is based on comparing test data (output data stream) to reference data (input data stream), symbol by symbol. However, a major disadvantage of this method is that the number of bits transmitted should be very large for a statistically significant P_e measurement to be made. The relative variance (VAR) of the P_e for N transmitted bits is:

$$VAR = \frac{(1 - P_e)}{N.P_e} \tag{5.7}$$

This implies that for a P_e of 10^{-6}, with a relative variance of 0.01, a sample size N of approximately 10^8 bits is required.

The probability of error was measured using the IIS technique [66], [67], [68]. The use of this technique is justified over the Monte Carlo technique since it requires a fewer number of bits to be simulated thereby reducing the simulation run time considerably. For example, using a QAM system with a P_e of 10^{-6}, a Monte Carlo simulation requires 10^8 simulation samples for a relative variance accuracy of 0.01.

For the IIS simulation, only 800 samples are needed for a similar accuracy [66]. However, the bit error rate sink in ADS utilizing this IIS technique, does not take into account external noise in the computation of the bit error rate. Instead, the user is required to have *a priori* knowledge of this information and express it in terms of the noise bandwidth, variance and ratio of energy per bit to noise power spectral density (E_b/N_o). Alternatively, the Monte Carlo method computes E_b/N_o using the formulae in equations (5.8) and (5.9) below. This value can then be used as one of the input parameters to the IIS measurement sink.

The P_e or BER is related to the signal-to-noise ratio (SNR) and the ratio of energy per symbol to the noise power spectral density (E_b/N_o). Both the SNR and E_b/N_o were computed at the output of the IF amplifier in figure (5.3) i.e. before demodulation. ADS uses the RF bandwidth ($1/T_{step}$) for the computation of these parameters. The following formulae are used in the simulation for the calculation of E_b and N_o:

$$E_b = P_{ESREF} T_b \tag{5.8}$$

Where E_b = Energy per bit

P_{ESREF} = source power in the reference RF signal (output of IF amplifier)

T_b = bit time

$$N_o = P_{ENREF} T_{step} \tag{5.9}$$

Where N_o = one-sided power spectral density of the bandlimited white noise in W/Hz

P_{ENREF} = noise signal power at output of IF amplifier

T_{step} = simulation time step

$$SNR = \frac{P_{ESREF}}{P_{ENREF}} \tag{5.10}$$

or in terms of E_b/N_o,

$$\frac{E_b}{N_o} = \frac{P_{ESREF} T_b}{P_{ENREF} T_{step}} = SNR \frac{T_b}{T_{step}} \tag{5.11}$$

Thus, with knowledge of the SNR value, the E_b/N_o value can be calculated. In [57] the processing gain (G_p) is related to the SNR and E_b/N_o value by the following equation,

$$\frac{E_b}{N_o} = SNR \times G_p \tag{5.12}$$

In order to be consistent with the standard definition of E_b/N_o in terms of the processing gain [57], it is appropriate that equation (5.11) be scaled by a factor of 6 (7.782dB). This effectively reduces the simulation bandwidth from 24.576MHz to the spread bandwidth of 4.096MHz. A further discussion on this scaling and other ADS simulation issues are provided in appendix A.4.

5.5 Simulation results and analysis

Simulation results for different front-end scenarios are shown in figures (5.4) to (5.20). The lookup table (table (5.2)) provides a quick reference to these simulation plots, showing varied and constant parameters.

Figure number	LNA NF (dB)	LNA gain (dB)	Mixer NF (dB)
5.4 – 5.8	3	3 –13 (variable parameter)	5
5.9 – 5.13	3 –13 (variable parameter)	13	5
5.14 – 5.18	3	13	5 –15 (variable parameter)
5.19 and 5.20	Comparison of system with LNA (LNA NF = 3dB and LNA gain = 13dB) and without LNA		5-15 (variable parameter)

Table 5.2: Lookup table showing constant and varied parameters of figures (5.4) to (5.20)

The obvious trend from these results is that an increase in component noise figure causes the BER, E_b/N_o and SNR to decrease, and vice-versa. Also, an increase in component gain (up to the gain that produces device saturation and compression) causes a decrease in BER, E_b/N_o and SNR. It should be noted that the SNR values are computed at the output of the IF amplifier i.e. before demodulation.

From figure (5.4), LNA gain in the range 3dB to 13 dB produce BERs between 7.6×10^{-12} and 7.5×10^{-3}. E_b/N_o values range between 13.9dB and 20.8dB for this range of LNA gain (figure (5.5)). A SNR value of –2.5dB was obtained for the lower limit

of LNA gain (3dB) while a SNR of 4.4dB was obtained for a 13dB upper limit LNA gain (figure (5.6)).

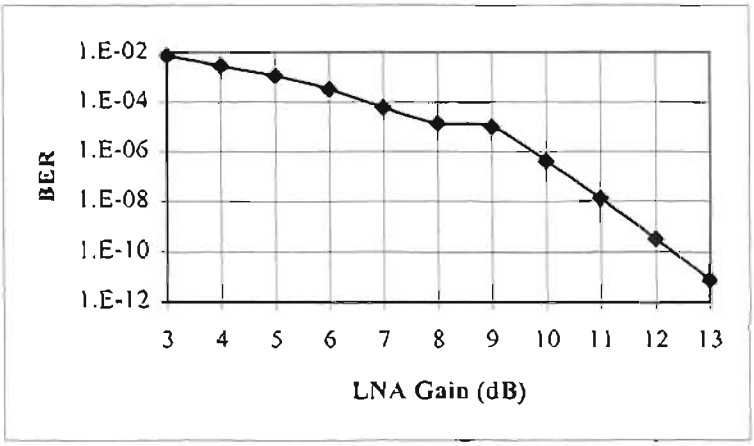

Fig. 5.4: LNA gain versus BER (LNA NF=3dB)

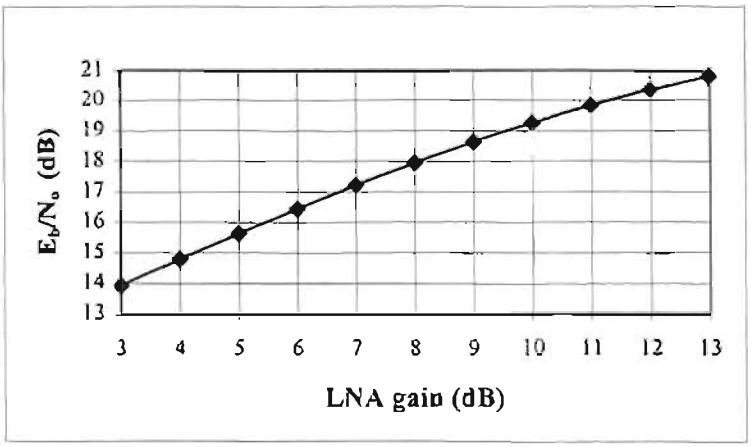

Fig. 5.5: LNA gain versus E_b/N_o (LNA NF=3dB)

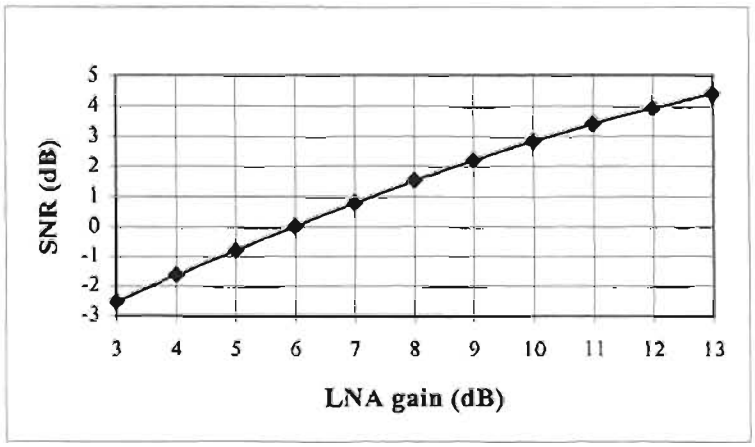

Fig. 5.6: LNA gain versus SNR (LNA NF=3dB)

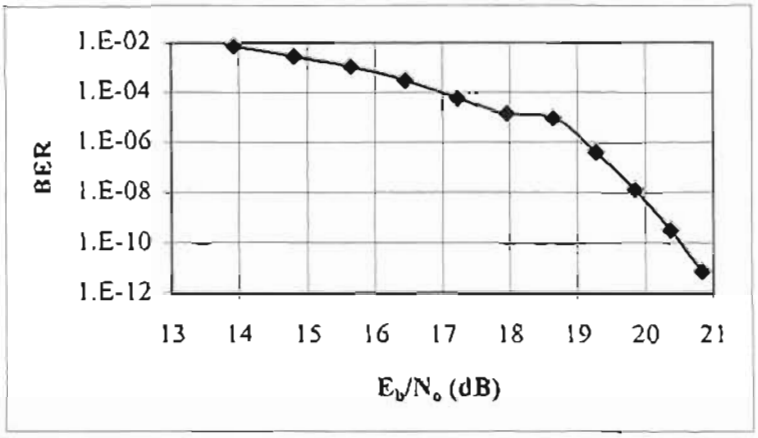

Fig. 5.7: E_b/N_o versus BER for varying LNA gain (3 to 13dB) (LNA NF=3dB)

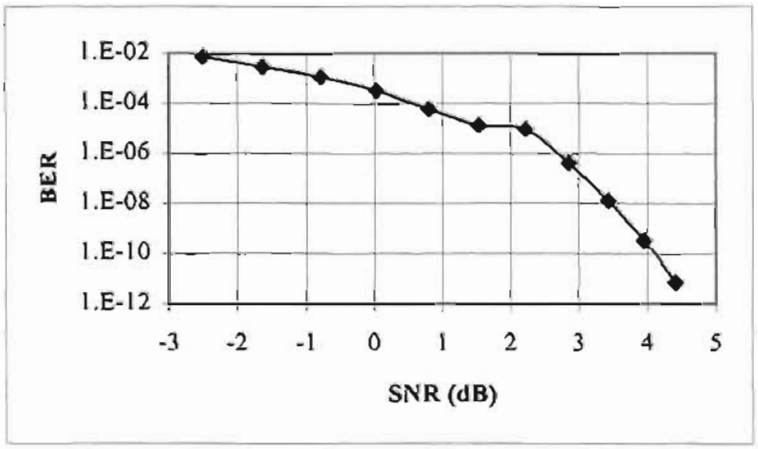

Fig. 5.8: SNR versus BER for varying LNA gain (3 to 13dB) (LNA NF=3dB)

Figure (5.9) shows a plot of LNA noise figure versus BER where it can be seen that for a LNA gain of 13dB and an unreasonably high noise figure of 13dB, the BER is 12.9×10^{-3} while the BER is 7.6×10^{-12} for a typical noise figure of 3dB. The E_b/N_o values range between 13dB and 20.8dB for noise figures between 3dB and 13dB (figure (5.10)). The SNR degrades from 4.4dB to –3.4dB with an increase in LNA noise figure from 3dB to 13dB (figure (5.11)).

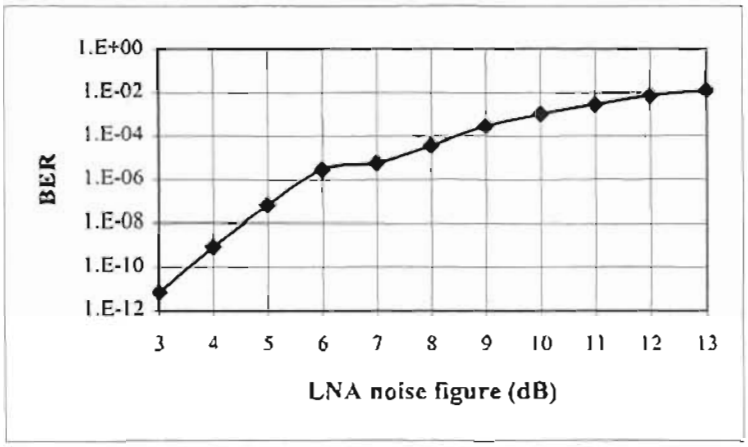

Fig. 5.9: LNA noise figure versus BER (LNA gain=13dB)

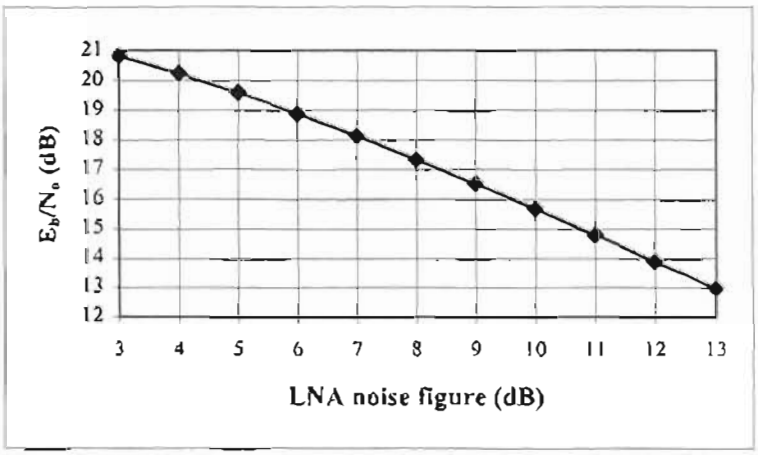

Fig. 5.10: LNA noise figure versus E_b/N_o (LNA gain=13dB)

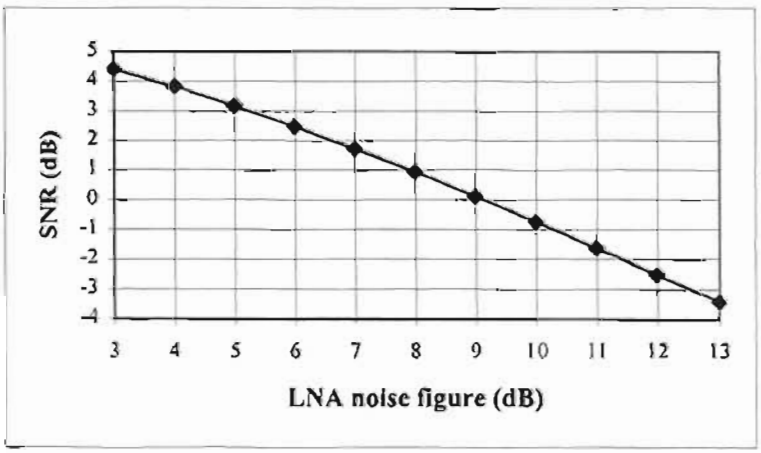

Fig. 5.11: LNA noise figure versus SNR (LNA gain=13dB)

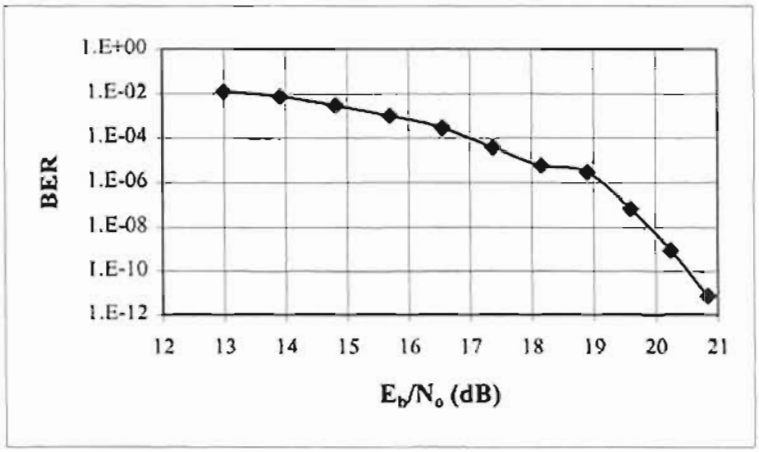

Fig. 5.12: E_b/N_o versus BER for varying LNA noise figure (3 to 13dB) (LNA gain=13dB)

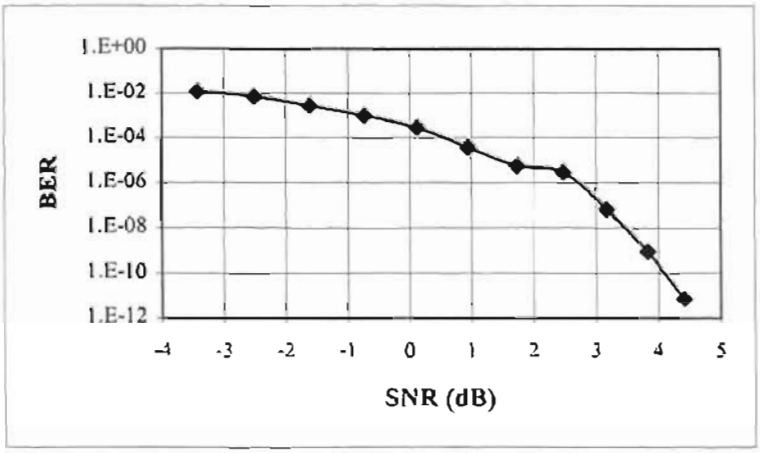

Fig. 5.13: SNR versus BER for varying LNA noise figure (3 to 13dB) (LNA gain=13dB)

It is commonly recognized that the selection of the mixer design topology dominates the receiver chain performance ahead of the LNA [65]. The mixer performance consideration is emphasized by the need to provide good local oscillator (LO) leakage isolation while maintaining a good balance between the front-end noise figure and intermodulation isolation [65]. Figure (5.14) shows a plot of mixer noise figure versus BER. The mixer noise figure is swept from 5dB to 15dB, in the range of typical noise figures of diode mixers. This range of mixer noise figures produce BERs between $7.6\text{x}10^{-12}$ and $7.7\text{x}10^{-3}$. Also, E_b/N_o values between 20.8dB and 13.8dB are obtained for this range of mixer noise figures (figure (5.15)). A degradation in SNR from 4.4dB to –2.6dB is produced as result of this increase in the mixer noise figure (figure (5.16)).

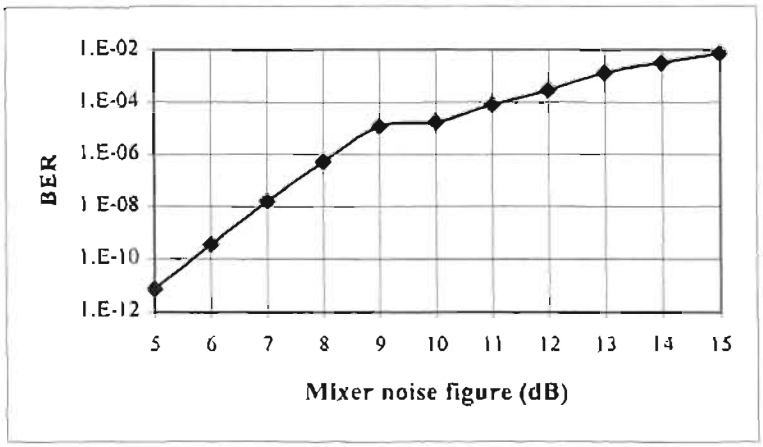

Fig. 5.14: Mixer noise figure versus BER (LNA gain=13dB and LNA NF=3dB)

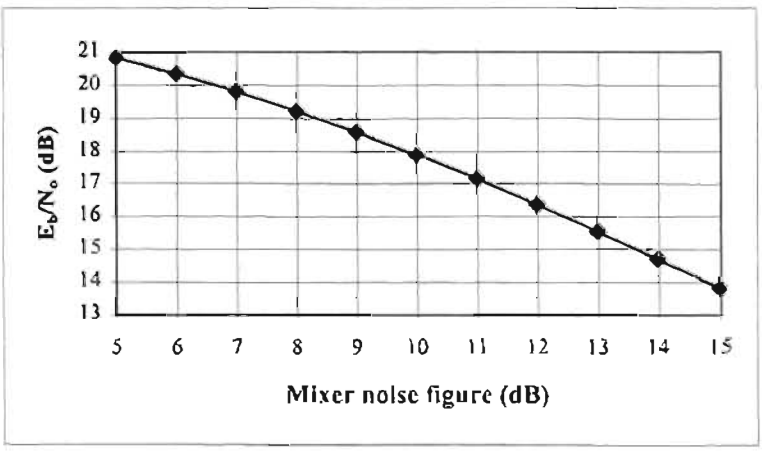

Fig. 5.15: Mixer noise figure versus E_b/N_o (LNA gain=13dB and LNA NF=3dB)

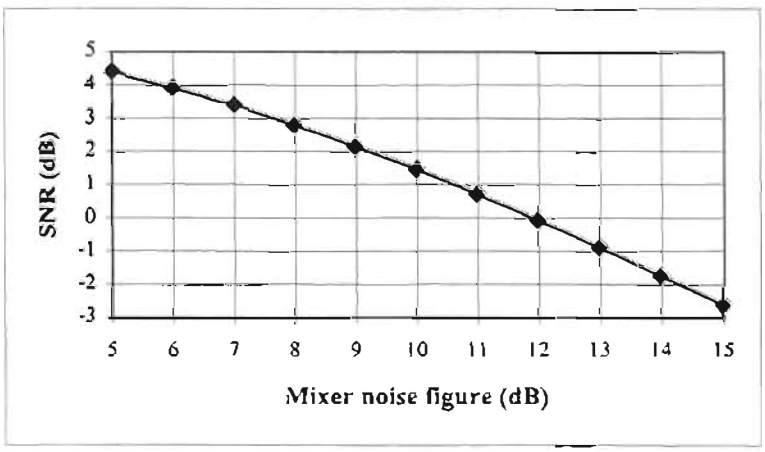

Fig. 5.16: Mixer noise figure versus SNR (LNA gain=13dB and LNA NF=3dB)

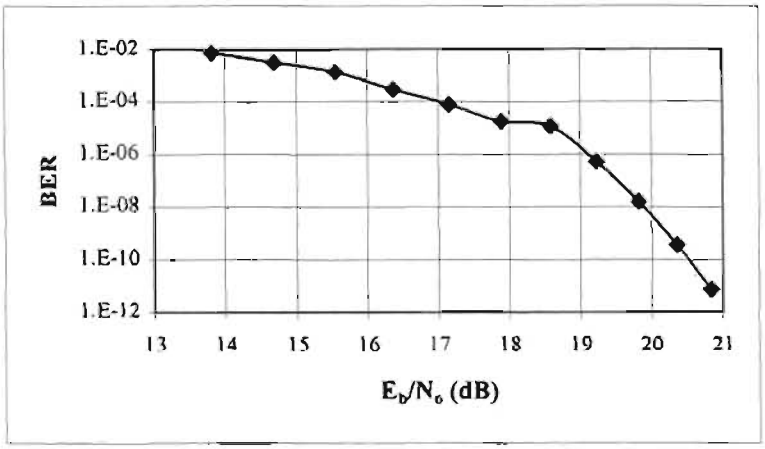

Fig. 5.17: E_b/N_o versus BER for varying mixer noise figure (5 to 15dB) (LNA gain=13dB and LNA NF=3dB)

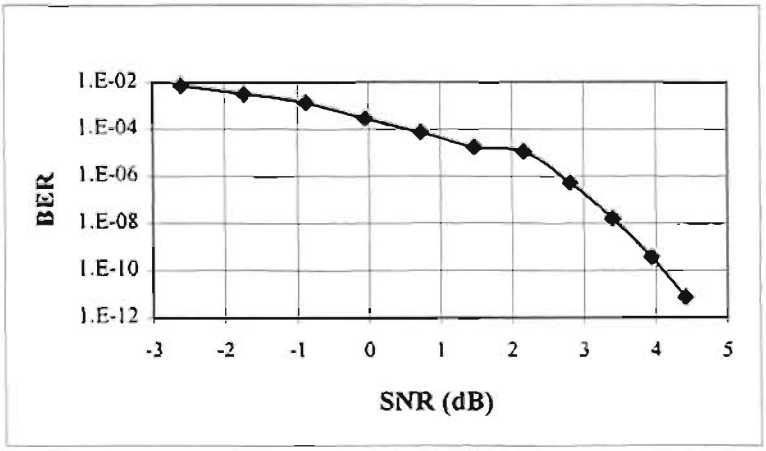

Fig. 5.18: SNR versus BER for varying mixer noise figure (5 to 15dB) (LNA gain=13dB and LNA NF=3dB)

As previously mentioned, the mixer noise figure is swept from 5dB to 15dB, in the range of typical noise figures of diode mixers. Diode mixers are passive components and consequently exhibit conversion loss. Typical conversion losses of diode mixers are between 6dB to 9dB [69]. This loss has a number of consequences: the greater the loss, the higher the noise of the system, and the more amplification is needed. High loss also indirectly leads to distortion because of high signals that result from the additional preamplifier gain required to compensate for this loss. It also adds to the cost of the system since the low-noise amplifier stages are usually expensive [65]. In a passive mixer, the noise figure is usually equal to, or only a few tenths of one decibel above, the conversion loss. In this sense, the mixer behaves as if it were an attenuator having a temperature equal to or slightly above the ambient. Diode mixers are the highest-frequency low-noise microwave components in existence: at high frequencies

a diode mixer is the only mixing device available. To the author's knowledge, low noise transistor amplifiers (LNAs) are unavailable above 120GHz, and receivers having mixer front-ends exhibit superior performance than than those using LNAs at frequencies above approximately 100GHz [70]. Virtually all such receivers employ Schottky-barrier diodes. In active mixers, the noise figure cannot be related easily to the conversion efficiency. In general, it cannot even be related qualitatively to the device's noise figure when used as an amplifier. The noise figure of an active FET mixer depends strongly on its design [65].

Active FET mixers have several advantages and disadvantages when compared to diode mixers. Most significantly, an active mixer can achieve conversion gain, while diode and other passive mixers always exhibit loss. This allows a system using an active mixer to have one or fewer stages of amplification, thus simplifying the front-end, thereby reducing its size and cost. However, generally, the distortion levels of well-designed active mixers are comparable to those of diode mixers. Paradoxically, it is easy to achieve good conversion efficiency in active mixers even when the design is poor. Thus it has been quoted in [65] that active mixers having good conversion gain but poor noise figures or high distortion. As a result, active FET mixers have gained a reputation for low performance. For active FET mixers, typical values for the conversion gain are of the order of 6 to 10dB (single-ended mixer) or 3-5dB (balanced mixer) with minimum noise figures of 4-6dB (single-ended mixer) or 6-8dB (balanced mixer) (LO and RF in the X-band (8-12GHz), IF=30MHz) [69].

Equation (5.6) theoretically confirmed the importance of an LNA to establish the system noise figure. Figures (5.19) and (5.20) emphasizes the importance of an LNA at the front-end. It can be observed in figures (5.19) and (5.20) that in both cases (system with and without LNA), an increase in the mixer noise figure causes an increase in the BER and a decrease in E_b/N_o and SNR.

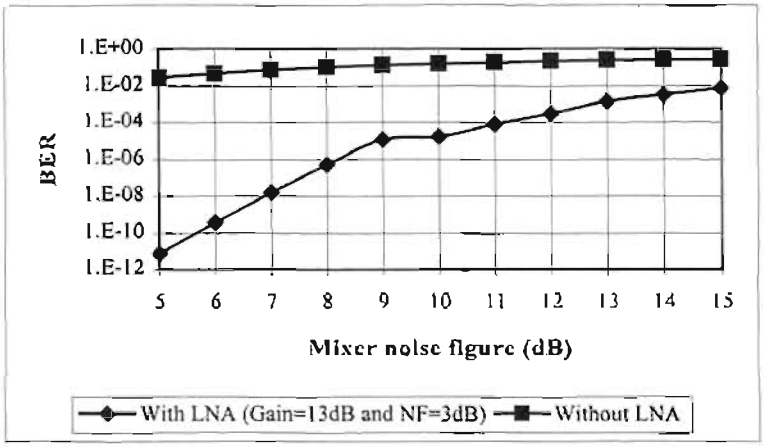

Fig. 5.19: Comparison of mixer noise figure versus BER for system with and without LNA

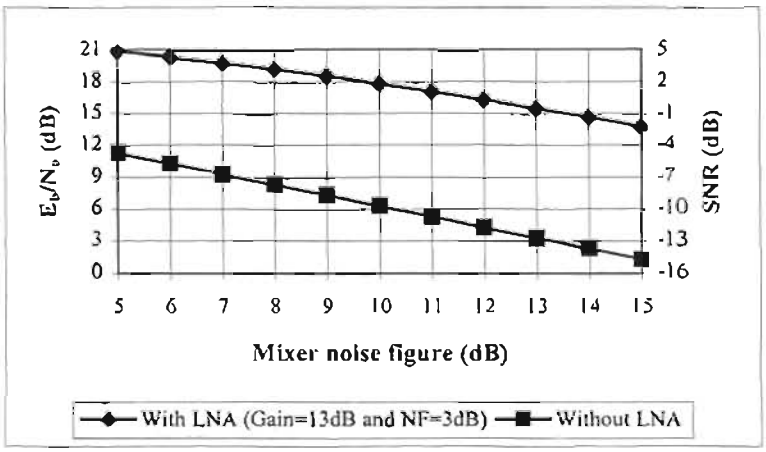

Fig. 5.20: Comparison of mixer noise figure versus E_b/N_o and SNR for system with and without LNA

For the proposed system utilizing an LNA, the BERs are between 7.7×10^{-3} and 7.6×10^{-12} for mixer noise figures (or conversion losses) in the range 5dB to 15dB. However, without an LNA, the BERs range from 2.8×10^{-2} to 2.7×10^{-1} for the same range of mixer noise figures. For the proposed system (utilizing a mixer with 5dB conversion loss/noise figure), E_b/N_o and SNR improvements of 9.53dB are obtained over the same system without an LNA. Also E_b/N_o and SNR improvements in the range 9.53dB to 12.51dB are obtained for mixer noise figures from 5dB to 15dB.

An expression for SNR improvement, which quantifies how much the SNR is improved by adding an LNA between the antenna and the radio, is derived in [57]. Since CDMA has reverse-link power control, the improvement in SNR is manifested in the reduction of mobile transmit power. This is intuitive because if there is an

improvement in SNR, reverse power control would command the mobile to power down so that the mobile transmit power is just enough to achieve the desired link SNR. As a result, the battery life-span of the mobile unit is increased.

5.6 Concluding remarks

The impact of internally generated RF component noise on a DS-CDMA system (via simulation) was investigated. The conclusions of this investigation are clear: Firstly, the importance of an LNA at the receiver front-end was established. For the proposed system (processing gain of 42) the use of an LNA yielded a BER below 10^{-11} while without an LNA the BER was more significant ($2.8\text{x}10^{-2}$). Secondly, it can be concluded that the use of commercially available RF components in the front-end do not cause severe BER degradation in a single-user DS-CDMA system. In a worst-case, highly improbable scenario, an LNA gain as low as 3dB and noise figure as high as 13dB produce BERs of $7.5\text{x}10^{-3}$ and $12.9\text{x}10^{-3}$, respectively for a modest processing gain of 42.

Thus far a system block diagram was established to ensure demodulation of a very weak –90dBm contant-level signal i.e. disregarding a change in the received signal strength. A change in the received signal strength can cause distortion to a complete wiping off and loss of the information. Variations in signal strength occurs when the receiver is a mobile. Large buildings and underpasses will greatly attenuate the signal. In reality, such signal strength variations require the receiver to incorporate automatic signal-level control or automatic gain control (AGC) in either the RF LNA or the IF amplifer. In the case of the receiver being a base station, this near-far effect is eliminated by power control (which is synonymous to AGC) ([1], [57], [60]).

CHAPTER 6

THE IMPACT OF LOCAL OSCILLATOR GENERATED PHASE NOISE ON DS-CDMA PERFORMANCE

6.1 Introduction

The local oscillator (LO) is often considered as being part of the mixer and is a common building block in wireless communication systems, since it provides precise reference frequencies for modulation/demodulation and frequency conversion.

Often the noise induced by the LO is classified as internally generated mixer noise. However, the LO induces amplitude (AM) noise, phase noise and spurious signals. An ideal oscillator or frequency synthesizer will produce a perfectly pure sinusoidal signal. The amplitude, phase and frequency of the source would not change under varying loading, bias or temperature conditions. However, such an ideal circuit is impossible to realize in practice. Therefore performance measures such as the amplitude noise, phase noise and spurious responses are used to characterize the deviation from the ideal.

The focus of this chapter is on the impact of LO generated phase noise on DS-CDMA performance. However, LO spurious signals and amplitude noise are briefly discussed.

6.2 Internally generated spurious signals

Local oscillators also cause spurious signals which are unwanted frequency components in the LO signal that are converted to the IF or simply leak through the mixer into the IF circuit. These spurious signals are applied to the mixer along with the LO and, depending on their frequencies, may be converted to a frequency within the IF band. The most serious problems arise when the spurious signals are within the RF

passbands; in this case the downconverted spurious signals may be much stronger than the RF signals. For example, consider a mixer having an RF input of –100dB, and a LO having an RF frequency spurious signal that is 60dB below the LO signal. Assuming a conversion loss of 7dB, the IF output level of the desired signal is –107dB. If the LO level is 10dBm, the spurious signal level is –50dBm. With 7dB conversion loss plus 20dB rejection due to mixer balance, the spurious IF signal is –77dBm or 30 dB above the desired output.

The source of such "spurs" is the frequency synthesizer used to generate the LO. Avoiding spurious signals requires careful selection of frequencies not only in the receiver front-end, but also in the LO synthesizer. Any frequency used in the synthesizer represents a potential spurious signal in the LO output. The use of a high IF frequency will allow effective LO filtering. The IF amplifier bandwidth should be kept as narrow as possible, so that spurs outside the IF passband are not amplified to the level where they might saturate the IF amplifier or generate intermodulation components.

6.3 Amplitude (AM) noise

AM noise which is generated by the LO source is injected into the mixer along with the LO signal. This noise is severe when the LO signal is generated at a low level and amplified.

A mixer's LO signal can be generated in many ways. The simplest is to use some type of oscillator operating directly at the LO frequency. In some cases, the LO signal is generated initially at a subharmonic of the desired LO frequency and multiplied to the desired frequency. The frequency multiplier often requires a high input level, and it is necessary to amplify the original subharmonic signal substantially. Amplifying the LO adds a certain amount of noise. This noise is AM noise; it consists of variations in the amplitude of the LO signal and can be treated as an additive noise process. When the noisy LO signal is applied to the mixer, its AM noise components at the RF and image frequencies are downconverted and appear at the IF port just as if they had been applied to the RF input. Therefore, the mixer noise temperature (or noise figure) is increased by an amount, depending on the type of mixer used, may be as high as the

LO noise temperature. If no measures are taken to eliminate the LO noise, the increase in the mixer's noise temperature may be very great.

The AM LO noise can be reduced by straight-forward techniques to a level where it is insignificant. The IF frequency is picked up high enough so that the RF and image frequencies are well separated from the LO frequency, so the noise at these frequencies can be removed effectively by filtering. The IF frequency should typically be at least 5% to 10% of the LO frequency if it is expected that AM noise will have to be removed by filtering. This may require a trade-off with IF amplifier noise temperature, since amplifier noise temperatures generally rise with frequency.

The general form of the expression for the output wave from a noisy oscillator can be written as

$$V(t) = \left[V_O + \varepsilon(t)\right]\cos\left[2\pi f_O t + \varphi(t)\right] \tag{6.1}$$

where f_o = nominal oscillation frequency

V_o = nominal oscillation amplitude

$\varepsilon(t)$ = fluctuations in amplitude

$\phi(t)$ = fluctuations in phase

Equation (6.1) indicates there is a concentration of noise power surrounding the RF local oscillator signal. A typical spectral distribution of such a signal is shown in figure (6.1).

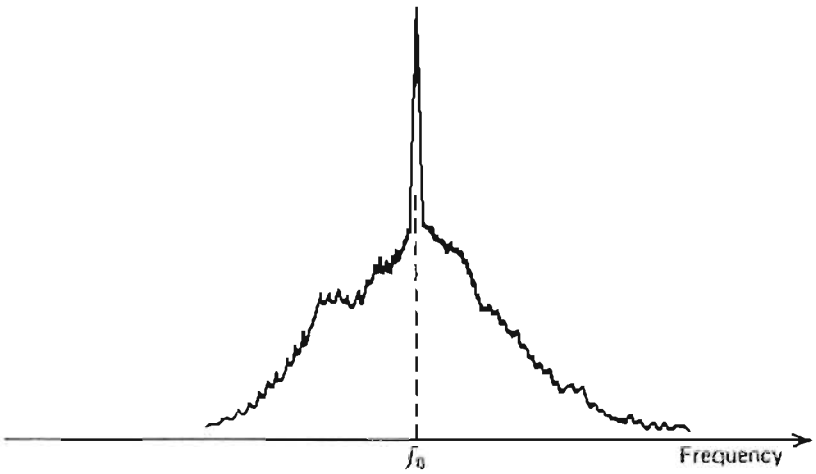

Fig. 6.1: Noise spectrum of a RF local oscillator signal (from [71])

In general, both the AM noise and FM or phase noise, $\varepsilon(t)$ and $\phi(t)$, respectively are present, accounting for the lack of symmetry in the envelope of the spectrum. The AM

noise component in this instance is negligible when compared to the phase/frequency noise component [72]. Thus it is often neglected in the analysis of phase noise.

6.3.1 Analysis

6.3.1.1 Sinusoidal modulation

With the phase noise component $\phi(t) = 0$, equation (6.1) can be rewritten as

$$V(t) = \left[V_o + \varepsilon(t)\right]\cos\left(2\pi f_o t\right) \tag{6.2}$$

Letting $\varepsilon(t) = \varepsilon_o \cos(\omega_{AN} t)$, equation (6.2) can be written as

$$\begin{aligned} V(t) &= \left[V_o + \varepsilon_o \cos(\omega_{AN} t)\right]\cos(\omega_o t) \\ &= V_o \cos(\omega_o t) + \varepsilon_o \cos(\omega_{AN} t)\cos(\omega_o t) \\ &= V_o \cos(\omega_o t) + \frac{\varepsilon_o}{2}\left[\cos(\omega_o + \omega_{AN})t + \cos(\omega_o - \omega_{AN})t\right] \end{aligned} \tag{6.3}$$

where $\omega_{AN} = 2\pi f_{AN}$ is angular frequency of modulation and $\omega_o = 2\pi f_o$ is the angular oscillation frequency.

The spectrum of a sinusoidally amplitude-modulated sinusoidal signal consists of three unmodulated sinusoidal signals located at three frequencies: f_o, $f_o - f_{AN}$, $f_o + f_{AN}$ (figure (6.2))

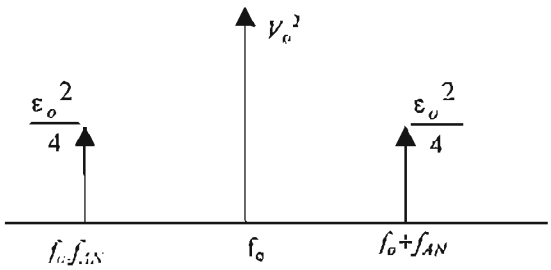

Fig. 6.2: Spectrum of sinusoidally amplitude-modulated sinusoidal signal

The vectorial representation of this consists of a vector of amplitude V_o rotating at ω_o and two vectors of amplitude $\varepsilon_o/2$ rotating at $\omega_o + \omega_{AN}$ and $\omega_o - \omega_{AN}$, whose resultant is collinear with V_o (figure (6.3)).

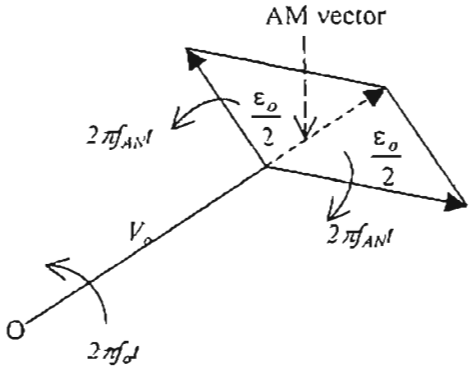

Fig. 6.3: Vector representation of sinusoidally amplitude-modulated sinusoidal signal

The maximum signal power is:

$$P_{max} = \frac{P_o}{V_o^2}\left[V_o + 2\left(\frac{\varepsilon_o}{2}\right)\right]^2 \tag{6.4}$$

The minimum signal power is:

$$P_{min} = \frac{P_o}{V_o^2}\left[V_o - 2\left(\frac{\varepsilon_o}{2}\right)\right]^2 \tag{6.5}$$

The fluctuation in power is then

$$\Delta P = P_{max} - P_{min} = \frac{8P_o\varepsilon_o}{2V_o} \tag{6.6}$$

6.3.1.2 Modulation by noise

By assuming that the modulating signal is noise of spectral density $S(f_{AN})$, the spectrum can be broken down into elementary components separated by differences in frequency of f_{AN} and each located within a frequency band Δf (figure (6.4)).

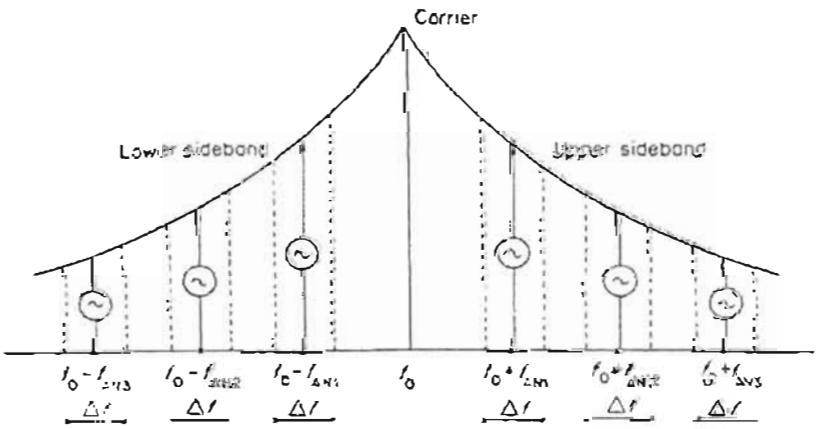

Fig. 6.4: Representation of a wave modulated by noise (from [69])

The noise power can then be represented in each frequency band by a sinusoidal generator with a frequency equal to that of the centre of the band concerned and with an amplitude proportional to $\sqrt{2S(f_{AN})\Delta f}$ (the proportionality coefficient takes account of the modulation of the oscillator by the noise). The general spectrum will have the form shown in figures (6.2) and (6.3), but there will be many vectors rotating with angular velocities distributed uniformly in a continuum. The above relationships are then valid for each equivalent generator and thus for the entire noise modulation.

Measurement of AM noise is generally achieved by applying the complete spectrum to a square-law detector of sensitivity S which produces fluctuations in steady voltage corresponding to the fluctuations of power produced by the noise. The voltage fluctuations then undergo standard low-frequency treatment for noise measurement. If $S = \Delta V/\Delta P$ and if an index for AM noise is defined by:

$$AM\ noise\ index = \frac{Noise\ power\ in\ the\ sidebands}{Power\ in\ the\ carrier} \tag{6.7}$$

$$\text{or}\quad AM\ noise\ index = 10\log_{10}\left[\frac{(\Delta V_{eff}/SP_o)^2}{4}\right] \tag{6.8}$$

in dB with respect to the carrier (dBc). The index is given in $dBcHz^{-1}$.

6.4 Phase noise

Present-day technology demands signal sources with better frequency stability for systems such as doppler radars, data communication links and multichannel receivers. Characterizing the randomness of frequency stability is a common requirement for all these systems. Phase noise is the term most widely used to describe this characteristic.

The analysis of the effect of phase noise in OFDM (Orthogonal Frequency Division Multiplexing) systems ([73], [74]) and a MC-CDMA (Multicarrier CDMA) system ([75]) has been presented. In [75], an analytical procedure was developed to evaluate the impact of carrier frequency offset and phase noise on the performance of a MC-CDMA system. The investigation in [75] concluded that phase noise introduces a spurious phase rotation on the useful signal and also introduces interchannel interference which is primarily responsible for performance degradation. It has also been concluded in [75] that MC-CDMA is very sensitive to the signal distortion

generated by the imperfect frequency downconversion at the receiver due to the local oscillator phase noise and frequency offset. The work presented in this section looks at the effect of phase noise on a simple DS-CDMA system thereby allowing evaluation of the degree of stability required of the oscillators to guarantee a moderate bit error rate performance degradation. An RF perspective is adopted in the analysis and representation of phase noise.

6.4.1 Effects of phase noise

Local oscillator sources always have a certain amount of phase jitter or phase noise which is transferred degree for degree via the mixer to the received signal. Because the mixer subtracts not only the LO and RF frequencies but also their phases, the local oscillator's phase noise is transferred directly to the received signal. This noise may be very serious in communication systems using either digital or analog phase modulation. In phase or frequency shift modulation systems, this phase jitter is demodulated along with the received signal. The trouble-some phase-noise components are usually close to the LO frequency, usually within 1MHz, which corresponds to modulation rates. These noise components arise from low frequency noise processes within the oscillator, such as 1/f noise in solid-state devices. Unfortunately, these noise components are very large. Because they are so close to the LO frequency, direct filtering is rarely a practical way to eliminate them. Phase noise can be minimized by careful design of the LO source. Phase noise in an oscillator is proportional to the inverse square of its resonator Q, so considerable improvement can be attained through the use of a cavity-or-dielectric-resonator-stabilized oscillator [70]. Crystal oscillators have low phase noise and are often used with a multiplier chain to generate microwave LO signals. However, frequency multiplication (which is in reality phase multiplication) enhances phase noise spectral density as the square of the multiplication factor, so high-order multiplication of a noisy source should be avoided. Phase noise is worse in higher frequency oscillators [72]. The usually high operating frequencies that are part of mobile communications has required a corresponding increase in local oscillator frequencies in upconverters and downconverters. Since phase noise is worse in higher frequency oscillators, there is thus a need to minimize this noise by careful design of the LO source.

The effects of receiver-LO phase noise are understood by considering the process of reciprocal mixing. This is an effect that occurs in all mixers, yet despite its name, reciprocal mixing is a LO, not a mixer, problem. The modulation on the mixer output (IF) is the combined modulations of the inputs. This means that modulating a receiver's local oscillator is indistinguishable from using a clean local oscillator and having the same modulation present on all incoming signals. The noise components of the LO are extra LO signals that are offset from the carrier frequency. Each of them mixes other signals that are appropriately offset from the LO carrier into the receiver's IF. Noise is the sum of an infinite number of infinitesimal components spread over a range of frequencies, so the signal it mixes into the IF are spread into an infinite number of small replicas, all at different frequencies. This amounts to scrambling these other signals into noise. It is tedious to look at the effects of receiver LO phase noise this way. The concept of reciprocal mixing provides an easier alternative that gives accurate results.

A poor oscillator can have significant noise sidebands extending out many tens of kilohertz on either side of its carrier. This is the same, as far as the signals in the receiver IF are concerned, as if the LO was clean and every signal entering the mixer RF input had these noise sidebands. Not only will the wanted signal (and its noise sidebands) be received, but the noise sidebands added by the LO to signals near, but outside, the receiver's IF passband will overlap it. In a multi-user system, each of many signals present will add its set of noise sidebands. The effect is cumulative. This produces the appearance of a high background-noise level on the spectrum band. Figure (6.5) illustrates this effect of phase noise in the receiver LO.

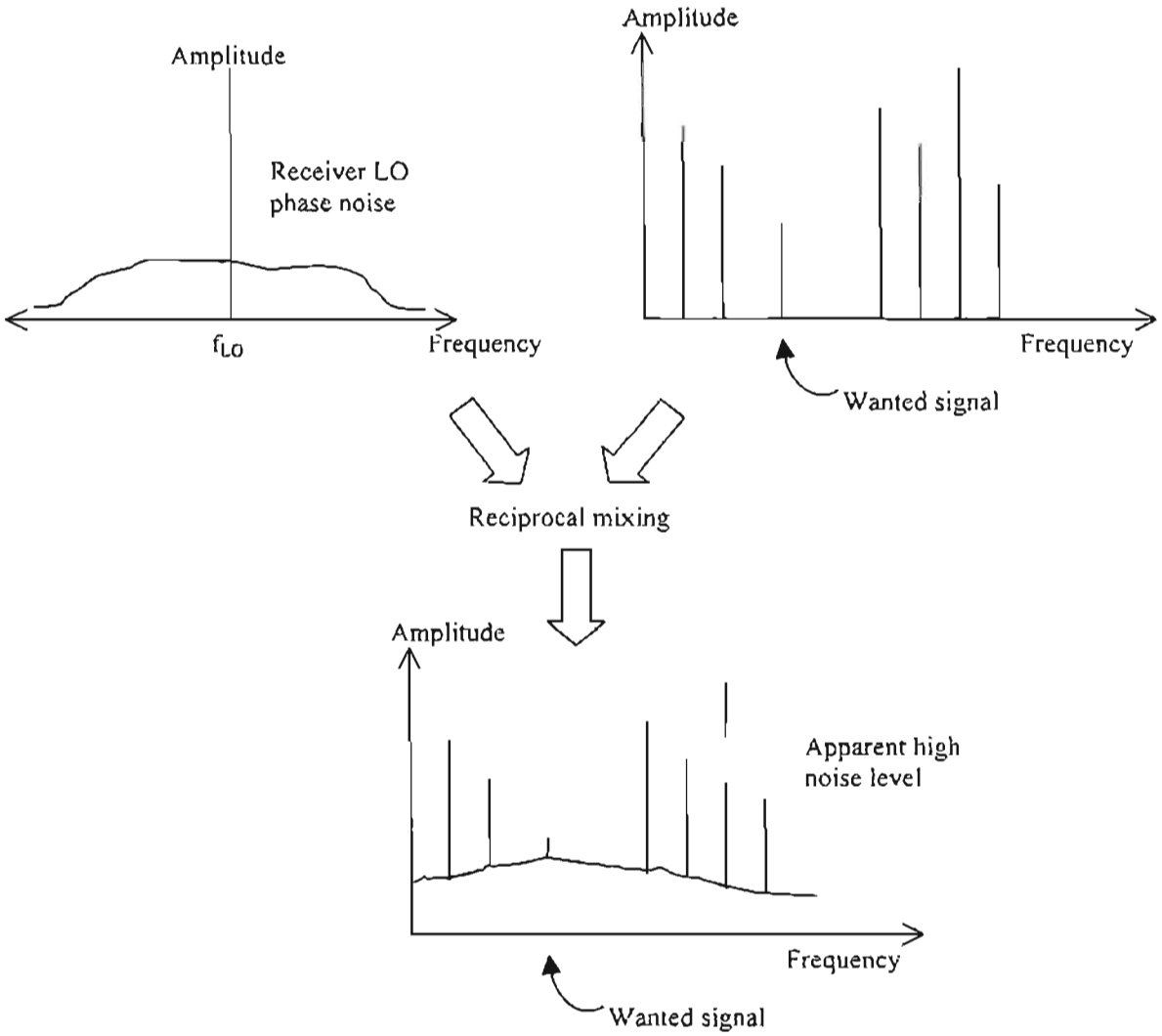

Fig. 6.5: Illustration of the effects of phase noise in the receiver LO

Thus, the phase noise is one of the limiting factors on determining how closely spaced (in the frequency domain) two communication channels can be.

6.4.2 Phase noise analysis and representation

In section (6.3) it was mentioned that the local oscillator spectrum consists of both amplitude (AM) and FM or phase noise that accounted for the lack of symmetry in the envelope of the spectrum. The AM portion of the signal is typically smaller than the FM portion and is usually neglected in the analysis/calculation of phase noise. The reason for this is that the oscillator output is often fed into some form of limiter that strips off AM components [72]. This is analogous to the function of the limiting IF amplifier in a FM receiver that removes any AM on incoming signals. The limiter is like a circuit that converts the signal to logic levels. For example, a diode ring mixer may be driven by a sine-wave LO of moderate power, yet this signal drives the diodes

hard-on and hard-off, approximating square-wave switching. This is a form of limiter, and it removes the effect of any AM on the LO. For these reasons, AM noise sidebands are rarely a problem in oscillators, and so are normally ignored. However, the analysis is relatively straightforward and was performed in section (6.3.1). To escape repetition, this section would just discuss the dominant FM component.

Figure (6.6) shows the symmetrical spectrum of a local oscillator as a result of phase noise. P_s is the LO signal power, P_{SSB} is the LO single sideband noise power while f_m is the offset frequency (also called the modulating frequency) from the centre frequency f_o. The output power is not concentrated exclusively at the carrier frequency alone. Instead it is distributed around it, and the spectral distribution on either side of the carrier is known as spectral sidebands.

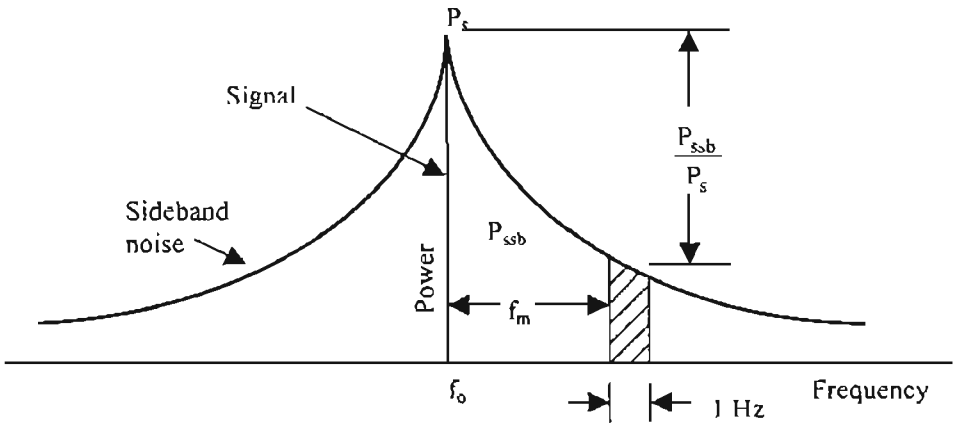

Fig. 6.6: Phase noise specification of frequency source. The noise is contained in the sidebands around the signal frequency at f_o (from [65])

6.4.2.1 Sinusoidal modulation

Phase noise can be represented as frequency or phase modulation of the carrier signal. Frequency modulation (FM) is a process of producing a wave whose instantaneous frequency varies as a function of the instantaneous amplitude of a modulating wave at a rate given by the frequency of the modulating source. A FM signal can be described by writing equation (6.1) as

$$V(t) = V_o \cos(2\pi f_o t + \phi_m \sin \omega_m t) \tag{6.9}$$

where the fluctuation in phase, $\phi(t)$ *is* $\phi_m \sin(\omega_m t)$ and the fluctuation in amplitude, $\varepsilon(t)$ is 0 (AM noise is zero). ω_m is the modulating angular frequency. The instantaneous

angular frequency ω is obtained by taking the time derivative of the cosine terms of equation (6.9):

$$\begin{aligned}\omega &= \frac{d}{dt}(2\pi f_o t + \phi_m \sin w_m t) \\ &= 2\pi f_o + \omega_m \phi_m \cos 2\pi f_m t\end{aligned} \tag{6.10}$$

or in terms of the instantaneous frequency f,

$$\begin{aligned}f &= \frac{1}{2\pi}\omega \\ &= f_o + f_m \phi_m \cos 2\pi f_m t\end{aligned} \tag{6.11}$$

The frequency variation Δf is given by

$$\begin{aligned}\Delta f &= f - f_o \\ &= \phi_m f_m \cos 2\pi f_m t\end{aligned} \tag{6.12}$$

so that the maximum frequency variation Δf_{max} is

$$\Delta f_{max} = \phi_m f_m \tag{6.13}$$

Δf_{max} is the maximum swing of the carrier from its mean or nominal frequency, f_o.

Hence $$\phi_m = \frac{\Delta f_{max}}{f_m} \tag{6.14}$$

ϕ_m is known as the peak phase deviation or modulation index. Expanding equation (6.9) gives

$$V(t) = V_o \cos(\omega_o t)\cos(\phi_m \sin \omega_m t) - V_o \sin(\omega_o t)\sin(\phi_m \sin \omega_m t) \tag{6.15}$$

If the modulation factor is small ($\phi_m << 1$ or $\phi_m << \pi/2$) as in the case of noise and narrowband FM),

$$\cos(\phi_m \sin \omega_m t) \cong 1$$

$$\sin(\phi_m \sin \omega_m t) \cong \phi_m \sin \omega_m t$$

hence

$$\begin{aligned}V(t) &= V_o \cos(\omega_o t) - V_o \phi_m \sin(\omega_o t)\sin(\omega_m t) \\ &= V_o \cos(\omega_o t) - \frac{V_o \phi_m}{2}\cos(\omega_o - \omega_m)t + \frac{V_o \phi_m}{2}\cos(\omega_o + \omega_m)t \\ &= V_o \cos(\omega_o t) - \frac{V_o \Delta f_{max}}{2 f_m}\cos(\omega_o - \omega_m)t + \frac{V_o \Delta f_{max}}{2 f_m}\cos(\omega_o + \omega_m)t\end{aligned} \tag{6.16}$$

Equation (6.16) indicates that the spectrum of a narrowband FM wave consists of the carrier plus two components, one on each side of the carrier (figure (6.7)).

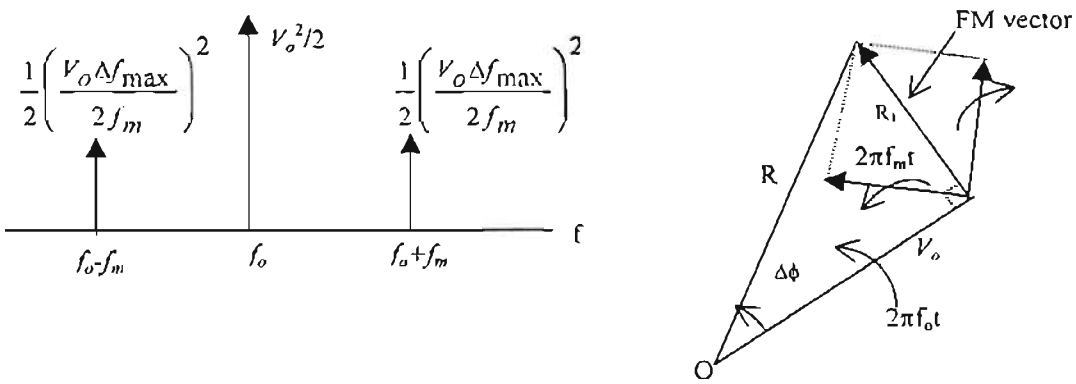

Fig. 6.7: Spectrum and vector representation of a FM wave

Thus, as for an AM signal, a FM signal with a small modulation factor is the sum of three sinusoidal signals located at frequencies f_o, f_o-f_m, f_o+f_m (figure (6.7)). In this sense, narrowband FM is equivalent to AM and cannot be distinguished from it by test equipment that is not capable of identifying the phase of a signal, such as spectrum analyzers. However, it is important in system evaluation and in measurement of spurious outputs and noise to distinguish between AM and FM waves: in the case of AM, the carrier envelope varies with the modulating signal, whereas the frequency of the AM wave remains unchanged; in FM, the carrier amplitude is constant, and the carrier instantaneous frequency varies with the modulating signal. However, the signal for which the frequency is lowest is in phase opposition to that for which the frequency is highest. From the vectorial representation, the carrier of amplitude V_o rotates at the angular velocity ω_o, while two vectors of amplitude $\Delta f_{max}/2f_m$ rotate at angular velocities $\omega_o + \omega_m$ and $\omega_o - \omega_m$ with an initial phase difference of π. They thus give a resultant vector R_1 perpendicular to the carrier. The phase fluctuation $\Delta\phi$ is given by:

$$\Delta\phi \approx \tan\phi = \frac{R_1}{V_o} \tag{6.17}$$

$$\Delta\phi_{max}^2 = \frac{R_{1\,max}^2}{V_o^2} = \frac{P_{2SB}}{P_o} = max\ FM\ noise\ power\ in\ sidebands\ /\ P_o \tag{6.18}$$

and thus [69]
$$\Delta f_{eff} = \sqrt{\frac{2f_m^2 P_{2SB}}{P_o}} \tag{6.19}$$

where Δf_{eff} is the effective or RMS frequency deviation, P_o is the power of the carrier f_o and P_{2SB} is the double sideband noise power.

6.4.2.2 Modulation by noise

All the relationships obtained previously are valid for a modulation signal consisting of noise, with the same considerations about the frequency distribution of the modulation generators as in the AM case.

Phase modulation (PM) and frequency modulation (FM) are closely related. Phase is the integral of frequency, so phase modulation resembles frequency modulation in which deviation decreases with increasing modulating frequency. From equations (6.12) and (6.13), the frequency variation (Δf) and maximum frequency variation (Δf_{max}) is $\phi_m f_m \cos 2\pi f_m t$ and $\phi_m f_m$, respectively. From equation (6.9), the phase deviation is $\phi_m \sin w_m t$ corresponding to a maximum phase deviation of ϕ_m. Thus with a sinusoidal modulating signal, it makes no difference whether one speaks of phase or frequency deviation because the two are related by the rate of modulation described by equation (6.14), i.e. $\phi_m = \frac{\Delta f_{max}}{f_m}$.

FM noise power is represented as a ratio of the power in some specified bandwidth (usually 1Hz) in one sideband to the power in the carrier itself. These ratios are usually specified in the quantity of dBc/Hz at some frequency offset from the carrier. As shall be seen later in this section, the entire noise power can be integrated over a specified bandwidth to realize a total angular error in the output of the oscillator. The calculation of the angular error from the FM noise performance is relatively straightfroward. A useful way of rating the FM (or PM) of a signal in synthesizer systems is to give the number of decibels by which the level of the one-sided FM/PM component is below the carrier, or

$$\text{single sideband - to - carrier ratio (dB)} = 10\log_{10}\left(\frac{\text{single sideband power}}{\text{carrier power}}\right) \quad (6.20)$$

From equation (6.16), it can be seen that the single sideband-to-carrier voltage ratio is

$$\text{single sideband - to - carrier voltage ratio} = \left(\frac{\frac{\varphi_m V_o}{2}}{V_o}\right) \quad (6.21)$$

The power ratio in the quantity of dBc/Hz at some offset frequency f_m from the carrier, commonly denoted as $L(f_m)$, is the square of equation (6.21),

$$L(f_m) = 10\log_{10}\left(\frac{\varphi_m}{2}\right)^2 \quad (6.22)$$

It should be noted that the units of dBc/Hz for $L(f_m)$ represent the sideband level in decibels relative to 1 rad^2 per unit bandwidth. Using the relation $\phi_m = \frac{\Delta f_{max}}{f_m}$, the following alternative expressions for $L(f_m)$ can be derived,

$$L(f_m) = 10\log_{10}\left(\frac{\Delta f_{max}}{2f_m}\right)^2 \tag{6.23}$$

$$L(f_m) = 10\log_{10}\left(\frac{\Delta f_{RMS}}{\sqrt{2}f_m}\right)^2 \tag{6.24}$$

For convenience, this expression is usually written as

$$L(f_m) = 20\log_{10}\left(\frac{\Delta f_{RMS}}{\sqrt{2}f_m}\right) \tag{6.25}$$

Since $\phi_m = \sqrt{2}\phi_{RMS}$, $L(f_m)$ can be written in terms of RMS phase deviation,

$$L(f_m) = \frac{\varphi_{RMS}^2}{2} \qquad (\text{rad}^2/\text{Hz}) \tag{6.26}$$

$$\text{or } L(f_m) = 10\log_{10}\left(\frac{\varphi_{RMS}^2}{2}\right) \qquad (\text{dBc/Hz}) \tag{6.27}$$

Phase noise is also expressed as the one-sided spectral density of phase fluctuations (denoted $S_\phi(f_m)$),

$$S_\varphi(f_m) = 2L(f_m) = \varphi_{RMS}^2 \tag{6.28}$$

Stability measurements with frequency comparators give the spectral density of frequency fluctuations,

$$S_{\Delta f}(f_m) = \Delta f_{RMS}^2 \qquad (\text{Hz}^2/\text{Hz}) \tag{6.29}$$

To relate the spectral density of frequency fluctuations to the spectral density of phase noise or phase fluctuations, recall from equation (6.11) that

$$\Delta f(t) = \frac{1}{2\pi}\frac{d\Delta\phi(t)}{dt} \tag{6.30}$$

By using the Fourier transform relation $\Im\left[\frac{d^n x(t)}{dt^n}\right] = (j2\pi f)^n X(f)$, $\Delta f(t)$ can be transformed into the frequency domain,

$$\Delta f(f_m) = f_m \Delta\varphi(f_m) \tag{6.31}$$

Using the relation $\Delta f_{RMS} = \phi_{RMS} f_m$ (derived from equation (6.13)) and substituting into equation (6.29),

$$\begin{aligned} S_{\Delta f}(f_m) &= \Delta f_{RMS}{}^2 \\ &= \varphi_{RMS}{}^2 f_m{}^2 \\ &= f_m{}^2 S_{\varphi}(f_m) \end{aligned} \tag{6.32}$$

To normalize the instantaneous frequency deviation to the carrier frequency f_o, define

$$\begin{aligned} y(t) &= \frac{\Delta f(t)}{f_o} \\ &= \frac{1}{2\pi f_o}\frac{d\phi(t)}{dt} \\ &= \frac{1}{\omega_o}\frac{d\phi(t)}{dt} \end{aligned} \tag{6.33}$$

Transforming equation (6.33) into the frequency domain,

$$y(f_m) = \frac{\Delta f(f_m)}{f_o} \tag{6.34}$$

Another standardized definition of phase noise is the spectral density of fractional frequency fluctuations $S_y(f_m)$ where the instantaneous RMS frequency deviation Δf_{RMS} is normalized to the carrier frequency f_o [71], [76], [77]. $S_y(f_m)$ is related to the spectral density of frequency fluctuations, $S_{\Delta f}(f_m)$ and spectral density of phase fluctuations, $S_\phi(f_m)$, by

$$\begin{aligned} S_y(f_m) &= y^2(f_m) \\ &= \frac{1}{f_o{}^2} S_{\Delta f}(f_m) \\ &= \frac{f_m{}^2}{f_o{}^2} S_{\phi}(f_m) \\ &= \frac{2 f_m{}^2}{f_o{}^2} L(f_m) \end{aligned} \tag{6.35}$$

In many cases, however, it is not the spectral density of the modulating source that is of interest but rather the actual sideband power of phase fluctuations with respect to the carrier level.

To illustrate the principles involved, consider the case of a single sideband-to-carrier ratio of –60dBc/Hz measured at 100Hz offset-from-carrier frequency. Using equation (6.25),

$$-60 = 20log_{10}\left(\frac{\Delta f_{RMS}}{\sqrt{2} f_m}\right)$$

or

$$10^{-3} = \frac{\Delta f_{RMS}}{\sqrt{2} \times 100}$$

or

$$\Delta f_{RMS} = 0.1414\text{Hz}$$

In terms of maximum phase deviation (equation (6.22)),

$$-60 = 10\,log_{10}\left(\frac{\varphi_m}{2}\right)^2$$

$$10^{-3} = \frac{\phi_m}{2}$$

$$\varphi_m = 2\times10^{-3} \text{ rad.}$$

The FM noise spectrum $S_y(f_m)$ of a RF signal is shown in figure (6.8).

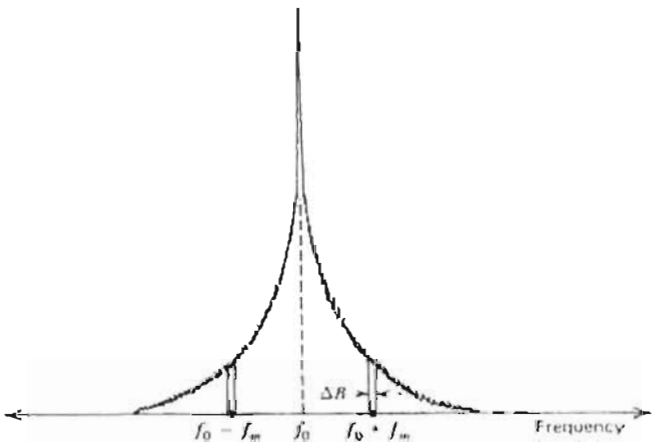

Fig. 6.8: Phase noise spectrum of a frequency source (from [71])

The spectrum is considered to be one-sided on a per hertz basis. The function $S_y(f_m)$ has the dimensions of Hz^{-1}. Although the noise distribution on each side of the signal is continuous, the spectrum can be subdivided into a large number of strips of width ΔB located f_m distance away from the signal f_o, and view the energy in ΔB as being caused by a sinusoidal frequency-modulating signal with a deviation proportional to the amplitude of the spectrum at f_m. It is assumed that ΔB is much smaller than f_m so that the envelope of the noise spectrum is flat within ΔB, though it may have 1/f or any other characteristic in the vicinity of f_m. This amounts to treating a continuous noise spectrum as if it consisted of a very large number of sinusoidal FM sideband

components symmetrically distributed about the signal so that, when all the equivalent sinusoidal voltages are added on a power or root-sum-square basis, the same total mean power as the actual noise spectrum is produced. This analogy is based on the assumption that contributions from amplitude modulation to the noise spectrum considered are negligible compared to those from frequency modulation.

The minimum resolution bandwidths of most spectrum analyzers are greater than 1Hz thereby restricting phase noise measurements to be performed in a bandwidth different from the specified bandwidth of 1Hz. If the equivalent single sideband noise-to-signal ratio was measured in a bandwidth different from 1Hz, the conversion from a single sideband ratio in x Hz bandwidth, ΔB_x, to $L(f_m)$ is expressed as

$$L(f_m) \cong \left.\frac{\text{single sideband noise power}}{\text{signal power}}\right|_{\Delta B_x} - 10\log_{10}(\Delta B_x) \quad \text{dBc/Hz} \tag{6.36}$$

In general, the conversion of a single sideband-to-signal ratio (in dB) from a bandwidth ΔB_1 to a bandwidth ΔB_2 is accomplished as

$$\left.\frac{\text{single sideband noise power}}{\text{signal power}}\right|_{\Delta B_2} = \left.\frac{\text{single sideband noise power}}{\text{signal power}}\right|_{\Delta B_1} - 10\log_{10}\left(\frac{\Delta B_1}{\Delta B_2}\right) \quad \text{dBc/Hz} \tag{6.37}$$

For the RMS frequency deviation (in Hz) this conversion is

$$\Delta f_2 = \Delta f_1 \sqrt{\frac{\Delta B_2}{\Delta B_1}} \tag{6.38}$$

Equations (6.36) to (6.38) apply to the noise-like content of the spectrum only. The power of a discrete FM sideband component is independent of the bandwidth of measurement.

Leeson [78] has developed an accurate and widely used model that describes the origins of phase noise in oscillators and frequency synthesizers. This model is depicted in figure (6.9) where it can be seen that there are four distinct regions of phase noise [71], [76].

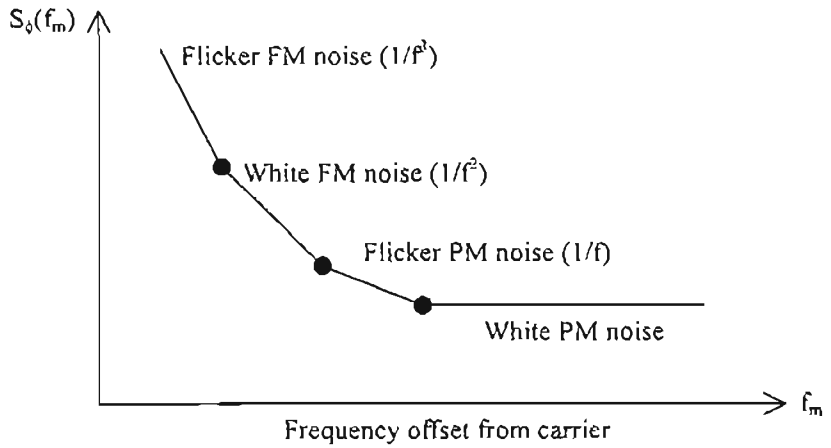

Fig. 6.9: Regions of phase noise

The lowest frequency region is dominated by flicker FM noise, which is device flicker noise that causes a random frequency modulation. This has a slope of $1/f^3$. The next region is denoted by white FM noise, which is white noise that causes a random frequency modulation. This has a slope of $1/f^2$. The third region is called flicker PM noise, which is modelled by flicker noise that mixes up to the oscillation frequency. This has a slope of 1/f. The last region is called white PM noise, which is simply white noise that mixes up to the oscillation frequency. This has the typical flat white-noise floor.

If the envelope of the predicted noise spectrum in the region of interest is approximated by n straight line segments with more than one slope, the spectrum derivation is achieved by successive approximations. Several curves representing various single phase noise-to-signal ratios in 1Hz bandwidth are plotted, each curve is integrated over the specified frequency band, and the curve that when integrated, satisfies the total noise requirement is selected as the synthesizer specification. Each line segment is integrated individually and the sum of noise powers for each curve is computed. If the envelope of the predicted spectrum is approximated by one line segment, a straightforward way of arriving at the envelope of the noise spectrum may be employed: The phase noise variance σ^2 (single sideband phase noise-to-signal ratio) is approximated by,

$$\sigma^2 = \int_{f_1}^{f_2} S_\phi(f_m)\,df_m \tag{6.39}$$

where $S_\phi(f_m)$ spectral density of phase fluctuations in dBc/Hz (i.e. decibels below $1\text{rad}^2/\text{Hz}$), f_1=low end of frequency band (Hz) and f_2=high end of frequency band (Hz).

Following Rohdes [76] analysis on the power law model for phase noise spectral density (figure (6.9)),

$$S_\phi(f_m) = Kf_m^{\,x} \tag{6.40}$$

Equation (6.40) can be reorganized as a straight line equation by taking the logarithmic values on both sides of the equation,

$$\log S_\phi = x \log f_m + \log K \tag{6.41}$$

The gradient of the line segment x and the antilog of the intercept point K, can be easily found by knowing 2 consecutive points $(dBc_1\ f_1)$ and $(dBc_2\ f_2)$ of the phase noise spectral density profile.

$$x = \frac{dBc_2 - dBc_1}{10(\log f_2 - \log f_1)} \tag{6.42}$$

$$\begin{aligned} K &= 10^{\left(\frac{dBc_1}{10} - x\log f_1\right)} \\ &= \frac{10^{\frac{dBc_1}{10}}}{f_1^{\,x}} \end{aligned} \tag{6.43}$$

The phase noise variance can then be,

$$\begin{aligned} \sigma^2 &= \int_{f_1}^{f_2} S_\phi(f_m)\,df_m \\ &= \int_{f_1}^{f_2} Kf_m^{\,x}\,df_m \\ &= \frac{K}{x+1}\left[f_2^{\,x+1} - f_1^{\,x+1}\right] \quad \text{for } x \neq -1 \end{aligned} \tag{6.44}$$

or

$$\begin{aligned} \sigma^2 &= \int_{f_1}^{f_2} S_\phi(f_m)\,df_m \\ &= \int_{f_1}^{f_2} Kf_m^{\,x}\,df_m \\ &= K\left[\ln f_2 - \ln f_1\right] \quad \text{for } x = -1 \end{aligned} \tag{6.45}$$

Since $\log_{10} f = \ln f / \ln 10$, equation (6.45) can be written as

$$\sigma^2 = K\left[\log f_2 - \log f_1\right] \quad \text{for } x = -1 \tag{6.46}$$

in which the constant $\ln 10$ is incorporated into the constant K.

It can be seen that the variance contains complicated expressions of x and K. A simple logarithmic manipulation and substituting $x = -1$ allows the following expressions to be derived:

By substituting (6.43) into (6.46), gives

$$\sigma^2 = 10^{\frac{dBc_1}{10}} f_1 \left[\log \frac{f_2}{f_1} \right] \quad \text{for } x = -1 \tag{6.47}$$

substituting (6.43) into (6.44) for the case of $x \neq -1$, gives

$$\begin{aligned} \sigma^2 &= \frac{10^{\frac{dBc_1}{10}}}{x+1} \left[f_2^{x+1} - f_1^{x+1} \right] \\ &= \frac{f_1}{x+1} \left[\left[\frac{f_2}{f_1} \right]^{x+1} - 1 \right] 10^{\frac{dBc_1}{10}} \quad \text{for } x \neq -1 \end{aligned} \tag{6.48}$$

Thus, the total variance σ_T^2 for n line segments is

$$\begin{aligned} \sigma_T^2 &= \sum_{i=1}^{n} 10^{\frac{dBc_i}{10}} f_1 \left[\log \frac{f_{i+1}}{f_i} \right] \quad \text{for } x = -1 \\ \sigma_T^2 &= \sum_{i=1}^{n} \frac{f_i}{x+1} \left[\left[\frac{f_{i+1}}{f_i} \right]^{x+1} - 1 \right] 10^{\frac{dBc_i}{10}} \quad \text{for } x \neq -1 \end{aligned} \tag{6.49}$$

where

$$x = \frac{dBc_{i+1} - dBc_i}{10(\log f_{i+1} - \log f_i)}$$

Using equation (6.49), the integrated signal sideband phase noise can be directly computed by a graphical integration method. In terms of the impact of phase noise on digital communication systems, the total rms jitter (σ) of a phase-modulated source is often specified. The RMS phase jitter is the square root of the variance (normalized noise power). If the envelope of the spectrum is approximated by one line segment, the integration of noise power is normally taken from f_1 between $0.01f_b$ and $0.05f_b$ and $f_2=f_b$ where f_b is the transmitted bit rate [18].

The designing of the LO source for communication systems often require optimization of its phase noise variance to meet a specific system requirement, such as the bit error rate. The effect of phase noise has different degrees of impact on the system's performance dependent on the modulation type. It is appropriate, however, to consider the spectrum efficient modulations such as PSK. The performance degradation of phase noise effect on digital communications can be characterized by a decrease in the energy per bit-to-noise ratio (E_b/N_o) and hence an increase in the bit error rate. From

the above analysis, the value σ^2 represents an RMS SSB phase noise variance. The noise contribution for both sidebands can be expressed as

$$\rho = \sqrt{2\sigma^2} = \sqrt{2}\sigma \tag{6.50}$$

A 3dB addition to spectral density is recommended to convert the SSB phase noise variance into a DSB one [76]. For clarity, the factor 2 is explicitly expressed in ρ.

An alternate expression can be used to evaluate the BER degradation due to phase noise. However, it should be noted that this expression was not used in this thesis, but is included here for interest. To obtain this BER degradation expression, it is necessary to select a suitable model for the probability density function of the phase error ϕ. From [79], the conditional probability of error averaged over ϕ is,

$$P_e = \frac{1}{\sqrt{2\pi}\rho}\int_{-\infty}^{\infty}\exp\left(-\frac{\phi^2}{2\rho^2}\right)erfc\left(\sqrt{\frac{2E_{bi}}{N_o}}\cos\phi\right)d\phi \tag{6.51}$$

where *erfc(x)* is the complementary error function. E_{bi}/N_o is the energy per bit over noise. Bit energy is used rather than symbol energy because the basic P_e curve will be universally true irrespective of the M'ary nature of the modulation of interest.

For ρ=0 or a small ρ, which is in the region of interest, the computation is very difficult using this direct form. To overcome this problem, a simple parametric substitution is made:

Let ϕ=ρθ, then the probability function can be written as,

$$P_e = \frac{1}{\sqrt{2\pi}}\int_{-\infty}^{\infty}\exp\left(-\frac{\theta^2}{2}\right)erfc\left(\sqrt{\frac{2E_{bi}}{N_o}}\cos\theta\rho\right)d\theta \tag{6.52}$$

In this way, the singularity in the region of interest is removed. The equivalent QPSK probability of error can be derived in a similar manner,

$$P_e = \frac{1}{2\sqrt{2\pi}}\int_{-\infty}^{\infty}\exp\left(-\frac{\theta^2}{2}\right)\left[erfc\left(\sqrt{\frac{2E_{bi}}{N_o}}(\cos\theta\rho+\sin\theta\rho)\right)+erfc\left(\sqrt{\frac{2E_{bi}}{N_o}}(\cos\theta\rho-\sin\theta\rho)\right)\right]d\theta \tag{6.53}$$

Figure (6.10) compares the noise sideband performance of a crystal oscillator, LC oscillator, cavity- tuned oscillator, switched reactance oscillator and YIG (Ytrium Iron Garnet) oscillator at their respective operating frequencies. Table (6.1) shows the

extrapolated data from figure (6.10), together with the phase noise performance at 2GHz (in the region of the desired local oscillator frequency (1930MHz or 2070MHz)). From column 3 of this table it should be noted that phase noise can be translated to any desired frequency by adding 20log(n) dB, where n is the multiplication/division factor ($n=f_{desired}/f_{specified}$) [71].

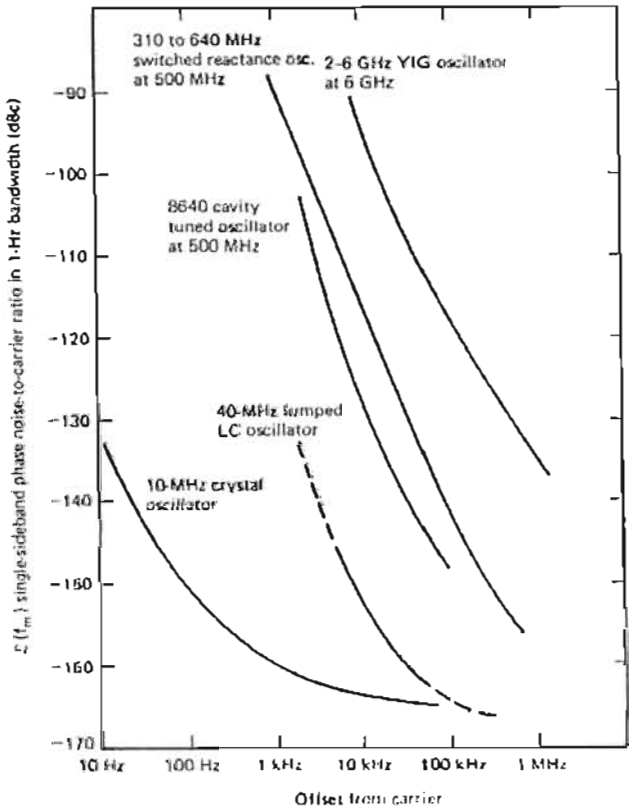

Fig. 6.10: Comparison of noise sideband performances of a crystal oscillator, LC oscillator, cavity-tuned oscillator and YIG oscillator (from [76])

Oscillator Type	σ_T^2 (dB) at specified frequency	σ_T^2 (dB) at 2GHz desired frequency
10MHz crystal	-114	-68
40MHz lumped LC	-101	-67
8640 cavity tuned oscillator at 500MHz	-75	-63
310MHz to 640MHz switched reactance oscillator at 500MHz	-61	-49
2GHz to 6GHz YIG oscillator at 6GHz	-55	-65
Avantek varactor tuned oscillators in 0.3GHz to 18GHz frequency range	<-34dB in 0.3GHz to 18GHz frequency range	
Avantek dielectrically stabilized oscillators in 3GHz to 18GHz frequency range	<-39dB in 3GHz to 18GHz frequency range	

Table 6.1: Comparison of phase noise variance for different oscillators

This data has either been extrapolated and calculated from the single-sideband noise performance versus offset frequency curves in [76] or calculated from two pairs of values from manufacturer's datasheets.

Table (6.2) compares the accuracy of the formula for the total variance σ_T^2 for n line segments in equation (6.49) with that obtained from ADS simulation at frequencies in the proximity of 2GHz. With a knowledge of the LO signal power (10dBm in this case) and σ_T^2 (table (6.1) column 3), the LO noise power can be easily calculated (table (6.2) column 2). In units of dBm, this can be expressed mathematically as $N_{LO} = \sigma_T^2{}_{dB} + S_{LO}$. The maximum number of segments used for estimation of the variance in this instance is eight. In the simulation (column 3), the phase noise power is obtained by integrating the LO spectrum between the minimum and maximum offset frequencies. However, estimation of this signal spectrum is obtained by computing a FFT (Fast Fourier Transform) on the signal. The FFT is a radix 2 FFT and uses 2^N data points with the number of line segments n equal to 2^N-1. With the minimum

number of data points of 2^{14} (16384), the minimum number of line segments used in the simulation is 16383. The comparison in table (6.2) indicates that both methods correlate very well. Clearly, the estimation of the LO noise power by use of equation (6.49) provides reasonably accurate results even for a spectrum approximated by only 4 line segments.

Oscillator Type	Noise power obtained by use of equation (6.49)	Noise power obtained in simulation
10MHz crystal	-58.18dBm (8 segments)	-57.63dBm
40MHz lumped LC	-57.20dBm (5 segments)	-56.54dBm
8640 cavity tuned oscillator at 500MHz	-53.30dBm (4 segments)	-53.81dBm
310MHz to 640MHz switched reactance oscillator at 500MHz	-39.67dBm (7 segments)	-38.03dBm
2GHz to 6GHz YIG oscillator at 6GHz	-55.70dBm (6 segments)	-55.70dBm

Table 6.2: Comparison of the calculation of LO noise power by the use of equation (6.49) with that of simulation

6.4.3 Simulation work

To escape repetition, the same transceiver architecture as in section (5.3) (figures (5.2) and (5.3) of chapter 5) was used. The LO source in ADS was specified to have a power level of 10dBm. This power is significantly higher than the power at the RF input of the mixer. This is essential for the mixer operation [70]. Also, a high LO drive is desirable since mixer conversion loss decreases asymptotically with increasing LO drive [70]. The LO source also accommodates insertion of phase noise. Phase noise is specified with pairs of values for offset frequency (Hz) and single sideband phase noise-to-carrier level (dBc/Hz). In order to resolve these components it is essential that the simulation sampling time (*Tstep*) be appropriately chosen. To resolve the phase noise component at the highest offset frequency ($f_m(max)$), the sampling time should be set such that $Tstep << 1/f_m(max)$. To resolve the phase noise component at the lowest offset frequency ($f_m(min)$), the simulation stop time (*Tstop*) should be set such that $Tstop >> 1/f_m(min)$. In this simulation the phase noise spectrum was approximated by a single line segment consisting of arbitrary chosen offset

frequencies of 1kHz and 10kHz. With a sampling time (*Tstep*) of chiptime/6 (40.69nS) and a stop time (*Tstop*) corresponding to 10000 bits (102.539mS), these components can be resolved easily. These choices of offset frequencies differs from the specified ones of in [18] (recall if the envelope of the spectrum is approximated by one line segment, the integration of noise power is normally taken from f_1 between $0.01f_b$ and $0.05f_b$ and $f_2=f_b$ where f_b is the transmitted bit rate [18]). Oscillator phase noise performance in manufacturer's datasheets are usually specified as single sideband noise-to carrier power level versus offset frequency. These values have to be either extrapolated from curves or simply just given as pairs of values. The latter is more commonly presented. However, these offset frequencies differ from manufacturer to manufacturer thus making comparison of phase noise performance by inspection, difficult. The phase noise variance (σ^2) is thus a more useful way to relate phase noise performance. It is also more appropriate to relate σ^2 to the bit error rate than either the offset frequencies or single sideband noise-to-carrier level. The degree of oscillator stability (in terms of σ^2) can thus be evaluated to guarantee a moderate performance degradation.

6.5 Analysis and interpretation of results

With reference to the simulated transceiver architecture (figures (5.2) and (5.3) in section (5.3) of chapter 5), figures (6.11) to (6.13) show plots of phase noise variance versus bit error rate (BER) for varying SNR at the input of the LNA.

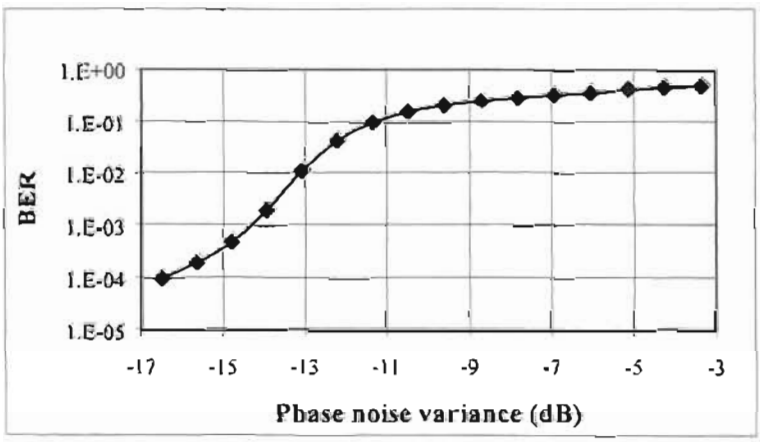

Fig. 6.11: Phase noise variance versus BER for 10dB SNR at the input of the LNA

In figure (6.11), the scales have been adjusted to reveal the most severe bit error rate degradation. For the proposed system (10dB SNR at the input of the LNA), phase

noise variance in the range –16.5dB to –3.3dB produce BERs in the range 10^{-4} to 0.51 for the system processing gain of 42. Phase noise variance less than –16.5dB produce negligible BERs (in the order of 10^{-24}). For a 7dB SNR at the input of the LNA, variance in the range –20.6dB to –3.3dB produce BERs between 0.51 and 10^{-4} (same BERs as 10dB SNR but for larger variance range). Negligible BERs (in the order of 10^{-24}) are produced for variance values less than –20.6dB. However, with a SNR at the input of the LNA of 5dB, phase noise variance between –39.4dB and –3.3dB produce BERs between 7×10^{-4} and 0.51. Clearly, the BER degradation due to phase noise is more severe for lower SNRs.

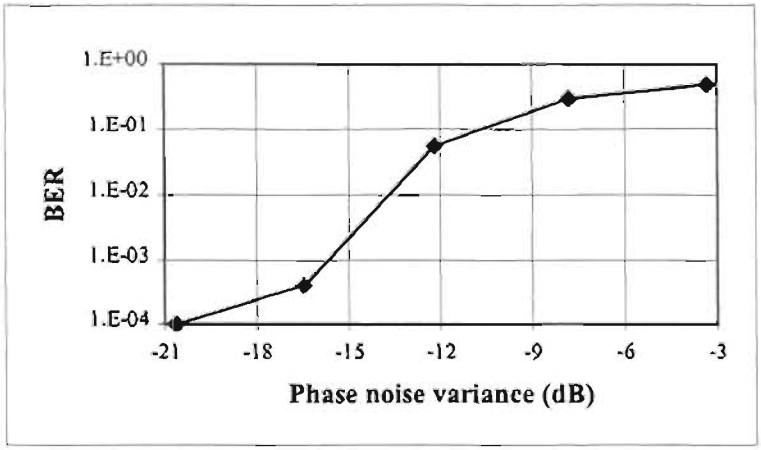

Fig. 6.12: Phase noise variance versus BER for 7dB SNR at the input of the LNA

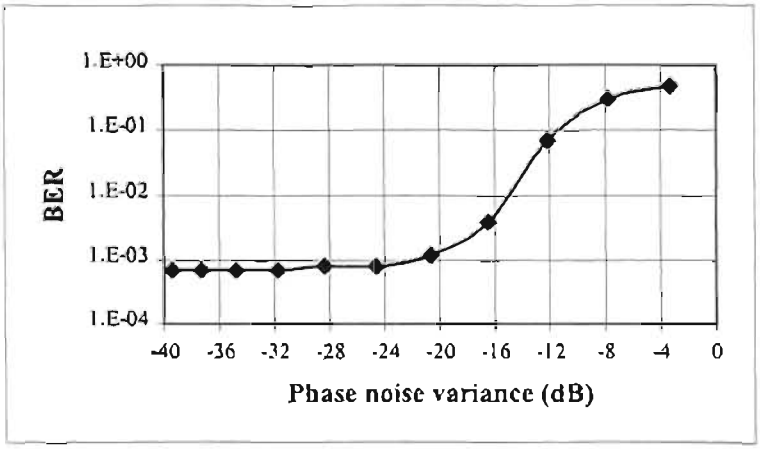

Fig. 6.13: Phase noise variance versus BER for 5dB SNR at the input of the LNA

From the phase noise variance of commercially available oscillators (table (6.1)), it can be concluded that the phase noise performance of typical oscillators have negligible effect on the BER of the proposed system (input SNR of 10dB and processing gain of 42). This can be substantiated by considering that the IF phase noise power (N_{IF}) exists in the same proportion to the RF receiver power, P_{RF} (at the RF input of mixer)

as the phase noise was to the oscillator power if it passes through no narrowband filtering capable of limiting its bandwidth [72]. Expressed mathematically, $N_{IF}|_{dB_m} = P_{RF}|_{dB_m} - SNR_{LO}|_{dB}$. This relation was verified in the simulation. As an example consider, the existing setup with a –80dBm signal power at the input of the mixer and a typical LO SNR of 50dB (variance = -50dB). The noise power additive to the IF port using the above equation is –130dBm. However, computation of the noise power (with the aid of Friis' equation [18]) in the absence of phase noise yielded an IF noise power of –91.35dBm. Thus the phase noise contribution of –130dBm to this noise power is negligible. The effect of phase noise has different degrees of impact on the system's performance dependent on the PSK modulation type. This is intuitive from the signal-space representation of various PSK formats. In [65] and [79] expressions have been derived for the BER as a result of phase noise for both BPSK and QPSK modulation. It has been mathematically shown that the phase noise contribution to the BER for π/4 QPSK modulation is not severe even when the phase noise performance is relatively poor. Thus it can be concluded that, in general, it is unnecessary for oscillator specifications to be overly restrictive in terms of phase noise. However, being overly restrictive with this phase noise specification, places less demand on the low-noise design of other components in the RF system. Phase noise can be minimized by careful design of the LO source. Phase noise in an oscillator is proportional to the inverse square of its resonator Q, so considerable improvement can be attained through the use of a cavity-or-dielectric-resonator-stabilized oscillator [70]. Crystal oscillators have low phase noise and are often used with a multiplier chain to generate microwave LO signals. However, frequency multiplication (which is in reality phase multiplication) enhances phase noise spectral density as the square of the multiplication factor, so high-order multiplication of a noisy source should be avoided since phase noise is worse in higher frequency oscillators [72].

CHAPTER 7

MIXER THEORY

7.1 Introduction

The mixing or frequency conversion process has been highly prevalent in the previous chapters: Recall in chapter 3, the concept of an all-digital adaptive array is currently impractical. This was solely due to the non-availability of signal processing and digitization hardware at typical communication frequencies. However, the use of a mixer for frequency downconversion, has made digital adaptive beamforming practically realizable. Although the mixer in this instance is an analog device, the entire receiver chain is often perceived to be digital. It must be borne in mind that the mixer is common to both analog and digital adaptive array receivers. The distinction in these receivers is made in the implementation of the phase shifting and summing circuits (chapter 3). Furthermore, some practical characteristics of mixers have been encountered in the previous two chapters (chapters 5 and 6). This device was quoted in chapter 5 as being the dominant source of noise in the receiver. Hence most of the simulation results present there were focused around the mixer noise figure. Even when considering the impact of LO phase noise in the DS-CDMA system of chapter 6, the LO phase noise that leaked from the LO port to the IF port of the mixer was of paramount concern (not the LO phase noise in isolation).

An overview on mixer theory is presented in this chapter. An understanding of some of the properties of this ubiquitous device are warranted, especially in the implementation of the BPSK RF front-end (chapter 9). For example, knowledge of the concepts of sum and difference frequencies (generated by the mixing process) are crucial for the selection of the appropriate LO frequency for a given RF and desired IF. Also an understanding of intermodulation products also provide insight on the IF filter requirements to filter unwanted intermodulation products. These become more apparent in chapter 9. Amongst other issues covered in this chapter are the parasitic signals (generated by the mixing process) and some principal characteristic of mixers (e.g. conversion gain/loss, VSWR, noise figure, etc). Intermodulation products are

demonstrated by a simple ADS simulation. This chapter ends with a discussion on intermodulation distortion and design techniques to avert these unwanted responses.

7.2 Mixing or frequency changing

Mixing or frequency changing is a nonlinear operation that transfers the characteristics of a signal of frequency f_A to one of frequency f_B. In most cases, this is done in order to take advantage of the fact that the conditions for propagation are better at high frequencies while the possibilities for signal processing are greater at low frequencies and the costs are less. Also, at the lower frequency, the signal can be amplified and demodulated most effectively. Mixers can also be used as phase detectors and in demodulators, must perform these functions while adding minimal noise and distortion.

When a sinusoidal signal is applied to a linear circuit, the output signal has the same single frequency as the input. If the same signal is applied to a nonlinear circuit, harmonics of the input frequency then appear at the output. When two sinusoidal frequencies are applied to a nonlinear circuit, not only does the output signal contain harmonics of both, but other frequencies appear that are not harmonics of either. The concepts of mixing and frequency multiplication are essentially bound up with the nonlinearity of the circuits involved and the amplitude of the input signal. A convenient way of describing the transfer characteristic of a nonlinear device is the use of a power series:

$$V_o = AV_i + BV_i^2 + CV_i^3 + DV_i^4 + ... \tag{7.1}$$

Where V_o = output voltage

V_i = input voltage

$A, B, C, D, \ldots$ = constants

When two sinusoidal signals V_1 and V_2 with respective frequencies f_1 and f_2 are applied to such a nonlinear circuit, the expression for the output voltage contains many terms. By substituting

$$V_i = V_1 + V_2 \tag{7.2}$$

into equation (7.1), then:

$$\begin{aligned} V_o &= A(V_1+V_2)+B(V_1+V_2)^2+C(V_1+V_2)^3+.... \\ &= \left[AV_1+BV_1^2+CV_1^3+K_mV_1^m\right]+\left[AV_2+BV_2^2+CV_2^3+K_mV_2^m\right]+ \\ &\quad \left[2BV_1V_2+3CV_1^2V_2+3CV_1V_2^2+...+KV_1^mV_2^n\right] \end{aligned} \tag{7.3}$$

The first set of bracketed terms represents the output voltage obtained when the signal V_1 alone is applied to the nonlinear circuit: it can be shown by using trigonometrical identities that the term in V_1^m generates the harmonic of frequency mf_1. The same reasoning can be applied to the second set of bracketed terms to show that the term in V_2^m generates the harmonic mf_2 from V_2. The third set of bracketed terms is the sum of cross products obtained from the expansion of the powers of $(V_1 + V_2)$. It can be shown that the general term $V_1^mV_2^n$ generates two frequencies, the sum and difference frequencies, given by:

$$\text{Sum frequencies: } mf_1 + nf_2 \tag{7.4}$$

$$\text{Difference frequencies: } mf_1 - nf_2 \tag{7.5}$$

where m and n are integers.

A highly nonlinear transfer characteristic generates many frequencies if two sinusoidal signals are applied. This is typical large-signal behavior: at the output there are two original (amplified) sinusoidal frequencies, the harmonics of both and all the sum and difference frequencies. The amplitudes decrease as m and n increase. The sum and difference frequency signals are known as intermodulation products. The first two sets of bracketed terms in equation (7.3) produce harmonic distortion, while the third produces intermodulation distortion. Note that an increase in these two types of distortion amounts to a dispersal of power and thus a loss of power from the fundamental frequencies.

A bandpass filter is used at the output of the mixer to allow only the desired frequency to pass – generally that of the desired intermodulation product and in practice normally the difference frequency (downconversion). The sum frequency is sometimes used for upconversion in transmitters. In most case one of the signals (here V_1) will be much greater than the other to ensure large-signal behaviour i.e. a large excursion around the operating point to obtain intermodulation products. The large signal is generally called the LO (local oscillator) signal. Since the RF signal V_2 often arrives from a receiving

antenna, it is small; this is reinforced by the fact that for f_2 the intermodulation products of high index will have a very small amplitude.

A mixer also incorporates an input circuit to combine the RF and LO signals correctly before applying them to the active nonlinear component. For this purpose, either a directional coupler, a transformer at relatively low frequencies or a hybrid coupler at high frequencies is used to combine the signals and to isolate them from each other. If conversion to a low or intermediate frequency is desired, the LO frequency f_{LO} is usually tuned to a frequency above that of the received RF carrier and the difference frequency signal ($f_{LO} - f_{RF}$) is selected while the other signals (f_{LO}, f_{RF} and $f_{LO} + f_{RF}$) are rejected by filtering [18]. The *LO* frequency is almost always higher than the RF carrier frequency, a characteristic referred to as the high-side injection of the mixer and the system is referred to as a superheterodyne system.

7.3 Parasitic signals

A mixer generates many difference frequencies with values given by $mf_1 - nf_2$, where m and n are integers. It is therefore possible for values of m and n to occur that produce frequency differences close to $f_1 - f_2$. These undesirable signals are liable to pass through the output bandpass filter, which must therefore have a narrow bandwidth. In addition, the operating point and the excursion along the characteristic curve (i.e. the amplitude of the local oscillator) should be such that cross products of order greater than 2 are negligible. Note that such parasitic frequencies are generated for high values of m and n.

Another type of undesirable signal, this time at the input, consists of the image frequency f_{im}. It is the second RF frequency that creates a response at the IF. For example, if a mixer is designed to convert 8GHz to 1GHz with a 7GHz LO, the mixer will also convert 6GHz to 1GHz using the same LO frequency. It is defined by:

$$\begin{aligned} f_{im} &= 2f_{LO} - f_{RF} \\ &= 2f_1 - f_2 \end{aligned} \tag{7.6}$$

Thus a mixer can accept a signal of frequency f_{im} as an input signal. This is the reason for all mixer circuits having an input filter to reject the image frequency. Consider the following examples: If the local oscillator is at 2750MHz, input frequencies at

2740MHz and 2760MHz will generate the same 10MHz output. Here the lower limit of the input frequency range is lower than the LO frequency. In a conventional receiver, where the lower limit of the IF output is higher than DC, this problem can be solved by adding a RF filter to limit the input bandwidth. For example, if the input is from 2750MHz to 3250MHz and the LO is at 1750MHz, the IF output is from 1000MHz to 1500MHz. The image entering the IF passband is from 250MHz to 750MHz in the RF input, which can be filtered out easily with a RF bandpass filter from 2750MHz to 3250MHz. If the LO frequency is at 2750MHz, with the same input bandwidth from 2750MHz to 3250MHz, the IF output is from 0 to 500MHz. The image is from 2250MHz to 2750MHz. This image (2250MHz to 2750MHz) will be very difficult to filter out because the desired input (2750MHz to 3250MHz) is adjacent to it. A filter with a finite slope to pass the 2750MHz – 3250MHz frequency range will not effectively stop the signals in the 2250MHz - 2750MHz range.

The spurious output is another undesirable aspect that should be considered during downconversion: A mixer used to downconvert an input signal to a proper IF range is usually considered as a linear device, but strictly speaking, it is a nonlinear device. In addition to the desired frequency, a mixer would produce many other frequencies, often called the spurious output. The spurious frequencies can be determined using equations (7.4) and (7.5) by

$$f_o = mf_1 + nf_2 \tag{7.7}$$

where m and n are integers and f_1 and f_2 are the input frequencies. Figure (7.1) shows a mixer spur chart for the determination of spurious responses. The desired output of a downconverter is on the diagonally straight line marked H-L. H and L represent the higher and lower frequencies of input signals f_1 and f_2. In a conventional superheterodyne receiver design, where the IF bandwidth is narrow, the output is chosen such that there are no low ordered spurs in the IF bandwidth, such as in the region A of the spur chart. If an IF is from dc to a certain range, the spurs of 2H-2L, 3H-3L, ...are always included. For example, if the input is from 2750MHz to 3250MHz and the local oscillator is at 2750MHz, the output is from 0 to 500MHz represented by square B where 6 spurs are included. Square B is obtained by use of the following two equations:

$$\frac{L}{H} \text{ or } \frac{f_1}{f_2} \tag{7.8}$$

$$\frac{H-L}{H} \text{ or } \frac{f_{IF}}{f_2} \tag{7.9}$$

The use of equations (7.8) and (7.9) yields values of 0.846 and 0.154, respectively. If the input is from 750MHz to 1250MHz and the local oscillator is at 750MHz, the output is from 0 to 500MHz represented by square C (equations (7.8) and (7.9) yields values of 0.6 and 0.4, respectively). This square contains many more spurs than square B. In general, the smaller the percentage bandwidth with respect to the local oscillator frequency, the less spurs the output contains.

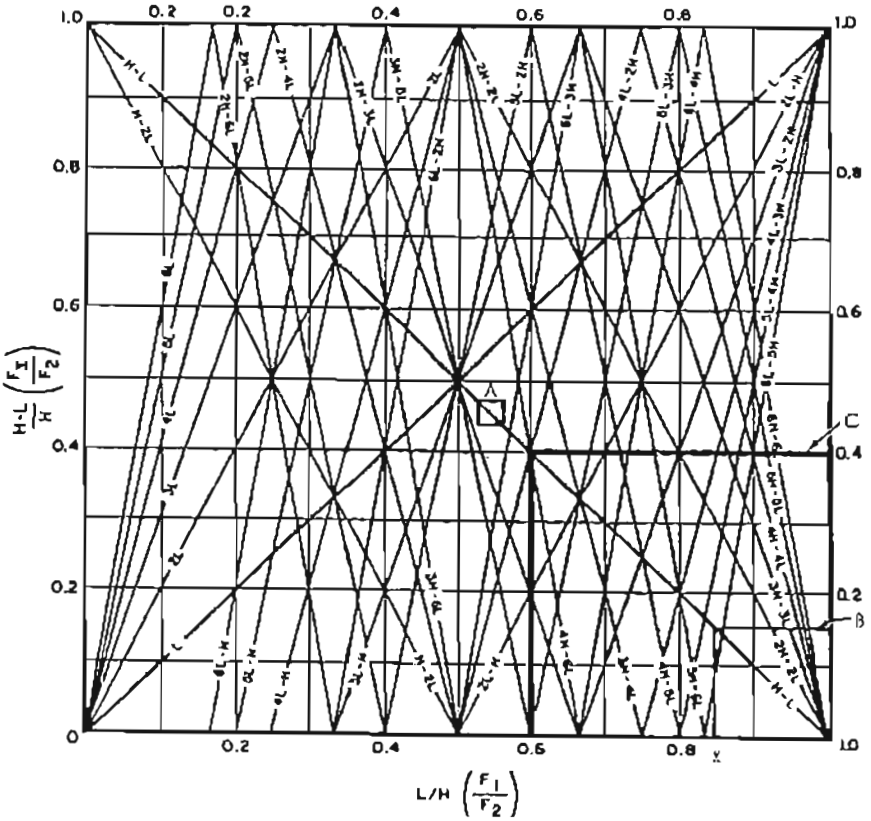

Fig. 7.1: Mixer spur chart (from [30])

7.4 Principal characteristics of mixers

7.4.1 Voltage standing wave ratio (VSWR) ρ

The VSWR gives a qualitative measure of the match for each of the mixer ports. It is expressed mathematically as

$$\rho = \frac{1+|\Gamma|}{1-|\Gamma|} \tag{7.10}$$

$$\Gamma = \frac{z_i - z_c}{z_i + z_c} \tag{7.11}$$

where z_i is the input impedance of the mixer at the frequency concerned (IF, LO, RF) and z_c is the characteristic impedance (usually 50Ω). The VSWR is closely related to LO amplitude which determines the operating point of the component. When the RF level is 20dB below the LO level, the VSWR that is used to calculate the filtering and matching circuits, is taken as unchanged. The value of ρ is generally defined by the manufacturer for a LO power having a value at the midpoint of its range of variation.

7.4.2 Isolation

The isolation is defined as the insertion loss between two terminals of the mixer for a given RF, LO or IF frequency. Its value is given by the manufacturer, over a range of frequencies, as a function of the LO level and sometimes of temperature. The LO input/RF input and LO input/IF output are the only ones quoted. The RF input/IF output isolations is only given if the RF level is such that there is a risk of some RF persisting at the IF output.

7.4.3 Dynamic range

This is the range of RF power over which it is possible to use the mixer. The minimum threshold is generally the noise, and the maximum limit is the 1dB compression point of the mixer.

7.4.4 The 1dB compression point

A mixer has an almost constant conversion gain (defined in section (7.4.7)) over the whole of its dynamic range, which implies that when the RF signal increases, the IF signal also increases. This only lasts until an RF level is reached at which P_{IF} versus P_{RF} characteristic begins to show saturation. The saturated output level of a mixer is

usually defined by its 1dB compression point. The RF amplitude that produces an IF level 1dB below that corresponding to a linear extrapolation of the characteristic is called the 1dB RF compression point. Alternatively, the 1dB compression point is the output power point at which the conversion loss increases by 1dB.

Beyond this point, intermodulation products of higher orders appear and there is a transfer of power from f_{IF} to $f = mf_{RF} + nf_{LO}$ (with $m \neq 1$ and $n \neq 1$), which is undesirable from the user's point of view. The value of the 1dB compression point is related to the amplitude of the LO signal.

7.4.5 The intermodulation intercept point and the corresponding powers

The intercept point I is defined as the point at which the output power in the intermodulation products is equal to the IF output power. The input and output powers P_{Ii} and P_{Io} at the point I are related by

$$P_{Io} = P_{Ii} + G_c \tag{7.12}$$

all in dBm. G_c is the mixer conversion gain. A high P_{Ii} guarantees a large dynamic range and a good value for the 1dB compression point. The manufacturer generally gives the value of P_{Ii} or P_{Io} for intermodulation products of the third order ($2f_{LO} - f_{RF}$, $2f_{RF} - f_{LO}$) or for double intermodulation products of the third order (with two RF sources, one wanted, one parasitic):($\pm 2f_{RF1} \pm f_{RF2} \pm f_{LO}$; $\pm f_{RF1} \pm 2f_{RF2} \pm f_{LO}$). This is warranted by the fact that the frequencies of the double products of the third order are very close to f_{IF} are not attenuated very much by normal mixers.

7.4.6 The noise factor, F

This is generally defined for a single sideband (SSB) system by the following relationship:

$$F_{SSB}(dB) = G_c(dB) + 10\log_{10}\left(\frac{IF\ noise\ power}{RF\ noise\ power}\right) \tag{7.13}$$

For a double sideband (DSB) system,

$$F_{DSB}(dB) = F_{SSB}(dB) - 3dB \tag{7.14}$$

The difference between the RF and IF noise power is produced by the active and passive components used in the mixer. The type of noise in question are 1/f (flicker) noise from carrier generation and recombination, thermal noise and shot noise. Mixers

with high intermediate frequencies are affected only by white noise (thermal and shot) and thus have better noise characteristics than those with low IFs which are subject to 1/f noise. This accounts for all the investigations being carried out with the aim of reducing 1/f noise level [69] for active components that can be used in low-IF mixers.

The noise factor of mixers is measured in the same way as for amplifiers, except that the signal and noise power levels are compared at different frequencies (f_{IF} and f_{RF}). From the point of view of noise, it is essential to reject the image frequency since, if a signal of frequency $f = f_{LO} - f_{IF}$ is the RF source for the mixer, the signal $f = f_{LO} + f_{IF} = f_{im}$ is also converted to the frequency f_{IF}. This doubles the amount of noise at the IF output and thus increases the noise factor of the mixer.

7.4.7 Conversion gain G_c

The conversion gain (or loss) of a mixer is defined mathematically as

$$G_c = 10\log_{10}\left(\frac{IF\ power}{RF\ power}\right) \tag{7.15}$$

All mixers have a 3dB loss because one of the two sidebands is eliminated. The conversion gain is always negative for a diode mixer (DM) and is on the whole positive for a transistor mixer (TM). The value of G_c is closely related to the local oscillator amplitude and the type of mixer [70].

A simulation using ADS software was performed to determine mixer conversion gain and the IF spectrum (intermodulation products). The IAM81081 mixer by Avantek was used. A RF frequency and power level of 2GHz and –50dBm, respectively was used. For a desired IF of 68MHz, the LO frequency was selected (using equation (7.5)) as 1932MHz. The LO level was chosen to be –5dBm (within the specified LO operating level of the IAM81081 mixer). Note that the LO level is much larger than the RF signal level. As discussed in section (7.2), this is to ensure large signal behaviour to obtain intermodulation products. Figure (7.2) shows the ADS simulation circuit schematic.

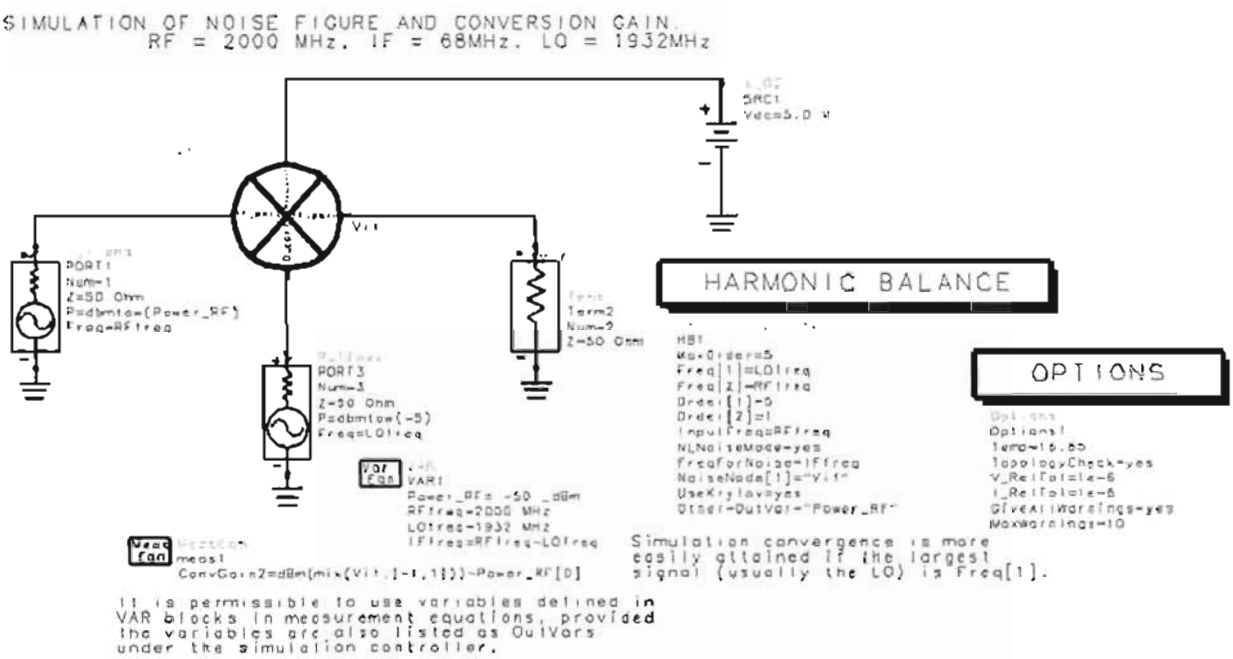

Fig. 7.2: ADS circuit schematic for simulation of mixer conversion gain and IF spectrum

The conversion gain was determined by writing an expression evaluating the difference between the RF and IF power levels. The conversion gain was computed to be 11.611dB (figure (7.3)).

Eqn ConversionGain=dBm(HB.Vif[1])-(-50)

ConversionGain
11.611

Fig. 7.3: Expression for determination of conversion gain

Figure (7.4) shows a plot of the IF spectrum. The relevant data is extracted and conveniently displayed in table (7.1). It should be noted that the desired 68MHz IF power level is above that of the –50dBm RF level by that of the conversion gain (11.611dB). The IF frequencies listed in table (7.1) are obtained by application of the sum and difference frequency equations (equations (7.4) and (7.5)) for $m + n \leq 5$. To speed up simulation time, the maximum order of the RF signal was set to 5. It should be noted that the IF spectrum consists of all intermodulation products for $m + n \leq 5$. In

practice an IF bandpass filter is used at the output (IF) port of the mixer to pass the desired product only (68MHz in this case). Also, the power levels of the 2GHz and 1.932GHz intermodulation products are different from the corresponding RF and LO levels at the input of the mixer. These levels can be calculated by the use of intermodulation product tables (spurious response charts) listed in manufacturer's datasheets. Section (7.5.2) briefly describes this chart.

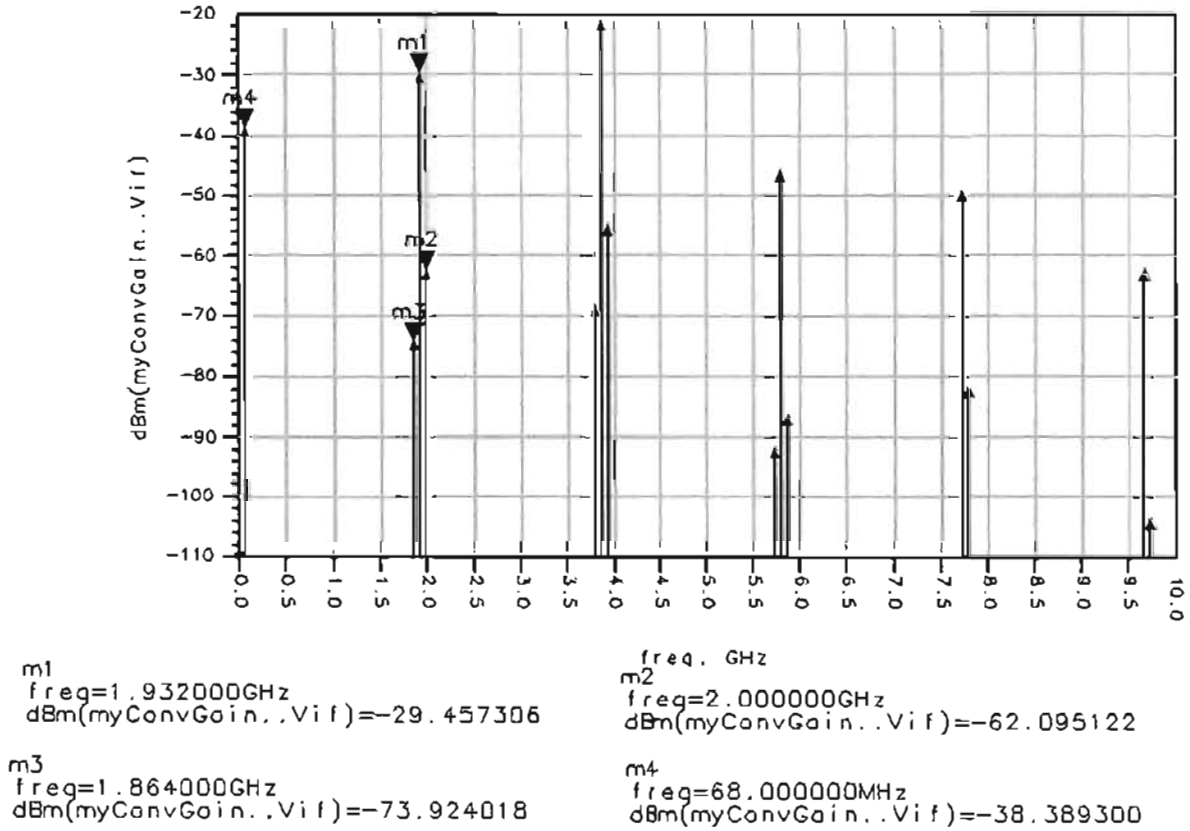

Fig. 7.4: IF spectrum

Eqn IF_Spectrum=dBm(HB,Vif)

freq	IF_Spectrum
0.000 Hz	<invalid>
68.000MHz	-38.389
1.864GHz	-73.924
1.932GHz	-29.457
2.000GHz	-62.095
3.796GHz	-68.193
3.864GHz	-20.931
3.932GHz	-54.813
5.728GHz	-91.825
5.796GHz	-45.899
5.864GHz	-86.228
7.728GHz	-49.080
7.796GHz	-81.759
9.660GHz	-62.297
9.728GHz	-103.588

Table 7.1: IF spectrum

7.5 LO-Induced noise, intermodulation and spurious signals

The sensitivity of a microwave receiver is usually limited by its internally generated noise. However, other phenomena sometimes affect the performance of a mixer front-end more severely than noise. These are AM noise (amplitude noise), phase noise, spurious signals and intermodulation products. AM noise and phase noise have been thoroughly discussed in the previous chapter (chapter 6). The discussion here is limited to intermodulation distortion and spurious responses.

7.5.1 Two-tone intermodulation and saturation [70]

Mixers are subject to gain saturation and two-tone intermodulation. Mixer operation requires that the RF input level be kept well below the LO level. As the RF level approaches the LO level, there is gain saturation and distortion. The saturated output level of a mixer is usually defined by its 1dB compression point, the output power at which its conversion gain decreases by 1dB. For the same LO level, active FET mixers have higher 1dB compression points than diode mixers. Increasing the output level of a mixer requires increasing its LO drive.

Diode mixers have high levels of multitone IM (intermodulation). IM is manifest as the creation of distortion products when two closely spaced RF input tones (e.g. at frequencies f_1 and f_2) generates other tones at the frequencies

$$f_{IM} = \pm qf_1 \pm rf_2 \pm sf_{LO} \tag{7.16}$$

where q, r, s are positive integers.

The worst of these are the third order ($q + r = 3$) products at $2f_1 - f_2$ and $2f_2 - f_1$ downconverted to the IF. These distortion products are generated by the nonlinearities in the solid-state device used to perform the mixing. The large-signal LO, in addition to the small-signal excitations, convert the intermodulation products to the IF frequency and to sidebands of all the LO harmonics.

The spectrum of intermodulation products in a mixer is shown in figure (7.5).

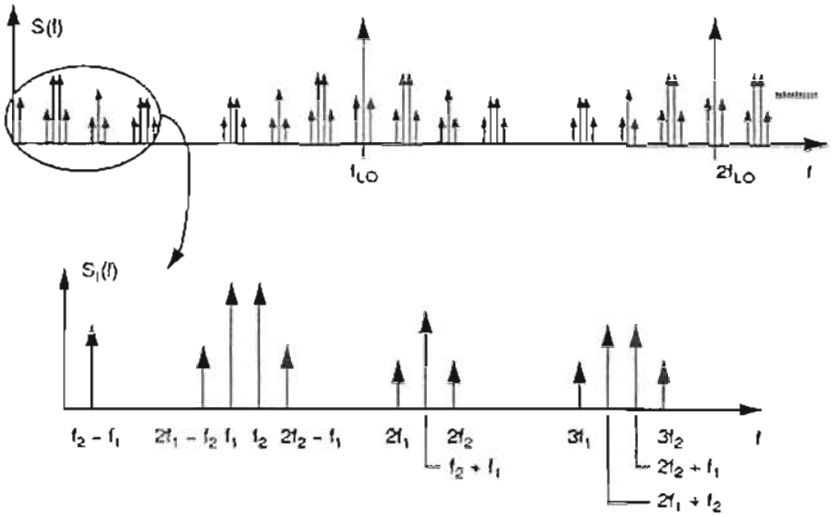

Fig. 7.5: Spectrum of the intermodulation products resulting from two RF inputs (from [70])

The intermodulation products up to third order are shown. These are "folded" around each LO harmonic. In the lower curve of figure (7.5), f_1 and f_2 are IF frequencies. As long as the mixer is not saturated by the RF tones, the levels of IM at the IF port depends on the levels of the excitation. A graph showing linear output levels and IM levels versus input levels is shown in figure (7.6).

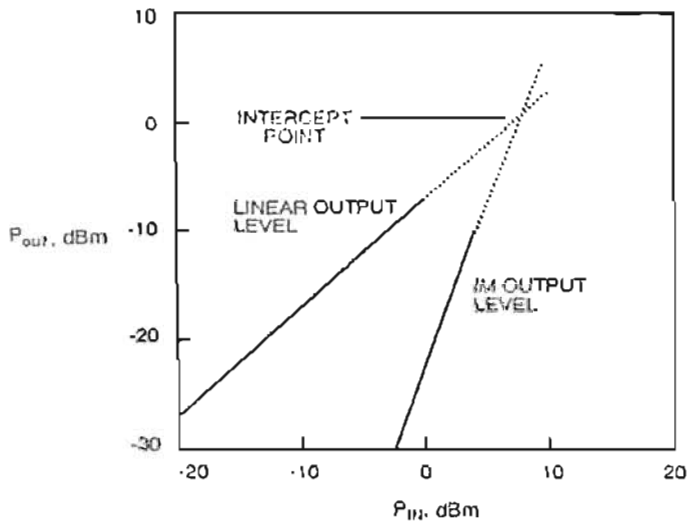

Fig. 7.6: The third-order intercept point (from [70])

The third-order intercept point is the extrapolated point where the IM levels and linear output levels meet. By convention P_{in} and P_{out} are the output levels of each tone. The level of intermodulation products at the output of the mixer is given by the well-known relation [81]:

$$P_{IM_n} = nP_1 - (n-1)IP_n \tag{7.17}$$

where n is the order of the IM product, IP_n is the nth-order intercept point of the IM product in question, and P_I is the output level of the linear responses, assumed to be equal. All power levels in equation (7.17) are in dBm. Note that IP_n is the extrapolated point, in terms of output power, at which the input-output curves of the linear and IM responses intersect.

Equation (7.17) shows that the levels of the nth-order IM product vary n dB for 1dB change in input level of both input tones. Closer inspection of the analysis leading to equation (7.17) would show that the nth order IM product given by equation (7.16), where $q + r = n$, varies q dB for every 1dB change in f_1, and r dB for every 1dB change in f_2. This principle, in combination with the intercept point and equation (7.17), can be used to find the IM level that results from any set of input levels.

When a mixer is cascaded with either RF preamplifiers or an IF amplifier, the calculation of intercept point for the cascade is complex. The intercept point for each stage is amplified or attenuated by the next stage, along with the desired signal, and new IM products are generated. These new IM products occur at the same frequency as those of the previous stage but their phase is indeterminate. Thus, the IM products may combine in such a way as to either enhance or reduce their magnitude. This process is repeated at each subsequent stage. An upperbound on the intercept point can be determined by assuming that the IM products generated in each stage, and those passed along from previous stages, add precisely in phase. This is a reasonable, worst-case assumption. Under this assumption, the worst-case output intercept point of a cascade of stages ([81], [82], [83]) is:

$$IP_n^{(1-n)/2} = IP_{n,m}^{(1-n)/2} + \left(G_m IP_{n,m-1}\right)^{(1-n)/2} + \left(G_m G_{m-1} IP_{n,m-2}\right)^{(1-n)/2} + \ldots + \left(G_2 \ldots G_m IP_{n,1}\right)^{(1-n)/2} \tag{7.18}$$

where n is the order of the IM product, m is the number of stages, and subscripts refer to the stage numbers.

In any receiver, the mixer is the dominant source of intermodulation distortion. Its contribution can be minimized by using minimal gain in the low-noise RF amplifiers preceding it. Minimizing the noise temperature of the receiver, however, requires the use of substantial amplifier gain. These are conflicting tradeoffs, which are resolved

only by using no more gain ahead of the mixer than is necessary to meet noise temperature goals. The better the mixer design, the less low-noise amplification is needed, and both noise temperature and intermodulation level will benefit. Minimizing preamplifier gain also improves spurious-response levels by reducing the input level at the mixer.

7.5.2 Spurious responses

Spurious responses are a type of single-tone intermodulation. The frequencies of spurious responses are given by equation (7.16) when either $q = 0$ or $r = 0$. However, unlike conventional multitone intermodulation, in a spurious response, a harmonic of the LO other than the one that causes the desired frequency translation often figures prominently. As mentioned earlier, the mixer generates output frequencies that satisfy the relation

$$f_{IF} = mf_{RF} + nf_{LO} \tag{7.19}$$

where m, $n = 0, \pm 1, \pm 2, \ldots$ and f_{IF}, f_{RF} and f_{LO} are the IF, RF and LO frequencies, respectively. This equation is similar to the sum and difference frequency equations of (7.4) and (7.5). Thus there exists a wide range of frequencies, many of which are outside the RF passband, whereby interfering signals can be converted to the IF.

If the input frequencies satisfying equation (7.19) are well outside the input passband, the interfering signals can be removed easily by filtering. If the spurious response is of a high order (i.e. high values of m and n), the mixer would not convert them efficiently to the IF. The problem becomes serious when the RF frequencies of low-order spurious responses are within the mixer's input passband, or are so close to it that they cannot be filtered effectively. The best way to avoid spurious responses is to select RF, LO and IF frequency ranges appropriately. An understanding of spurious responses can be gained through the following example. Although the frequency range from this example is different from that used in the project, the knowledge attained is useful. Figure (7.7) shows a spurious-response plot and table (7.2) shows a level chart for a 29GHz to 30GHz mixer having a 3GHz to 4GHz IF passband.

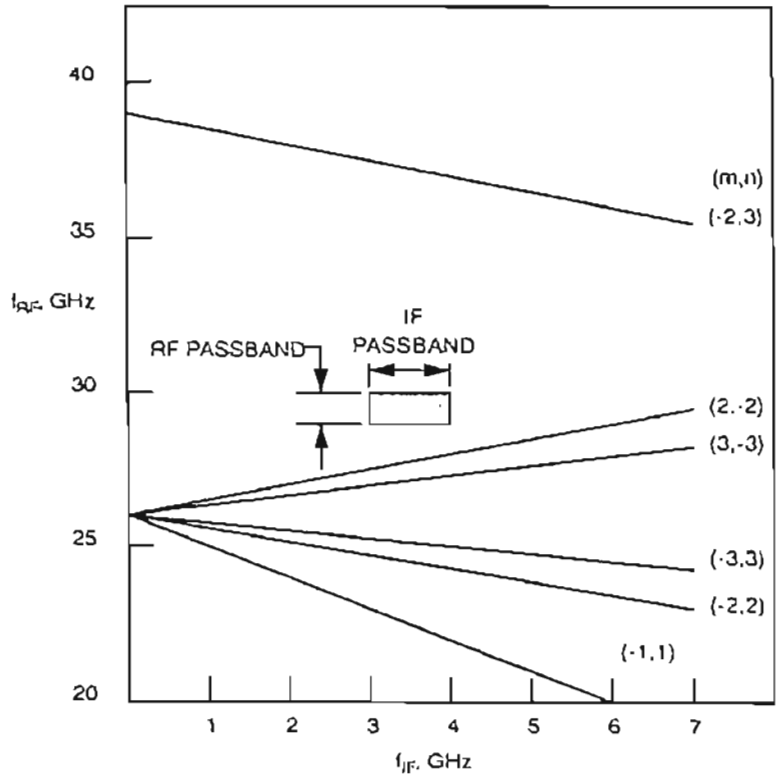

Fig. 7.7: Spurious response plot for a 30GHz mixer (LO frequency = 26GHz) (from [70])

Since none of these curves intersect the shaded area, this mixer has no in-band spurious responses.

Spurious-Response Levels of a 29- to 30-GHz Mixer
× indicates that no spur exists within the 20- to 40-GHz RF range

IF Frequency: 3 to 4 GHz
LO Frequency: 26 GHz
LO Level: +13 dBm
RF Level: −10 dBm

LO Harmonic (n):		-3	-2	2	3
	3	−70	×	×	×
	2	×	−45	×	×
	1	×	×	×	×
RF Harmonic (m):	-1	×	×	×	×
	-2	×	×	−46	−80
	-3	×	×	×	−70

Table 7.2: Spurious-response levels of a 29GHz to 30GHz mixer (from [70])

The plot in figure (7.7) is simply a plot of equation (7.19) for several low-order combinations of m and n. Spurious responses (including the image, which can be treated as the low-order spurious response $(m,n) = (-1, 1)$) are plotted over the range

of input frequencies from 20GHz to 40GHz and IF frequencies from zero to 8GHz. Note that the defined RF and IF ranges have been exceeded, because spurious responses outside the defined passband may still be a source of trouble. The response of greatest concern in this example is the (2, -2) response from 27.5GHz to 28GHz, close to the lower edge of the passband, because it has relatively low order. It is close enough to the RF passband that it may be difficult to eliminate by means of a filter.

The spurious-response chart, table (7.2), shows the spurious-response levels of the mixer. The response levels in the chart were measured with the LO level set at the mixer's standard value, in this case 13dBm, and at an RF input level of –10dBm (this input level has become an informal standard for specifying spurious–response levels). The chart includes the effects of filtering and matching circuits that may be used in the mixer. In some cases, the input frequencies that give rise to a particular spurious response cannot be measured – thus there is no entry in the table for this. For other types of mixers, such as a broadband balanced mixer, the table would be nearly full.

The –10dBm level is a compromise: it is not high enough to cause saturation, so the data in the table can be scaled to different input levels, yet it is still high enough to allow accurate determination of some fairly high-order (and therefore weak) responses. These data can be scaled to different RF input levels [82] by recognizing that spurious responses are a type of intermodulation. Like other intermodulation products, the response associated with the mth harmonic of the RF input changes m dB for each dB change in RF input level. Thus, a reduction in RF level of 10dB reduces the (2, -2) response by 20dB, or the (-2,3) by 30dB. This principle can be used to determine the amount of filtering needed to reduce any spurious response to an acceptable level. Note that this principle does not apply to the LO level, or to RF levels strong enough to saturate the mixer.

One of the fundamental uses of LNAs ahead of a mixer is to minimize a receiver's noise temperature. This has been established in chapter 5. Because of the way mth order spurious responses and intermodulation products vary with input level, the use of an LNA can seriously degrade the receiver's intermodulation and spurious-response performance. For example, suppose an LNA having 20dB gain is added to the input of a receiver having a mixer front-end. The extra 20dB of signal level at the input of

the mixer will increase the level of a (2,*n*) spurious-response by 40dB, and will degrade the carrier-to IM level by 20dB; a (3,*n*) response will be degraded (in terms of carrier-to-IM ratio) by 40dB.

7.6 Conclusion

Some important issues and properties of mixers were highlighted in this chapter. An understanding of simple concepts such as the generation of sum and difference frequencies (that are often taken for granted), enable selection of the appropriate LO frequency for a given RF and desired IF. The issue of the LO drive level always being specified larger than the RF drive level in manufacturer's datasheets also become apparent. Also, as discussed, the mixing process generates, in addition to the desired IF, other unwanted intermodulation products. These unwanted products are removed by an IF bandpass filter. Thus, it is not uncommon to find these IF bandpass filters in RF front-ends. This is also evident in the implementation of the BPSK RF front-end (chapter 9). These characteristics where taken into consideration in the implementation of the RF front-end of chapter 9.

Other issues, though not related to this project, not only are of interest to the reader, but also provides insight into this ever-present device.

CHAPTER 8

LOW NOISE AMPLIFIER DESIGN

8.1 Motivation

This chapter presents the design, simulation, construction and characterization of a low noise amplifier (LNA) intended for use in the BPSK RF front-end system (chapter 9). The LNA specifications of interest (noise figure and gain) are crucial to this investigation. With knowledge of these specifications for each of the front-end blocks, the overall noise figure (using Friis' equation) can be computed. Thus the SNR and the Error Vector Magnitude (EVM) degradation of the system can be measured. Hence the LNA can be specified for a given SNR or EVM system requirement.

Due to the initial expected delay in the arrival of the commercially available LNA (ZEL-1724LN) used in the BPSK system, the need for the design and construction of an in-house LNA was further motivated. However, it was not possible to characterize the noise figure of this LNA at the frequency of interest (2GHz). The reasons for this have been outlined in section (8.6.1). As a result, the delay cost incurred in the arrival of the commercial product was accepted, and the ZEL-1724LN was included in the BPSK RF front-end (figure (9.1)). Nevertheless, a low-cost, in-house solution, with the possibility of demonstrating acceptable system performance, is an attractive and viable option.

8.2 Introduction

In wireless communication systems, a fundamental function of the RF front-end section is signal amplification. In the case of a receiver, the lowest possible signal level at its input must be amplified to a level that can be detected by the demodulator. In the transmitting case, the transmitted signal must be amplified sufficiently so that

despite losses inherent in wireless transmission, the signal can be received by the base station.

There are several types of amplifiers that serve specific functions in the RF front-end of the communication system. In the receiving chain, amplifiers that are closest to the antenna contribute directly to the noise performance. As established in chapter 5, these LNAs must have a low noise figure and provide adequate gain so that noise contributions from the remaining of the receiving components are negligible. In the transmit path, the amplifiers closest to the antenna are power amplifiers (PAs). They must amplify the signal linearly and efficiently [65]. However, noise is not a primary consideration in PAs. Chapter 5 also made brief mention of the near-far effect which is eliminated by power control. In this instance, the receiver incorporates automatic gain control (AGC) in either the RF LNA or IF amplifier. The function of these variable gain amplifiers (VGAs) is to help keep the receiver output constant over the expected range of signal level. The noise and linearity specifications/requirements of VGAs are not stringent as that for LNAs and PAs, respectively. However, the dynamic range of VGAs must be reasonable i.e. it must be able to handle both the levels of small and large signals.

The basic topology of microwave amplifier circuit design is straightforward. Often the only components involved are an active device (transistor or FET) plus four or five microstrip transmission line elements of various lengths and widths. Compared to a large analog I.C. chip or a digital microprocessor chip, such a microwave circuit seems very simple. However, the design of microwave amplifiers poses many technical challenges to electronic circuit designers.

High-frequency amplifier design has traditionally followed the route of an art rather than a science. Engineers would carry out approximate calculations and then make the amplifier circuit work by means of tuning, shielding, grounding and the design of a good layout. However, in addition to the above techniques, scattering parameters are today used in microwave amplifier design work because they are easier to measure and work with at high frequencies than are other kinds of parameters. They are

conceptually simple, analytically convenient, and capable of providing insight into a design problem.

The approach followed in the designing of a practical high-frequency amplifier is based on the following six steps:

I. Define a specification
II. Select an active device
III. Select a topology
IV. Select a bias circuit
V. Perform a computer simulation and optimization of the circuit to realize the specification.
VI. Construct and test to verify that the design meets the specification.
VII. Adjust simulation to achieve measured results (Steps V to VII are performed iteratively).

The necessary tools for the design of microwave amplifiers are found from an understanding of transmission lines, two port networks and impedance matching networks. With the knowledge and understanding of scattering parameters, the design of amplifier circuits is essentially an impedance matching problem. In order to understand this design, it is assumed that the reader is familiar with basic network analysis and the elementary concepts of microwave amplifier design theory. A detailed theoretical analysis of microwave amplifier design can be found in [63], [84], [85], [86], [87] and [88].

The first step in the design process is the definition of the specifications. It is intended to use to this amplifier in the proposed CDMA adaptive array system. The specifications have been appropriately defined as:

- Centre frequency of 2GHz
- Required operating power gain $\geq$ 10dB
- Minimum 3dB bandwidth of 10MHz (This bandwidth is commensurate with the 4.096MHz chip rate of WCDMA. A bandwidth of 8.192MHz (2 x chip rate) is required for BPSK modulation)

- Noise figure less than 3dB in the 10MHz bandwidth (corresponding to noise figures of commercially available LNAs)
- System characteristic impedance (Z_o) of 50Ω

The design process in steps II to IV for active device, topology and bias circuit selection, respectively, are documented in the appendix (appendix A.3). A discussion on the simulation, optimization and construction aspects (steps V and VI) will now be provided.

8.3 Initial circuit simulation

The initial circuit was simulated using ADS [7]. Figures (8.1) and (8.2) show the circuit schematic and s-parameter simulation results, respectively.

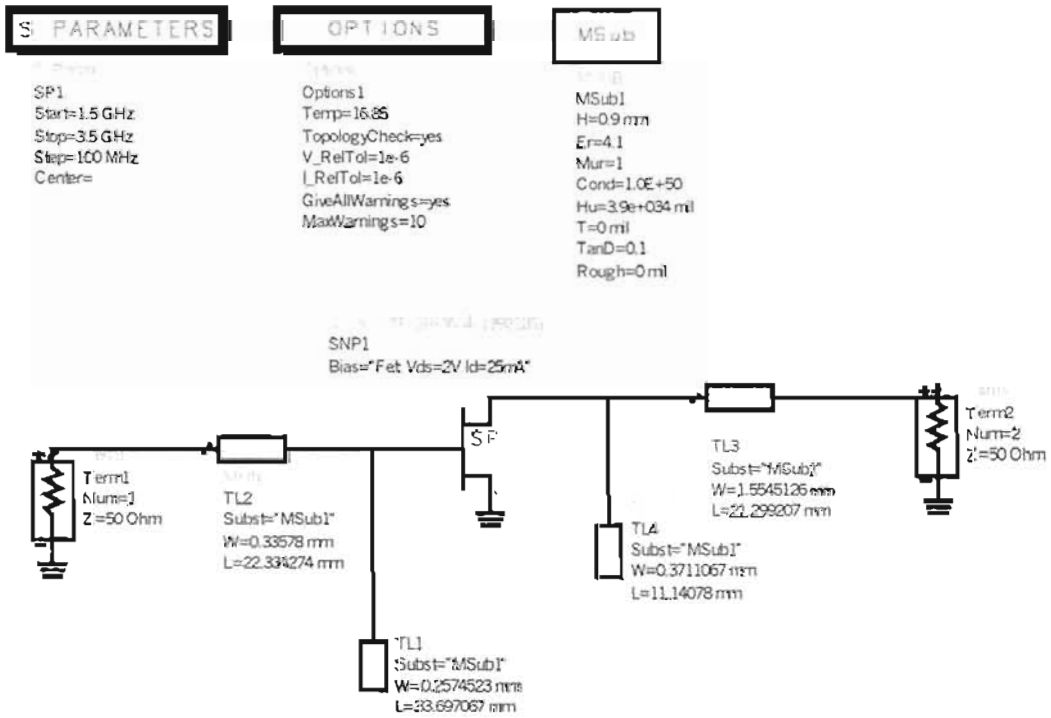

Fig. 8.1: Circuit schematic

With regard to the s-parameter simulation results (figure (8.2)), the following points are of interest: At 2GHz, the transducer gain of the amplifier ($|S_{21}|$) is 12.89dB. Thus, this meets the 10dB minimum specified gain. The input reflection parameter ($|S_{11}|$) is –7.906dB. It is also apparent that the 3dB bandwidth is much greater than the specified minimum bandwidth of 10MHz (3dB bandwidth ≈ 400MHz). Figure (8.3)

shows the noise figure versus frequency simulation results. Once again it is apparent that the noise figure is less than 3dB within an approximate bandwidth of 1.25GHz.

The simulation results indicate that the amplifier meets all the specifications. However, the large value of the input reflection parameter (-7.906dB) is a cause for concern. The input reflection parameter ($|S_{11}|$) is a measure of the quality of the input match. It is the ratio of reflected power to transmitted input power at port 1 of the device. It is thus desirable to make this parameter as small as possible. The next section focuses on optimization of the circuit for an improved input match.

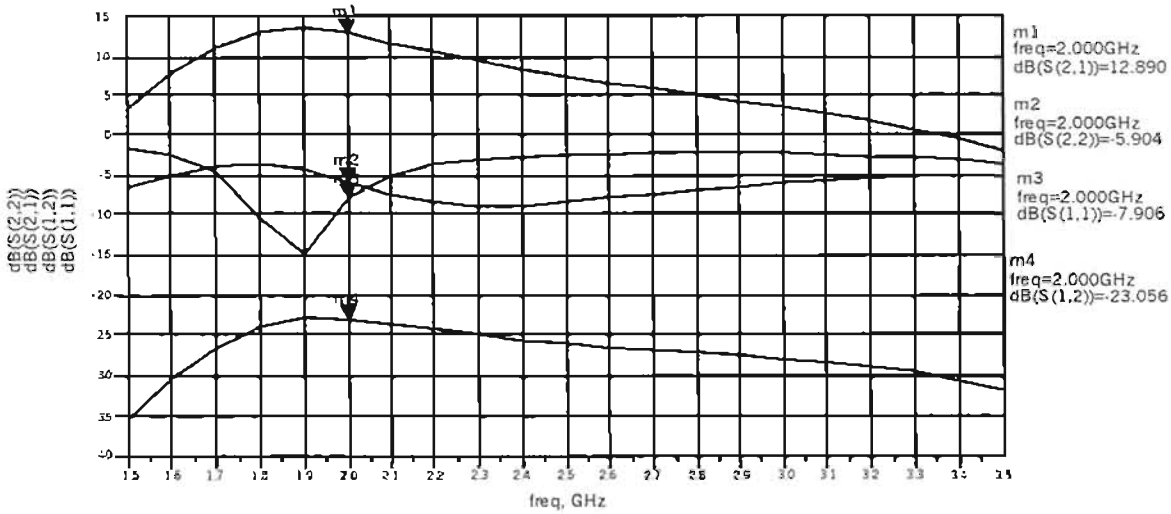

Fig. 8.2: S-parameter simulation results

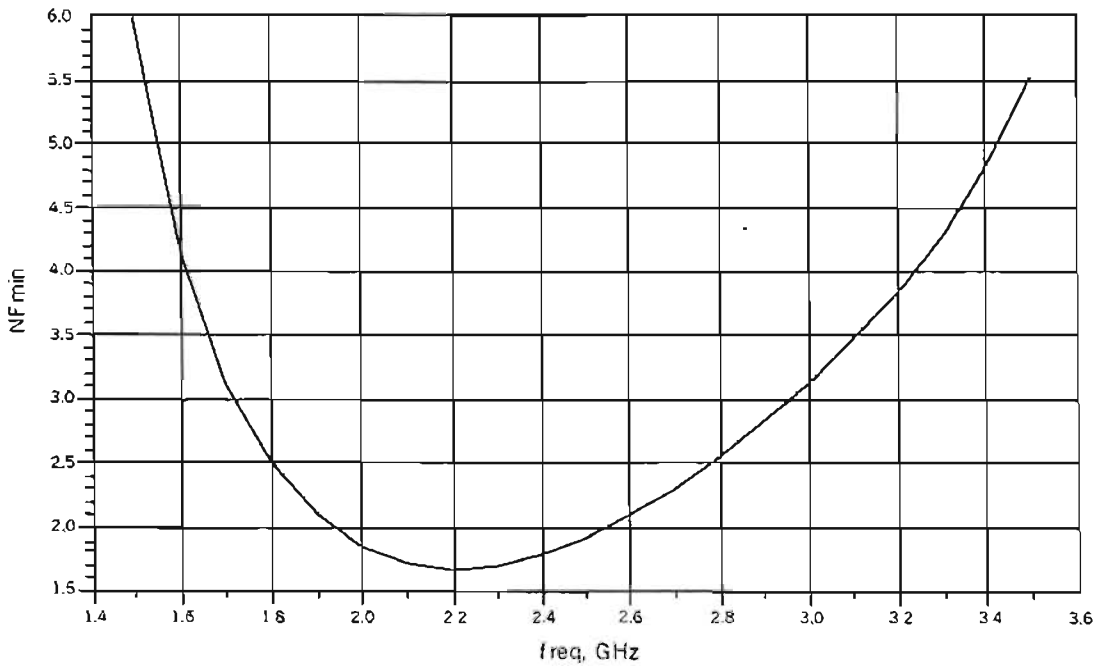

Fig. 8.3: Noise figure versus frequency

8.4 Optimization

8.4.1 Fundamentals of optimization

Often in the design of a microwave amplifier, the initial responses - gain, noise figure, input or output VSWR, and so on - do not exactly match the specified values over the frequency band of interest for many reasons. For example, the model may not exactly represent the measured data; other causes of error include the unilateral assumption in the case of transistors, or the distributed approximation of the lumped elements.

In order to obtain the specified response, the elements of the original network can be adjusted by the cut-and-try method (tuning); this usually limits a network to a few elements and a narrowband response. For a large broadband network, this type of tuning is a tremendous and often impossible task. Therefore it is more appropriate to adjust the response of the initial network by varying its elements iteratively according to some numerical algorithm carried on a digital computer. This process is called optimization. Since optimization is an iterative process, the procedure is laborious, and for a broadband amplifier the number of iterations could easily be a few hundred - even with the most efficient currently available optimization methods - if the response of the initial network deviates too far from the specified one. Furthermore, the optimization process may fail or may converge to an inferior network with poor starting values.

8.4.2 Optimization of input matching network

The simulation results in section (8.3) indicate that the amplifier meets all the specifications. As mentioned, the large value of the input reflection parameter (-7.906dB) is a cause for concern. This can be attributed, inter alia, to the non-consideration of the biasing lines, step-width change discontinuity [89], coupling and bypass capacitors in the simulation model. There is thus a need to optimize the circuit for an improved input match or lower input reflection parameter ($|S_{11}|$).

Tuning is one of the simplest optimization tools in ADS. In this instance, the length of the quarter-wave transformer (between 50Ω input line and input open circuit stub) was tuned/optimized for an improved input match. An optimum value of –26.765dB

for the input reflection parameter ($|S_{11}|$) was obtained for a 13.867mm transmission line length. Thus, a reduction in the length of the quarter-wave section from 22.334mm to 13.867mm resulted in a reduction in $|S_{11}|$ from –7.906dB to –26.765dB. Figures (8.4) and (8.5) shows the optimized s-parameter simulation results and noise figure versus frequency plot, respectively.

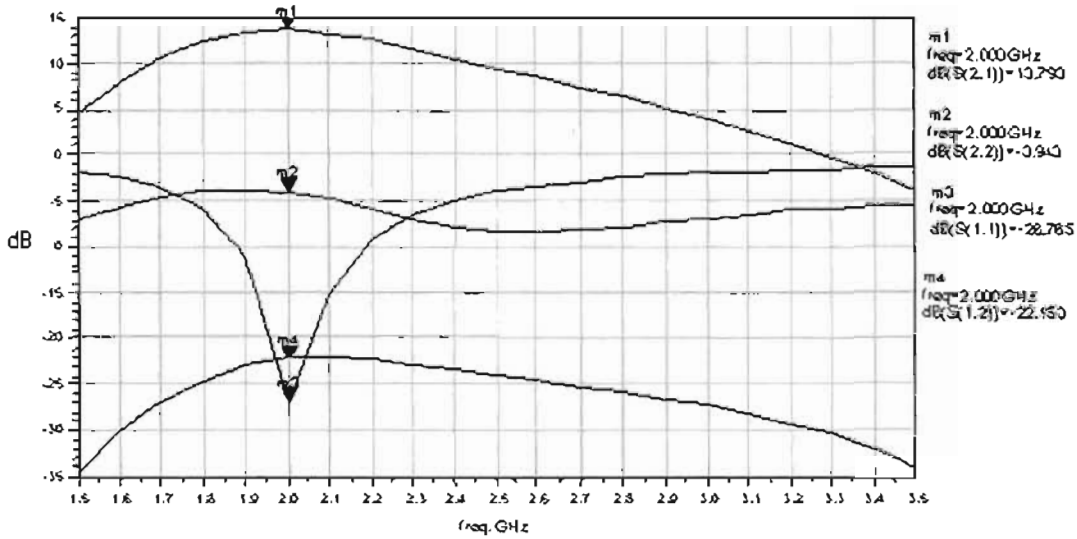

Fig. 8.4: Optimized s-parameter simulation results

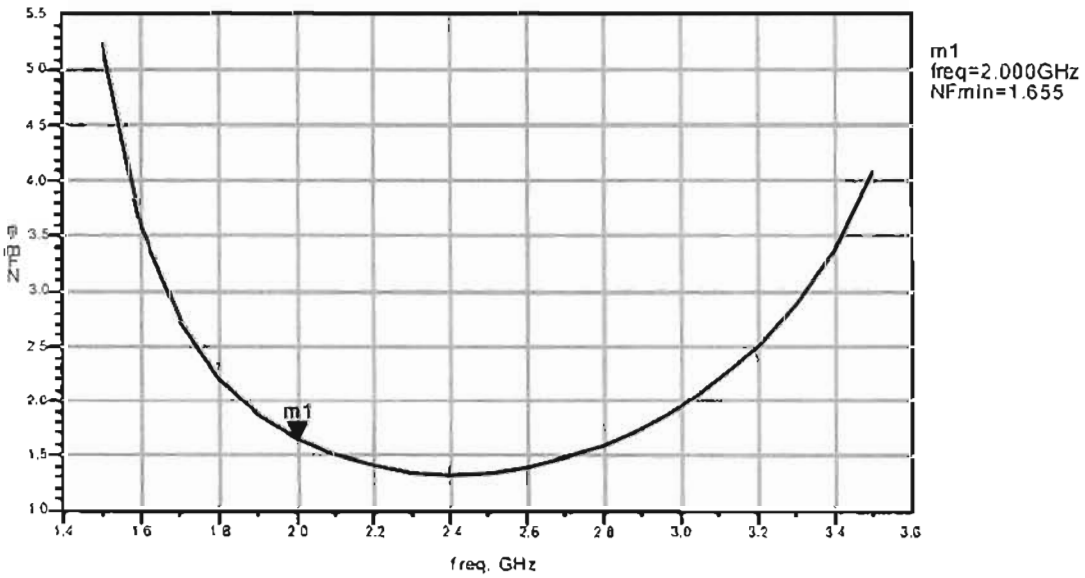

Fig. 8.5: Noise figure versus frequency (after optimization)

On comparison of the optimized simulation results of figures (8.4) and (8.5) with that of the initial circuit (figures (8.2) and (8.3)), optimization also resulted in a marginal improvement in gain ($|S_{21}|$) from 12.89dB to 13.793dB and a decrease in the noise figure from 1.858dB to 1.655dB. It is evident that the 3dB bandwidth is greater than

200MHz while the noise figure is less than 3dB within a 1.6GHz bandwidth – still well within the amplifier specifications. Figure (8.6) shows the optimized input matching network (dimensions in millimetres).

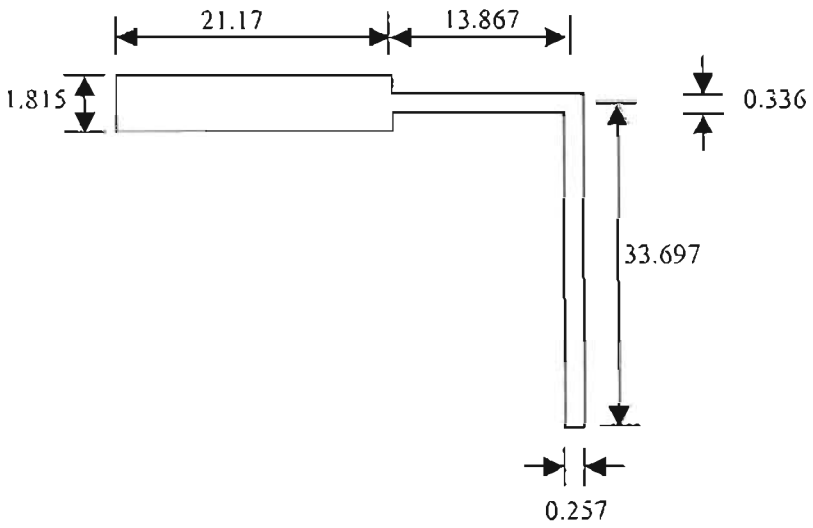

Fig. 8.6: Optimized input matching network

8.5 Layout and construction

The circuit layout was implemented in ADS. A 1:1 artwork was obtained and is shown in figure (8.7). The circuit was constructed on double-sided PCB substrate with one side used as the ground plane. Return paths between topside ground connections and the bottom ground plane are obtained by using wire "feedthroughs" soldered on either side. Holes were drilled through the board to accommodate these "feedthroughs". Two millimeter (2mm) gaps were left on the input and output 50Ω lines to allow 0805 chip coupling capacitors to be added later. Radio frequencies were prevented from entering the DC bias power supply by inserting DC bias transmission lines of width 0.114mm. These lines have a characteristic impedance of 150Ω - larger than that of the other microstrip lines. The DC bias lines were effectively made $\lambda_g/4$ (22.787mm) in length to present an effective open-circuit at the gate and drain of the ATF10136 device. These lines serve as RF chokes. RF in the DC supply could cause the supply to oscillate. These lines were terminated in capacitors, thus presenting a RF short circuit to ground. All capacitors (coupling and bypass) were 10nF 0805 chip capacitors. The "GND", "Vg" and "Vd" pads shown, provides connectivity to the

ground, gate and drain inputs, respectively of the power supply (see figure (A.11) in appendix A.3). Figure (8.8) shows a picture of the complete amplifier.

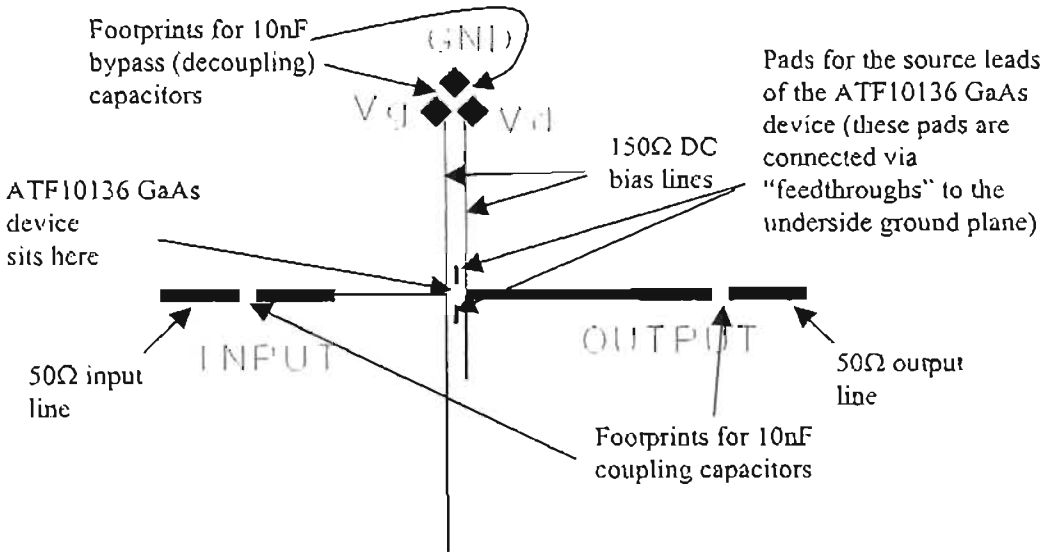

Fig. 8.7: Circuit artwork (1:1)

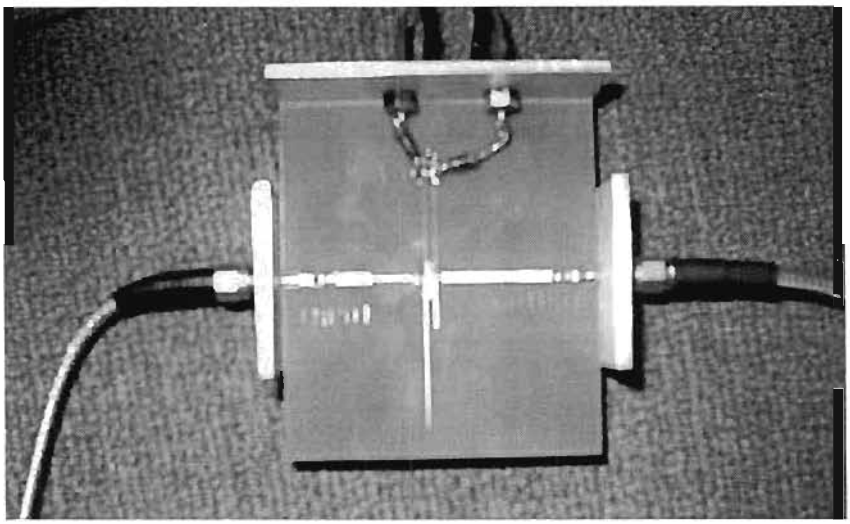

Fig. 8.8: Complete amplifier

8.9 Measurements and results

Testing of the amplifier was conducted using the Hewlett Packard Network analyzer HP8510A. Figure (8.9) shows the measurement set-up. Extreme caution was taken when connecting the amplifier to the network analyzer. Since both ports are only capable of handling a maximum of 17dBm of power, an external variable attenuator had to be used as a precautionary measure to prevent the expected output power of the amplifier from exceeding this rated power at port 2 of the analyzer. The power source at port 1 of the network analyzer was set to 0dBm. The external attenuation was set to 10dB thereby sourcing a –10dBm signal into the amplifier. This power level is significantly lower than the maximum power rating of the ATF10136 GaAs FET (430mW or 26.33dBm). With a maximum anticipated amplifier gain of 14dB, the expected power input at port 2 should be approximately 4dBm – well within the 17dBm power handling capability of the HP8510A.

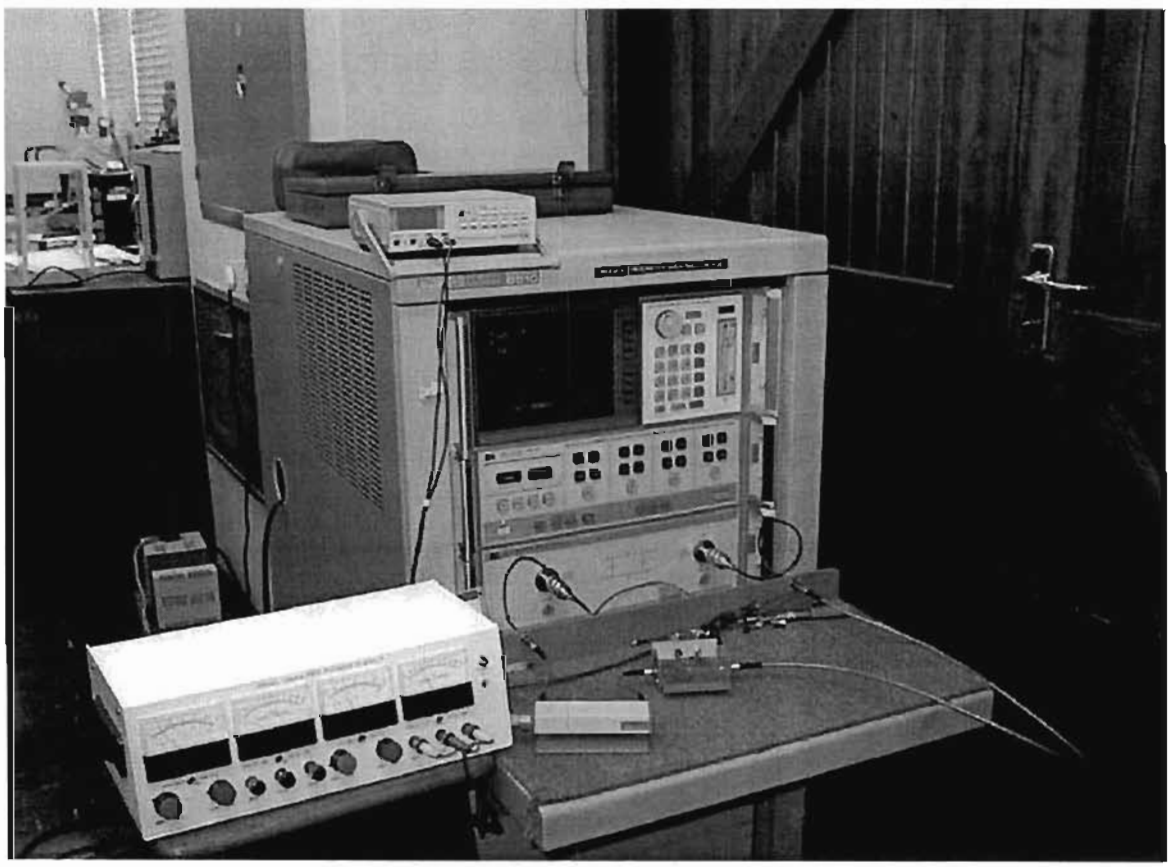

Fig. 8.9: Measurement set-up

Figures (8.10) to (8.13) show plots of the s-parameter measurement results.

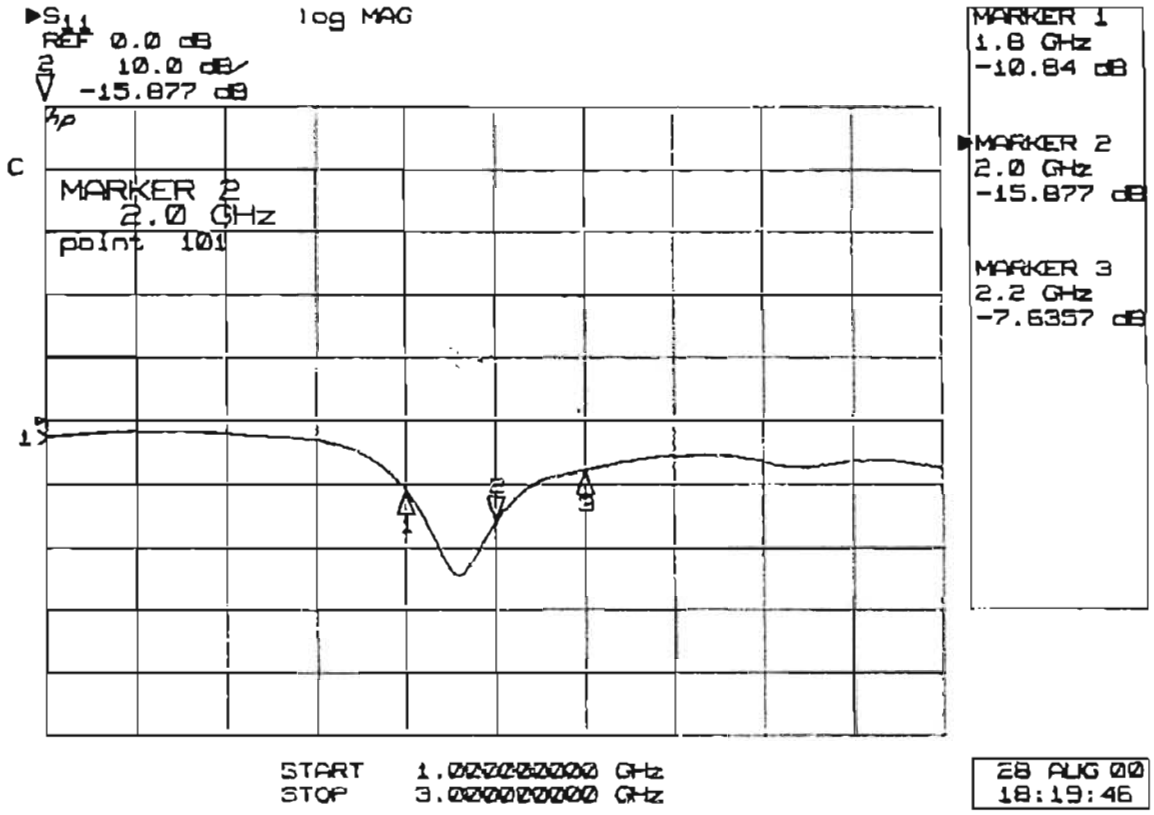

Fig. 8.10: S-parameter measured result $|S_{11}|$

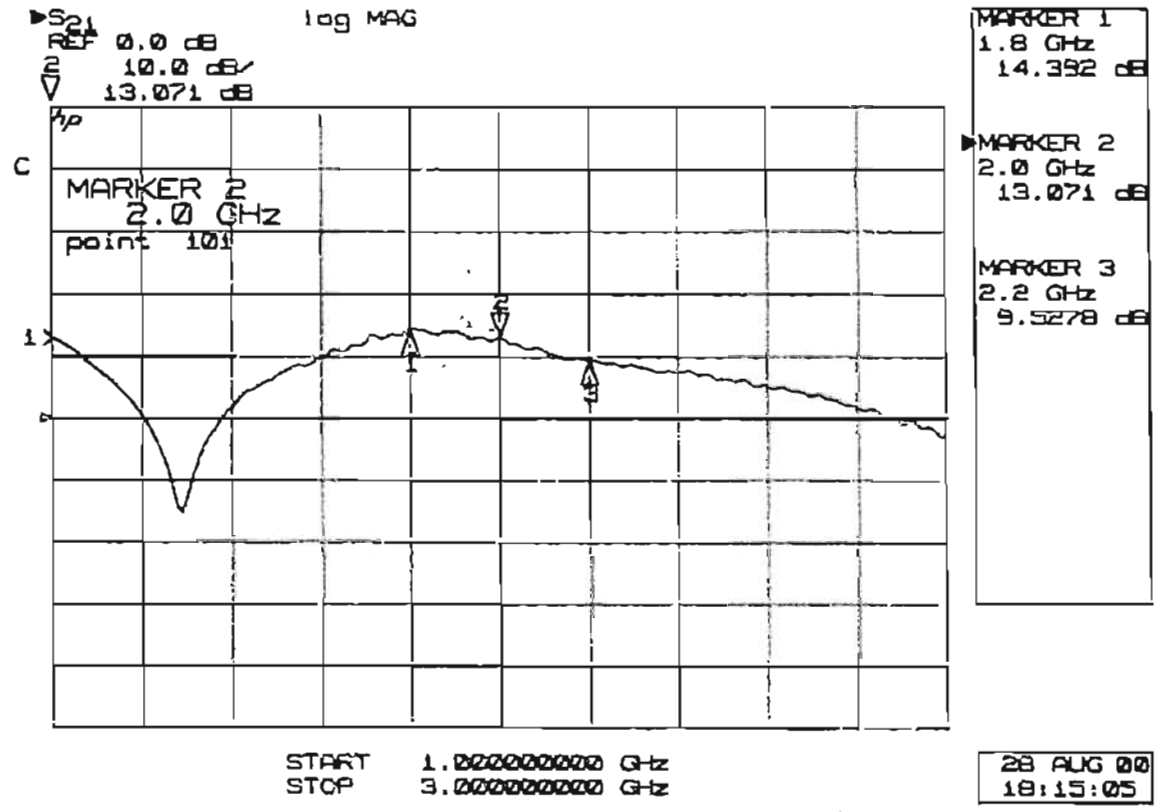

Fig. 8.11: S-parameter measured result $|S_{21}|$

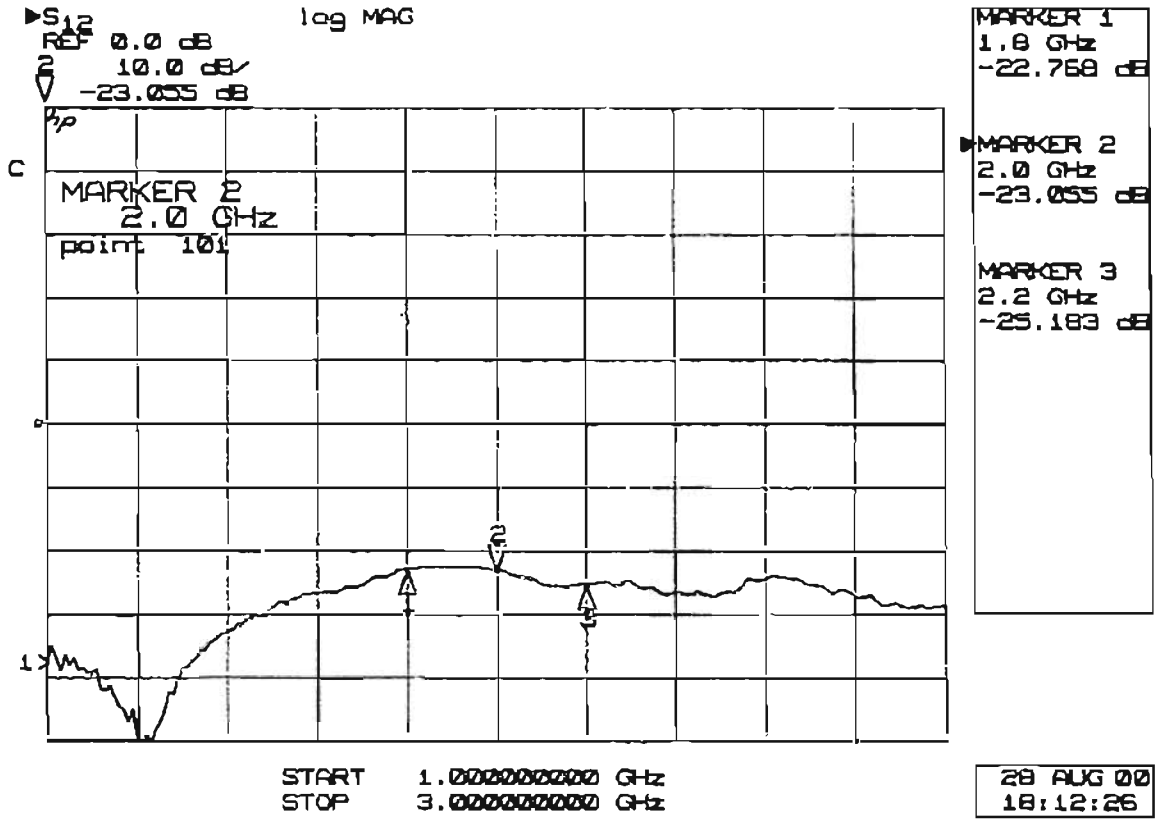

Fig. 8.12: S-parameter measured result $|S_{12}|$

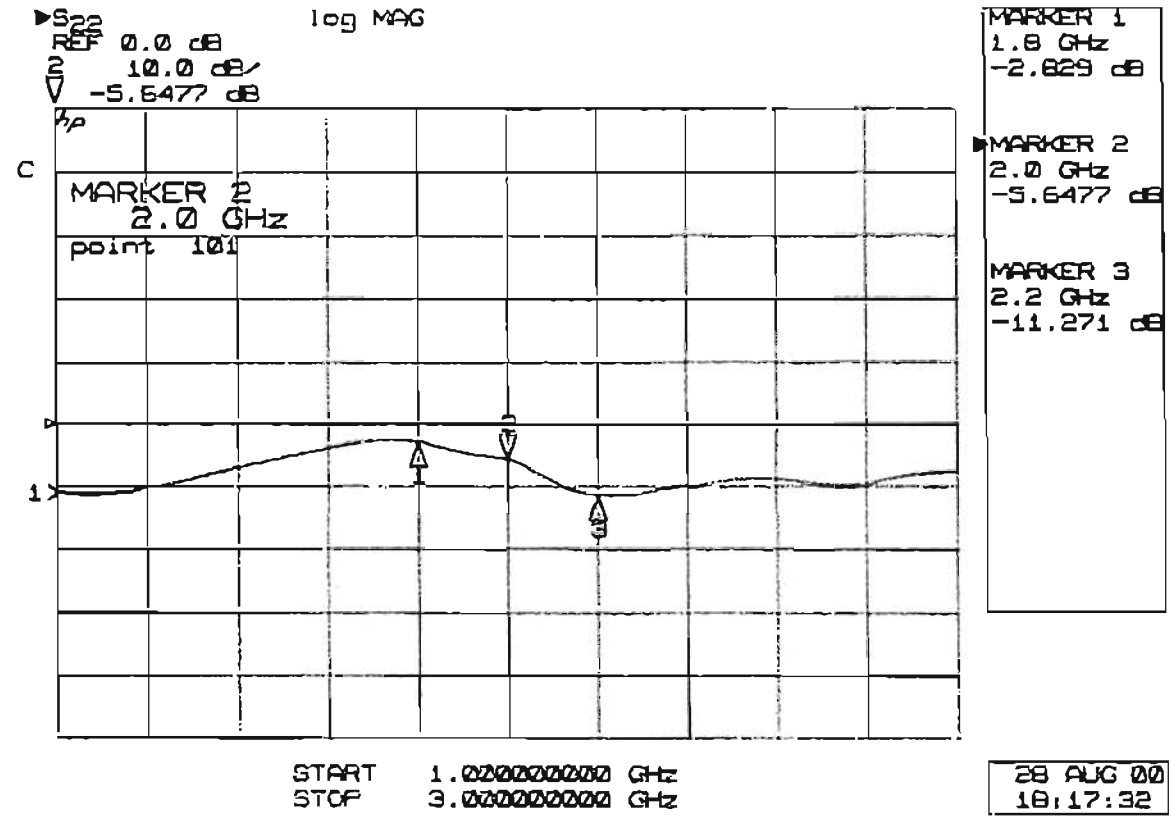

Fig. 8.13: S-parameter measured result $|S_{22}|$

Table (8.1) compares the measured s-parameter results with that of the simulation (after optimization) at the 2GHz centre frequency.

S-parameters	Simulation results (after optimization)	Measured results
$\|S_{11}\|$	-26.8dB	-15.9dB
$\|S_{21}\|$	13.8dB	13.1dB
$\|S_{12}\|$	-22.2dB	-23.1dB
$\|S_{22}\|$	-3.9dB	-5.6dB

Table 8.1: Comparison of simulated and measured s-parameter results

As can be seen in table (8.1), there is good correlation between measured and simulated s-parameter results, with the exception of the input reflection parameter ($|S_{11}|$). Nevertheless, an input reflection parameter of –15.9dB is reasonable.

The gain of the device was measured to be 13.1dB. The 3dB bandwidth was computed as 520MHz (Q factor of 3.85) which exceeded the minimum specified 10MHz bandwidth. A broadband design has thus been achieved.

8.6.1 Noise figure measurements

Procedures and techniques for noise figure measurements are described in [91], [92] and [93]. The technique described in [91], utilizing a spectrum analyzer, has been deemed the best measurement choice for the following reasons:

a) The noise figure can be measured at any frequency within a spectrum analyzer's frequency range. This enables measurement at the device's operating frequency without changes in the test set-up.
b) Due to the frequency selectivity of spectrum analyzers, noise figure measurements are independent of device bandwidth or spurious responses.

However, as with any other measurement, the analyzer's sensitivity and accuracy become limiting factors in noise figure measurements. The technique outlined in [91] has a limitation: the noise output of the device under test (DUT) must be greater than

the analyzer's internal noise level so that it can be measured. If the noise output of the DUT is below the analyzer's sensitivity level, its power must be raised by a low-noise, high-gain preamplifier. Then the noise level measured by the spectrum analyzer is greater than the device's output noise by the preamp's gain.

Due to inadequate gain of the designed amplifier and the inavailability of a preamp at the desired frequency, this technique (utilizing a spectrum analyzer) could not be used. Instead, another straightforward technique utilizing a HP346B noise source and HP8970B noise figure meter.

The basis of noise figure measurements using a noise source and noise figure meter depends on the noise linearity characteristic of linear two-port devices. The noise power out of a device is linearly dependent on the input noise power or noise temperature (T_s) as shown in figure (8.14). N_a is the noise power added by the DUT.

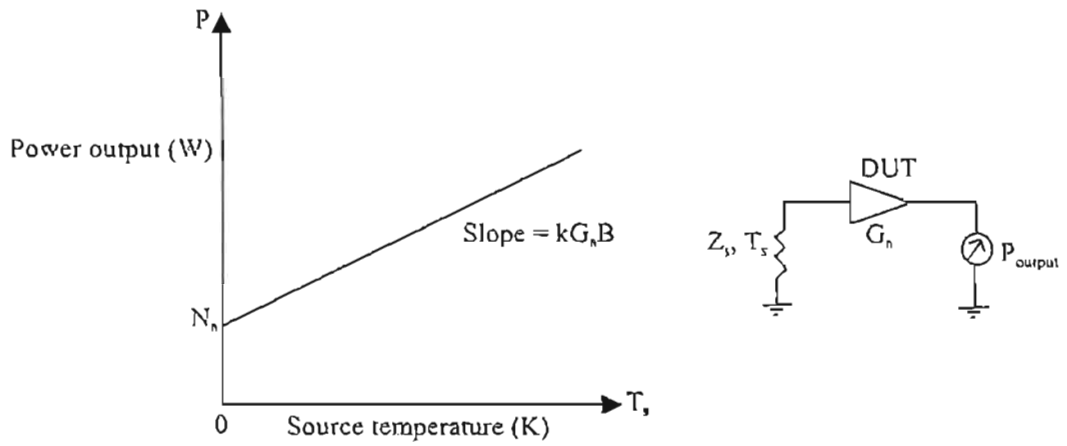

Fig. 8.14: Noise linearity characteristic of a linear two-port device

If the slope of this characteristic and a reference point is known, the output power corresponding to a noiseless input power, N_a can be found. From N_a, the noise figure F can be calculated using the well-known relation,

$$F = \frac{N_a + kT_oBG}{kT_oBG} \tag{8.1}$$

This equation appeared in chapter 5.

From figure (8.14), for a source impedance with a temperature of absolute zero, the power output consists solely of added noise N_a from the DUT. For other source temperatures the power output is increased by thermal noise from the source amplified by the gain of the DUT. The noise slope is determined by applying two different levels of input noise and measuring the output power change. A noise source is used to provide these two known levels of noise.

The HP346B noise source consists of a low-capacitance diode that generates noise when reversed biased into avalanche breakdown with a constant current [94]. When the diode is biased, the output noise will be greater than kT_CB (thermal noise) due to avalanche noise generation in the diode. When unbiased, the output will be the thermal noise (kT_CB) produced in the attenuator of the noise source. These levels are called T_h and T_C corresponding to the terms "hot" and "cold".

The HP346B produces noise levels approximately equal to 10000K when on and 290K when off. To make noise figure measurements a noise source must have a calibrated output noise. The excess noise ratio (*ENR*), expressed in dB is the ratio of the difference between T_h and T_C, divided by 290K,

$$ENR_{dB} = 10\log\frac{T_h - T_c}{T_o} \tag{8.2}$$

It should be noted that a 0dB *ENR* noise source produces a 290K temperature change between its on and off states. It is often erroneously believed that the *ENR* is the "on" noise relative to *kTB*. However, this is not the case.

T_C in equation (8.2) is assumed to be 290K when it is calibrated. Noise sources are supplied with an *ENR* table giving the *ENR* versus frequency values. The noise figure meter uses *ENR* and the *Y*-factor method as the basis of noise figure measurements. Using a noise source, this method allows the determination of the internal noise in the DUT and thus the noise figure. With a noise source connected to the DUT, the output power can be measured corresponding to the noise source on (N_2) and the noise source off (N_1). The ratios of these two powers is called the *Y*-factor,

$$Y = \frac{\text{output power with noise source on}}{\text{output power with noise source off}} = \frac{N_2}{N_1} \tag{8.3}$$

or in dB units, $Y_{dB} = 10\log Y$.

The *Y*-factor and *ENR* can be used to find the noise slope of the DUT that is depicted in figure (8.14). Since the calibrated *ENR* of the noise source represents a reference level for input noise, an equation for the internal noise (N_a) of the DUT can be derived. In a noise figure meter, this is automatically determined by modulating the noise source between the on and off states and applying internal calculations,

$$N_a = kT_oBG\left(\frac{ENR}{Y-1} - 1\right) \tag{8.4}$$

From this an expression for the noise figure can be derived. The noise figure that results is the total system noise figure, F_{sys}. It includes the noise contribution of all the individual parts of the system. In this case the noise generated in the noise figure meter has been included as a second stage contribution. If the gain of the DUT is large, the noise contribution from this second stage will be negligible. By substituting equation (8.4) into equation (8.1),

$$F_{sys} = \frac{ENR}{Y-1} \tag{8.5}$$

When the noise figure is much higher than the *ENR*, the device noise tends to mask the noise source output. In this case the *Y*-factor will be very close to 1. It is difficult to measure small ratios of the *Y*-factor accurately. For this reason, the *Y*-factor method is generally not used when the noise figure is more than 10dB above the *ENR* of the noise source, depending on the measurement instrument.

Table (8.2) shows the noise figure results for the designed amplifier at three frequencies. These results were obtained using the HP346B noise source and HP8970B noise figure meter. Measurements were restricted to a frequency of 1.8GHz which is the maximum operating frequency of the noise figure meter. At 1.8GHz the simulated noise figure (after optimization) from figure (8.5) was 2.2dB while the noise figure measurement yielded 2.7dB. At 1.7GHz and 1.75GHz, noise figures of 3.2dB and 4.97dB respectively, were measured. Simulated noise figures (after

optimization) of 2.8dB and 2.5dB at 1.7GHz and 1.75GHz, respectively were obtained. Unfortunately, no correlation/comparison between simulated and measured noise figure (at the desired frequency of 2GHz) could be made.

Frequency	Noise figure
1700MHz	3.2dB
1750MHz	4.97dB
1800MHz	2.7dB

Table 8.2: Noise figure measurements using the HP346B noise source and HP8970B noise figure meter

8.7 Conclusion

It was the intention of the author to specify, design and construct an LNA with parameters that would provide acceptable performance of the BPSK RF front-end of chapter 9. However, due to the reasons cited in section (8.6.1), the noise figure of the LNA could not be measured. Nevertheless, a low-cost, in-house 2GHz broadband low-noise amplifier (with 13.1dB gain and 520MHz 3dB bandwidth), for possible use in the adaptive CDMA system, was developed.

Relevant theory focusing on amplifier stability was presented and a suitable design technique, discussed and implemented. The topology of a low-noise high-frequency amplifier seems very simple. Tuning, shielding, proper grounding techniques and the design of a good layout plays an important role in the design of a fully functional amplifier. To conclude, a firm theoretical and practical basis on microwave low-noise amplifier design has been laid down in this chapter.

CHAPTER 9

MEASUREMENTS

9.1 Objectives

The intention of this chapter is to verify and support the theory and simulation results of the preceding chapters. The effect of RF component noise on DS-CDMA system performance was evaluated in chapter 5. Essentially, RF component noise (as a result of the noise figure) causes degradation of the signal-to-noise ratio (SNR) and hence an increase in the bit error rate (BER). Thus it is intended to replicate the SNRs within the measurement setup and compare the performance degradation between simulated and measured results. In the previous chapters, the BER was used as a figure of merit to quantify system performance. However, this chapter introduces a different measurement method, the Error Vector Magnitude (EVM), which has been gaining rapid acceptance in the wireless communication industry. In addition to providing a figure of merit for system performance, it introduces a methodology for troubleshooting possible impairments sources within a transceiver system that could cause signal degradation.

The phase noise theory in chapter 6 is reinforced by phase noise measurements. This section does not include all possible phase noise measuring schemes nor does it examine any single method in detail. Attention here is given to the more sensitive methods of phase noise measurement. Two such methods are the delay line method and the phase detector method. Using the HP89410A vector signal analyser in conjunction with the theory developed in chapter 6, a quantitative phase noise comparison of two frequency sources is performed.

9.2 System description

Figure (9.1) shows a block diagram of the system measurement setup. The receiver RF front-end was implemented using commercially-available (off-the-shelf) components. Recall, at the onset of the project, it was intended to use the Alcatel software radio as the CDMA transceiver platform. However, only during the implementation stages of the project, did it become apparent that the transceivers do not support carrier demodulation. Carrier demodulation is not a simple process requiring both precise frequency and phase locking of the incoming modulated carrier. Thus the design of a demodulator is complex and hence beyond the scope of this research. As a result, a HP89410A vector signal analyzer was used to demodulate the signal. Since the HP89410A has an operating frequency range between DC and 10MHz, the desired 70MHz IF was further downconverted to 5MHz using another mixer. However, the HP89410A is incapable of demodulating a CDMA signal i.e. it cannot perform the despreading operation. As a result a simple BPSK transceiver system was configured. A 2GHz, -20dBm BPSK modulated transmitted signal was generated using the Rohde and Schwarz SMIQ 03 signal generator. This signal was generated internally by modulating a 2GHz, -20dBm carrier by a 4.096MHz digital signal. This digital signal was set to consist of the repetitive PN code (0011101) that was used in the various ADS simulations. Figure (9.2) shows this sequence as viewed on an oscilloscope.

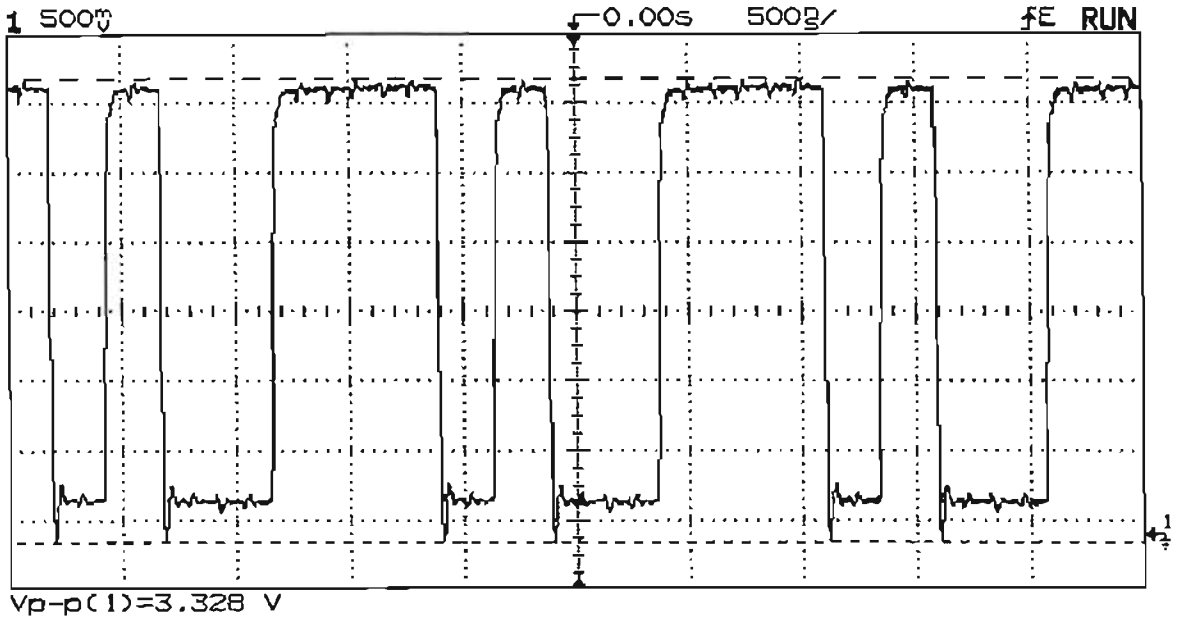

Fig. 9.2: Repetitive 4.096MHz digital signal used to BPSK modulate the carrier

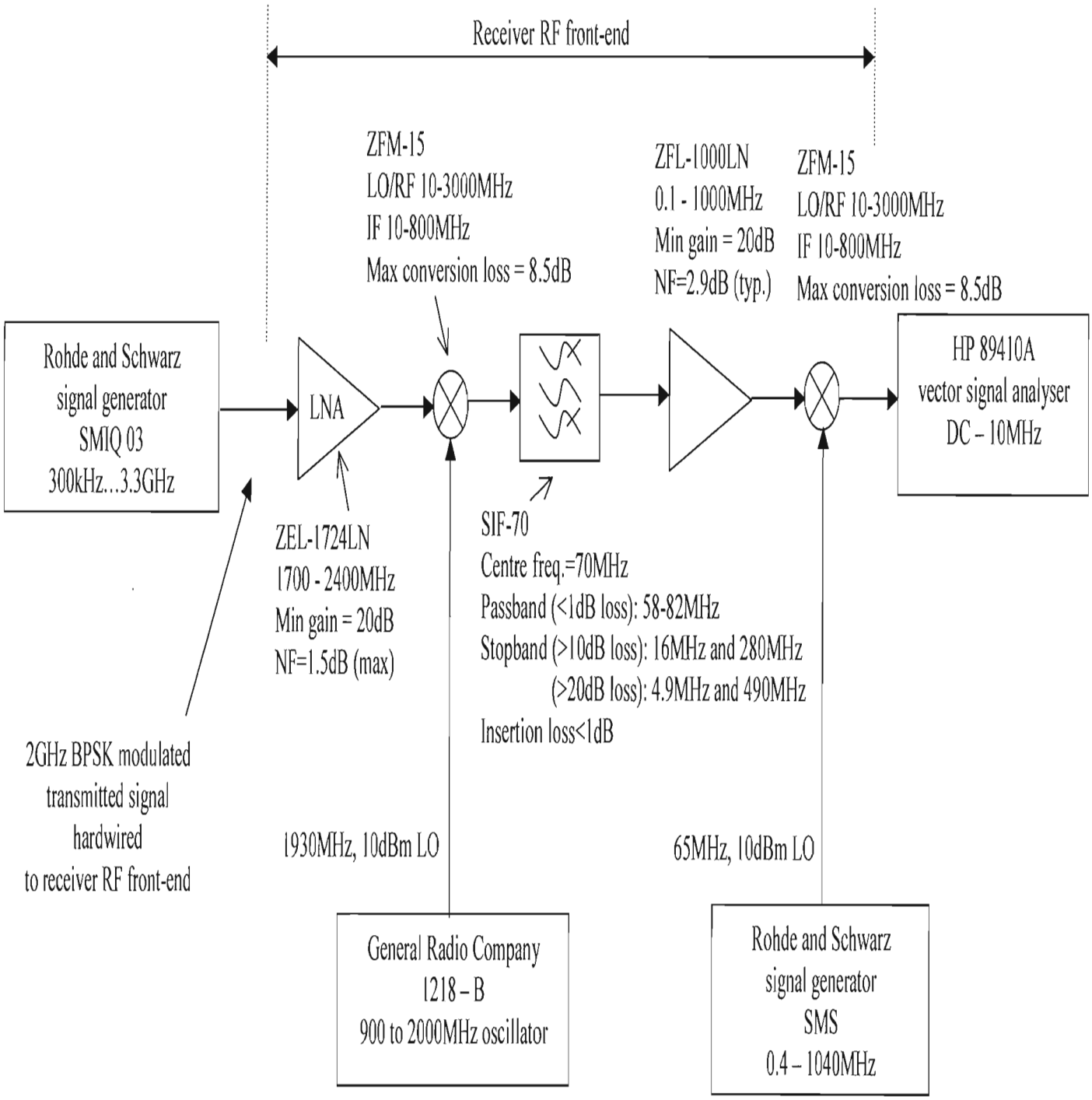

Fig. 9.1:Block diagram of measurement setup

The 2GHz, -20dBm BPSK spectrum (for different frequency spans are shown in figures (9.3) and (9.4).

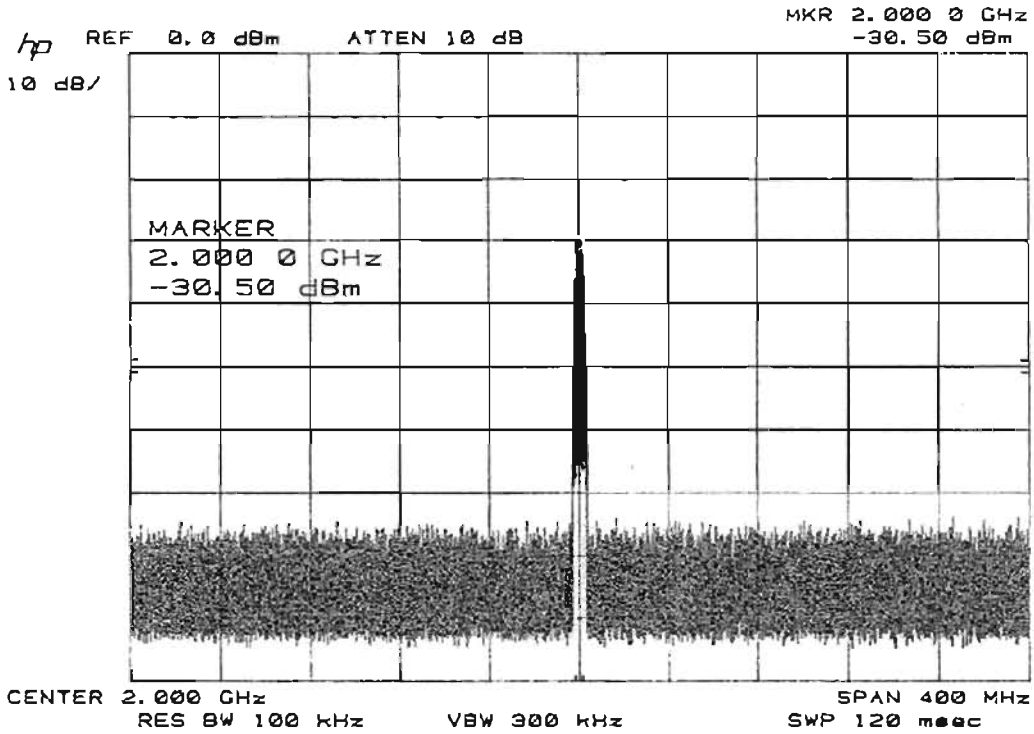

Fig. 9.3: 2GHz, -20dBm BPSK modulated spectrum (400MHz span) measured at output of Rohde and Schwarz SMIQ 03 signal generator

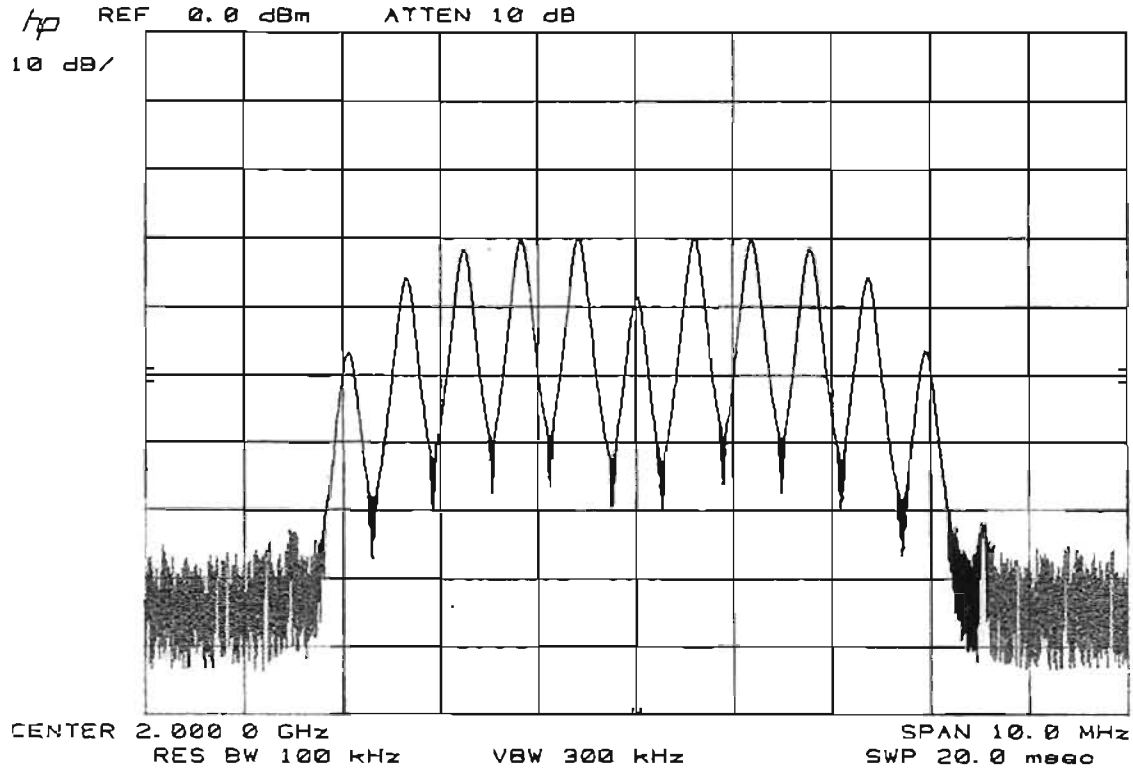

Fig. 9.4: 2GHz, -20dBm BPSK modulated spectrum (10MHz span) measured at output of Rohde and Schwarz SMIQ 03 signal generator

From chapter 4, using the null-to-null bandwidth criterion, a 4.096MHz data signal has an approximate RF bandwidth of 8.192MHz ($2f_b$) for BPSK modulation. This is evident in figure (9.4). Figure (9.5) shows the ADS simulation equivalent of figure (9.4). The estimation of this BPSK spectrum is obtained by computing the Fast Fourier Transform (FFT) of the signal. The FFT is a radix 2 FFT that uses 2^N data points (N = ceil[ln(number of data points)/ln2]). The number of data points is related to the resolution bandwidth and simulation sampling rate (2^N=sampling rate/resolution bandwidth). Thus for a resolution bandwidth of 100kHz and a sampling rate of 10 times the chip rate (10 x 4.096MHz), 410 data points are obtained and N=9. The spectrum is thus approximated by 410 points over a simulation bandwidth of 40.96MHz (ADS uses an RF bandwidth of 1/sampling time). Since the number of data points is less than 2^9, the simulated spectrum consists of spectral splatter which is caused by zero padding of the data set. The ADS documentation provides further information on this. Nevertheless, there is a reasonable correlation between the measured and simulated spectrum for the 1997MHz to 2003MHz band: There are 5 lobes on either side of the 2GHz centre frequency. The power levels of these corresponding lobes are within 5dB to each other.

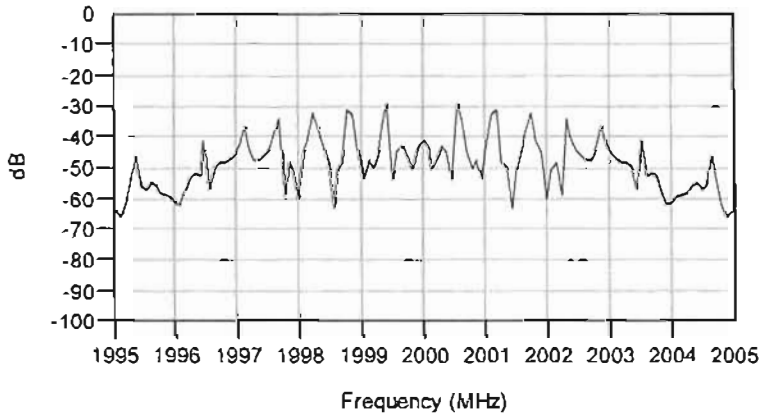

Fig. 9.5: ADS simulation equivalent of 2GHz, -20dBm BPSK modulated spectrum (10MHz span)

Referring to the block diagram (figure (9.1)), one notices that a commercially available LNA (ZEL-1724LN) as opposed to the designed LNA of chapter 8 was used in the measurement setup. As mentioned previously, the noise figure of the designed amplifier could not be measured at the desired frequency of interest (2GHz). Figures (9.6) and (9.7) show the 1930MHz, 10dBm LO signal and 70MHz IF BPSK spectrum, respectively. Note from the sum and difference frequency equations of chapter 7, a

LO frequency of 2070MHz could also be used to generate the 70MHz IF. However, the maximum operating frequency of the LO generator used here is 2GHz. The LO signal power was set to 10dBm, commensurate with the specified LO drive level of the ZFM-15 mixer. The ADS simulation equivalent of the measured 70MHz IF BPSK spectrum (figure (9.7)) is shown in figure (4.17) (chapter 4). On comparison of figure (4.17) with that of figure (9.7), it should be noted that the spectra have a similar appearance. However, the power levels of the spectra differ. The simulation model used in chapter 4 did not consider component gains and noise figures. Furthermore, the spread data was used to BPSK modulate a 10dBm 2GHz RF carrier (as opposed to the –20dBm RF carrier in this measurement setup). The simulation model in chapter 4 was merely intended to demonstrate CDMA concepts.

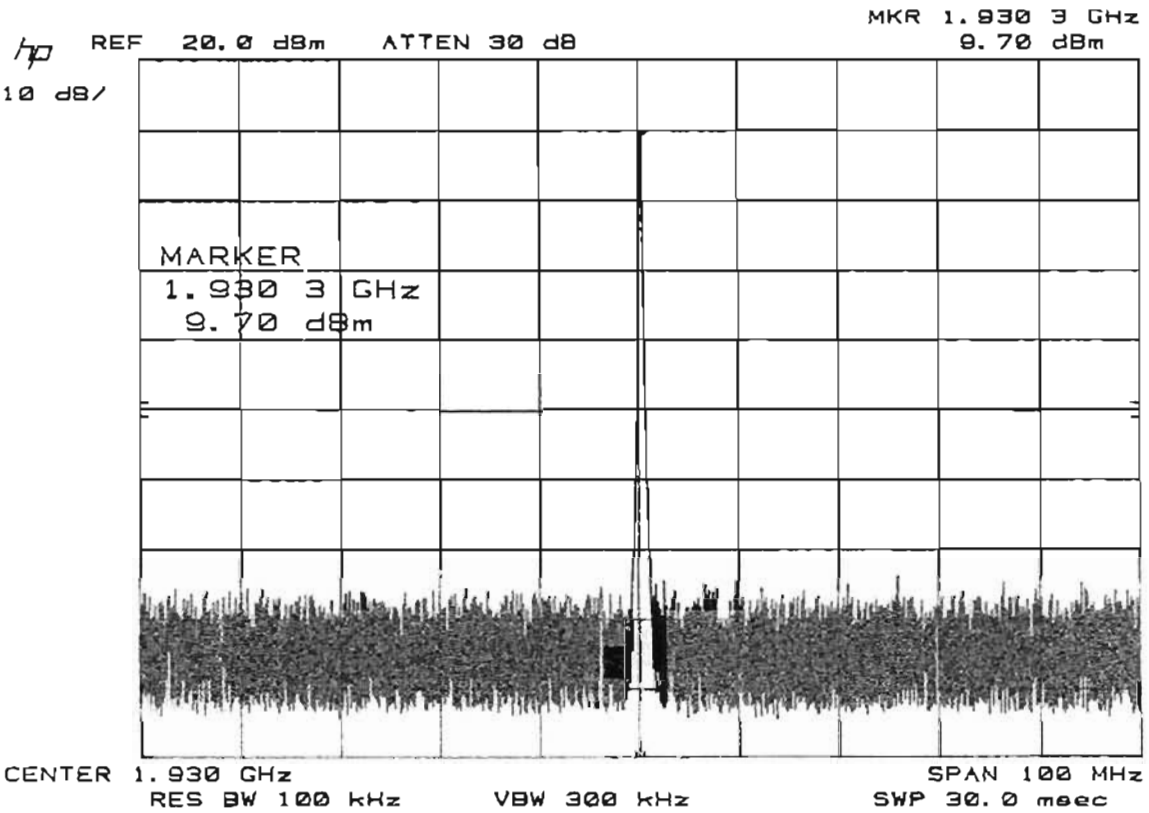

Fig. 9.6: 1930MHz, 10dBm LO signal measured at output of General Radio Company 1218-B oscillator

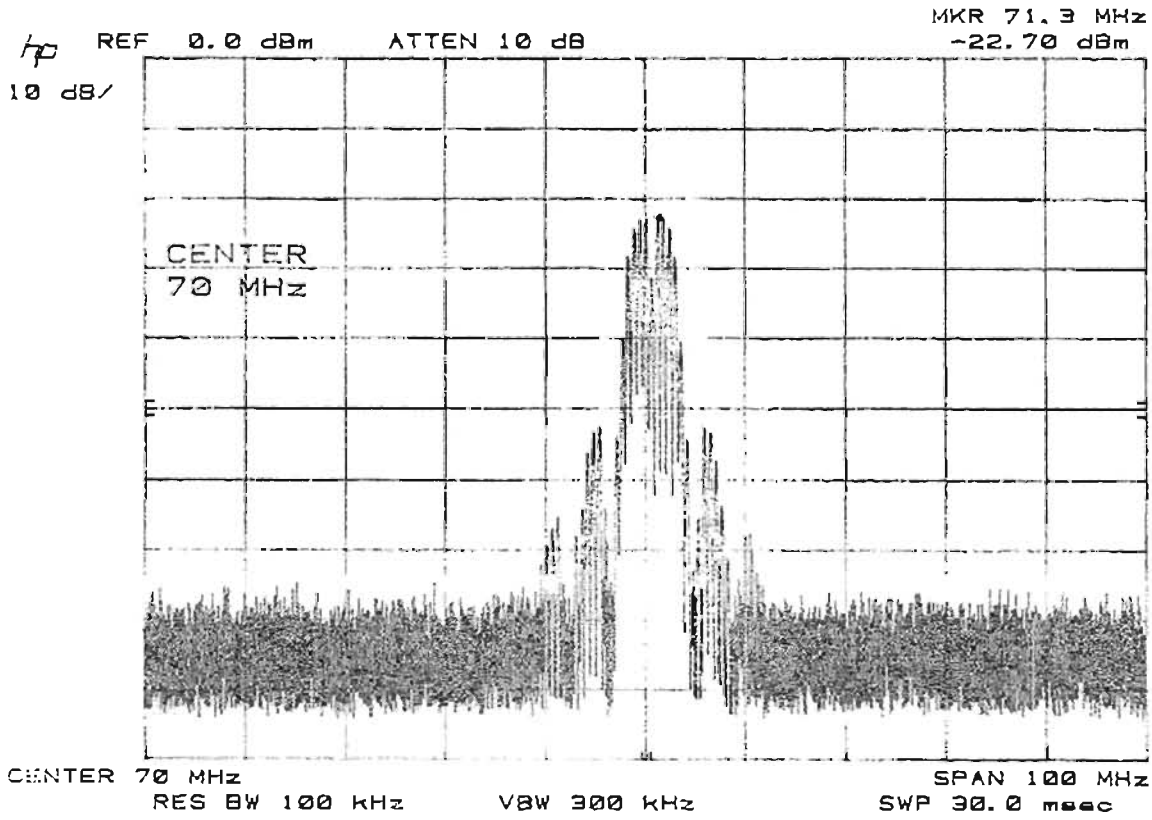

Fig. 9.7: 70MHz IF BPSK spectrum measured at input of SIF-70 IF bandpass filter

The gain/conversion loss for each of the RF front-end components were measured by using an unmodulated (single-tone) carrier of known power level and measuring the carrier power at the output of the device under test. The measured and specified values are compared in table (9.1).

RF device	Specified gain / conversion loss	Measured gain / conversion loss
ZEL-1724LN (LNA)	20dB (min)	20.4dB
ZFM-15 (mixer)	8.5dB (max) conversion loss	7.6dB conversion loss
SIF-70 (IF BPF)	<1dB insertion loss	1.1dB insertion loss
ZFL-1000LN (IF amp.)	20dB (min)	23dB
ZFM-15 (mixer)	8.5dB (max) conversion loss	11.1dB conversion loss

Table 9.1: Comparison between specified and measured gain / conversion loss

The overall gain of the front-end is computed as 23.6dB. Using the specified noise figure for each component and the measured gain, the approximate overall noise figure using Friis' equation [18], [61], [63] is computed to be 1.873dB.

9.3 Phase noise measurement

The most convenient way to measure phase noise is to use a common phase noise test system. Such a system usually contains a state-of-the-art frequency synthesizer, a low frequency spectrum analyzer and some dedicated hardware. Often, a second DSP-based spectrum analyzer is included to speed up and extend measurements close to the carrier by using a Fast Fourier Transform (FFT) technique. The whole system is then controlled by a computer with proprietary software. With these systems, it is possible to determine phase noise levels both very close to and very far from the carrier.

As mentioned in chapter 6, the sidebands of a LO signal may represent both AM and PM noise. Asymmetry in the sidebands indicates that both AM and PM noise are present. However, in many cases, the PM sidebands are dominant. For example, if a reasonably clean synthesized signal is multiplied up to be used as a high frequency reference, the phase noise sidebands are multiplied by the same factor as the frequency while the AM sidebands are unchanged or are limited. In this case, direct RF spectrum measurements at the multiplied frequency are a good approximation of the phase noise sidebands. The sidebands, when corrected and normalized to the carrier powers, represent the *L(f)* spectral density described in chapter 6. One way to achieve better resolution is to translate the signal down in frequency to the range of an analyzer with the desired IF bandwidth. Figure (9.8) shows a typical setup using a doubly-balanced mixer and a low pass filter. AM noise on the LO signal is rejected by a balanced mixer. Also all (m,n) spurious responses (chapter 7) where m, n or both are even are rejected by doubly balanced mixers.

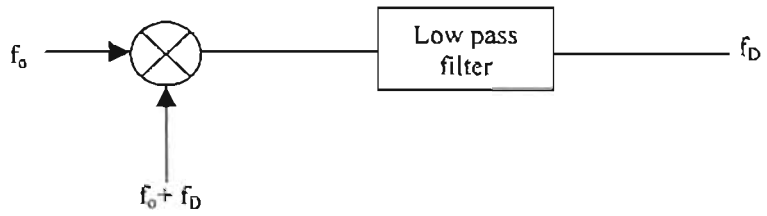

Fig. 9.8: Sideband translation

One of the advantages of this technique is that AM sidebands on the measured signal will be stripped off if it is to be used as the high level signal at the mixer. However, there are two potential problems:

a) The difference frequency will contain sidebands which are folded up from below zero frequency. Whether or not the sidebands are significant depends on the nature of the particular source being measured.
b) The phase noise sidebands from the reference frequency at the mixer will also be translated down. This problem is avoided by using a source with better phase noise specifications than the one being tested.

Two requirements must be met in a phase-noise measuring scheme to reach a noise floor low enough for the best oscillators:

a) The carrier's phase noise must be separated from its AM components.
b) Carrier must be eliminated. It must somehow be cancelled to measure its close-in phase noise sidebands. A frequency discriminator is used to do this. Information on this is contained in [95].

9.3.1 Delay line method

Figure (9.9) illustrates this method where the above two requirements are satisfied

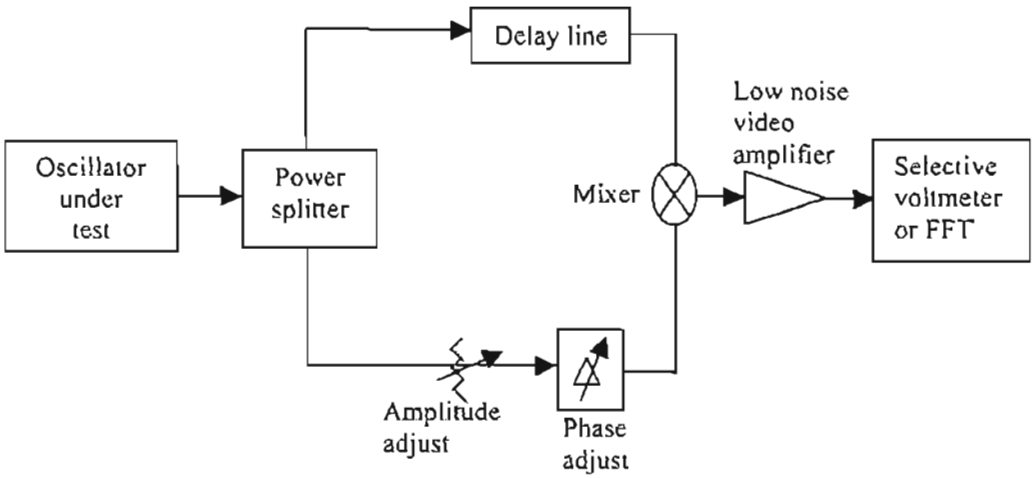

Fig. 9.9: Delay line phase noise test equipment block diagram

The signal to be measured is divided into two equal parts. One-half goes through a delay line, producing a quadrature phase shift of the carrier. The other-half, undelayed except for an incremental adjustment is mixed with the delayed signal in a homodyne detector. This cancels the carrier. The quadrature shift places one carrier

in phase with the other's quadrature or phase noise sidebands, as the mixing signal. The demodulated signal is amplified for measurement. This scheme is insensitive to AM noise. This technique does not require an extremely stable test oscillator, but it has limitations imposed by the delay line requirements:

a) A long delay line means a low instrument noise floor
b) A long line also implies high transmission losses, so it must be driven by a power amplifier to give the detector a minimum signal level. This amplifier contributes its own phase noise and converts signal amplitude noise to phase noise. If no amplification is used, optimum delay requires that the product of its length and attenuation be unity. The product of its delay and offset frequency must be less than unity. This latter condition limits measurements close to the carrier, as the delay must be high to measure small offset frequencies.

The delay line may be made of any form of microwave transmission line. Coaxial and waveguide lines are the most common. A coaxial air line gives minimum loss but it is large. The waveguide line has the advantage that its group velocity is less than that of light and decreases as frequency approaches cut-off. Attenuation also increases at the same time. It is an optimum delay line but is bulky. A transmission form of resonant cavity also may be used as a delay line. It has a much greater delay per unit volume than a transmission line. However, it and the oscillator under test must be quite stable, because the cavity must be tuned accurately to the oscillation frequency.

9.3.2 Phase detector method

A phase detector scheme can be used to cancel the carrier and give quadrature mixing. Figure (9.10) shows an elementary circuit for the phase detector method.

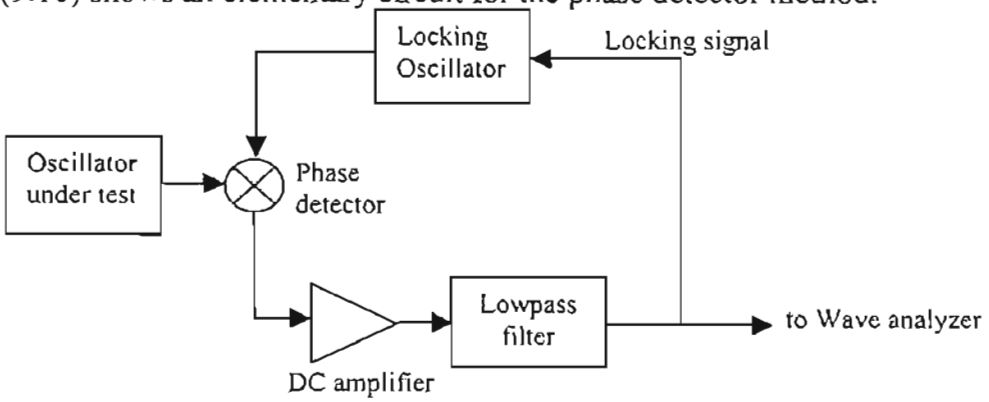

Fig. 9.10: Block diagram of the phase detector phase noise measuring system

The test and locking oscillators must be on the same frequency, and the locking oscillator's phase noise must be either very low or a known quantity. The two oscillator's signals are mixed, their difference frequency amplified, filtered and used for phase lock. At offset frequencies above the locked bandwidth, the noise is the sum of the two oscillator's phase noise powers. This setup requires very stable free-running oscillators. The difference frequency must remain within a few hundred hertz of the locking frequency for a short time (up to a minute or so).

9.3.3 Phase noise measurement and comparison of 2 frequency sources

The HP89410A vector signal analyzer was used to measure and compare the phase noise performance of the Rohde and Schwarz SMIQ 03 and SMS frequency sources (figure (9.1)). The HP89410A has a phase noise measurement utility that eliminates external hardware or circuitry (described above) thereby simplifying the measurement process considerably. However, measurements are restricted to a carrier frequency of 10MHz (within the operating frequency range of the instrument). The setup simply requires direct connection of the frequency source to the HP89410A. The instrument then performs phase demodulation to eliminate the carrier thereby allowing the phase noise to be measured. The power level and frequency of both sources was set to 10dBm and 5MHz respectively. Figures (9.11) and (9.12) show the power spectral density of phase fluctuations of both frequency sources for a resolution bandwidth and frequency span of 300Hz and 20kHz, respectively. Note from chapter 6, the power spectral density of phase fluctuations, denoted as $S_\phi(f)$ ($= \phi_{RMS}^2$), is expressed in units of decibels below $1rad^2$ in a bandwidth of 1Hz. Tables (9.2) and (9.3) show the single sideband (SSB) level versus offset frequencies. Also shown are the single sideband noise-to-signal ratio or variance (σ_T^2) computed by use of equation (6.49) in chapter 6. The SSB levels in tables (9.2) and (9.3) have been extrapolated from figures (9.11) and (9.12) respectively. From the variance values of both frequency sources, it can be concluded that the Rohde and Schwarz SMIQ 03 signal generator has considerably better spectral purity or phase noise performance than that of the SMS signal generator. This was anticipated at the onset of the measurement since the SMIQ 03 is a much more recent model than the SMS.

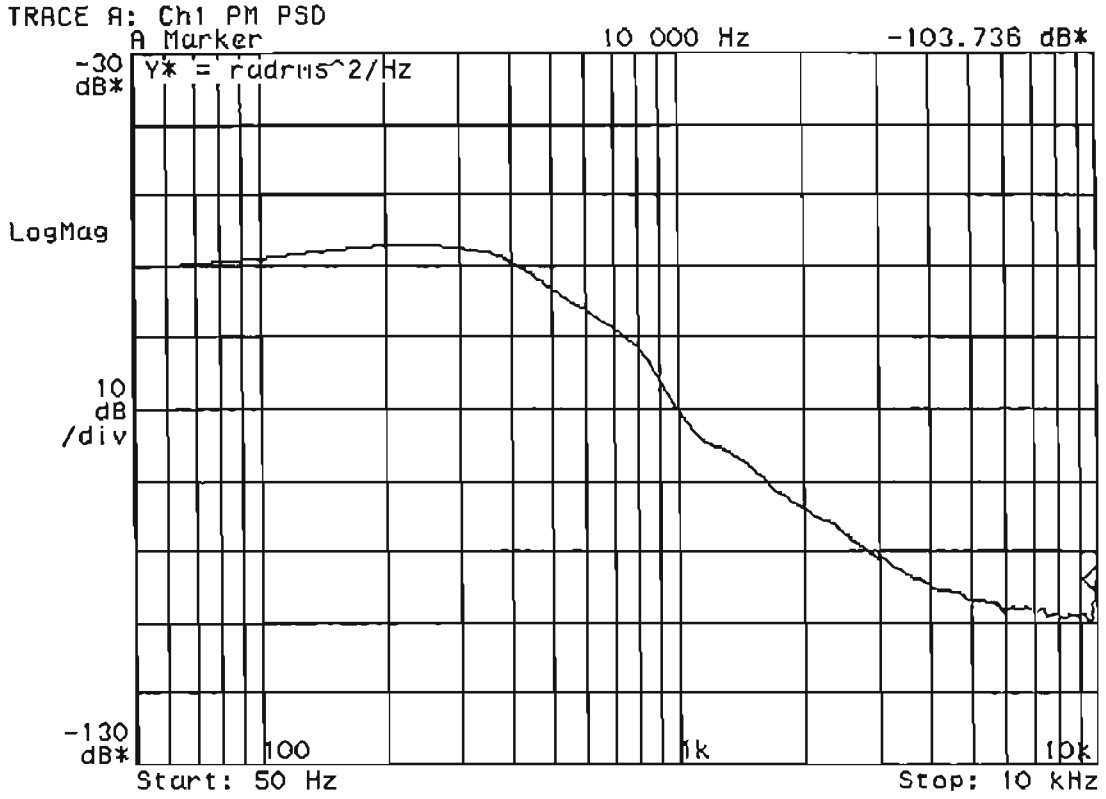

Fig. 9.11: Phase noise spectral density profile of the Rohde and Schwarz SMS 0.4MHz – 1040MHz signal generator (f_o=5MHz, resolution bandwidth=300Hz, frequency span=20kHz)

Offset frequency	SSB level (dBc/Hz)	variance (σ_T^2)
50Hz	-61	-40.5dB
100Hz	-59	
1kHz	-82	
10kHz	-104	

Table 9.2: Phase noise parameters of the Rohde and Schwarz SMS 0.4MHz – 1040MHz signal generator

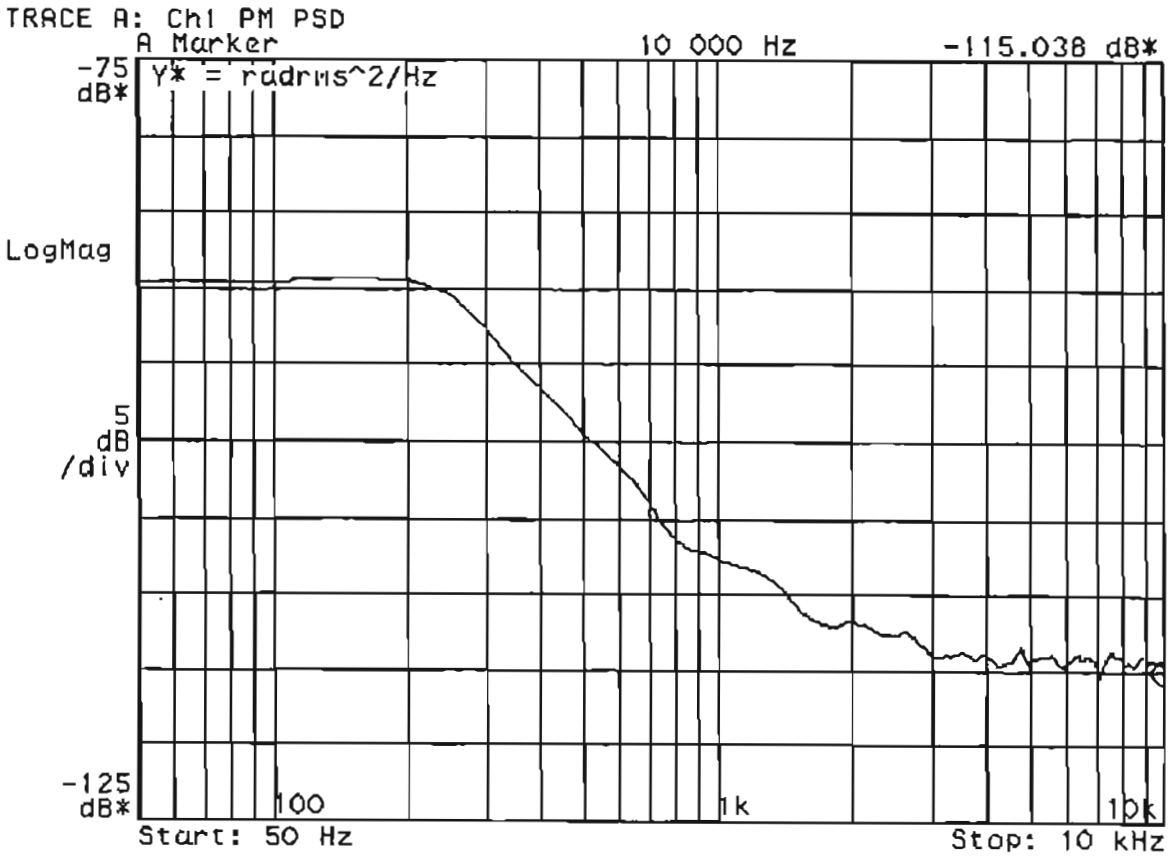

Fig. 9.12: Phase noise spectral density profile of the Rohde and Schwarz SMIQ 03 300kHz – 3.3GHz signal generator (f_o=5MHz, resolution bandwidth=300Hz, frequency span=20kHz)

Offset frequency	SSB level (dBc/Hz)	variance (σ_T^2)
50Hz	-89.6	-66.4dB
100Hz	-89.5	
1kHz	-108	
10kHz	-114	

Table 9.3: Phase noise parameters of the Rohde and Schwarz SMIQ 03 300kHz – 3.3GHz signal generator

The resolution bandwidth and frequency span of the measurement instrument are crucial to accurate phase noise measurements. Both these parameters are inter-related. The smaller the resolution bandwidth, the greater the measurement accuracy and the larger the instrument sweep time. For the HP89410A vector signal analyser, the lower and upper bounds on the resolution bandwidth (RBW) are given by:

$$RBW_{min} = \frac{ENBW \times [span]}{(num\ of\ freq.\ pts.) - 1} \tag{9.1}$$

$$RBW_{max} = 0.3 \times [span] \tag{9.2}$$

where $ENBW$ = normalized equivalent noise bandwidth

$span$ = frequency span

$num\ of\ freq.\ pts$ = number of frequency points required to interpolate the plots

To measure phase noise at a large offset frequency requires a corresponding increase in both the frequency span and resolution bandwidth. This case is demonstrated in figure (9.13) where it is desired to measure the SSB level at an offset frequency of 20kHz. Table (9.4) shows the extrapolated data corresponding to some of the offset frequencies (100Hz, 1kHz and 10kHz) of table (9.3). The SSB levels at offset frequencies of 100Hz and 1kHz do not correlate reasonably. This is due to the interpolation of the spectrum as a result of an increase in frequency span and hence the resolution bandwidth.

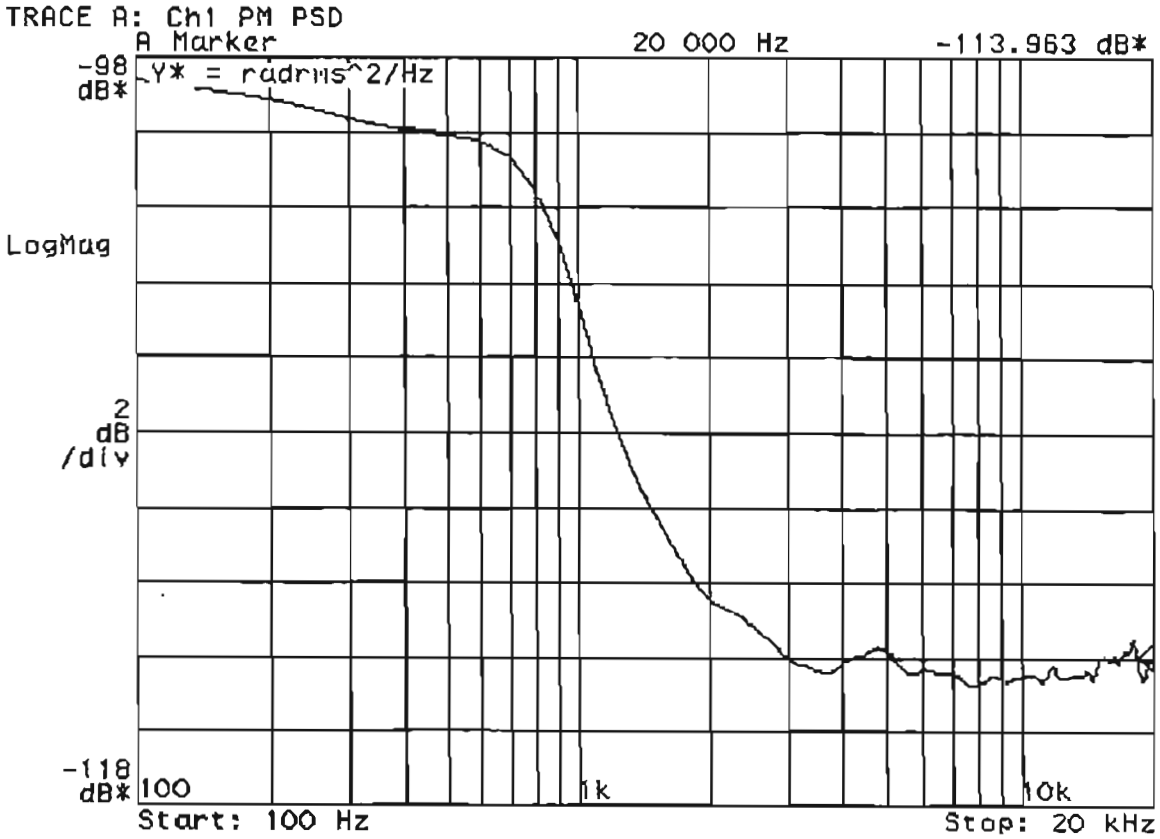

Fig. 9.13: Phase noise spectral density profile of the Rohde and Schwarz SMIQ 03 300kHz – 3.3GHz signal generator (f_0=5MHz, resolution bandwidth=1kHz, frequency span=40kHz)

Offset frequency	SSB level (dBc/Hz)
100Hz	-99
1kHz	-105
10kHz	-114
20kHz	-114

Table 9.4: Phase noise parameters of the Rohde and Schwarz SMIQ 03 300kHz – 3.3GHz signal generator for resolution bandwidth of 1kHz and 40kHz frequency span

9.4 Error Vector Magnitude (EVM) measurements

A fundamental function of the HP89410A vector signal analyzer, apart from carrier demodulation, is to perform error vector magnitude (EVM) measurements. Thus far, the bit error rate (BER) was used as a figure of merit for system performance. Poor quality transmission can be seen as low or poor signal quality which may result in a high BER. BER testers count the number of errors which cross certain limits/thresholds. These instruments do not indicate why or how far out of limit the signal is, or even if the error occurred in the transmitter or receiver. However, EVM in addition to providing a simple, quantitative figure of merit for a digitally modulated signal, it also introduces a methodology to pinpoint exactly the type of degradations present in a signal, and even help identify their sources. Among the impairments that can be pinpointed are compression, LO feedthrough, IQ origin offset, IQ gain imbalance, quadrature error, phase noise, symbol timing errors and intersymbol errors. EVM measurements are growing rapidly in acceptance, having already been included in standards such as GSM, NADC and PHS (Personal Handyphone System).

It should be noted that even though the HP89410A performs demodulation as a prerequisite to the EVM process, the demodulated signal is not available as an analog output or bitstream for analysis or BER measurements. The HP89410A digitizes the RF signal and then performs demodulation using internal DSPs. Hence BER measurements are not possible with this instrument.

9.4.1 EVM definition

Vector modulation involves the transfer of digital bits onto an RF carrier by varying the carrier's magnitude and phase such that at each data transition the carrier occupies any one of several specific locations on the I versus Q plane. A constellation diagram shows the valid locations (magnitude and phase relative to the carrier) for all permitted symbols, of which there must be 2^n, given n bits transmitted per symbol. Thus to demodulate the incoming data, the exact magnitude and phase of the received signal must be accurately determined for each clock transition. The layout of the constellation diagram and its ideal symbol locations are determined by the modulation format (e.g. BPSK, QPSK, 16QAM).

At any moment in time, the signal's magnitude and phase can be measured. These values define the actual or measured phasor. At the same time, a corresponding ideal or reference phasor can be calculated, given knowledge of the transmitted data stream, the symbol clock timing, baseband filtering parameters, etc. The difference between these two phasors form the basis for EVM measurements. Figure (9.14) defines EVM and several related terms.

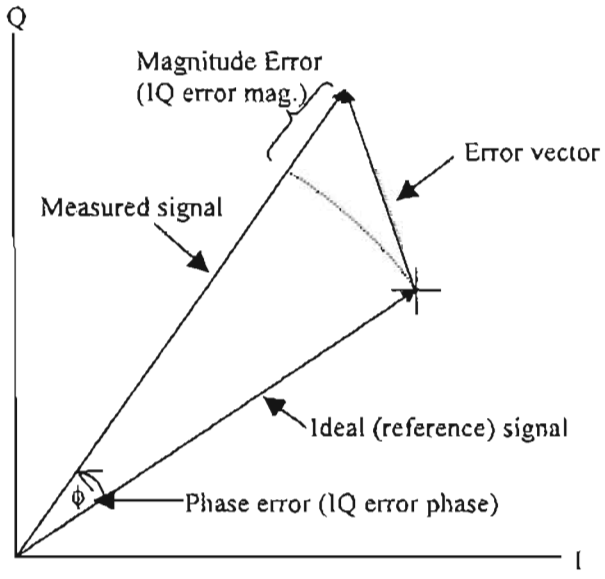

Fig. 9.14: Phasor description of EVM and related quantities

As shown, EVM is the scalar distance between the two phasor end points (the magnitude of the difference vector). Expressed another way, it is the residual noise. By convention, EVM is expressed as a percentage of the peak signal level, usually

defined by the constellation's corner states. While the error vector has a phase value associated with it, this angle is random because it is a function of both the error itself (which may or may not be random) and the position of the data symbol on the constellation (which is also random). A more useful angle is measured between the actual and ideal phasors (IQ phase error) which contain information useful in troubleshooting signal problems. Likewise, IQ magnitude error shows the magnitude difference between the actual and ideal signals.

9.4.2 Using EVM analysis to troubleshoot digital RF communication systems

Figure (9.15) shows an EVM troubleshooting tree that can be used as a general guideline for troubleshooting digital RF communication system using the HP89410A vector signal analyzer.

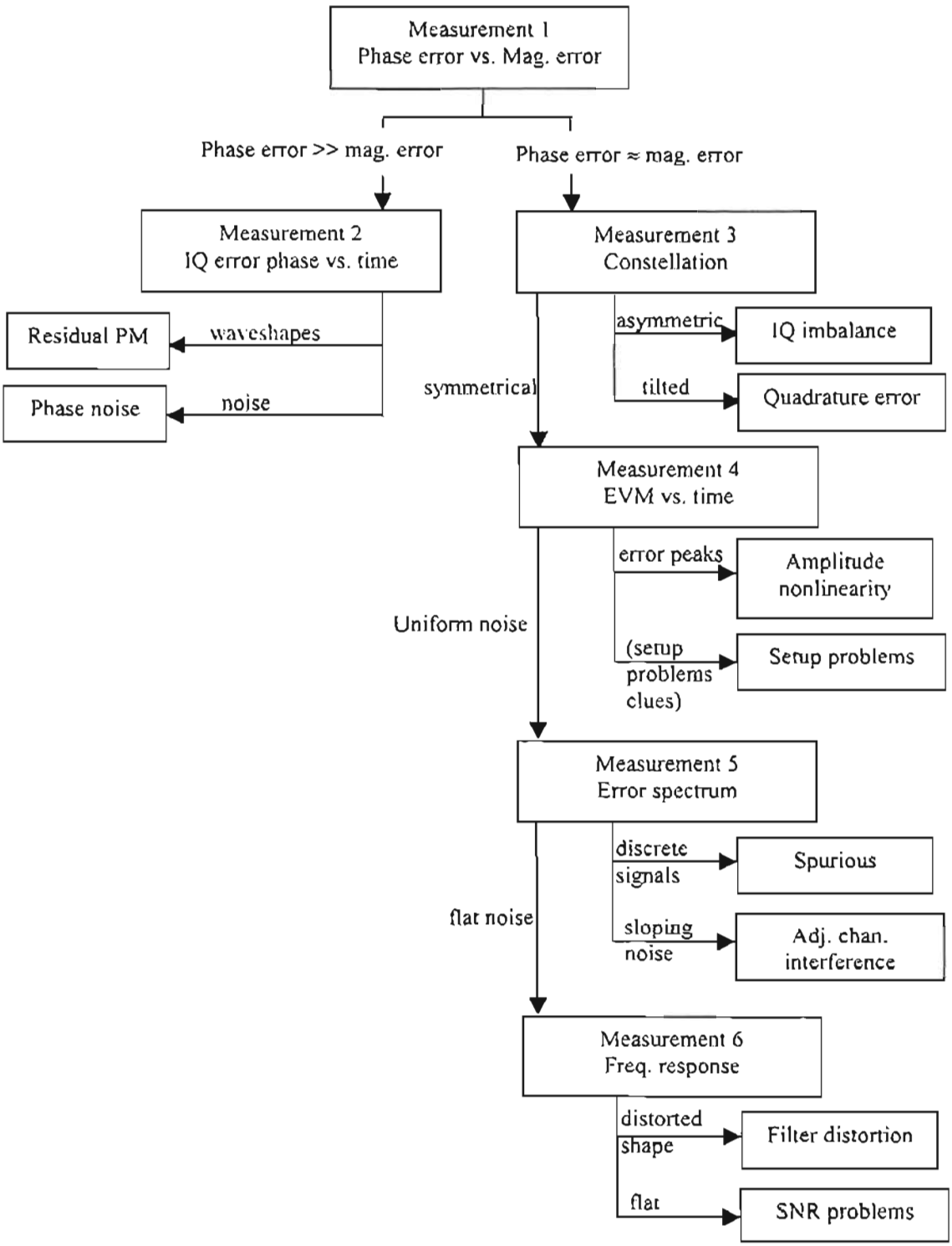

Fig. 9.15: EVM troubleshooting tree (from [96])

The following sections provide a brief description of the troubleshooting tree. Note that the description here is not intended as step-by-step procedures but rather as

guidelines for those who are already familiar with the basic operation of the HP89410A. Additional information can be obtained by consulting the instrument's on-screen help facility or [96], [97].

9.4.2.1 Measurement 1: Magnitude vs. phase error

The first diagnostic step in troubleshooting a digital RF communication system is to resolve EVM into its magnitude and phase error components (figure (9.14)) and compare their relative sizes. When the average phase error (in degrees) is larger than the average magnitude error (in percent) by a factor of about five or more, this indicates that some sort of unwanted phase modulation is the dominant error. Proceed to measurement 2 to look for noise, spurs or cross-coupling problems in the frequency reference, phase-locked loops or other frequency generating stages. Residual AM is evidenced by magnitude errors that are significantly larger than the phase angle errors. In many cases, the magnitude and phase errors will be approximately equal, indicating a broad category of potential problems, which will be further isolated in measurements 3 to 6.

9.4.2.2 Measurement 2: IQ phase error vs. time

Phase error is the instantaneous angle difference between the measured signal and the ideal reference signal. When viewed as a function of time (or symbol) it shows the modulating waveform of any residual or interfering PM signal. Sinewaves or other regular waveforms indicate an interfering signal. Uniform noise is a sign of some form of phase noise (random jitter, residual PM/FM, etc).

9.4.2.3 Measurement 3: IQ Constellation diagram

This is a common graphical analysis technique utilizing a polar plot to display a vector-modulated signal's magnitude and phase relative to the carrier, as a function of time or symbol. The phasor values at the symbol clock times are highlighted by a dot, and are important. A perfect signal will have a uniform constellation that is perfectly symmetric about the origin. IQ imbalance is indicated when the constellation is not "square" i.e. when the Q-axis height does not equal the I-axis width. Quadrature error is seen in any "tilt" to the constellation. It is caused when the phase relationship between the I and Q vectors is not exactly 90°. Gain imbalance or quadrature errors can be caused by matching problems due to component differences (filters, DACs,

etc.) between the I side and Q side of a network. Imbalances can also be caused by errors in IF filtering, for example, when a filter's response is not flat.

9.4.2.4 Measurement 4: Error vector magnitude vs. time

As described earlier, EVM is the difference between the input signal and the internally generated ideal reference. When viewed as a function of symbol or time, errors may be correlated to specific points on the input waveform such as peaks or zero crossings. Note that EVM is a scalar (magnitude-only value). The EVM vs. time waveform is compared with the IQ measured vs. time waveform. Both traces are observed for the same moment time. Error peaks occurring with signal peaks indicate compression or clipping. Error peaks that correlate to signal minima suggest zero-crossing non-linearities in an amplification stage. An example of zero-crossing nonlinearities is in a push-pull amplifier, where the positive and negative halves of the signal are handled by separate transistors. In high power amplifiers, it is usually a challenge to precisely bias and stabilize the amplifiers such that one set is turning off exactly as the other set is turning on, with no discontinuities. The critical moment is the zero-crossing point that can lead to zero-crossing errors, distortion or nonlinearities.

9.4.2.5 Measurement 5: Error spectrum (EVM vs. frequency)

The error spectrum is calculated from the FFT of the EVM vs. time waveform and results in a frequency domain display that can show details not visible in the time domain. The centre frequency of this measurement's display is the carrier frequency input to the instrument (5MHz in the case of the proposed BPSK system). The error-noise spectrum of the signal shows the noise concentrated within the bandpass and then rolling off rapidly on either side. In most digital systems, non-uniform distribution or discrete signal peaks indicate the presence of externally coupled interference (e.g. switching power supply interference).

9.4.2.6 Measurement 6: Channel frequency response

This measurement calculates the ratio of the measured signal to the reference signal. Because the latter is internally generated and ideal, it allows a frequency response measurement to be made across an entire modulated system without physically

accessing the modulator input. Having this baseband access point is important because in most cases, such a stimulus point is usually unavailable either because it is

a) inaccessible

b) digitally implemented

c) the aggregate of separate I and Q inputs

This measurement result shows the aggregate, complex transfer function of the system for the baseband I and Q inputs of the modulator to the point of measurement. This can be viewed as a magnitude ratio, a phase response or group delay. If there is a small deviation from the flat response / linear phase, serious performance problems can result.

9.4.3 Demonstration of EVM analysis for the proposed BPSK system

In this section, the EVM theory and concepts developed thus far, would be used to troubleshoot / analyze the proposed BPSK transceiver system (figure (9.1)). First, the different measurement displays (some described in section (9.4.2)) for the analysis of vector modulated signals, would be illustrated. Figure (9.16a) and (9.16b) show a typical HP89410A screenshot of the EVM results.

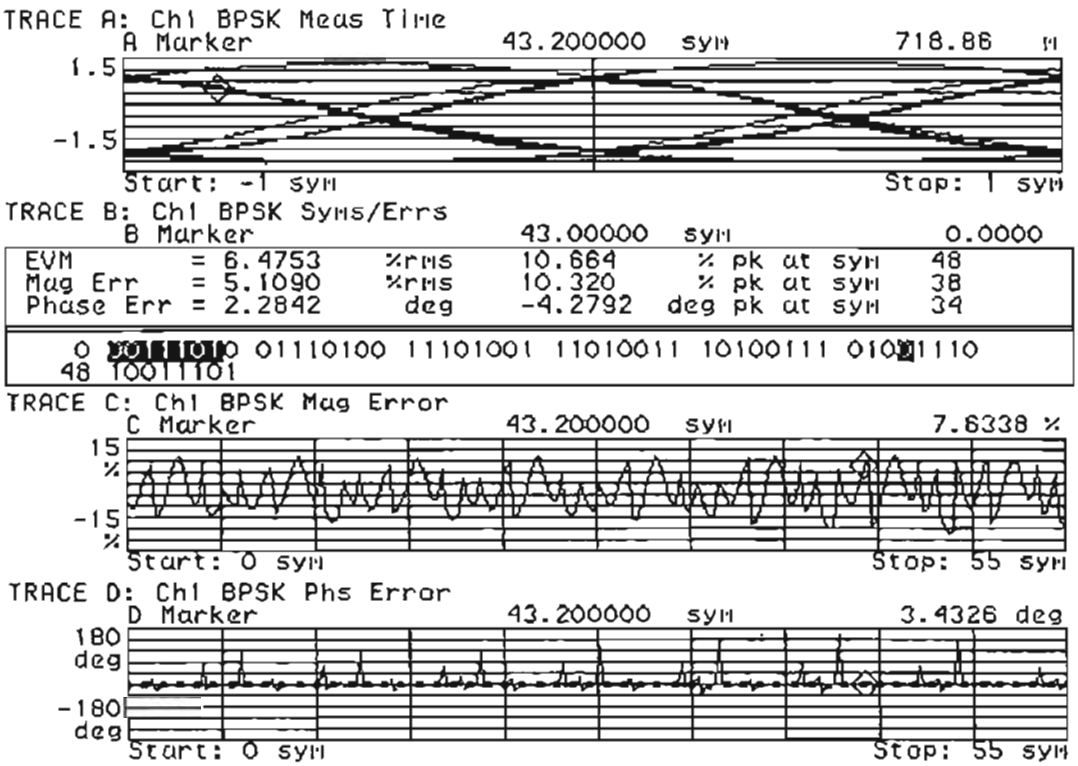

Fig. 9.16a: HP89410A EVM results display

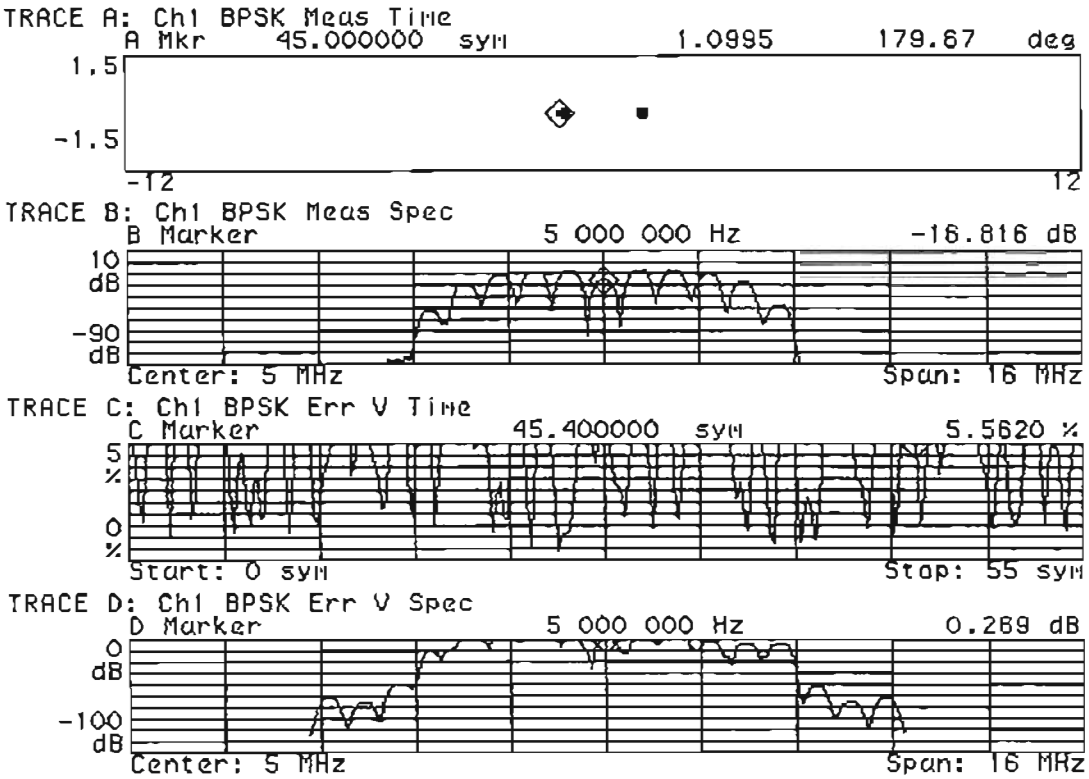

Fig. 9.16b: HP89410A EVM results display

In this instance, the signal power at the input of the front-end (see block diagram in figure (9.1)) was set to –25dBm corresponding to a SNR of 60.5dB at the input of the demodulator (HP89410A). Trace A in figure (9.16a) shows an eye diagram which is another way to view digitally modulated signals. Separate eye diagrams can be generated, one for the I-channel data and another for the Q channel data. These diagrams display I and Q magnitude versus time in an infinite persistence mode, with retraces. The I and Q transitions are shown separately and an "eye" (or eyes) is formed at the symbol decision times. A "good" signal has wide open eyes with compact crossover points. Trace B is a symbol table and error summary. The demodulated bitstream/symbols is shown at the bottom of this table. The present setup shows 56 bits. It should be reiterated that this bitstream is not available as an analog output or bitstream for BER measurements. The error values given in this table are the RMS averages of the error at each at each displayed symbol point. On the righthand side of this table, the errors are expressed as a percentage of the peak signal level with the symbol number displayed for the peak position. Traces C and D show the magnitude error vs. time (or symbol) and phase error vs. time, respectively. The magnitude error vs. time measurement is simply the IQ error magnitude (figure

(9.14)) as a function of time/symbol. The significance of the phase error vs. time/symbol is discussed in section (9.4.2.2).

With reference to figure (9.16b): Trace A is an IQ constellation diagram (discussed in section (9.4.2.3)). Trace B is the IQ measured spectrum. The error vector magnitude vs. time (section (9.4.2.4)) and its FFT, the error spectrum (section (9.4.2.5)) are shown in traces C and D, respectively.

The effects of filtering can be viewed using an IQ vector diagram. This is simply an IQ constellation diagram but with transitional paths between the states. The transitions between the states affects the transmitted bandwidth. Figures (9.17) and (9.18) show the effects of filtering. These figures confirm the theoretical aspects of filtering in chapter 4 (section (4.5)). For the system without filtering (figure (9.17), the transitions between states are instantaneous. No filtering means an excess bandwidth factor (α) of infinity. However, with filtering (figure (9.18)), the transitions between states are much smoother. In this case a root raised cosine filter with an excess bandwidth factor of 0.5 is used. So, decreasing the excess bandwidth factor (α) smoothens the transitions between states and narrows the spectrum required.

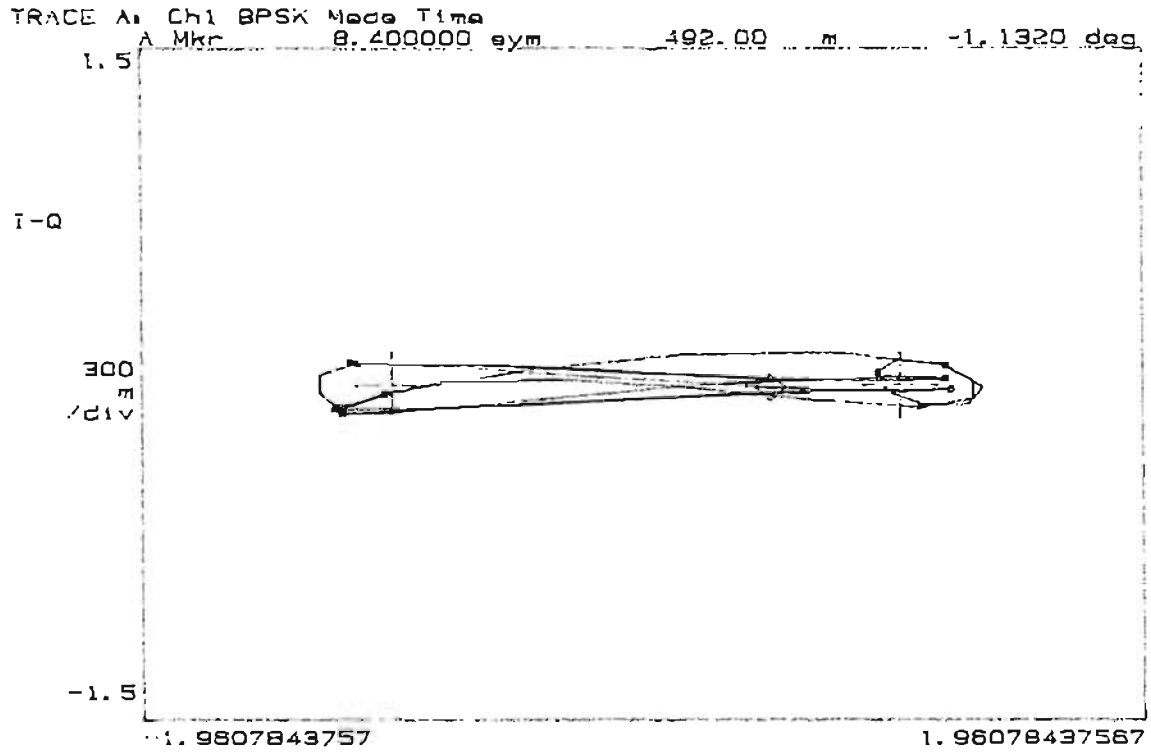

Fig. 9.17: IQ vector diagram for system without filtering (α of infinity)

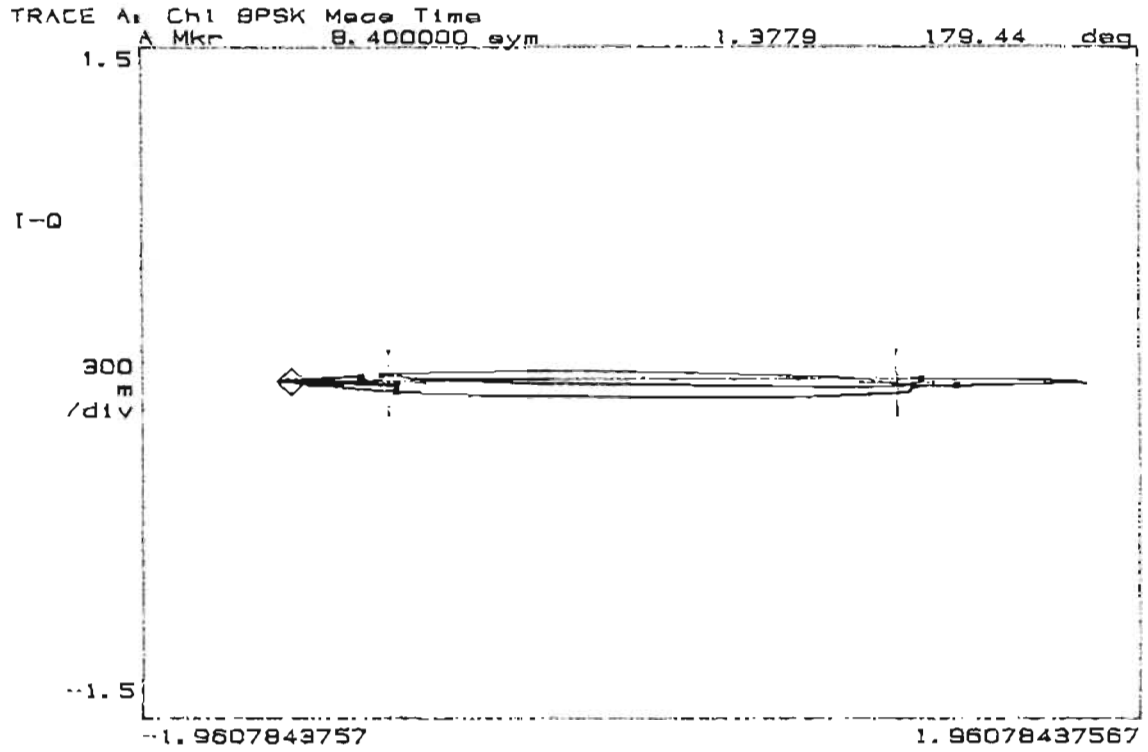

Fig. 9.18: IQ vector diagram for system with filtering (root raised cosine - α=0.5)

Figures (9.19a) and (9.19b) show EVM results for the case of an LNA input power of –90dBm corresponding to a SNR of 14.5dB at the input of the HP89410A. A skillful eye can easily (visually) detect many types of errors or signal degradation. The eye diagram (figure (9.19a) trace A) indicates the signal is of inferior quality when compared to that of figure (9.16a) (-25dBm LNA input power and SNR = 60.5dB). This is due to the eyes being not as wide open and also the crossover points are not as compact. This is also confirmed by the constellation diagram (figure (9.19b) trace A) where the states are much more dispersed/scattered from the ideal (reference states). However, the EVM values in the symbol/error summary table provides a faster and more conclusive result. In this case, the EVM is 39.977% RMS when compared to 6.4783% RMS for the –25dBm, 60.5dB SNR case. The magnitude (29.708% RMS) and phase (18.385°) errors are approximately equal, ruling out the possibility of unwanted phase modulation. The IQ phase error vs. time display (figure (9.19a) trace D) shows a regular or periodic waveform. This hints some form of interfering signal with an approximate frequency of 7.56MHz (periodic every 1.85 symbols). The error spectrum of trace D (figure (9.19b) indicate the non-existence of externally coupled

interference. This is based on the uniform/ symmetrical distribution of the error spectrum. Also, no discrete signal peaks are present.

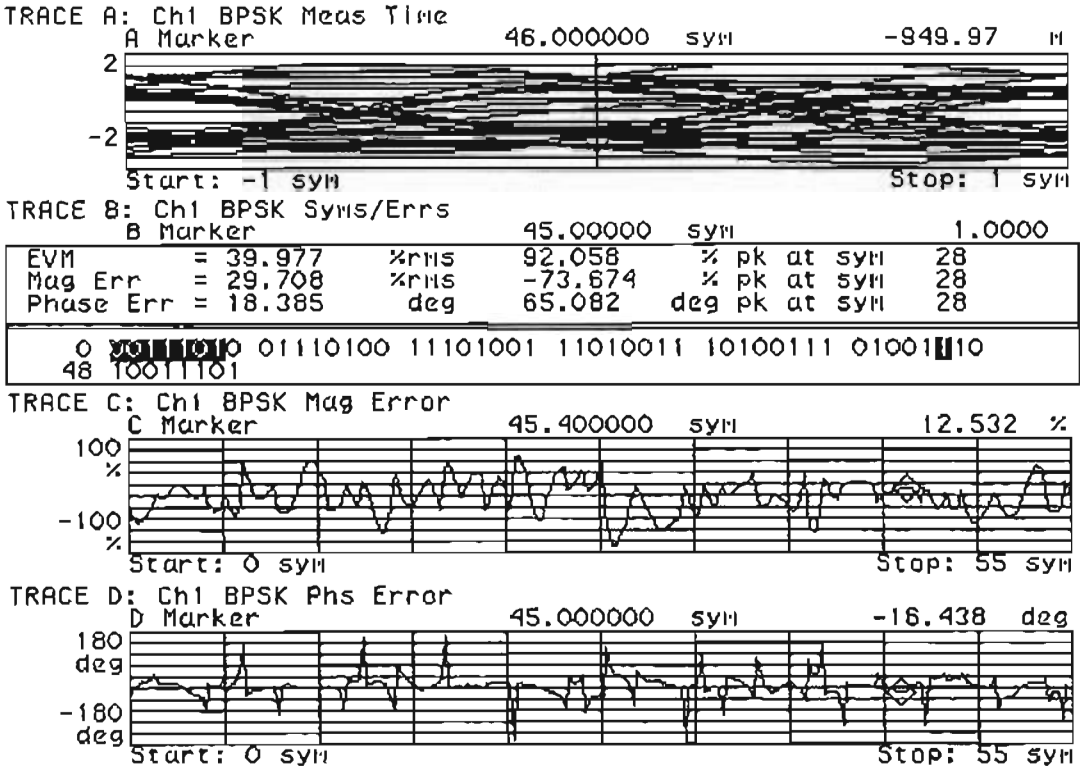

Fig. 9.19a: EVM results for –90dBm LNA input power (SNR = 14.5dB at input of HP89410A)

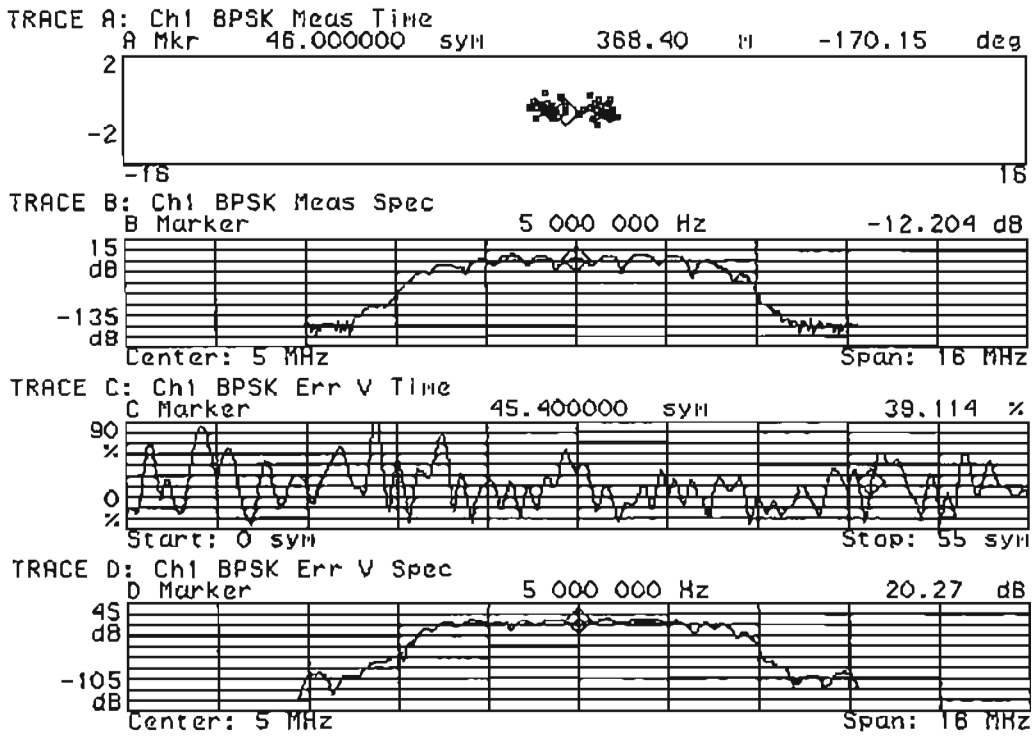

Fig. 9.19b: EVM results for –90dBm LNA input power (SNR = 14.5dB at input of HP89410A)

EVM measurement results are tabulated comprehensively in table (9.5) for various signal powers (and hence SNRs). The EVM, magnitude and phase errors were read up to 4 decimal places from the HP89410A screen display. Note that the SNRs were computed at the input of the demodulator (HP89410A vector signal analyzer). With reference to table (9.5): The frequency error indicates the frequency deviation (in kHz) between the internally generated RF carrier (from the HP89410A) and the incoming modulated carrier. The IQ offset is the magnitude of the carrier feedthrough signal, relative to the magnitude of the modulated carrier at the detection decision points. Carrier feedthrough is an indication of the balance of the IQ modulator used to generate the modulated signal. Imbalance in the modulator results in carrier feedthrough and appears as a DC offset on the demodulated signal. This imbalance can be due to a bad mixer or extraneous DC terms. The amplitude droop is a measure of the change in the magnitude of the signal at the detection decision points over the measured burst in units of dB per symbol. This parameter is most significant for pulsed signals. A high number indicates a problem with the pulse modulation process.

Signal power at input of LNA (dBm)	Signal power at input of demodulator (HP89410A) (dBm)	SNR at input of demodulator (HP89410A) (dB)	EVM (%RMS)	Magnitude error (%RMS)	Phase error (deg.)	Frequency error (KHz)	IQ offset (dB)	Amplitude droop (dB/symbol)
-25	0.16	60.5	6.4753	5.1090	2.2842	-282	-33.4	-15.1ndB/sym
-45	-14.2	57	4.6377	2.6401	2.1837	46.823	-36.3	-1.17μdB/sym
-65	-34.4	38	4.6935	3.1053	2.0114	18.604	-36.5	-1.23μdB/sym
-75	-44.3	29.6	8.6780	5.0756	4.0573	213.37	-36.1	-56.3μdB/sym
-85	-54.5	19.1	24.650	17.651	9.8411	149.82	-32.9	-291μdB/sym
-90	-59.2	14.5	40.804	28.699	18.055	-77.515	-48.7	-81.4μdB/sym
-93	-62.5	10.6	60.073	34.574	31.682	-427.06	-34.9	335μdB/sym
-95	-64.4	9.5	88.648	38.266	50.383	-714.11	-40	-652μdB/sym
-97	-66	7.6	84.250	46.179	48.141	411.68	-7.5	1mdB/sym
-100	-69.5	4.4	88.443	45.589	49.785	-493.73	-13.2	1.5mdB/sym
-103	-72.5	0.66	93.304	46.552	53.504	866.54	-13	-267μdB/sym
-105	-74.2	-0.72	93.361	50.409	50.818	-65.332	-19	-531μdB/sym
-107	-76.2	-2.68	94.718	47.383	53.678	276.12	-24	-380μdB/sym

Table 9.5: EVM measurement results for various signal powers and SNRs

Figures (9.20) to (9.23) show various plots extracted from table (9.5). Figure (9.20) shows a plot of LNA input signal power versus SNR. An intuitive obvious trend here is that an increase in the signal level at the input of the LNA causes an increase in the SNR (at the input of the HP89410A). Signal levels between –107dBm and –25dBm produce SNRs in the range –2.7dB to 60.5dB. However, it should be noted that the SNRs start to level-off at the lower and upper extremes of signal power. The levelling-off at the lower extreme (input signal power < -100dBm) can be attributed to the signal level reaching the noisefloor of the instrument. The levelling-off at the upper extreme (input signal level > -45dBm) can possibly be due to the HP89410A being overdriven by the receiver RF front-end. There is a high probability that the "ranging" calibration procedure for the HP89410A, for these power levels, was omitted.

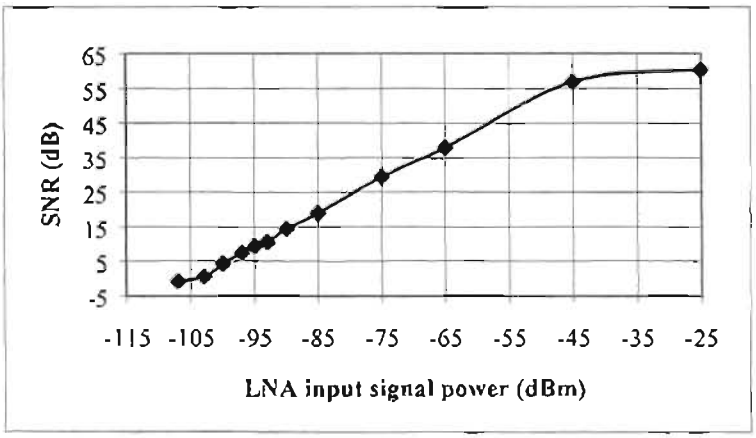

Fig. 9.20: LNA input signal power versus SNR

A plot of SNR versus EVM is shown in figure (9.21). The general trend, once again here, is an increase in SNR causes the EVM to decrease. EVM values between 4.6% RMS and 94.7% RMS are produced for SNRs in the range –2.7dB to 60.5dB. Figures (9.22) and (9.23) show plots of SNR versus magnitude error and SNR versus phase error, respectively. The magnitude error increases from 5.1% RMS to 47.4% RMS for a decrease in the SNR from 60.5dB to –2.7dB. The phase error varies between 2° and 53.7° for the same range of SNRs. It is evident from figures (9.21) to (9.23) that the EVM (and hence the magnitude and phase errors) do not exhibit a regular trend for a SNR range of between –3dB to 9.5dB. This irregularity may possibly be due to the sensitivity limitation of the HP89410A (the signal levels

corresponding to this range of SNRs may be approaching the noise floor of the instrument).

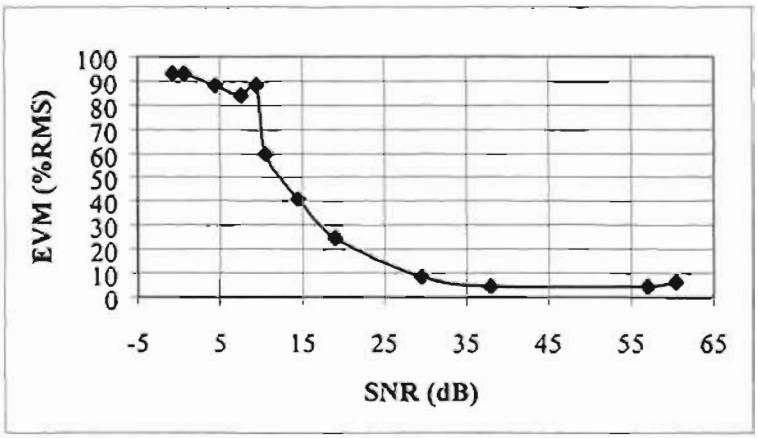

Fig. 9.21: SNR versus EVM

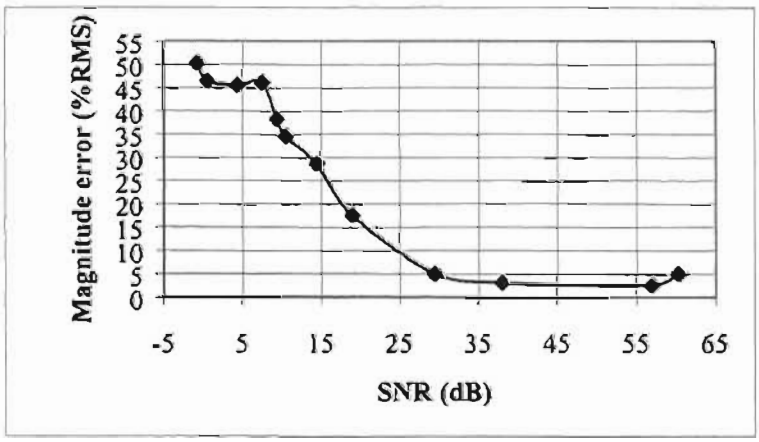

Fig. 9.22: SNR versus magnitude error

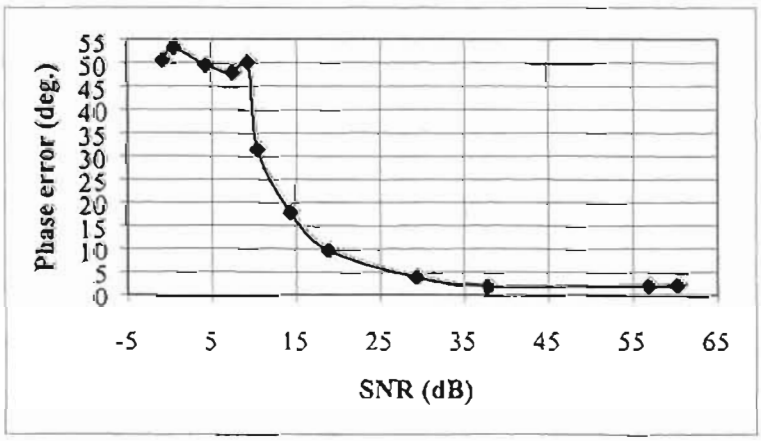

Fig. 9.23: SNR versus phase error

The importance of an LNA in the receiver RF front-end has been emphasized in the simulation results of chapter 5. The measurement results in table (9.6) conclusively verifies this importance for a –90dBm signal power into the receiver RF front-end. As can be seen, the use of an LNA not only causes an improvement in the SNR but also a decrease in the magnitude and phase errors and hence a decrease in the EVM.

	Signal power into demodulator (HP89410A)	SNR at input of demodulator (HP89410A)	EVM (% RMS)	Magnitude error (% RMS)	Phase error
System with LNA	-59.2dBm	14.5dB	40.804	28.699	18.055°
System without LNA	-81.5dBm	3.1dB	99.073	51.323	57.150°

Table 9.6: Comparison of EVM results for system with and without LNA

9.5 Conclusion

This chapter has supported the theory and simulation results of the preceding chapters through the implementation of a receiver RF front-end for a BPSK system. Using the phase noise theory in chapter 6 in conjunction with the HP89410A vector signal analyzer, a quantitative phase noise comparison of two frequency sources were performed. The phase noise density profiles were used to extrapolate the single sideband levels. Hence by use of equation (6.49) in chapter 6, the single sideband noise-to-signal ratios or variance (σ_T^2) were computed. Variance values of –40.5dB and –66.4dB were obtained for these frequency sources (at a frequency of 5MHz), allowing a comparison to be made.

In chapter 5, the BER was used as a figure of merit to evaluate the effect of RF component noise. In this chapter, a different figure of merit, the EVM, was used for this purpose. In chapter 5, it was established that RF component noise as a result of the noise figure) causes degradation of the SNR and hence an increase in the BER. These range of SNRs were replicated (to an extent) in the measurement setup to evaluate the effect of RF component noise. The general trend from the results is that

an increase in the SNR causes the EVM to decrease, and vice-versa. EVM values between 4.6%RMS and 94.7%RMS are obtained for SNRs in the range –2.7dB to 60.5dB. Only a quantitative comparison between the simulated CDMA setup (chapter 5) and the implemented BPSK setup can be made. Linking these SNR values to the simulation setup and results of chapter 5 (figure (5.11)), a SNR of 4.42dB corresponds to an LNA noise figure of 3dB (LNA gain = 13dB and mixer noise figure = 5dB). Figure (9.24) shows a trace of the symbol and error summary (after demodulation) for 512 bits. This is the maximum number of bits that can be displayed for BPSK demodulation (with 1024MB RAM and a minimum sampling rate of 2 samples per symbol, the maximum number of bits that can be displayed by the HP89410A is 512).

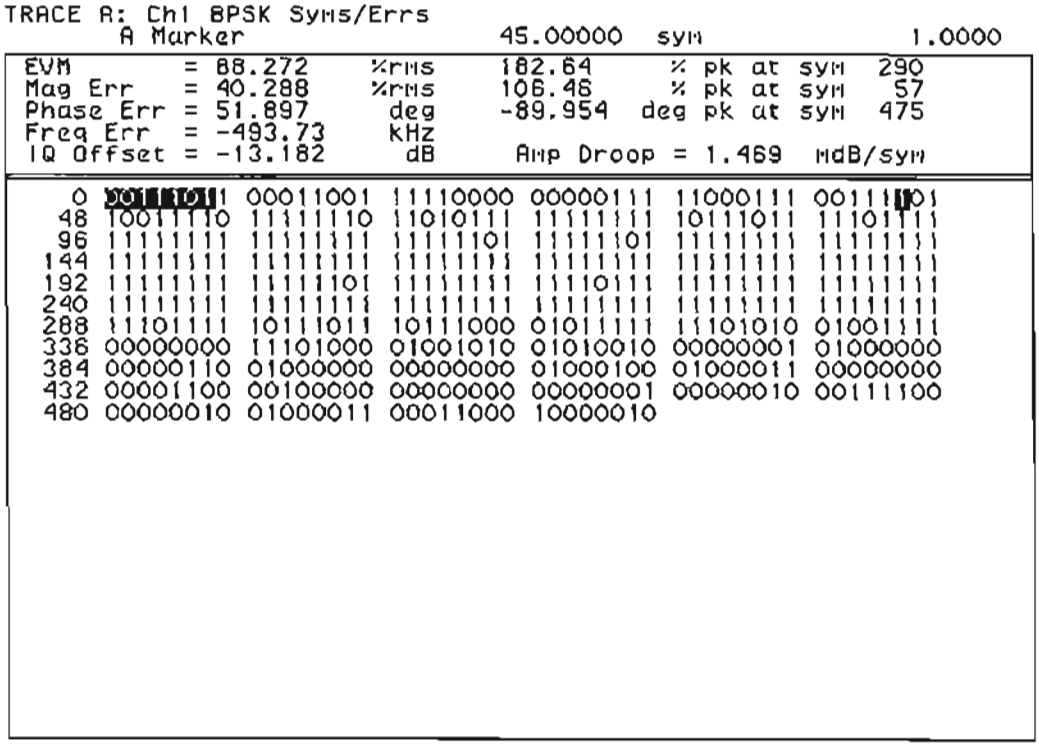

Fig. 9.24: Symbol and error summary for SNR of 4.4dB (at input of HP89410A) and –100dBm LNA input power

Figure (9.24) shows the errors for a SNR (at the input of the HP89410A) of 4.4dB corresponding to an LNA input power (see block diagram of figure (9.1)) of -100dBm. From this trace, 238 out of the 512 bits are in error. For a realistic bit length of 10^9, this translates to a best-case BER of 5.12×10^{-7}. However, the CDMA simulation setup in chapter 5, yielded a BER of 7.6×10^{-12} for the same SNR (figure (5.13)). Recall that the simulation setup consisted of spread (or chipped) data BPSK modulating a RF carrier and the BER measurement was performed on the received data after the despreading process. In contrast, this measurement setup consists solely

of data BPSK modulating a RF carrier and the BER computed after carrier demodulation. Essentially, the BER computed from the measurement is the simulated CDMA system equivalent of "chip error rate". Thus it can be concluded that the effect of RF component noise is more severe in a non-CDMA BPSK system than in a CDMA system employing BPSK modulation. CDMA's ability to suppress in-band interference and noise through its processing gain is apparent.

Methodologies for troubleshooting the RF front-end using EVM were also discussed. Signal quality was demonstrated visually using IQ constellation diagrams. The effects of filtering were also shown using IQ vector diagrams. These diagrams confirmed that filtering smoothens the transitions between states (chapter 4). EVM results from table (9.6) also conclusively verified the theoretical and simulation importance of an LNA in the receiver RF front-end (chapter 5).

CHAPTER 10

CONCLUSIONS

10.1 Summary and conclusions

This thesis examined the topic of design considerations and implementation of a RF front-end for a CDMA adaptive array system. A detailed study of the RF implementation issues were presented, beginning with a literature survey on antenna arrays and beamforming in chapters 2 and 3 and ending with an implementation and evaluation of a receiver RF front-end for a BPSK transceiver system in chapter 9.

A literature survey on antenna arrays and beamforming was presented in chapters 2 and 3. In chapter 2, the basic concepts of antenna arrays (specifically the linear array) were described. Also discussed were the principles of beamscanning, pattern multiplication and antenna element spacing criteria for the avoidance of grating lobes. All these concepts were demonstrated by a simulation that plots the array beam pattern as a function of the number of elements, element spacing and scan angle using a half wavelength dipole as the antenna element. Amongst the conclusions that can be drawn out from this simulation are: an increase in the number of antenna elements increases the main beam directivity of the array response (increase in gain and decrease in main beamwidth). However, it also results in an increase in the number of sidelobes in the total pattern.

Chapter 3, was essentially a literature survey of analogue and digital beamforming and the implementation implications of adaptive antennas at RF, IF or baseband. An adaptive beamforming configuration for CDMA (using Compton's loop) and the implementation issues thereof were described. Due to the fact that each CDMA user would require a separate loop, it would be cost-effective in a multiuser system to implement this loop in software in baseband. The loop can also be implemented at IF using hardware followed by digital processing. This setup not only places increased requirements on the digital processor (which now has to process a much higher

frequency signal), but is also costly in a multiuser system where hardware would be required for each user. The loop cannot be processed at RF (digital technology at RF is awaited). Although analogue beamforming and loop implementation (using hardware) can be performed at RF, the RF error signal would not be able to be processed by a present-day adaptive processor. Hence RF adaptive beamforming of the above loop is presently impossible. However, the weights themselves can be implemented in hardware using analog phase shifters and attenuators at either RF (following the antenna elements) or IF (following the IF amplifiers). The processing of the weights in this case can be performed at baseband/IF. In a large array, this setup is costly and increases the complexity of the front-end. The best alternative is to perform adaptive beamforming at baseband with the weights being implemented digitally in software.

An overview on CDMA theory and concepts were provided in chapter 4. Issues such as its background, advantages over other multiple access schemes and the all-important process of filtering was also included. The CDMA theory and concepts in this chapter were demonstrated by simulation work using Advanced Design System (ADS) software. The work here formed the basis for the simulation models utilized in the latter chapters of this thesis.

Chapter 5 investigated the effect of internally generated RF component noise on the bit error rate of a DS-CDMA system. Essentially, RF component noise (as a result of component noise figure) cause degradation of both the ratio of energy per bit to noise power spectral density (E_b/N_o) and the signal-to-noise ratio (SNR) and hence an increase in the bit error rate (BER). The importance of an LNA to establish the system noise figure was confirmed via simulation. For the proposed system (processing gain of 42) utilizing an LNA, the BERs are between 7.7×10^{-3} and 7.6×10^{-12} for mixer noise figures in the range 5dB to 15dB. However, without an LNA, the BERs range from 2.8×10^{-2} to 2.7×10^{-1} for the same range of mixer noise figures. For the proposed system (utilizing a mixer with 5dB conversion loss/noise figure), E_b/N_o and SNR improvements of 9.53dB are obtained over the same system without an LNA. Also E_b/N_o and SNR improvements in the range 9.53dB to 12.51dB are obtained for mixer noise figures from 5dB to 15dB. The simulation also concluded that the use of commercially available RF components in the front-end do not cause severe BER

degradation in a single-user DS-CDMA system. In a worst-case, highly improbable scenario, an LNA gain as low as 3dB and noise figure as high as 13dB produce BERs of 7.5×10^{-3} and 12.9×10^{-3}, respectively for a modest processing gain of 42. It can be anticipated that the effect of RF component noise in a multi-user DS-CDMA environment would be much more severe than that of the single-user case. Multiuser interference (MI) would cause a decrease in the SNR and hence an increase in the BER.

Chapter 6 examined the impact of local oscillator generated phase noise on DS-CDMA performance. A thorough discussion and analysis of phase noise from an RF engineer's perspective was initially provided. This was followed by simulation work. For the proposed system (10dB SNR at the input of the LNA), phase noise variance in the range –16.5dB to –3.3dB produce BERs in the range 10^{-4} to 0.51 for the system processing gain of 42. Phase noise variance less than –16.5dB produce negligible BERs (in the order of 10^{-24}). For a 7dB SNR at the input of the LNA, variance in the range –20.6dB to –3.3dB produce BERs between 0.51 and 10^{-4} (same BERs as 10dB SNR but for larger variance range). Negligible BERs (in the order of 10^{-24}) are produced for variance values less than –20.6dB. However, with a SNR at the input of the LNA of 5dB, phase noise variance between –39.4dB and –3.3dB produce BERs between 7×10^{-4} and 0.51. These results indicate that the BER degradation due to phase noise is more severe for lower SNRs. By comparing the phase noise variance of commercially available oscillators with these variance ranges, it can be concluded that the phase noise performance of typical oscillators have negligible effect on the BER of the proposed system (input SNR of 10dB and processing gain of 42). This was substantiated in chapter 6 by considering that the IF phase noise power (N_{IF}) exists in the same proportion to the RF receiver power, P_{RF} (at the RF input of mixer) as the phase noise was to the oscillator power if it passes through no narrowband filtering capable of limiting its bandwidth ($N_{IF}|_{dB_m} = P_{RF}|_{dB_m} - SNR_{LO}|_{dB}$). However, the effect of phase noise has different degrees of impact on the system's performance dependent on the PSK modulation type. This is intuitive from the signal-space representation of various PSK formats. The higher the PSK modulation format, the greater is the impact of phase noise. Thus it can be concluded that, in general, it is unnecessary for oscillator specifications to be overly restrictive in terms of phase noise. However,

being overly restrictive with this phase noise specification, places less demand on the low-noise design of other components in the RF system.

An overview on mixer theory was presented in chapter 7. As mentioned previously, due to its extensive presence in the previous chapters, a single chapter on this device was warranted. Its functionality and presence have been highlighted in chapters 3, 5 and 6. In chapter 3, frequency downconversion has made the digital adaptive array receiver realizable. Downconversion was necessitated to make use of currently-available digitization and processing hardware. Mixers have also been encountered in chapters 5 and 6. The results of the investigation on the effect of RF component noise (in chapter 5) were hinged around the mixer noise figure since it has been quoted as being the dominant source of noise and distortion in the receiver. The topic of local oscillator phase noise was considered in chapter 6. Being an inseparable entity of the mixing process, the LO phase noise that leaks from the LO port to the IF port of the mixer, was considered. So, it is not surprising that a single chapter was devoted to some mixer theory. The theory and understanding of some concepts in this chapter provides some insight into the implemented BPSK RF front-end of chapter 9. Most of these concepts are often taken for granted. For example, the simple concept of sum and difference frequencies, enable selection of the appropriate LO frequency for a given RF and desired IF. Also through discussion and simulation of intermodulation products, the importance of an IF bandpass filter (to reject unwanted intermodulation products) in this BPSK system becomes apparent. Furthermore, the non-linear mixing process also provides a reason for the LO drive level always being specified higher than the RF level in manufacturer's datasheets/catalogues.

The contents of chapters 8 and 9 constituted the RF design and implementation sections of this thesis. Chapter 8 was dedicated to the design, simulation, construction and characterization of a low noise microwave amplifier originally intended to quantify its performance in the BPSK RF front-end (chapter 9). However, the noise figure of this LNA could not be measured thus prohibiting its performance evaluation in the BPSK system. Nonetheless, a low-cost, in-house 2GHz broadband LNA with 13.1dB gain and 520MHz 3dB bandwidth, for possible use in the proposed CDMA adaptive array system, was developed. The specifications were defined as: 2GHz center frequency, required operating power gain $\geq$ 10dB, minimum 3dB bandwidth of

10MHz, noise figure less than 3dB in this 10MHz bandwidth (corresponding to the typical range of noise figures of commercially-available LNAs). This 10MHz bandwidth is commensurate with the 4.096MHz chip rate of WCDMA – a bandwidth of 8.192MHz (2 x chip rate) is required for BPSK modulation. On design and simulation of the initial circuit, the simulation results revealed a transducer gain ($|S_{21}|$) of 12.89dB at 2GHz, 3dB bandwidth of approximately 400MHz and a noise figure less than 3dB within an approximate bandwidth of 1.25GHz. Although these results met the specifications, the large value of the input reflection parameter ($|S_{11}|$) of –7.906dB was undesirable. Thus there was a need to optimize the initial circuit for an improved input match (lower input reflection parameter). An optimum input reflection parameter of –26.765dB was obtained by reducing the quarter-wave transformer length (between the 50Ω input line and input open circuit stub) from 22.334mm to 13.867mm. This was achieved by using the optimization tuning tool in ADS. In addition to the improved input match, optimization also resulted in a marginal improvement in gain ($|S_{21}|$) from 12.89dB to 13.793dB and a decrease in the noise figure from 1.858dB to 1.655dB (@2GHz). The 3dB bandwidth was greater than 200MHz while the noise figure was less than 3dB within a 1.6GHz bandwidth – still well within the amplifier specifications. Finally, this optimized circuit was constructed and characterized. There was good correlation between the simulated and measured s-parameter results, with the exception of the measured input reflection parameter ($|S_{11}| = -15.877$dB). This can possibly be attributed to the non-consideration of the biasing lines, step-width change discontinuity, coupling and bypass capacitors in the simulation model. Nevertheless, an input reflection parameter of –15.877dB is acceptable. The gain of the amplifier was measured to be 13.1dB while the 3dB bandwidth was computed as 520MHz. Thus a broadband design has been achieved (Q factor of 3.85). Noise figure measurements were performed using the HP346B noise source and the HP8970B noise figure meter. The theory and operation behind these instruments were discussed. Unfortunately, no correlation/comparison between the simulated and measured noise figure (at the desired frequency of 2GHz) could be made. This was due to the 1.8GHz operating frequency limitation of the HP8970B noise figure meter. At 1.8GHz, the noise figure of the amplifier was measured to be 2.7dB. A low-cost, in-house, operational LNA

was achieved in this design. The theoretical and practical aspects of LNA design has been presented in this chapter.

In chapter 9, a receiver RF front-end, excluding the antenna (using off-the-shelf/commercially available components) for a BPSK transceiver was implemented. The objective of this chapter was to support or reinforce the theory of the preceding chapters (specifically chapters 5 and 6). The chapter began with a description of the system. Waveforms for most of the stages were shown. The gain, conversion loss or insertion loss for each of the RF components were measured. The overall gain of the front-end was computed to be approximately 23.6dB. By using the specified noise figure (from the manufacturer's datasheet) for each component and the measured gain, the overall noise figure was computed to be 1.873dB. The focus of the next subsection was on phase noise measurements. Here, two techniques, the delay line method and the phase detector method, for measuring phase noise were discussed. However, a straightforward technique, using the HP89410A vector signal analyzer, was employed for the phase noise measurements. The phase noise performance of two Rohde and Schwarz frequency sources (models SMIQ 03 and SMS) were compared. The power level and frequency of both sources were set to 10dBm and 5MHz, respectively. The phase noise density profiles (represented in terms of the power spectral density of phase fluctuations, $S_\phi(f)$) were obtained. From these the single sideband level versus offset frequency were extrapolated. By use of equation (6.49) in chapter 6, the single sideband noise-to-signal ratio or variance (σ_T^2) were computed. This was calculated for 3 line segments (n = 3) i.e. the phase noise density profile was approximated by 3 line segments. Variance values of –40.5dB and –66.4dB were obtained for the SMS and SMIQ 03 models, respectively. A quantitative phase noise comparison of these frequency sources could thus be made. The latter part of chapter 9 was dedicated to Error Vector Magnitude (EVM) measurements, using the HP89410A vector signal analyzer. In addition to providing a figure of merit for a digitally modulated signal, it also helps to identify the type and source of signal degradation by using different troubleshooting methodologies. The section began with a definition of EVM followed by a description of a troubleshooting tree that can be used as a guideline to troubleshoot digital RF communication systems. Some of these troubleshooting methodologies were demonstrated on the BPSK

transceiver system. In chapter 5, it was established that RF component noise (as a result of component noise figure) cause degradation of the SNR and hence an increase in the BER. SNR values within the same range as used in the simulation were replicated for the measurement setup. The signal level at the input of the LNA was varied between –25dBm and –107dBm, producing SNRs at the input of the demodulator (HP89410A) between 60.5dB and –2.7dB. The general trend, is an increase in SNR causes the EVM to decrease. EVM values between 4.6% RMS and 94.7% RMS are produced for SNRs in the range –2.7dB to 60.5dB. The magnitude error increases from 5.1% RMS to 47.4% RMS for a decrease in the SNR from 60.5dB to –2.7dB. The phase error varies between 2° and 53.7° for the same range of SNRs. By linking a particular SNR value to the SNR value in the simulation setup and results of chapter 5, a quantitative comparison between the simulated CDMA setup (chapter 5) and the implemented BPSK setup could be made. This revealed that the effect of RF component noise is more severe in a conventional BPSK system than in a CDMA system. IQ constellation diagrams were used to demonstrate the quality of modulated signals. IQ vector diagrams were used to demonstrate and confirm the effects of filtering. The system with root raised cosine filtering ($\alpha = 0.5$) and without filtering ($\alpha = \infty$) were compared. These diagrams confirmed the theory in chapter 4 that filtering smoothens the transitions between states. The importance of an LNA in the receiver RF front-end has been emphasized in the simulation results of chapter 5. The measurement results conclusively verified this importance: the use of an LNA not only causes an improvement in the SNR but also a decrease in the magnitude errors, phase errors and hence a decrease in the EVM. For the system without an LNA, the EVM was measured to be 99.1% RMS while with an LNA it was 40.8% RMS. The magnitude errors were 51.3% RMS and 28.7% RMS for systems without and with LNA, respectively. The corresponding phase errors were 57.2° and 18.1°.

10.2 Possible extensions and topics of further study

Finally, to conclude this thesis, some possible extensions and/or further topics of study to this research are presented:

(a) The first part of this thesis presented a literature survey on antenna arrays and beamforming. No mention of the type of antennas used in cellular communications were made. The choice of antennas for the array are important

and depends on the requirements that need to be satisfied. Some of the requirements that need to be considered are their gain, coverage pattern, the power available to drive them and polarization. As a possible extension, further research on these aspects is proposed.

(b) The simulation model for the generation of the array beam pattern in chapter 2 did not take into account the effects of mutual coupling. Similarly, it is suggested that an expression (incorporating the effects of mutual coupling) for the array factor be derived. This expression will depend on the antenna element type.

(c) Furthermore, in the investigation in chapter 5, it may be of interest to evaluate the BER degradation as a result of overdriving the receiver RF front-end into compression.

(d) Consideration should also be given to extend the phase noise simulation model (in chapter 6) to a multiple carrier (MC) environment. Although the existing DS-CDMA model, in effect, used a typical loaded SNR of 10dB, it would be interesting to study the impact of LO-generated phase noise in a MC-CDMA system. Although documented in the literature, the existing theory and understanding would be enhanced.

(e) A "hardwired" BPSK transceiver was implemented and documented in chapter 9. Recall, initially it was intended to utilize the Alcatel software radio as the CDMA transceiver platform. However, the carrier demodulation process is not supported by this radio. As a result, the HP89410A vector signal analyzer was used for this purpose. As mentioned previously, there are two downsides to this instrument:

- The HP89410A is incapable of demodulating a CDMA signal i.e. it cannot perform the despreading operation. Thus, the idea of implementing a simple BPSK transceiver was conceived.
- The demodulated signal is not available as an analog output or bitstream for analysis. Thus, BER measurements are not possible with this instrument.

For the above reasons, it is proposed that research towards the implementation of a carrier demodulator, be conducted. It is envisaged that such demodulation

circuitry would interface with the software radio, completing the missing link, to form a complete CDMA transceiver. The performance of the receiver RF front-end in a CDMA environment can thus be evaluated. Another possible future extension will involve the performance evaluation of the receiver RF front-end in a wireless CDMA environment (including the effects of multipath and fading).

REFERENCES

1. T. Ojanpera and R. Prasad, "Wideband CDMA for third generation mobile communications," Artech House, Norwood, 1998.

2. S. Anderson, M. Milnert, M. Viberg and B. Wahlberg, "An adaptive array for mobile communication systems," Trans. on Veh. Tec., Vol. 40, 1991.

3. S.C. Swales, M.A. Beach, D.J. Edwards and J.P. McGeehan, "The performance enhancement of multibeam adaptive base-station antennas for cellular land mobile radio systems," IEEE Trans. Veh. Technol., vol. 39, p56-57, 1990.

4. Shiam-Shiun Jeng et al, "Experimental evaluation of smart antenna system performance for wireless communications," IEEE Trans., Vol. AP-46, June 1998, P749-757.

5. J.S. Thompson, P.M. Grant, B. Mulgrew, "Smart antenna arrays for CDMA systems," IEEE Personal communications, Vol. 3 (1996), P16-25.

6. Yingjie Li, Martin J. Feuerstein, Douglas O. Reudink, "Performance evaluation of a cellular base station multibeam antenna," Trans. IEEE Veh. Tech., Vol.46, no. 1, Feb. 1997, P1-9.

7. Agilent Technologies Advanced Design System release 1.3: This is an electronic design automation (EDA) software that allows design, simulation, optimization and verification of DSP, RFIC, communication systems, RF board, microwave and electromagnetic designs.

8. Bernard D. Steinberg, "Principles of aperture and array system design," John Wiley and sons, New York, 1976.

9. Richard C. Johnson and Henry Jasik, "Antenna applications reference guide," McGraw-Hill, New York, 1987.

10. J.E. Hudson, "Adaptive array principles," Short Run Press Ltd., England, 1981.

11. C.A. Balanis, "Antenna theory, analysis and design," 2nd edition, John Wiley and sons, New York, 1997.

12. L.C. Godara, "Application to antenna arrays to mobile communications, part 1: performance, feasibility, and system considerations," Proc. IEEE, Vol. 85, July 1997, P1029-1060.

13. Robert A. Monzingo and Thomas W. Miller, "Introduction to adaptive arrays," John Wiley and sons, New York, 1980.

14. L.C. Godara and A. Cantoni, "Uniqueness and linear independence of steering vectors in array space," J. Acoust. Soc. Amer.,Vol. 70, P467 – 475,1981.

15. A.F. Naguib, A. Paulraj, and T. Kailath, "Capacity improvement with base-station antenna arrays in cellular CDMA," IEEE Trans. Veh. Technol., Vol. 43, P691 – 698, 1994.

16. D.G. Brennan, "Linear diversity combining techniques," Proc. IRE., Vol. 47, P1075 – 1102, 1959.

17. J. Litva and T.K.Y. Lo, "Digital beamforming in wireless communications," Artech House, Inc., 1996.

18. Paul H. Young, "Electronic Communication techniques," fourth edition, Prentice Hall, 1994.

19. A.R. lopez, "Performance prediction for cellular switched beam intelligent antenna system," IEEE commun. Mag., Vol. 34, P152-154, Oct 1996.

20. B. Suard, A.F. Naguib, G. Xu and A. Paulraj, "Performance of CDMA mobile communication systems using antenna arrays," Proc. IEEE Int. Conf. Acoust.,Speech and Signal processing (ICASSP), Minneapolis, MN, 1993, P153-156.

21. Y.Wang and J.R. Cruz, "Adaptive antenna arrays for the reverse link of CDMA cellular communication systems," Inst. Elect. Eng. Electron. Lett., Vol.30, P1017-1018, 1994.

22. Robert J. Mailloux, "Phased array antenna handbook," Artech House, Boston, 1994.

23. Robert C. Hansen, "Microwave scanning antennas," Peninsula publishing, California, 1985.

24. J.D. Kraus, "Antenna arrays with closely spaced elements," Proc. IRE, Vol. 28, P76-84, February 1940.

25. Lamont V. Blake, "Antennas," John Wiley and sons, New York, 1966.

26. J.L. Allen, "Gain and impedance variation in scanned dipole arrays," IEEE Trans. on antennas and propagation, AP-10, no.5, P567-569, September 1962.

27. M. Barrett and R. Arnott, "Adaptive antennas for mobile communications," Electron. Commun. Eng. J., Vol. 6, P203-214, 1994.

28. B. Widrow et al, "Adaptive antenna systems," Proc. IEEE, Vol. 55, Dec.1967, P2143-2159.

29. W.F. Gabriel, "Adaptive arrays – an introduction," Proc. IEEE, Vol. 64, February 1976, P239-272.

30. James Bao-Yen Tsui, "Digital microwave receivers – theory and concepts," Artech House, Norwood, 1989.

31. Butler J.L. and Lowe R., "Beamforming matrix simplifies design of electronically scanned antennas," electronic Design, Vol. 9, Apr. 12, 1961, P170-173.

32. R.C. Hansen, "Phased array antennas," John Wiley and sons, New York, 1998.

33. M.I. Skolnik, "Introduction to radar systems," 2nd edition, McGraw Hill book company, New York, 1980.

34. Raymond Tang and Richard W. Burns, "Phased arrays," from "Antenna engineering handbook," by R.C. Johnson and H. Jasik, 2nd edition, McGraw-Hill, New York, 1984, P20-1 to 20-67.

35. Edward A. Wolff and Roger Kaul, "Microwave Engineering and system applications," John Wiley and sons, U.S.A., 1988.

36. R.D. Gaudenzi, "The influence of signal quantization on the performance of digital receivers for CDMA radio networks," ETT, Vol. 8, No. 1, January – February 1997, P89 – 97.

37. F.G. Weiss, "A 1Gs/s 8-bit GaAs ADC with on-chip current source," Proc. GaAs IC Symposium, P209, 1986.

38. T. Dcourant et al., "3GHz, 150mW, 4-bit GaAs analog to digital converter," Proc. GaAs IC Symposium, P301-304, 1986.

39. B.P. Del Signore, "Monolithic 20-b delta-sigma A/D converter implemented in standard 3μm CMOS technology," IEEE J-SC, Vol. 8, Dec. 1990.

40. J. Valburg, "8-b 650MHz folding A/D converter with analog error correction," IEEE J-SC, Vol. 10, Dec. 1992.

41. H. Kimura, "10-b 300MHz interpolated-parallel ADC implemented in double-polysilicon self-aligned bipolar technology," IEEE J-SC, Vol. 11, Apr. 1993.

42. A.N. Karanicolas, "15-b 1Msample/s digital self-calibrated pipeline ADC," IEEE J-SC, Vol. 11, Dec. 1993.

43. C. Schiller, "4GHz 8-bit ADC system using sample and filter sampling techniques," IEEE J-SC, Vol. 9, Dec. 1991.

44. F. Goodenough, "ADCs become application specific," Electronic Design, P42-50, Apr. 1993.

45. E.O. Brigham, "The fast fourier transform and its applications," Prentice-Hall, Englewood Cliffs, NJ, 1988.

46. Taub and Schilling, "Principles of communication systems," 2nd edition, McGraw-Hill Book company, Singapore, 1986.

47. R.T. Compton, "An adaptive antenna in a spread spectrum communication system," Proc. IEEE, vol. 66, March 1978, P289-298.

48. R.T. Compton, R.J. Huff, W.G. Swarner and A.A. Ksienski, "Adaptive arrays for communication systems: An overview of research at the Ohio State University," IEEE Trans. Antennas Propagation, Vol. AP-24, P599-607, 1976.

49. E. Bouktache, "On the stability of adaptive antenna arrays with weights at an intermediate frequency," IEEE Trans., Vol. AP-40, November 1992, P1438-1444.

50. Dean E. Svoboda, "A phase-locked receiving array for high-frequency communications use," IEEE Trans., Vol. AP-12, March 1964, P207-215.

51. Jonas Strandell et al, "Experimental evaluation of an adaptive antenna for a TDMA mobile telephony system,"

52. Y.J. Guo, S. Vadgama, M. Davies, J. Khalab, M. Zarri and D. Spink, "An adaptive antenna for CDMA," IEEE 5th International symposium on spread spectrum techniques and applications, Sun City, South Africa, 2-4 September, 1998.

53. Joel L. Dawson, Jenshan Lin, "An adaptive antenna integrated with automatic gain control for receiver front end," IEEE MTT-S International Microwave Symposium Digest, Vol. 3, June 1997.

54. Kimmo Kalliola and Pertti Vainikainen, "Characterization system for radio channel of adaptive array antennas,"

55. Tom Gratzek, Brad Brannon, Jim Camp and Frank Murden, "A new paradigm for base station receivers: High IF sampling + digital filtering," IEEE radio frequency integrated circuits (RFIC) Symposium, June 1997.

56. F. Swarts, P. van Rooyan, I. Oppermann and M.P. Lotter, "CDMA techniques for third generation mobile systems," Kluwer Academic Publishers, U.S.A., 1999.

57. Samuel C. Yang, "CDMA RF system engineering," Artech House, Inc., Norwood, 1998.

58. Vijay K. Garg, Kenneth Smolik, Joseph E. Wilkes, "Applications of CDMA in wireless/personal communications," Prentice-Hall NJ, 1997.

59. Lilja H., "Characterizing the effect of nonlinear amplifier and pulse shaping on the adjacent channel interference with different data modulations," Licentiale Thesis, Oulu University, Finland, 1996.

60. Asha Mehrotra, "Cellular radio performance engineering," Artech House, Inc., Norwood, 1994.

61. F.R. Connor, "Noise," 2nd edition, Macmillan India Ltd., Bangalore, 1982.

62. Nyquist H., "Thermal agitation of electric charge in conductors," physical review, Vol. 32, P10, 1928.

63. Peter C.L. Yip, "High-frequency circuit design and measurement," 1st edition, Chapman and Hall, 1991.

64. www.mprg.ee.vt.edu/research/glomo/antenna/arch.html

65. Lawrence E. Larson, "RF and microwave circuit design for wireless communications," Artech House, Norwood, 1996.

66. D. Lu and K. Yao, "Improved importance sampling technique for efficient simulation of digital communication systems," IEEE J. Selet. Areas Commun., Vol. 6, P67 – 75, Jan. 1988.

67. D. Lu and K. Yao, "Estimation variation bounds of importance sampling simulations in digital communication systems," IEEE Trans. Commun., Vol. 39, P1413 – 1417, Oct. 1991.

68. J. Chen, D. Lu, J. Sadowski and K. Yao, "On importance sampling in digital communications – Part 1: fundamentals," IEEE J. Select. Areas in Commun., Vol. II, No. 3, P289-299, April, 1993.

69. P.F. Combes, J. Graffeuil, J.F. Sautereau, "Microwave components, devices and active circuits," John Wiley and sons Ltd., Great Britain, 1987.

70. Stephen A. Maas, "Microwave mixers," 2nd edition, Artech House, Norwood, 1993.

71. Vadim Manassewitsch, "Frequency synthesizers theory and design," second edition, John Wiley and sons, 1980.

72. "The American Radio Relay League Handbook (ARRL)" 1998.

73. T. Pollet, M. Van Bladel and M. Moeneclaey, "BER sensitivity of OFDM systems to carrier frequency offset and Wiener phase noise," IEEE Trans. Commun., Vol. 43, P191-193, Feb./Mar./Apr., 1995.

74. P. Robertson and S. Kaiser, "Analysis of the effect of phase noise in orthogonal frequency division multiplex (OFDM) systems," in Proc. ICC'95, Seattle, WA, June 1995, P1652-1657.

75. L. Tomba and W.A. Krzymien, "Sensitivity of the MC-CDMA Access scheme to carrier phase noise and frequency offset," IEEE Trans. On Veh. Tech., Vol. 48, no. 5, September 1999, P1657-1665.

76. U.L. Rohde, "Digital PLL frequency synthesizers," N.J, Prentice-Hall, 1983.

77. Hewlett Packard staff, "Understanding and measuring phase noise in the frequency domain," application note 207, October 1976.

78. Leeson D.B., "A simple model of feedback oscillator noise spectrum,"Proc. IEEE, Vol. 54, P329-330, 1966.

79. J.J. Stiffler, "Theory of synchronous communications," NJ, prentice Hall, 1971.

80. L.C. Godara and A. Cantoni, "Uniqueness and linear independence of steering vectors in array space," J. Acoust. Soc. Amer.,Vol. 70, P467 – 475,1981.

81. S.A. Maas, "Nonlinear microwave circuits," Artech house, Norwood, M.A., 1988.

82. F.C. McVay, "Don't guess the spurious level," Electronic Design, Feb. 1, 1967, P70.

83. S.E. Wilson, "Evaluate the distortion of modular cascades," Microwaves, Vol. 20, No. 3, 1981, P67.

84. Tri T. Ha, "Solid-state microwave amplifier design," John Wiley and sons, 1981.

85. Stuart D. MacPherson, "An introduction to high frequency design" DIT Publications, Microwave systems course notes, Natal Technikon, 1st edition, 1997.

86. Gonzalez, Guillermo, " Microwave transistor amplifiers analysis and design," Prentice-Hall, 1984.

87. Allen Sweet, " MIC and MMIC amplifier and oscillator circuit design," Artech House, 1990.

88. George D. Vendelin, "Design of amplifiers and oscillators by the S parameter method," John Wiley and sons, 1982.

89. Bahl I.J. and Trivedi D.K., " A designers' guide to microstrip line," Microwaves, May 1977, P174 - 182.

90. Hewlett Packard, "Microwave transistor bias considerations" Application note 944-1.

91. Hewlett Packard, "Spectrum analysis...noise figure measurements," application note 150-9.

92. Hewlett Packard, "Noise figure measurement accuracy," application note 57-2.

93. Agilent technologies, "Fundamentals of RF and microwave noise figure measurements," application note 57-1.

94. Chambers D.R., "A noise source for noise figure measurements," Hewlett Packard Journal, April 1983, P26 – 27.

95. "Wave analyzer dynamic range and bandwidth requirements for signal noise analysis," Technical report RE 76-26, U.S. Army Missile Command, Redstone Arsenal, Alabama 35809.

96. Hewlett Packard, "10 steps to perfect digital demodulation measurement," product note 89400-14A.

97. Hewlett Packard, "Using vector modulation analysis in the integration, troubleshooting and design of digital RF communications systems," product note 89400-8.

APPENDIX

A.1 Coordinate system for the analysis of arrays

In order to analyze the array response as a result of beamscanning, it is necessary to introduce a three-dimensional coordinate system. This coordinate system is convenient since it leads to a simple method of analyzing the response of any array configuration (figure (A.1)).

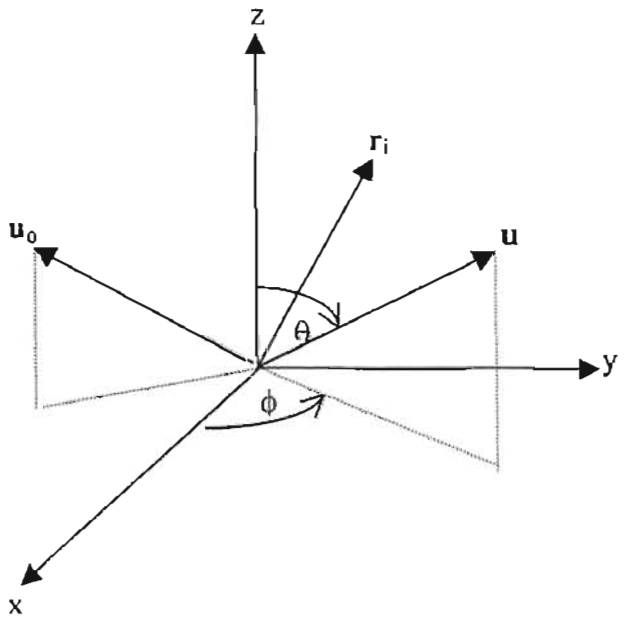

Fig. A.1: Three-dimensional coordinate system used

The angle ϕ of figure (A.1), describes the rotation in the xy-plane (azimuth), while the angle θ describes the elevation from the z-axis towards the xy-plane. The vector $\mathbf{u} = [u_x, u_y, u_z]$ is a unit vector perpendicular to a planar wavefront, travelling towards the array, and pointing in the direction of the source of the wavefront. The vector $\mathbf{r}_i = [r_x, r_y, r_z]$ describes the position of the i^{th} element of the array. The main beam of the array will be steered in the direction indicated by $\mathbf{u}_o$ associated with angles ϕ_o and θ_o. The vector $\mathbf{u}$ can be written in terms of the direction cosines as

$$\mathbf{u} = \hat{x}\sin\theta\cos\phi + \hat{y}\sin\theta\sin\phi + \hat{z}\cos\theta \qquad (A.1)$$

A.2 MATLAB program for the analysis of linear arrays

```
%*********************************************************************
%This program calculates and plots the array factor for a linear array with uniform
%amplitude excitation, uniform spacing and non-uniform phasing between array
%elements in terms of the number of elements, spacing of the elements (in
%wavelengths) for elements positioned on the z- axis
%*********************************************************************

N=input('Enter the number of elements:');
d=input('Enter the spacing d between elements in terms of wavelengths lambda: ');
scanang=input('Enter the angle thetha in degrees where you wish main beam to be
scanned to: ');

thetha=0:pi/180:2*pi;
scanang1=(scanang/180)*pi;
phi=2*pi*d*(cos(thetha)- cos(scanang1));

AF=0;
for n=1:N,
AF=AF+exp(j*(n-1)*phi);
end

magsq=abs(AF.*AF);
x=N^2;
normaliz=magsq/x;
figure(1);
polar(thetha,normaliz)
title('Polar plot of the normalized array factor power density ')

%Figure 2 plots the normalized array factor pattern
figure(2)
polar(thetha,1/N*abs(AF))
title('Polar pattern of normalized array factor')

figure(3);
gaindB=10*log10(magsq/x);   %Both AF and number of elements are squared
thetha1=thetha*180/pi;
plot(thetha1,gaindB);
axis([0 180 -30 max(gaindB)]);
xlabel('Degrees');
ylabel('Normalized gain in dB');
title('Plot of the normalized array factor power density');


%This section of the program plots the normalized element power density pattern for
%a half-wavelength dipole that is parallel to the z-axis
figure(4);
range1=eps:pi/360:(1-eps)*pi;
range2=(1+eps)*pi:pi/360:(2-eps)*pi;
```

```
range=[range1 range2]
E=cos((pi/2).*cos(range))./sin(range);
power=abs(E.*E);
norm=power/max(power);
polar(range,norm)
title('Polar plot of the normalized half wavelength dipole power density');


%Figure 5 just plots the E-field pattern for the 1/2 wavelength dipole with its axes
%parallel to the z-axis
figure(5);
polar(range,abs(E));
title('Half-wavelength dipole element E-plane pattern')


%Demonstrating the multiplication principle using the half-wavelength dipole
phi1=2*pi*d*(cos(range)- cos(scanang1));
AF1=0;
for n=1:N,
AF1=AF1+exp(j*(n-1)*phi1);
end

%Figure 6 plots the normalized array factor pattern
figure(6)
normaf1=1/N*abs(AF1);
polar(range,normaf1)
title('Polar pattern of normalized array factor')

%Figure 7 plots the total normalized array response AF1
figure(7);
mult=abs(normaf1.*abs(E));
mult1=mult/max(mult);
polar(range,mult1)
title('Total normalized array response');

%Figure 8 plots the normalized array response pattern in a linear dB scale
figure(8);
gain=10*log10(mult1);
rangedeg=180*range/pi;
plot(rangedeg,gain);
axis([0 180 -30 max(gain)]);
xlabel('Degrees');
ylabel('Normalized gain in dB');
title('Plot of the normalized array response');
%Figure 9 plots the normalized array power density pattern in a linear dB scale
figure(9);
powergain=20*log10(mult1);
plot(rangedeg,powergain);
axis([0 180 -30 max(powergain)]);
```

```
xlabel('Degrees');
ylabel('Normalized power gain in dB');
title('Normalized array response power density pattern');
```

Discussion of simulation

The shape of the far-field pattern for the λ/2 dipole is given by

$$E_\theta = \frac{\cos\left[\frac{\pi}{2}\cos\theta\right]}{\sin\theta} \qquad \text{(A.2)}$$

The fact that the angle ϕ does not appear in the expression means that the pattern of E in any plane parallel to the xy-plane (i.e. a plane in which ϕ varies but θ does not) is a perfect circle (omnidirectional). It also means that the pattern of E in all planes containing the z-axis (θ = 0-axis) will be exactly alike; e.g. pattern in xz-plane will be the same as the pattern in the yz-plane.

The three-dimensional pattern of the half-wavelength dipole with its axis parallel to the z-axis is shown in figure (A.2).

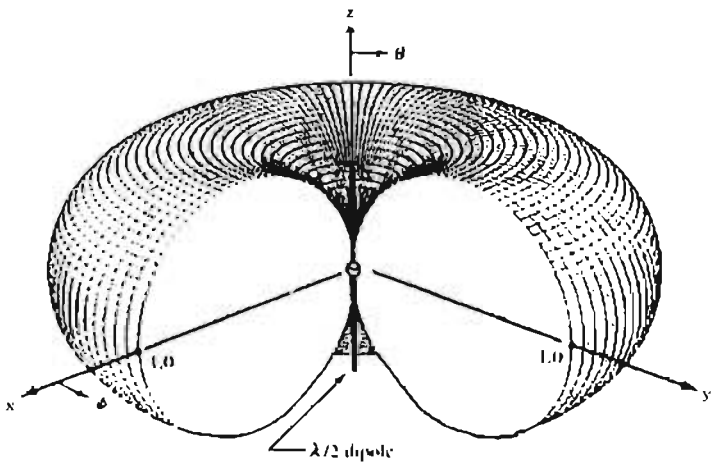

Fig. A.2: Three-dimensional pattern of a λ/2 dipole (from [11])

As can be seen, the H-plane (plane perpendicular to the axis of the antenna – azimuthal in this case) pattern is omnidirectional. The E-plane (plane parallel to the axis of the antenna – elevation in this case) pattern is the figure-eight. In figure (A.2), a 90° sector has been removed to illustrate this figure-eight elevation plane pattern.

The array thus consists of $\lambda/2$ dipole antennas arranged collinearly (element axes parallel to the line of the array) on the z-axis. This collinear arrangement is very popular amongst dipole antennas since it reduces the effect of mutual coupling between dipole elements.

To better illustrate the pattern multiplication rule, the normalized pattern of the single element $\lambda/2$ dipole, the array factor and the total array response are shown in figures (A.3), (A.4), (A.5) and (A.6). In each figure, the total pattern of the array is obtained by multiplying the pattern of the single element by that of the array factor. In each case, the pattern is normalized to its own maximum.

Figure (A.3) for $N = 2$, $d = 0.25\lambda$ and beam steered to broadside ($\theta_o = 90^o$): Since the array factor is nearly isotropic (within 3dB), the element pattern and the total pattern are almost identical in shape. However, the total array response is more directive (higher gain) than the individual element. Since both the element and array factor pattern are maximum at broadside, the total array response is also maximum at broadside (i.e. beam steered to broadside).

Figure (A.4) for $N = 2$, $d = 0.25\lambda$ and beam steered to endfire ($\theta_o = 0^o$): Since the array factor is of cardioid form, its corresponding element and total patterns are considerably different. In the total array response, the null at $\theta_o = 0^o$ is due to the element pattern. Thus, even though the array factor is steered to 0^o, the total response of the array is not steered to 0^o. Clearly, the element pattern prevents the total array pattern from being steered to 0^o. Therefore, the radiation pattern/characteristic of an element can sometimes place restrictions on the scan angle of the array.

Figure (A.5) for $N = 10$, $d = 0.25\lambda$ and beam steered to broadside ($\theta_o = 90^o$): The array factor and the total array response are similar to the broadside array of figure (A.3). However, an increase in the number of elements has resulted in the presence of sidelobes and a decrease in the main beamwidth. Thus, an increase in the number of elements increases the main beam directivity of the array response (increase in gain and decrease in main beamwidth). However, it also results in an increase in the number of sidelobes in the total pattern.

Figure (A.6) for N = 10, d = λ and beam steered to broadside ($\theta_o = 90^o$): To form a comparison with the broadside array of figure (A.5), figure (A.6) shows the same array but with the spacing increased to λ. From the plots of the normalized array factor polar pattern and power density pattern, it can be seen, in addition to the main beam directed broadside ($\theta_o = 90^o$), there also exists other maxima (grating lobes) at $\theta = 0^o$ and $\theta = 180^o$. However, since the element pattern of the λ/2 dipole consist of nulls at 0^o and 180^o, the overall array response also consists of nulls at these angles. Therefore the grating lobes that were present in the array factor pattern are suppressed in the total array pattern.

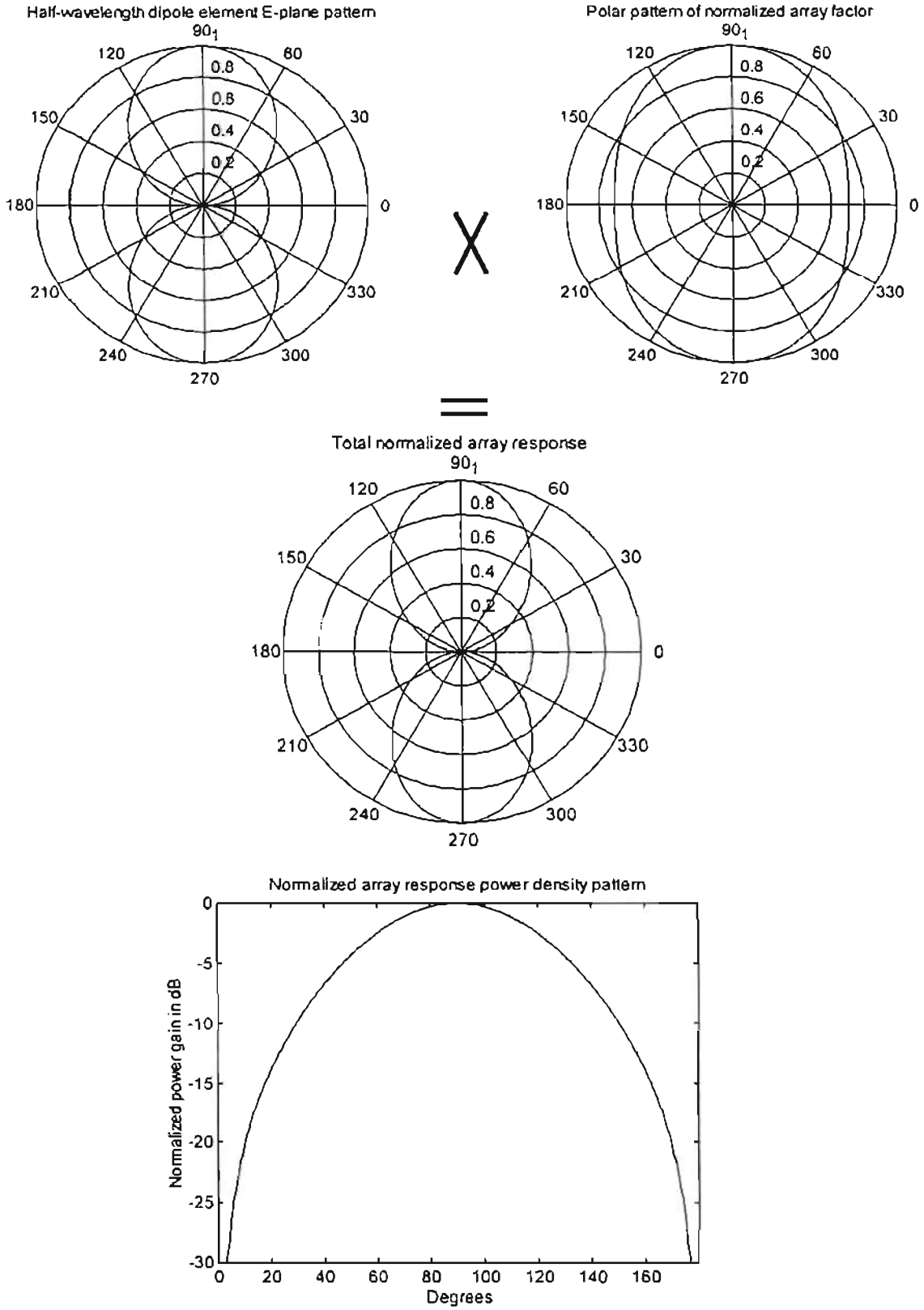

Fig. A.3: Element, array factor and total array response for an array of collinear λ/2 dipoles steered to broadside (N = 2, d = 0.25λ, $\theta_o = 90^\circ$)

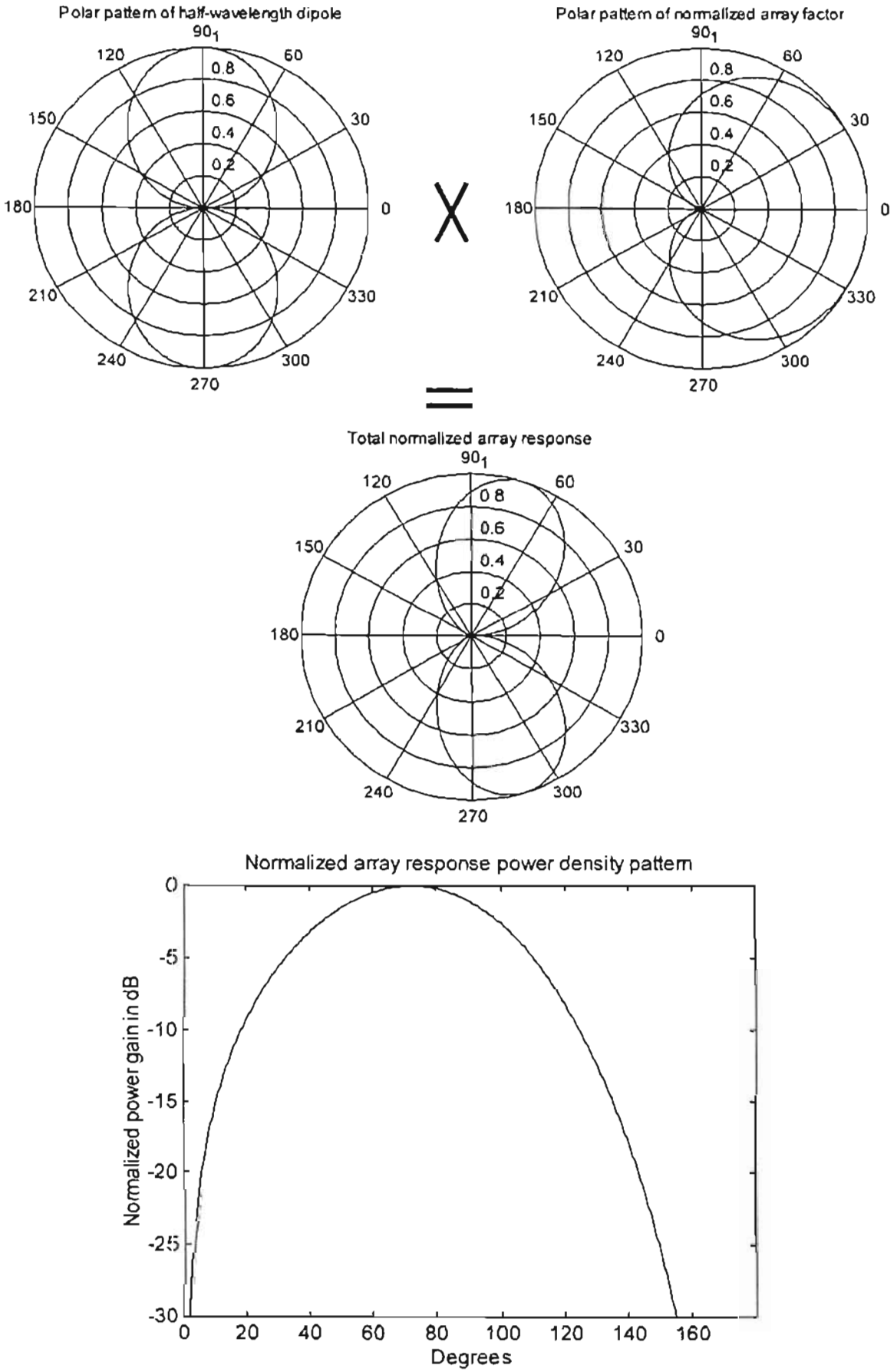

Fig. A.4: Element, array factor and total array response for an array of collinear λ/2 dipoles steered to endfire (N = 2, d = 0.25λ, $\theta_0 = 0^\circ$)

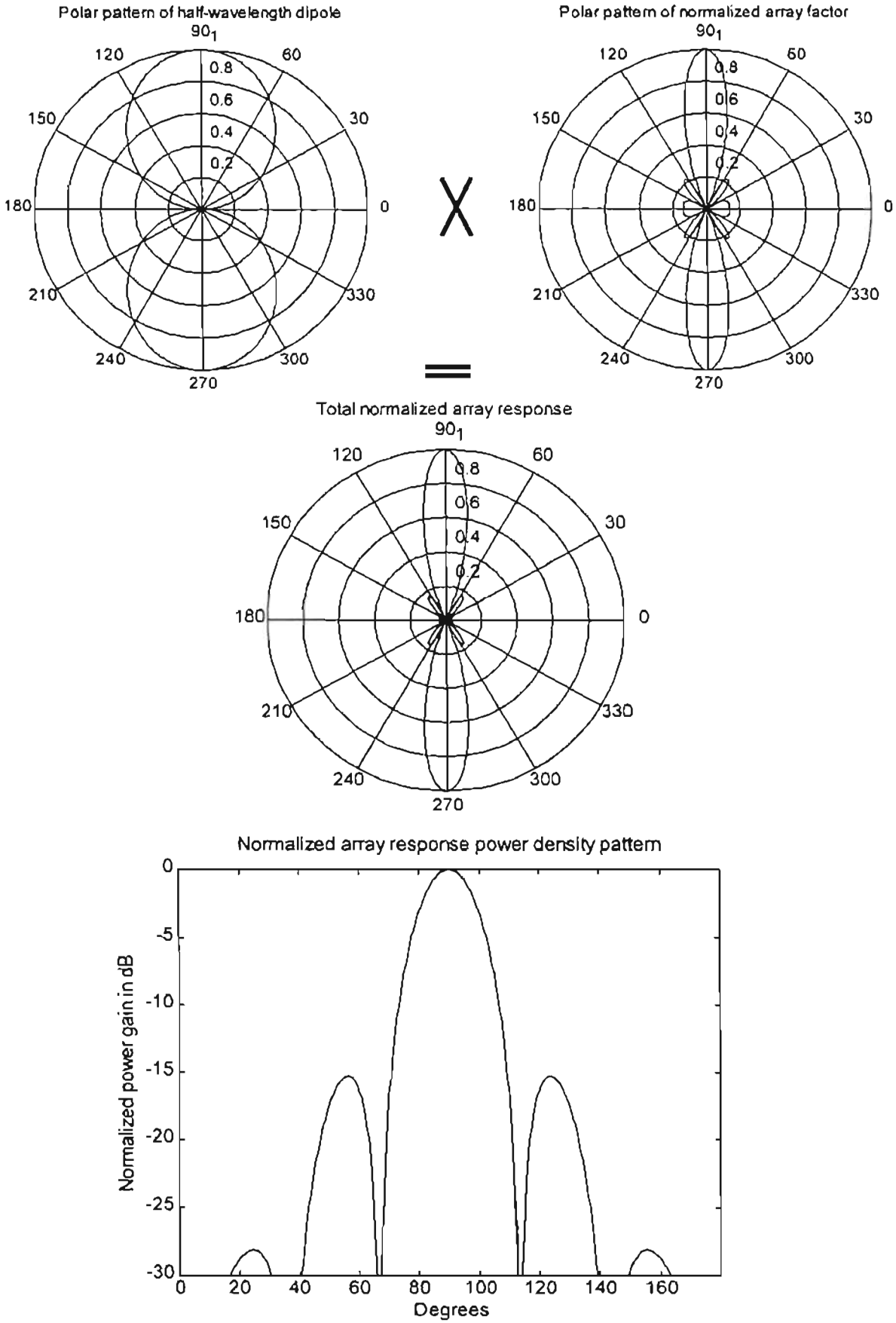

Fig. A.5: Element, array factor and total array response for an array of collinear λ/2 dipoles steered to broadside (N = 10, d = 0.25λ, θ_o =90°)

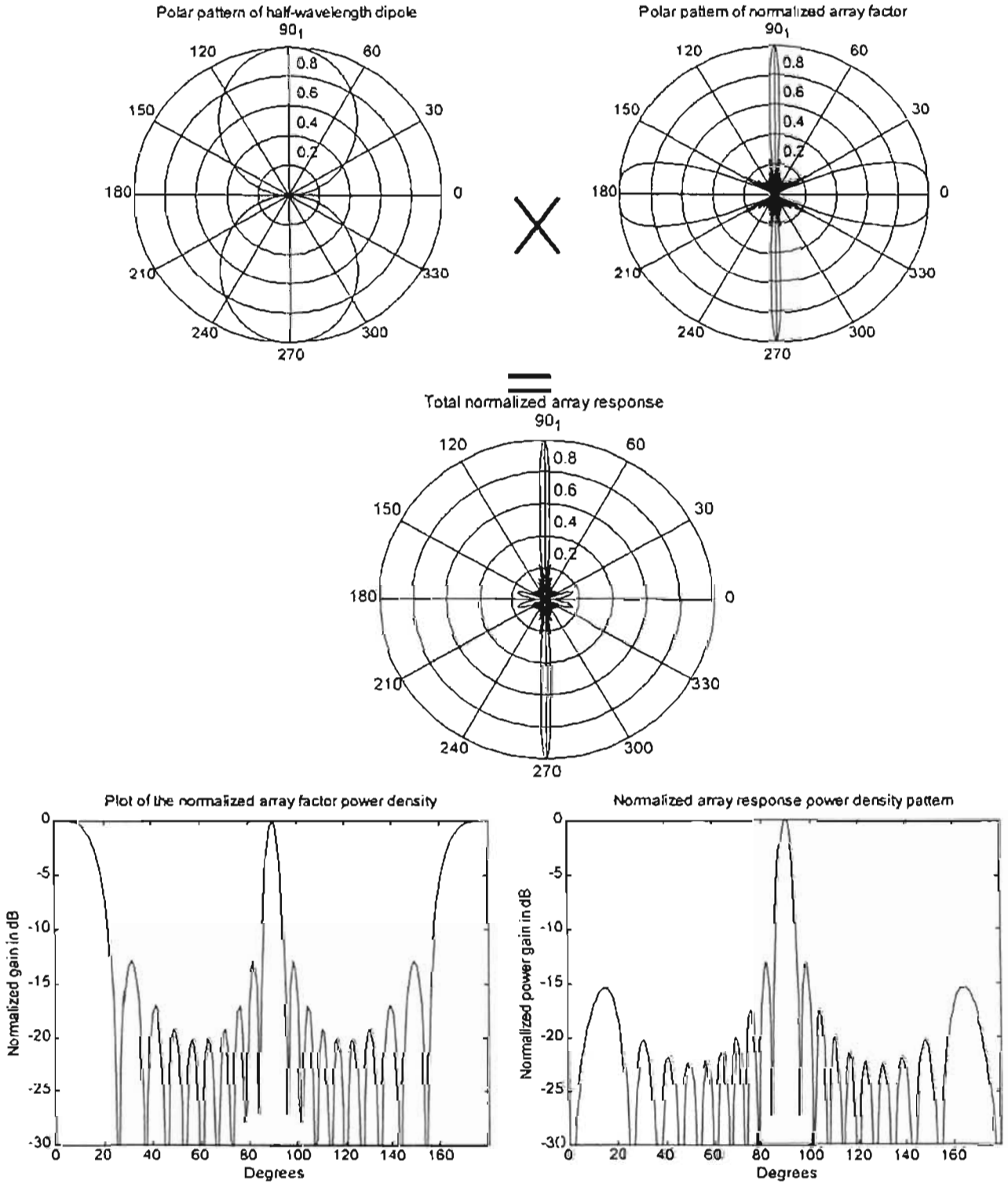

Fig. A.6: Element, array factor and total array response for an array of collinear λ/2 dipoles steered to broadside (N = 10, d = λ, $\theta_o = 90^o$)

A.3 LNA design

A.3.1 Active device selection

The gallium arsenide field-effect transistor (GaAs FET) and the bipolar junction transistor (BJT) are the two most commonly used devices in the design of amplifiers. BJTs used in UHF and microwaves are usually of planar npn silicon type. The advantages of silicon planar BJTs over other types of transistors at high frequencies are that they represent mature technology both in the understanding of physics and the device design, low cost and proven reliability. Compared with its microwave BJT counterpart, the GaAs FET has high gain and lower noise figure and can operate at a higher maximum frequency. The difference in frequency handling capacity between BJTs and GaAs FETs is due to the slower minority carriers in the base region of the BJT whereas conduction in a GaAs FET depends mainly on majority carriers.

The ATF-10136 GaAs FET was selected on the basis of the description of the device by the manufacturer as being suitable for use in low noise amplifier applications in the 0.5 to 12GHz range. It was also selected on the basis of availability and cost effectiveness.

A criterion to check whether a single stage amplifier will suffice is to check that the device has a maximum available gain, *MAG* (in the case of an unconditionally stable device) greater than the specified gain at the frequency of interest. In the case of a potentially unstable device, a single stage will suffice when the maximum stable gain (*MSG*) greater than the specified gain at the frequency of interest. The specified minimum gain is 10dB, so the device must have a *MAG* or *MSG* greater than 10dB at 2GHz for a single stage to suffice. The S parameters of the device at V_{DS} = 2V and I_{DS} = 25mA are given in the manufacturer's data sheet and partially reproduced in table (A.1) below.

Freq.	S_{11}		S_{21}		S_{12}		S_{22}	
(GHz)	Mag.	Angle	Mag.	Angle	Mag.	Angle	Mag.	Angle
2	0.79	-66^0	4.64	113^0	0.074	59^0	0.30	-31^0

Table A.1: S parameters of ATF-10136 GaAs FET at V_{DS} = 2V and I_{DS} = 25mA

The scattering matrix determinant Δ is given as

$$\begin{aligned}\Delta &= S_{11}S_{22} - S_{12}S_{21} \\ &= 0.421\angle -42.3^\circ\end{aligned} \tag{A.2}$$

The Rollet stability factor,

$$\begin{aligned}K &= \frac{1-|S_{11}|^2-|S_{22}|^2+|\Delta|^2}{2|S_{12}S_{21}|} \\ &= 0.674\end{aligned} \tag{A.3}$$

Since $|S_{11}| < 1$, $|S_{22}| < 1$ and $K < 1$, this implies that the device is potentially unstable. Hence, the design for maximum available gain is impossible.

The maximum stable gain (MSG) is given by

$$\begin{aligned}MSG &= \frac{|S_{21}|}{|S_{12}|} \\ &= \frac{4.64}{0.074} \\ &= 62.703 \\ &= 17.97dB\end{aligned} \tag{A.4}$$

Hence, a single stage amplifier will suffice.

A.3.2 Single stage amplifier design

The configuration of a single stage microwave transistor amplifier is shown in figure (A.7).

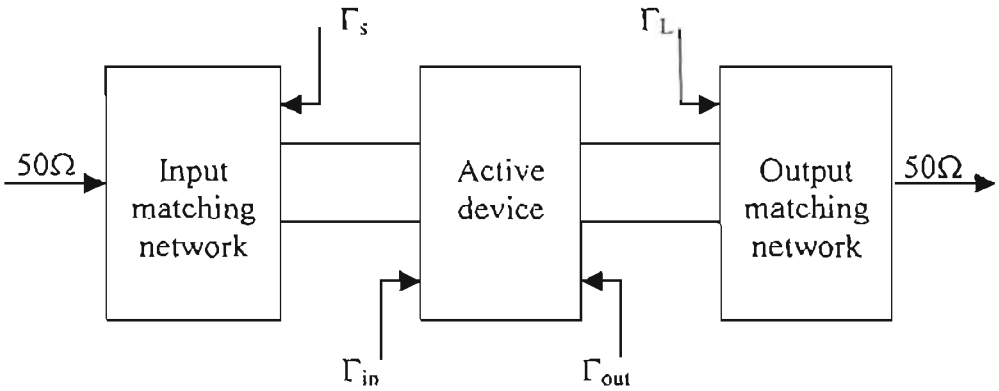

Fig. A.7: Single stage amplifier configuration

The design of an amplifier usually consists in the optimization of one of the following requirements:

(a) overall high gain

(b) overall low noise figure

In a design requiring overall high gain, the reflection coefficients are selected as follows.

$$\Gamma_s = \Gamma_{in}^{*}$$
$$\Gamma_L = \Gamma_{out}^{*} \quad \text{(A.5)}$$

In a low-noise design, the reflection coefficients are selected as follows.

$$\Gamma_s = \Gamma_{opt}$$
$$\Gamma_L = \Gamma_{out}^{*} \quad \text{(A.6)}$$

where Γ_s and Γ_L are the source and load reflection coefficients, respectively. Γ_{in} and Γ_{out} are the input and output reflection coefficients, respectively. Γ_{opt} is the optimum noise source reflection coefficient. The low noise design option was chosen. Table (A.2) shows the typical noise parameters of the GaAs FET at V_{DS} =2V and I_{DS} = 25mA at the desired frequency of 2GHz. This table was partially reproduced from the manufacturer's datasheets.

Freq (GHz)	Γ_{opt} (Mag./angle)	$r_n = R_n/50$	F_{min} (dB)
2	$0.7\angle 47^{\circ}$	0.46	0.4

Table A.2: Typical noise parameters for the ATF-10136 at V_{DS} =2V and I_{DS} = 25mA

It should be noted that F_{min} is a function of the device bias point and operating frequency and there is one value of optimum source reflection coefficient Γ_{opt} associated with each value of F_{min}.

The design for lowest possible noise figure is always possible in an unconditionally stable device (K>1). However, in a potentially unstable device (K<1), this is not always the case. Also, the process is not as straightforward as with an unconditionally stable device, involving the construction of source and load stability circles, and checking the stability of the optimum source reflection coefficient Γ_{opt} together with its corresponding load reflection coefficient Γ_L. The design procedure is as follows:
The centre of the load stability circle is given by

$$\Gamma_{2S} = \frac{\left(S_{22} - \Delta S_{11}^{*}\right)^{*}}{|S_{22}|^2 - |\Delta|^2} \quad \text{(A.7)}$$
$$= 3.359\angle 99.3^{\circ}$$

The radius of the load stability circle is given by

$$R_{2S} = \frac{|S_{12}S_{21}|}{\left||S_{22}|^2 - |\Delta|^2\right|} \qquad (A.8)$$

$$= 3.951$$

The centre of the source stability circle is given by

$$\Gamma_{1S} = \frac{\left(S_{11} - \Delta S_{22}^*\right)^*}{|S_{11}|^2 - |\Delta|^2} \qquad (A.9)$$

$$= 1.620\angle 74.2^\circ$$

The radius of the source stability circle is given by

$$R_{1S} = \frac{|S_{12}S_{21}|}{\left||S_{11}|^2 - |\Delta|^2\right|} \qquad (A.10)$$

$$= 0.768$$

The source and load stability circles are plotted on the Smith chart shown overleaf. A normalized impedance of 1 corresponds to 81.5mm. Since $|S_{11}|$ and $|S_{22}|$ are less than 1 at 2GHz, the Smith chart represents a stable operating point for both source and load terminations i.e. the stable regions are outside the stability circles. However, since the load stability circle encloses (encompasses) the centre of the Smith chart, all areas inside the load stability circle are stable for load terminations i.e. the areas outside the load stability circle are unstable load terminations. To check whether a minimum noise figure of F_{min} = 0.4dB (@ 2GHz) is achievable with a potentially unstable device, it is necessary to ensure that $\Gamma_S = \Gamma_{opt}$ lies in the stable region of the source stability circle plot. If this is not the case, then a value other than Γ_{opt} must be chosen for the source reflection coefficient Γ_S, at the expense of having a noise figure higher than F_{min}. After selecting Γ_S, whether it is equal to Γ_{opt} or not, conjugate matching is normally employed on the output of the device i.e. the load reflection coefficient is made equal to the complex conjugate of the output reflection coefficient. The computed value of Γ_L must of course lie within the stable region of the load stability plot.

The value of $\Gamma_S = \Gamma_{opt} = 0.7\angle 47^\circ$ (corresponding to F_{min} = 0.4dB) is plotted on the Smith chart. It lies within the stable region of the source stability circle. The corresponding value of load reflection coefficient Γ_L is computed as

The Complete Smith Chart

Black Magic Design

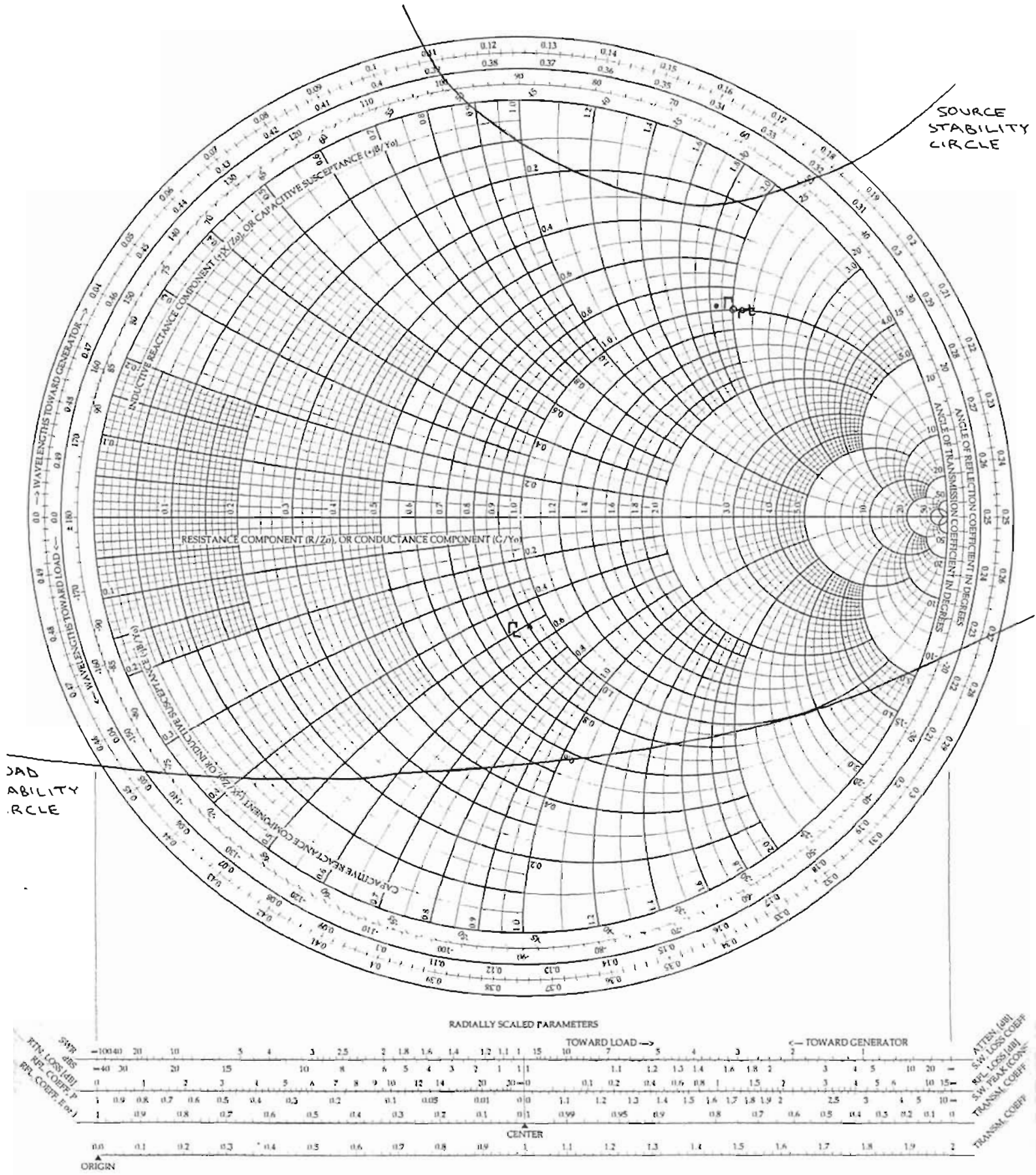

$$\Gamma_L = \left(\frac{S_{22} - \Delta\Gamma_{opt}}{1 - \Gamma_{opt} S_{11}} \right)^* \qquad (A.11)$$
$$= 0.265\angle -84.9°$$

This is now plotted on the Smith chart. It lies within the stable region of the load stability circle. Since both Γ_L and Γ_{opt} lie in the stable region of the load and source stability circles, it is possible to design for minimum noise figure of 0.4dB.

The transducer power gain G_T for this minimum noise figure can now be calculated as

$$G_T = \frac{|S_{21}|^2 \left(1 - |\Gamma_L|^2\right)\left(1 - |\Gamma_S|^2\right)}{\left|1 - S_{11}\Gamma_S - \Gamma_L S_{22} + \Delta\Gamma_L \Gamma_S\right|^2}$$
$$= 33.319 \qquad (A.12)$$
$$= 15.523dB$$

A.3.3 Topology

One of the most important aspects of high-frequency circuit design and microwave engineering is the problem of impedance matching. Impedance matching is the design of a circuit to be inserted between a source and load (both used in the general sense) so as to provide maximum power transfer between them. One of the most fundamental criteria is that a matching network must at least be theoretically lossless. The reason is obvious. As a consequence, matching networks in high-frequency circuit design always take the form of a LC (never R) circuit in the discrete case, or in the form of transmission line sections and stubs in the distributed case.

The bandwidth specification is ≥10MHz at a centre frequency of 2GHz. This gives a Q factor of:

$$Q \le \frac{f_o}{\Delta f}$$
$$\le \frac{2GHz}{10MHz} \qquad (A.13)$$
$$\le 200$$

The Q factor is a useful measure of the bandwidth performance of a filter/amplifier [18]. With a Q factor less than 10, the device is classified as wideband whereas with a Q factor greater than 10, the device is classified as narrowband. In wireless communications, higher frequency bands are being sought to avoid congestion. As a result, wider bandwidth amplification would be required. There are a number of

techniques used to maximize the bandwidth of an amplifier [65]. One technique is the employment of wideband matching.

Wideband matching can be accomplished by means of multisection quarter-wavelength transformer matching networks. Multisection transformer matching offers increased bandwidth at the expense of having a large number of $\lambda/4$ sections. Depending on the frequency of operation, substrate permittivity and thickness, this can lead to impractical circuit sizes. In a multi-stage amplifier, the use of multisection $\lambda/4$ transformers (2 or more sections) results in a circuit that is considerably much larger than with its single section counterpart (for the same substrate and frequency of operation). Hence single section $\lambda/4$ matching networks were chosen because of its practicality.

A quarter-wavelength transformer can only be used to match a purely resistive source to a purely resistive load. However, should either/both the source or load be complex, it is necessary to first cancel the reactive component(s) before using a quarter-wavelength transformer. Cancellation of the reactive components can be achieved in two ways:

(a) By insertion of a length of transmission line (of arbitrary characteristic impedance) in series with the source and/or load so that the impedance seen at the input of the length of transmission line is purely resistive. The length of the transmission line is determined by using a Smith chart. It should be noted that the precision obtainable from the chart is not very good.

(b) By insertion of a stub in parallel with the complex source and/or load. The stub cancels the susceptance of the source and/or load impedance so that the impedance seen at the input of the stub is purely resistive. The stub can take the form of an open-circuit or short-circuit length of transmission line in parallel with the source and/or load. Good short-circuit stubs are difficult to implement and realize in microstrip as it requires the use of through-hole plating which is costly. Also in some instances the stubs are so thin (large characteristic impedance) that they require precision drilling equipment (ultrasonic drill and small diameter bits) to prevent cracking of the substrate. Therefore short-circuit stub implementation requires skill. Hence the use of short-circuit stubs is discouraged.

Hence, single section quarter-wavelength transformers with open-circuit stubs as matching networks were only considered in this design. The choice of substrate is important in the design of microstrip circuitry. Circuit performance can be degraded by the choice of a poor substrate. Electrical, mechanical and thermal stability properties should be considered when choosing a substrate. However, in spite of its lossyness, PCB was used in this design due to its availability and cost-effectiveness. The main specifications of the PCB substrate are listed in table (A.3) below.

Dielectric constant ε_r	4.1 ± 0.2
Dielectric thickness d	0.9mm

Table A.3: PCB main specifications

The relatively low value of the dielectric constant coupled with the relatively low frequency of operation (lower end of microwave frequency band) allows for easy etching of the circuit. Thus there is no need for ultra-precision etching facilities that would otherwise be required in the case of a high dielectric constant (for the same dielectric thickness and frequency of operation).

A.3.3.1 Input matching

Input matching is required to match the 50Ω source to Z_{opt}^* where Z_{opt}^* is given by

$$Z_{opt}^* = \frac{Z_o\left(1+\Gamma_{opt}^*\right)}{1-\Gamma_{opt}^*}$$
$$= 106.864\angle -63.5° \qquad \text{(A.14)}$$
$$= 47.65 - j95.65\Omega$$

The –j95.65Ω reactive component of Z_{opt}^* can be cancelled with a parallel (shunt) reactance to ground. The admittance Y_{opt}^* is given by

$$Y_{opt}^* = \frac{1}{Z_{opt}^*} \qquad \text{(A.15)}$$
$$= 0.0041721 + j0.0083761$$

The +j0.0083761 susceptance needs to be cancelled with a susceptance value of -j0.0083761 in parallel. To realize this susceptance, we note that an open-circuited stub is seen to have an input admittance of

$$Y = jY_o \tan\theta \qquad \text{(A.16)}$$

where Y_o is the characteristic admittance and $\theta = 2\pi l / \lambda$. If $\theta = 3\pi/4$ i.e. $l = 3\lambda/8$, then $Y = -jY_o$. Thus an open-circuited stub that is three-eights of a wavelength long looks like a shunt element with admittance $-jY_o$. In this case, $Y = -jY_o$ = -j0.0083761

and thus Y_o = 0.0083761 or the characteristic impedance of the open-circuited stub is given by $Z_o = 1/Y_o$= 119.387Ω.

Since the source generator is 50Ω and in order to realize the parallel conductance element of 0.0041721S, a quarter-wave transformer ($l = \lambda/4$) of impedance

$$\begin{aligned} Z_o &= \sqrt{Z_s Z_L} \\ &= \sqrt{50\frac{1}{0.0041721}} \\ &= 109.473\Omega \end{aligned} \qquad \text{(A.17)}$$

is employed.

A.3.3.1.1 Microstrip implementation

(a) Calculation of line widths

Bahl and Trivedi [89] have proposed two formulae to calculate line widths (w), given substrate thickness (d) and line impedance (Z_o):

$$\frac{w}{d} = \frac{8e^A}{e^{2A} - 2} \qquad \text{for } \frac{w}{d} < 2 \qquad \text{(A.18)}$$

where $A = \frac{Z_o}{60}\sqrt{\frac{\varepsilon_r + 1}{2}} + \frac{\varepsilon_r - 1}{\varepsilon_r + 1}\left[0.23 + \frac{0.11}{\varepsilon_r}\right]$

and

$$\frac{w}{d} = \frac{2}{\pi}\left[B - 1 - \ln(2B - 1) + \frac{\varepsilon_r - 1}{2\varepsilon_r}\left\{\ln(B - 1) + 0.39 - \frac{0.61}{\varepsilon_r}\right\}\right] \quad \text{for } \frac{w}{d} > 2 \qquad \text{(A.19)}$$

where $B = \frac{377\pi}{2Z_o\sqrt{\varepsilon_r}}$

50Ω input line width

using equation (A.19): $\frac{w}{d} = 2.01630283$ or $w = 1.815mm$

109.473Ω quarter-wave section line width

using equation (A.18): $\frac{w}{d} = 0.3730937$ or $w = 0.336mm$

119.387Ω open-circuit stub width

using equation (A.18): $\frac{w}{d} = 0.2860581$ or $w = 0.257mm$

(b) Calculation of line lengths

Two parameters that are of importance in the calculation of microstrip line lengths are the effective dielectric constant (ε_e) and the guided wavelength (λ_g). These are given respectively, by:

$$\varepsilon_e = \frac{\varepsilon_r + 1}{2} + \frac{\varepsilon_r - 1}{2} \frac{1}{\sqrt{1 + 12\frac{d}{w}}} \qquad \text{(A.20)}$$

and

$$\lambda_g = \frac{\lambda_o}{\sqrt{\varepsilon_e}} \qquad \text{(A.21)}$$

where $\lambda_o = \frac{c}{f} = \frac{3 \times 10^8 ms^{-1}}{2 \times 10^9 Hz} = 150mm$

50Ω input line length

The 50Ω input line length was chosen to be $\lambda_g/4$.

using equation (A.20): $\varepsilon_e = 3.1378856$

using equation (A.21): $\lambda_g = 84.678$mm

$\therefore$ length of 50Ω line is 21.17mm

109.473Ω quarter-wave section line length

using equation (A.20): $\varepsilon_e = 1.724$

using equation (A.21): $\lambda_g = 89.337$mm

$l = \lambda_g/4 = 22.334$mm

119.387Ω open-circuit stub length

using equation (A.20): $\varepsilon_e = 2.7865117$

using equation (A.21): $\lambda_g = 89.859$mm

$l = 3\lambda_g/8 = 33.697$mm

Figure (A.8) shows the microstrip input matching network (dimensions in millimetres).

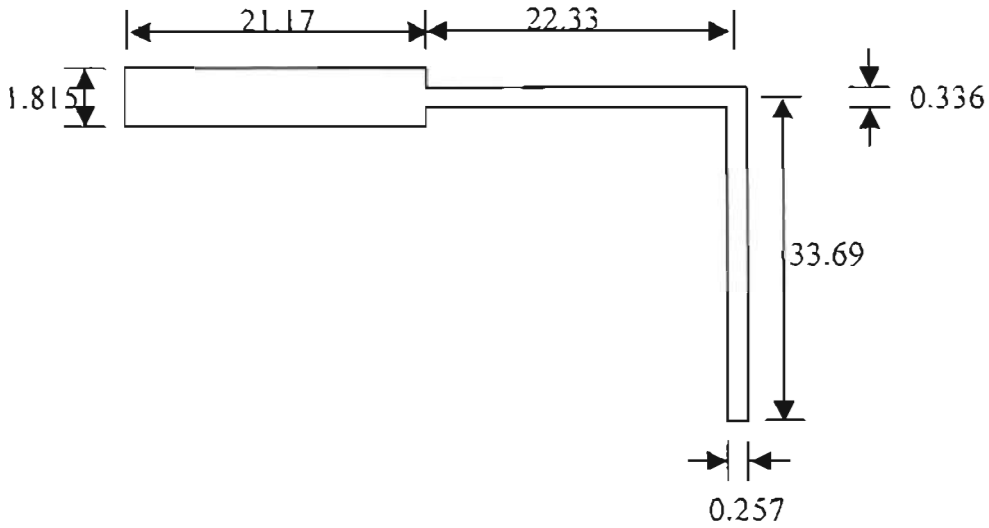

Fig. A.8: Microstrip input matching network

A.3.3.2 Output matching

Output matching is required to match the output of the amplifier to the 50Ω load i.e. Z_L^* to 50Ω.

$$Z_L^* = \frac{Z_o\left(1+\Gamma_L^*\right)}{1-\Gamma_L^*}$$
$$= 52.263\angle 29.6° \qquad \text{(A.22)}$$
$$= 45.434 + j25.829\Omega$$

where Γ_L^* is computed as $0.265\angle 84.9°$ from equation (8.10).

The +j25.829Ω reactive component of Z_L^* can be cancelled with a shunt reactance to ground. The admittance $Y_L^* = 1/Z_L^* = 0.0166338 - j0.0094562$. The -j0.0094562 susceptance needs to be cancelled with a susceptance value of +j0.0094562 in parallel. Using the same procedure as the input matching network, the open-circuited stub should be one-eight of a wavelength long ($\theta = \pi/4$) with a characteristic impedance of $Z_o = 1/Y_o = 1/0.0094562 = 105.751\Omega$.

With the reactive component of Z_L^* cancelled, a quarter wavelength transformer can now be used to match the parallel conductance element of 0.0166338S to the 50Ω load. The characteristic impedance of the λ/4 transformer is

$$Z_o = \sqrt{Z_s Z_L}$$
$$= \sqrt{\frac{1}{0.0166338}}50 \qquad \text{(A.23)}$$
$$= 54.826\Omega$$

A.3.3.2.1 Microstrip implementation

(a) Calculation of line widths

105.751Ω open-circuit stub width

using equation (A.18): $\frac{w}{d} = 0.4123408$ or $w = 0.371mm$

54.826Ω quarter-wave section line width

using equation (A.18): $\frac{w}{d} = 1.7272363$ or $w = 1.555mm$

50Ω output line width

using equation (A.19): $\frac{w}{d} = 2.01630283$ or $w = 1.815mm$

(b) Calculation of line lengths

105.751Ω open-circuit stub length

using equation (A.20): $\varepsilon_e = 2.8325095$

using equation (A.21): $\lambda_g = 89.126$mm

$l = \lambda_g/8 = 11.141$mm

54.826Ω quarter-wave section line length

using equation (A.20): $\varepsilon_e = 3.0998143$

using equation (A.21): $\lambda_g = 85.197$mm

$l = \lambda_g/4 = 21.299$mm

50Ω output line length

The 50Ω output line length was chosen to be $\lambda_g/4$ (same length as 50Ω input line).

using equation (A.20): $\varepsilon_e = 3.1378856$

using equation (A.21): $\lambda_g = 84.678$mm

$\therefore$ length of 50Ω line is 21.17mm

Figure (A.9) shows the microstrip output matching network (dimensions in millimetres).

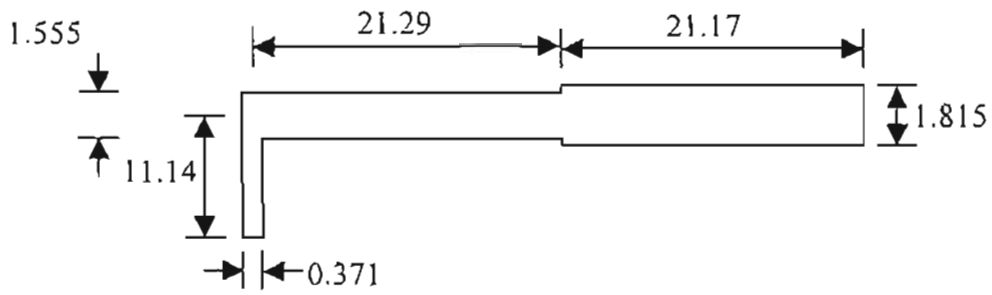

Fig. A.9: Microstrip output matching network

A.3.4 Bias circuit

It has been said that the least considered factor in microwave transistor amplifier design is the bias network [90]. While considerable effort is spent in designing for a given gain, noise figure and bandwidth, little effort is spent in the dc bias network. The cost per decibel of microwave power gain or noise figure is high, and the designer cannot sacrifice the amplifier performance by having a poor dc bias design.

The purpose of a good dc bias design is to select the proper quiescent point and hold the quiescent point constant over variations in transistor parameters and temperature. A resistor bias network can be used with good results over moderate temperature changes. However, an active bias network is usually preferred for large temperature changes.

GaAs FETs can be biased in several ways. One common bias circuit used for low noise, high gain, high power and high efficiency is shown in figure (A.10).

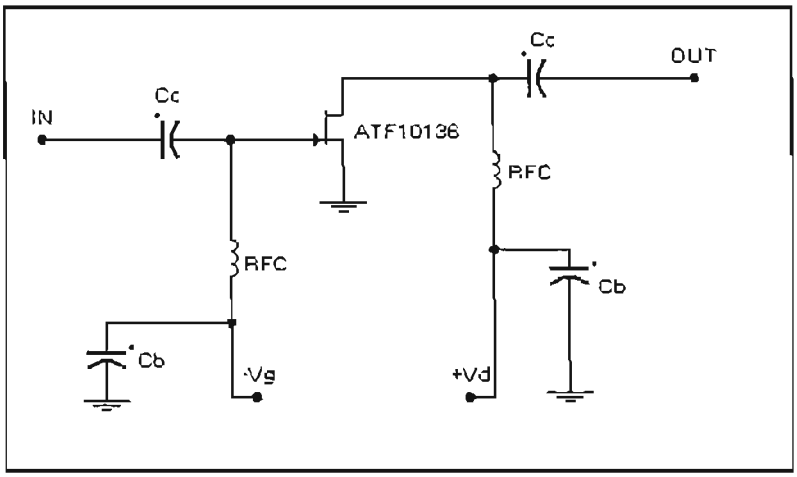

Fig. A.10: Bias circuit

Low noise amplifiers operate at relatively low drain-source voltage V_{DS} and current I_{DS}, usually $I_{DS} = 0.15I_{DSS}$ (I_{DSS} is the drain-source current when $V_{GS} = 0$). This configuration gives the lowest source inductance and hence lowest noise figure and higher gain. Most high-frequency amplifier circuit designs for high gain or low noise figure requires that the source lead be dc grounded as close to the package as possible so that the source series feedback is kept to an absolute minimum. However, I_D becomes sensitive to variations in temperature and I_{DSS}.

The above bias circuit requires a bipolar power supply i.e. one positive and one negative supply. The proper turn-on sequence must be applied to prevent transient burnout of the GaAs FET device. If the drain is biased positive before the gate, the device will operate momentarily beyond its safe operating region. Therefore, the proper turn-on sequence is: first apply a negative bias to the gate ($V_G < 0$) and then apply the drain voltage ($V_D > 0$). One method to accomplish the previous turn-on procedure is to turn both power supplies at the same time and to include a long RC time constant in the V_D supply and a short RC time constant network in the negative supply V_G.

A bipolar power supply incorporating the above turn-on sequence is available in the Programme of Electronic Engineering. This is shown in figure (A.11).

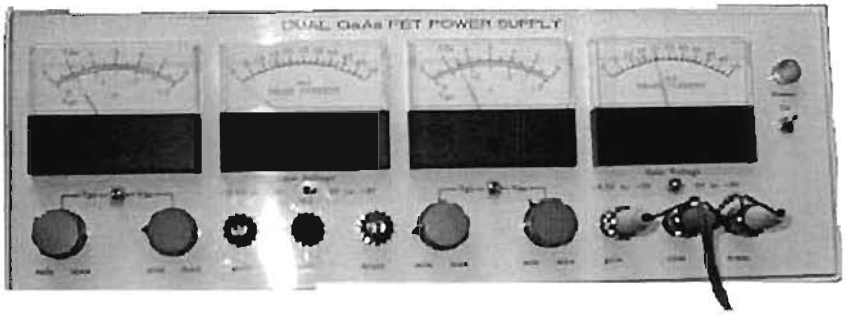

Fig. A.11: Power supply available in the Programme of Electronic Engineering for the biasing of GaAs FET amplifiers

RF chokes and decoupling (bypass) capacitors (C_B) are used to isolate RF from the DC power supply. Typical values for the chip bypass capacitors are 50pF to 500pF. The RF choke should have a reactance of at least five times the impedance of the circuit at the point where the choke is to be connected. Chip coupling capacitors (C_c) are used to AC couple the input and output of the amplifier. Typical values for the coupling capacitors are 100pF to 1000pF, high Q capacitors. They are also chosen to have low loss at the frequency of interest and low impedance compared to 50Ω. For this design, coupling and bypass capacitors (0805 size) of value 10nF were chosen. Their impedance X_c at 2GHz is

$$\begin{aligned} X_c &= \frac{1}{2\pi fC} \\ &= \frac{1}{2\pi \times 2\times 10^{9} \times 10\times 10^{-9}} \\ &= 7.958\times 10^{-3}\Omega \end{aligned} \qquad \text{(A.24)}$$

As can be seen that this impedance is negligible when compared to the 50Ω system characteristic impedance.

The bias conditions of the ATF10136 is V_{DS} = 2V and I_{DS} = 25mA. From the datasheet, the value of I_{DSS} and V_p (pinchoff voltage) are obtained as 130mA and -1.3V, respectively. The gate voltage can be calculated using the following formula:

$$I_{DS} = I_{DSS}\left(1-\frac{V_{gs}}{V_p}\right)^2 \qquad \text{(A.25)}$$

Solving for V_{gs}, yields V_{gs} = -1.87V or -0.73V. Choosing $|V_{gs}| < |V_p|$ $\Rightarrow V_{gs}$ = -0.73V. Since the source is grounded, $V_g = V_{gs}$ = -0.73V.

A.4 ADS simulation issues

This section provides a detailed description on some of the different issues that had to be considered to enable the simulations in this thesis to run successfully. These issues arose from the BER simulations in chapter 5 and 6.

A.4.1 BER simulation setup

As mentioned in chapter 5, the Improved Importance Sampling (IIS) BER measurement technique was used instead of the Monte Carlo technique because it requires a fewer number of bits to be simulated thereby reducing the simulation run time considerably. Figure (A.12) shows the IIS BER ADS sink that was used.

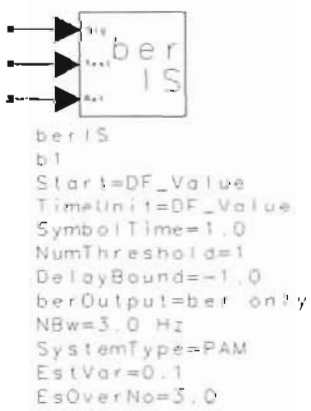

Fig. A.12: Improved Importance Sampling (IIS) BER sink used in ADS

As can be seen from figure (A.12), this block has (among other input fields), an input field for the E_b/N_o value where E_b is the energy per bit and N_o is the one-sided power spectral density of bandlimited white noise. However, in the existing simulation setup, the user has no prior knowledge of this value. However, there are two methods to determine this value

(i) Calculation

(ii) Using the Monte Carlo BER measurement sink

(i) Calculation

The following formulae are used in ADS for the calculation of E_b and N_o:

$$E_b = P_{ESREF} T_b \tag{A.26}$$

where P_{ESREF} = source power in the reference RF signal at output of the IF amplifier (see figure (5.3) in chapter 5), T_b = bit time.

$$N_o = P_{ESREF} T_{step} \tag{A.27}$$

where P_{ENREF} = noise power at output of IF amplifier, T_{step} = simulation time step or sampling time. So

$$\frac{E_b}{N_o} = \frac{P_{ESREF} T_b}{P_{ENREF} T_{step}} \tag{A.28}$$

E_b/N_o can also be related to the SNR (at the output of the IF amplifier) by the following equation:

$$\frac{E_b}{N_o} = SNR \frac{T_b}{T_{step}} \tag{A.29}$$

where $SNR = \frac{P_{ESREF}}{P_{ENREF}}$.

Recall from the simulation, the signal and noise powers at the input of the LNA were predetermined (-90dBm and −100dBm, respectively). Thus with a knowledge of the gain and noise figure of each RF component block, the overall noise figure (by use of Friis' equation) can be calculated. Hence, the SNR, signal (P_{ESREF}) and noise powers (P_{ENREF}) on at the output of the IF amplifier (input to demodulator can also be evaluated.

Note that P_{ESREF} and P_{ENREF} can also be determined by measuring these powers using ADS spectrum analyzer sinks. However, in this case there must be a way to distinguish these powers from each other. Recall, the output of the IF amplifier consists of both signal and noise. This distinction was made by having three RF front-ends in the simulation model (figure (A.13)).

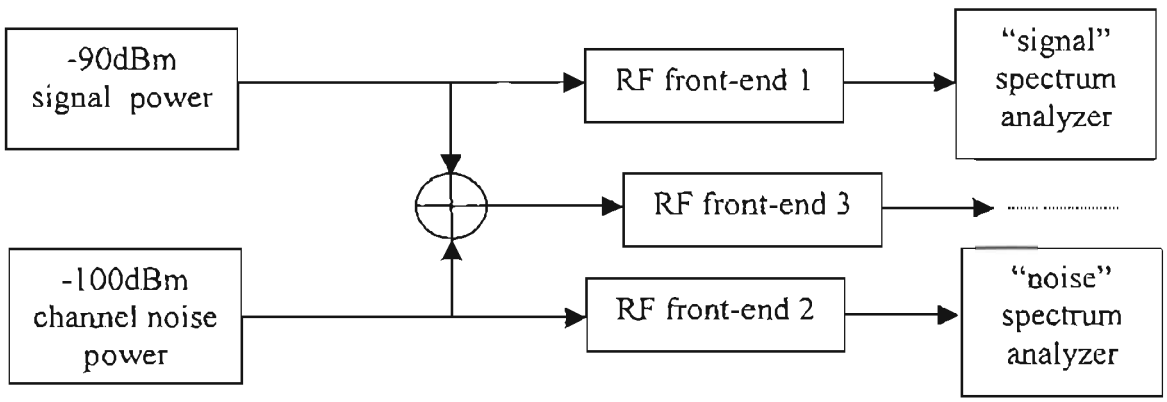

Fig. A.13: ADS setup to distinguish between signal and noise components

The setup in figure (A.13) consists of three identical front-end. Front-end 1 is connected to the –90dBm signal only. There is no noise here. Front-end 2 has only

noise power while front-end 3 has a combination of both noise and signal power. Front-end 3 is the actual receiver used to perform demodulation, despreading and BER measurements. Now that the noise and signal components can be distinguished individually, their spectrums can be integrated to find their respective powers. This is achieved using the spec_power function in ADS. The ADS documentation has more information on this.

(ii) Using the Monte Carlo BER measurement sink

Figure (A.14) shows this sink.

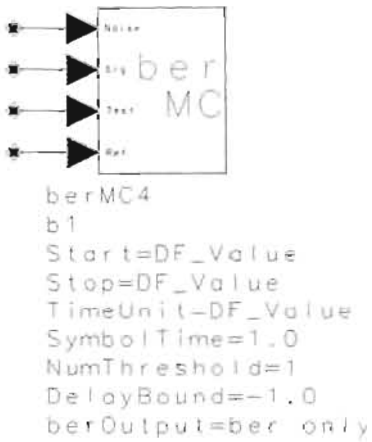

Fig. A.14: Monte Carlo BER measurement sink used in ADS

Notice that this sink has inputs for both signal (P_{ESREF}) and noise (P_{ENREF}) components. This implies that these must be distinguishable in the simulation setup. The setup of figure (A.13) could be used to differentiate between the signal and noise components. However, with this method, the Monte Carlo sink computes the E_b/N_o value (using equations (A.26), (A.27) and (A.28)) as part of the BER measurement. Thus it is unnecessary to have spectrum analyzer sinks and write functions for calculating the spectrum powers. Also, the E_b/N_o value is independent of the number of samples.

In the simulation setup, both methods (described above) were used to verify and correlate the E_b/N_o value.

A.4.2 Scaling of E_b/N_o

As mentioned in chapter 5, the E_b/N_o values were scaled by a factor 6 (7.782dB) prior to be used as an input to the IIS BER sink. The reasons for this are as follows: From equations (A.28) and (A.29) it should be noticed that E_b/N_o is a function of the simulation time step (*Tstep*). However, in CDMA, the processing gain G_p is related to the E_b/N_o by the following equation [57]:

$$\frac{E_b}{N_o} = SNR \times G_p \tag{A.30}$$

On comparison of equation (A.29) with equation (A.30), it is appropriate that E_b/N_o to be consistent with the standard definition of E_b/N_o in terms of the processing gain [57]. With a chip rate (4.096MHz) of 42 times the data (bit) rate (G_p = 42) and a simulation sampling rate of 6 times the chip rate, the scaling factor K is computed as

$$G_p = \frac{T_b}{T_{step}} \times K = 42$$

$$\frac{42}{\frac{4.096MHz}{1}} \times K = 42$$

$$\frac{}{6 \times 4.096MHz}$$

$$\Rightarrow K = \frac{1}{6} = -7.782dB$$

Thus the E_b/N_o values (obtained by the methods described earlier) had to be reduced by 7.782dB prior to input of the IIS BER measurement sink. This effectively reduces the simulation bandwidth from 24.576MHz (1/*Tstep*) to a spread bandwidth of 4.096MHz. This 4.096MHz bandwidth is used as the noise bandwidth (NBw) input field in the IIS BER sink.

A.4.3 BER curve irregularities

It can be noticed that the BER plots in chapter 5 are not smooth i.e. they do not have the expected "waterfall" BER appearance. Instead there are "flat areas" on these curves. An attempt to find the cause of this irregularity has been unsuccessful. These "flat areas" occur for a fixed range of E_b/N_o or (*SNR*). They also occur for both the IIS and Monte Carlo BER measurement techniques. This irregularity may be due a software bug. A response from Agilent Technologies' product technical support division, on this phenomenon, is still awaited.